

https://dspace.org/

Investigation of the Ore Mineralisation Styles and Alteration Zones of Messina Copper Deposits

Hlahla, Dimakatso Lauretta

2025-01

University of the Witwatersrand, Johannesburg

https://hdl.handle.net/10539/47653

Hlahla, Dimakatso Lauretta. (2025). Investigation of the Ore Mineralisation Styles and Alteration Zones of Messina Copper Deposits. [Master's dissertation, University of the Witwatersrand, Johannesburg]. WIReDSpace. https://hdl.handle.net/10539/47653

Downloaded from a DSpace repository. https://dspace.org/

INVESTIGATION OF THE ORE MINERALISATION STYLES AND ALTERATION ZONES OF MESSINA COPPER DEPOSITS, SOUTH AFRICA



By

Hlahla Dimakatso Lauretta (1730650)

Supervisor: Dr Linda Iaccheri
Co-supervisor: Prof Robert Bolhar

School of Geosciences
A research report submitted to the Faculty of Science, University of the Witwatersrand, Johannesburg, in fulfilment of the requirements for the degree of Master of Science.

Declaration

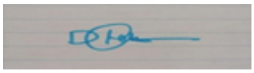
I, Dimakatso Hlahla (student number: 1730650), declare that this research report is my own, unaided work. It is being submitted for the Degree of Master of Science at the University of the Witwatersrand, Johannesburg. It has not been submitted before for any degree or examination at any University.

I am aware that plagiarism (the use of someone else's work without their permission and/or without acknowledging the original source) is wrong.

I confirm that the work submitted for assessment for the above course is my own unaided work except where I have explicitly indicated otherwise.

I have followed the required conventions in referencing the thoughts and ideas of others.

I understand that the University of the Witwatersrand may take disciplinary action against me if there is a belief that this is not my own unaided work or that I have failed to acknowledge the source of the ideas or words in my own writing.

Signature:  **Date:** 03/01/2025

Dedication

To my supportive family and friends. To Dr. Linda Iaccheri for her support and utmost patience.

Acknowledgements

My special thanks go to my supervisor, Dr. Linda Iaccheri for encouraging me to pursue this project. Her support and guidance throughout the project are unmatched. I thank Dr. Humbulani Rejune Mundalamo of the University of Venda for shedding light about Messina Cu deposit. I am grateful to Mr Louis Mudalahotlhe and Mr Samuel Tshabalala for preparing thin sections even when they had to redo some of them without hesitation. I am deeply indebted to Bibi Ayesha Jogee for her help with Wits Imaging and Microscopy (WIMLab) and always finding time to help. I thank my Co-supervisor Robert Bolhar for his constructive feedback that improved the quality of this project. I am also grateful to Dr. Nonkuselo Madlakana and Mr Borbor Gibson for helping me with Tescan Integrated Mineral Analyser (TIMA) and being patient during tough times of load shedding. I also acknowledge CIMERA for funding TIMA analysis and Mining Qualification Authorities for funding my MSc.

Table of Contents

Declaration i

Abstract ii

Dedication iii

Acknowledgements iv

List of Figures vi

List of Tables xii

The Abbreviations xiii

1 Introduction 1

2 Geological background 3

3 Previous studies of Messina Cu deposit 6

3.1 Source of hydrothermal fluids and alteration 6

3.1.1 Sulphide paragenesis 7

3.1.2 Silicate paragenesis and alteration zones 10

4 Methodology 12

5 Results 14

5.1 Petrographic descriptions 14

5.2 SEM-EDS (TIMA) analysis 47

6 Interpretation of results 65

7 Discussion 71

7.1 Ore types 71

7.2 Messina hydrothermal fluid processes 74

7.3 Critical and base metals associated with sulphides and Fe oxides 79

7.4 Comparison of Messina Cu deposit with other hydrothermal copper deposits 79

8 Conclusion 83

9 Limitations 84

10 Recommendations for future work 84

11 Reference list 86

Appendix A 90

Appendix B 112

List of Figures

Figure 1: Google Earth image showing the location of Musina town and different mines within Messina mining district. The stippled line shows Messina Fault 1

Figure 2: A cross-section showing mineralisation styles within the metamorphic country rocks of Musina area in Harper mine (Bahnemann, 1986) 2

Figure 3: Simplified geology of the location of (a) Musina area within the Central Zone of the Limpopo Mobile Belt and (b) the distribution of mines along the Messina fault in Messina mining district. Breccia pipes are represented by the small, black circular-like shapes (after Cox *et al*., 2019; Mundalamo, 2019) 5

Figure 4: Geological cross-section of Artonvilla mine shafts showing occurrence of mineralisation within mafic and felsic granulites at Frost Lode, Emery Lode, and Reggie Lode (after Jacobsen and McCarthy, 1976) 6

Figure 5: Sketch showing sulphide zonation in the L Lode breccia pipe of Messina mine (from Jacobsen, 1967) 8

Figure 6: Sketch showing the concentric zonation of (a) the sulphides and (b) associated hydrothermal alteration zones in Emery Lode of Artonvilla mine (after Jacobsen and McCarthy, 1976). The white areas within sulphide zoning represent leached ore 9

Figure 7: Sample 19068 showing massive bornite (Bn) enclosing discrete subhedral quartz (Qz) fragments and fine-grained irregular chlorite (Chl) veins. Fine-grained multiple chlorite veinlets cut through the massive bornite, whereas another fine-grained chlorite groundmass occurs around it. The chlorite has orange-red iron oxide stains (red arrow in a). White arrow in (b) indicates needle-like specularite between the massive bornite and fine-grained chlorite 14

Figure 8: Plane polarised light photomicrographs for sample 19068, showing silicate minerals and their associated opaque minerals 15

Figure 9: Reflected light photomicrographs showing copper sulphides, mainly bornite (Bn) and chalcocite (Cc), associated with hematite (Hem) and magnetite (Mag). The different colours of bornite are due to different exposures. Some were dark under low exposure and some bright under slightly higher exposure. It is not identified as chalcopyrite because of the absence of chalcopyrite in the hand sample. Magnification scale = 500 µm. 16

Figure 10: Sample 19077 showing massive interconnected and brecciated quartz crystals (Qz) which contain minor chlorite (Chl) and bornite (Bn). Red arrows in (a) show the elongation of individual quartz crystals, typical of comb veining 17

Figure 11: Photomicrographs showing: (a-b) fragments of clinopyroxene (Cpx), quartz (Qz), and amphibole (Amp) concentrated within a fracture; (c) granular chlorite (Chl) with subhedral-subangular quartz grains filling an open space between large quartz grains; (d) small-medium-sized, angular, and subrounded quartz clustered between large quartz grains; (e) disseminated fine-grained chalcocite

(Cc); (f) bornite (Bn) blebs partially replaced by Cc and disseminated Cc (white arrow). Magnification scale = 500 µm and 200 µm..... 18

Figure 12: Sample 19073 comprises very fine-grained quartz (Qz) groundmass with subhedral, elongated, and irregular chlorite grains (Chl) in the groundmass. Quartz groundmass is heavily coated by orange-red iron oxide (Fe-stain). Interstitial bornite occurs within the quartz groundmass and is cut by chlorite in places. Some subhedral quartz grains occur within interstitial bornite. Fine-grained chalcopyrite grains (Ccp) are enclosed within the quartz groundmass. Other chalcopyrite (white arrow) is in contact with interstitial bornite (Bn) 19

Figure 13: Photomicrographs showing: (a) chlorite (Chl) grains within Fe-stained cryptocrystalline quartz (Qz) are partially altered into epidote (Ep) along cleavage planes; (b) Fe-stained vein cut through cryptocrystalline groundmass and opaque minerals. Irregular grains of green chlorite grains within cryptocrystalline quartz; (c) subhedral quartz and irregular chlorite-epidote veinlets within the opaque minerals; (d) subhedral coarse-grained bornite (Bn) in contact with disseminated chalcopyrite. Hematite platelets rim the bornite along margins; (e) bornite with minor chalcopyrite (Ccp) flame-like relics within bornite. Subhedral hematite developing into elongate blades (light bluish-green) in a fracture in host bornite; (f) tiny blades of hematite and chalcocite along minor fractures of bornite under high magnification (white square in Fig. 13e). Magnification scale = 500 µm and 200 µm. 20

Figure 14: Sample 19075 showing: (a) a mineralised vein of brecciated milky quartz crystals hosting massive tarnished bornite with minor chalcopyrite inclusions. Quartz crystals are coated with orange-red iron oxide stains; (b) contact between fine-grained chloritised country rock with the mineralised vein. Thin veins and discrete quartz crystals also occur within the chloritised country rock 21

Figure 15: Photomicrographs showing: (a) brecciated quartz (Qz) fragments with interstitial granular chlorite-epidote; (b) quartz fragments with irregular fibrous epidote (Ep) between the fragments; (c) interstitial granular chlorite (Chl) with quartz inclusions form invade the opaque minerals; (d) disseminated and anhedral lenses of bornite with minor chalcopyrite replaced by bornite along a fracture; (e) anhedral hematite (Hem) enclosing grey magnetite grains (Mag); (f) coarse-grained bornite (Bn) with minor bright yellow chalcopyrite is abutted by irregular to elongated hematite blades along the margins. Magnification scale = 500 µm..... 22

Figure 16: Sample 19078 showing one part representing epidotised (Ep) country rock and the other part representing a mineralised brecciated milky white quartz vein. The contact between them shows irregular quartz (Qz) as a rim. In other parts, bornite is in direct contact with the epidotised country rock. Minor large, subhedral quartz crystals also occur within the epidotised country rock. Fine-grained epidote (Ep) groundmass is also in direct contact with the massive bluish-purple black bornite (Bn) 23

Figure 17: Photomicrographs showing: (a) epidote (Ep) aggregates invading massive opaque minerals. The tiny white and grey grains represent broken material during sample preparation; (b) the opaque minerals are interstitial between large, subhedral cloudy quartz (Qz) and epidote aggregates; (c) epidote aggregates developing into prismatic zoisite (Zo); (d) massive, tarnished bornite (Bn) with minor disseminations cementing epidote aggregates; (e) interstitial bornite replaced partially by chalcocite (Cc) along the margins; (f) disseminated chalcocite. Magnification scale = 500 µm and 200 µm 25

Figure 18: Photomicrographs showing: (a-b) subhedral quartz (Qz) with fine-grained sericite (Ser) rimmed by epidote (Ep) along its margins. Irregular epidote grains also occur within the opaque

minerals; Chlorite-epidote (Chl+Ep) veinlets or aggregates occur within the opaque minerals; (c) fine-grained sericite partially rims subhedral quartz grains along the margins and it is overprinted by epidote, where they enclose the opaque minerals. Other euhedral, prismatic epidote grains overprint subhedral quartz grains; (d) massive bornite (Bn); (e) massive bornite with chalcocite (Cc) minute grains in places (white circles); (f) curvilinear coarse-grained bornite between the subhedral quartz rimmed by fine-grained sericite. Magnification scale = 500 µm 27

Figure 19: Photomicrographs showing: (a) albitised plagioclase (Pl) partially altered by fine-grained sericite (Ser); (b-c) fractured orthopyroxene (Opx) and plagioclase fragments associated with chloritic (Chl) networks veins filling the fractures, rimming opx and pl, and cementing and overprinting some pl fragments. Some veins occur within the opaque minerals; (d) anhedral pyrrhotite (Pyh) cements albitised plagioclase fragments and is associated with anhedral chalcopyrite (Ccp, white arrow) encroaching onto pyh; (e) massive, granular, interstitial pyh intergrown with individual euhedral and subhedral pyrite (Py) grains; (f) disseminated subhedral and anhedral pyrrhotite filling corroded halos within albitised plagioclase and chloritised biotite and orthopyroxene. Magnification scale = 500 µm 29

Figure 20: Photomicrographs showing: (a-c) subhedral and subrounded quartz (Qz1) grains intergrown with iron-stained biotite (Bt). Quartz veinlets (Qz2) cut through quartz 1, biotite and opaque minerals. Biotite is partially altered and replaced by chlorite; (d-e) subhedral and anhedral lenses of bornite (Bn) with flame-like lamellae and islands of chalcopyrite (Ccp) occur between quartz and biotite gangue. Hematite-magnetite exsolution lamellae is seen abutting bornite; (f) subhedral disseminations of bornite within corroded spaces of quartz 1 grains. Minor chalcocite spots occur along bornite margins (white circles). Irregular hematite (Hem) grains occur along cleavage planes of biotite and are in places enclosing chalcopyrite. Figure (e) represents a high magnification image of the area outlined by a white square in Fig (d). Magnification scale = 500 µm and 200 µm 31

Figure 21: Photomicrographs showing: (a-b) epidote (Ep) aggregates (brownish-yellow in PPL) associated with subangular quartz (Qz2) cement. Light green angular amphibole (Amp) relics occur within epidote aggregates; (c) fine-grained, subrounded chlorite (Chl) between relatively large quartz grains (Qz1) and interstitial sericite (Ser); (d-e) chalcocite (Cc) rims bornite and chalcopyrite (Ccp) and is in turn rimmed by thin hematite (white arrow). Disseminated chalcocite between epidote aggregates and secondary quartz 2 gangue; (f) small subhedral hematite (Hem) grains within quartz 1 halos. The pale colours of the sulphides could be due to polishing. Magnification scale = 500 µm and 200 µm . 33

Figure 22: Photomicrographs showing: (a-b) fine-grained sericite (Ser) associated with large, clear quartz grains (Qz) and alters K-feldspar (Kfs, dark brown); (c-d) anhedral quartz grains surrounded by partially sericitised K-feldspar associated with a single plagioclase grain. Sericite partially rims quartz and the opaque minerals. Corroded ser, pl, and kfs occur within the opaque minerals; (e-f) clustered pyrite (Py) grains with inclusions of corroded gangue minerals. Some smaller pyrite grains also occur as disseminated grains within sericite gangue. Pyrite grains are tarnished due to polishing. Magnification scale = 500 µm 35

Figure 23: Photomicrographs showing: (a) brecciated country rock matrix of primary quartz (Qz) intergrown with fractured garnet (Grt) and partially altered K-feldspar (Kfs) and plagioclase (Pl) grains. Fine-grained sericite (Ser) partially alters Kfs and Pl. Chlorite (Chl) has completely replaced biotite and it is also altering into epidote; (b-c) irregular stockwork veins of secondary quartz 2 (Qz2) cutting through quartz 1 (Qz1), alkali feldspars, and the opaque minerals within a thick vein. The alkali

feldspars also occur as inclusions within quartz 1; (d) subhedral and anhedral disseminated chalcopyrite (Ccp) within brecciated matrix. Molybdenite (Mol) laths are associated with anhedral sericite; (e-f) subhedral chalcopyrite within the thick vein is cut by quartz 2 veins. Disseminated smaller chalcopyrite also occurs within quartz 2 veins. Magnification scale = 500 µm 37

Figure 24: Photomicrographs showing: (a-c) fine-grained sericite (Ser) groundmass encloses altered garnet (Grt) and subhedral secondary quartz (Qz) grains. Elongated biotite (Bt) and subrounded-subangular quartz grains are included within sericite groundmass. Garnet and biotite are altered and replaced by chlorite (Chl). Fine-grained sericite and quartz enclose the opaque minerals and are corroded by opaque minerals; (d) small lenses of magnetite (Mag) within altered garnet and biotite; (e) disseminated subhedral and subrounded grains of pyrite (Py) within corroded spaces of the silicates. Coarse-grained irregular vein and thin anhedral lenses of chalcopyrite (Ccp) between sericite-quartz. Some pyrite grains are partly clustered; (f) thick pyrite vein and irregular lenses of pyrite disseminations. The vein contains sericite-quartz inclusions corroded from the contact between sericite-quartz and vein. Minor molybdenite (Mol) euhedral laths occur within the gangue and are in close contact with altered biotite grains. Magnification scale = 500 µm 39

Figure 25: Photomicrographs showing: (a) interconnected, large clear quartz (Qz) grains, typical of blocky vein cementing the opaque minerals; (b) subhedral blue chlorite (Chl) with sericite (Ser) cut through the opaque minerals. Sericite also occurs along quartz margins and granular chlorite; (c) contact between the quartz vein and brecciated country rock. The country rock contains fragments of partially altered garnet (Grt), amphibole (Amp), clinopyroxene (Cpx), and biotite (Bt) embedded within plagioclase (Pl). These fragments penetrate the quartz vein; (d) disseminated pyrite grains preferentially aligned around quartz grain boundaries; (e) fractured and porous clusters of pyrite with inclusions of tiny magnetite grains; (f) subhedral magnetite within the altered country rock. Magnification scale = 500 µm and 200 µm 41

Figure 26: Photomicrograph showing: (a-b) interconnected plagioclase (Pl) grains enclosing interstitial opaque minerals; (c) a curvy epidote vein cuts fractured garnet (Grt) intergrown with plagioclase and quartz. The garnet is weakly altered by pale green chlorite in places; (d) brecciated, corroded, and partially altered clinopyroxene (Cpx) and plagioclase intergrown with quartz. Epidote (Ep) aggregates partially altered and replaced plagioclase and clinopyroxene; (e) interstitial chalcopyrite (Ccp) cementing plagioclase; (f) subhedral and anhedral disseminated chalcopyrite within corroded gangue minerals. Magnification scale = 500 µm 43

Figure 27: Photomicrographs showing: (a-b) relatively small (1 mm) amorphous and subrounded quartz (Qz) grains overprinting large, fractured garnet (Grt); (c-d) biotite (Bt) and amphibole (Amp) grains surrounding partially sericitized (Ser) plagioclase (Pl) grains. Biotite grains are partially altered and replaced by anomalous blue chlorite (Chl). Subrounded quartz grains overprint altered plagioclase, biotite, and amphibole grains. Uncemented fracture cuts through plagioclase and amphibole grains; (e-f) anomalous blue chlorite mass altered and replaced garnet and contains inclusions of fragmented garnet and biotite. Elongated slabby quartz with smaller subrounded quartz grains overprinting chlorite. Magnification scale = 500 µm. 45

Figure 28: Photomicrographs showing: (a-b) epidote (Ep) aggregates enclose and partially alter subhedral amphibole (Amp) grains. Subhedral secondary quartz 1 cements epidote aggregates and amphibole relics. Some epidote grains are included within quartz 1; (c-d) discontinuous thin veins of secondary quartz 2 cuts through epidote aggregates and occur between elongated amphibole prismatic

grains; (e-f) subhedral magnetite grains within epidote and amphibole grains. Magnification scale = 500 µm 47

Figure 29: Phase maps showing detected minerals in sample 19068: (a) Full scan phase map; (b) high-resolution phase map 48

Figure 30: (a-e) Elemental maps of the selected area showing concentrations of Cu=copper, S=sulphur, Fe=iron, Co=cobalt, and Sn=tin in sample 19068 copper sulphides and iron oxides 49

Figure 31: (a) Full scan image for sample 19077 under transmitted light; (b) Phase map showing detected minerals. 50

Figure 32: Phase map showing mineralogy of the selected area in sample 19077 51

Figure 33: (a-d) Elemental maps showing concentrations of Co=copper, S=sulphur, Fe=Iron, and Co=cobalt in sample 19077 copper sulphides 52

Figure 34: (a-b) Transmitted and reflected light full scan images for sample P579; (c) Phase map showing the detected minerals 53

Figure 35: (a-e) Elemental maps showing concentrations of Cu=copper, S=sulphur, Zn=zinc, Fe=iron, and Co=cobalt in sample P579 sulphides and iron oxides 54

Figure 36: (a) Transmitted light full scan image for sample P774; (b) Phase map showing detected minerals 55

Figure 37: (a) Full scan image under reflected light for sample P774; (b) Selected area (white circle in a) for high-resolution TIMA imaging 56

Figure 38: (a-f) Elemental maps showing concentrations of Cu=copper, S=sulphur, Zn=zinc, Fe=iron, Sn=tin, and Co=cobalt in sample P744 sulphides and iron oxides 57

Figure 39: (a) Full scan image under transmitted light; (b) TIMA phase map showing detected minerals in sample P817. 58

Figure 40: (a) Full scan image under reflected light for sample P817; (b) TIMA phase map showing the selected area for high-resolution imaging (area circled red in a) 59

Figure 41: (a-e) Elemental maps showing concentrations of Cu=copper, S=sulphur, Fe=iron, Zn=zinc, and Co=cobalt in sample P817 iron sulphides and oxides 60

Figure 42: (a-b) Full scan images under transmitted and reflected light for sample P782; (b) TIMA phase map showing detected minerals 61

Figure 43: (a-e) Elemental maps showing concentrations of Cu=copper, S=sulphur, Fe=iron, Zn=zinc, and Co=cobalt in sample P782 iron and copper sulphides 62

Figure 44: (a-b) Full scan images under transmitted and reflected light for sample P613; (c) TIMA phase map showing detected minerals 63

Figure 45: (a-d) Elemental maps showing concentrations of Cu=copper, S=sulphur, Fe= iron, and Co=cobalt in sample P613 copper sulphides 64

Figure 46: Sketch showing characteristics of Messina Cu deposit breccia pipe(s). Black fillings between fragments are alteration minerals, quartz, and sulphides 77

Figure 47: Idealised sketch of the concentric zonation of alteration and associated sulphides and iron oxides of the Messina Cu deposit. The overlapping sequences of mineral crystallisation due to alteration and metasomatism is shown by irregular shapes of alteration zones. The red zone is evident in samples P817, P812, P782, P814, P579, dark green zone in samples 19075, 19077, 19068, P679, P613, and lime-green zone in samples 19078, 19073, P744, and P580 77

Figure 48: Zonation of hydrothermal halos in (A) Greisen deposits (from Elliot *et al*., 1995) and (B) Porphyry copper systems (Lowell and Guilbert, 1970). Kao=Kaolinite, Alun=Alunite, Anh=Anhydrite, Car=Carbonates..... 80

Figure 49: A sketch of the Olympic Dam IOCG breccia complex intrusion into early granitoid rocks showing mineralisation and the associated alteration within the breccia (after Reid, 2019 and Skirrow, 2022) 82

List of Tables

Table 1: List of the samples used in this project 12

Table 2: List of the primary and secondary minerals observed in the samples 65

Table 3: List of iron oxide and sulphide minerals observed in the samples 66

Table 4: List of silicate minerals detected using SEM-EDS 66

The abbreviations

List of IMA-CNMNC approved mineral names and abbreviations (Whitney and Evans, 2010; Warr, 2021).

Amp = Amphibole
Bt = Biotite
Bn = Bornite
Cc = Chalcocite
Ccp = Chalcopyrite
Cpx = Clinopyroxene
Chl = Chlorite
Ep = Epidote
Grt = Garnet
Hem = Hematite
Kfs = K-Feldspar
Mag = Magnetite
Mol = Molybdenite
Opx = Orthopyroxene
Pl = Plagioclase
Py = Pyrite
Pyh = Pyrrhotite
Qz = Quartz
Ser = Sericite
Zo = Zoisite
PPL = Plane Polarised Light
XPL = Crossed Polarised Light
RF = Reflected Light
IOCG = Iron-Oxide Copper Gold
SEM-EDS = Scanning Electron Microscope-Energy Dispersive Spectrometer
TIMA = Tescan Integrated Mineral Analyser

1 Introduction

Various copper-sulphide deposits around the world are classified based on the processes that formed them (Taylor, 2009). They usually form by either magmatic, strata-bound, or hydrothermal ore-forming processes. They are hosted within a variety of rocks and are mostly localised by fluids along structural conduits (Lindgren, 1933; Guilbert and Park, 1986; Cox *et al*., 2007). The Messina copper deposit is found in the far north of the Limpopo province at 22.3°S 30°E, near the town of Musina (Fig. 1). The copper mineralisation has been the subject of Cu mining in the area, with several operations extending for 15 km from the north-eastern to south-western direction along the so-called Messina Fault (Chaumba *et al*., 2016; Mundalamo, 2019). The Musina area, formerly known as Messina, also hosts a wealth of coal, diamond, graphite, asbestos, magnetite, and iron ore (Cairncross, 1991; Mundalamo 2019). Currently, the Venetia diamond mine is the active mining operation in the Musina area (Mundalamo, 2019).

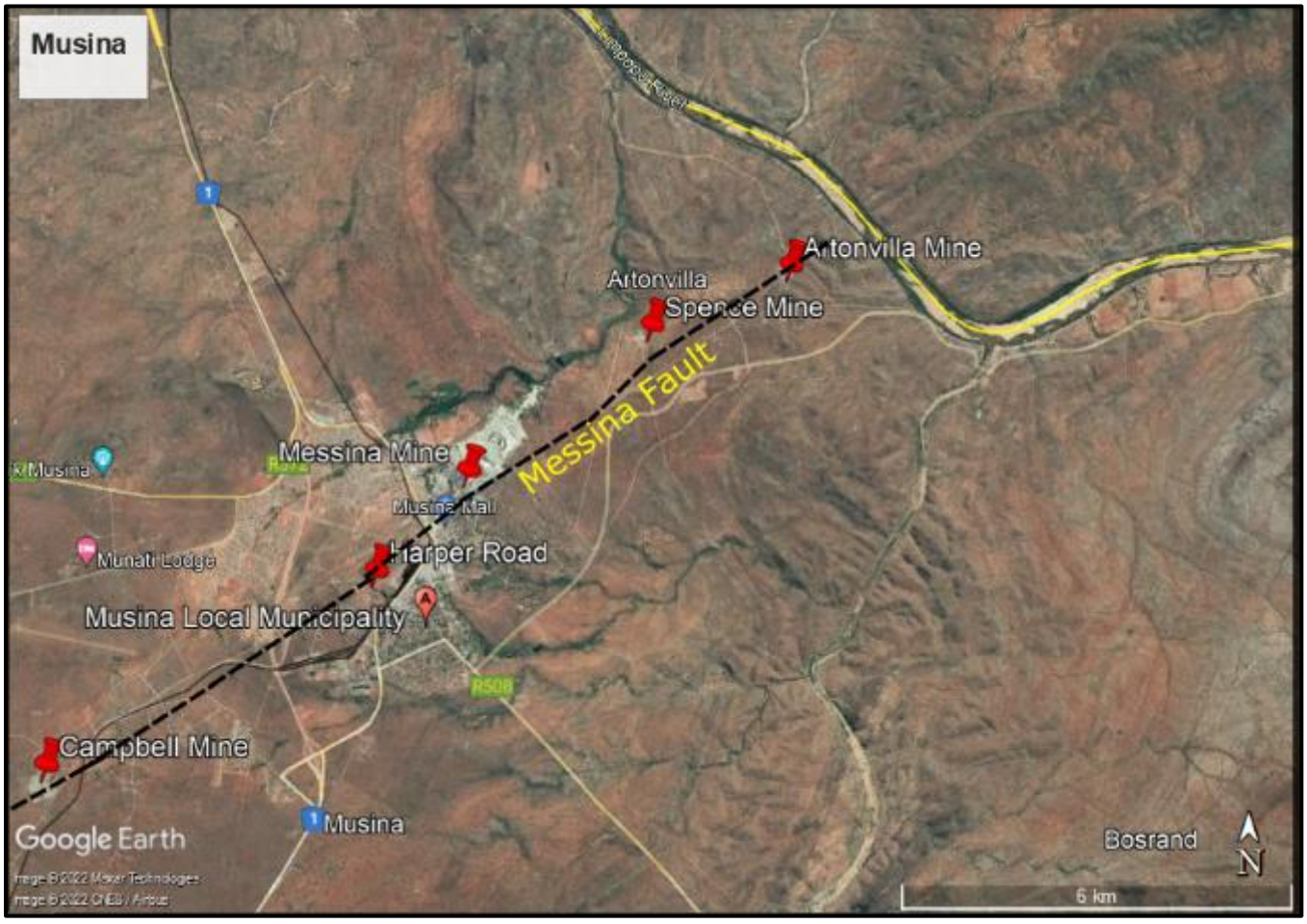


Figure 1: Google Earth image showing the location of Musina town and different mines within Messina mining district. The stippled line shows Messina Fault.

The Messina Cu deposit is an unusual breccia-hosted hydrothermal deposit that appears to be unique in its kind in South Africa (e.g., Jacobsen and McCarthy, 1976). It is characterised by an important group of breccia pipes, disseminated replacement, and vein mineralisation, which occur within granulite-facies metamorphic rocks (Fig. 2; Jacobsen and McCarthy, 1976; Sawkins, 1977). Most of the research about the deposit was performed in the seventies. Therefore, many aspects of the ore-forming processes are poorly studied and yet to be constrained. Furthermore, the deposit has been exploited mostly for

copper. However, other base, precious, and critical metals associated with the copper sulphides are not well documented.

Chalcopyrite and bornite form the primary ore minerals with lesser amounts of chalcocite and minor native copper, whereas the associated gangue minerals are dominantly represented by sericite, chlorite, epidote, quartz, magnetite, and hematite (Jacobsen, 1967; Jacobsen and McCarthy, 1976; Jacobsen *et al*., 1976; Bahnemann, 1986). The Cu mineralisation is associated with pervasive alteration and metasomatism of the metamorphic country rocks. The ore is zoned and the zonation of sulphides together with variations of the alteration mineral assemblages observed specifically in breccia pipes, has been interpreted to reflect the continuous evolution of the ore hydrothermal mineralising fluid(s). This evolved hydrothermal fluid led to redistribution of mineral constituents and selective reactions during cooling (Jacobsen and McCarthy, 1976; McCarthy and Jacobsen, 1976). The zonation of the sulphides and associated alteration was reported to have been controlled by the deformed structures, which created an impervious barrier that trapped the hydrothermal solution, causing inversed zonation (Jacobsen, 1967; Jacobsen and McCarthy, 1976; Jacobsen *et al*., 1976; Bahnemann, 1986). Although there is a general agreement that the deposit is hydrothermal, the source of the hydrothermal mineralising fluids has not yet been constrained.

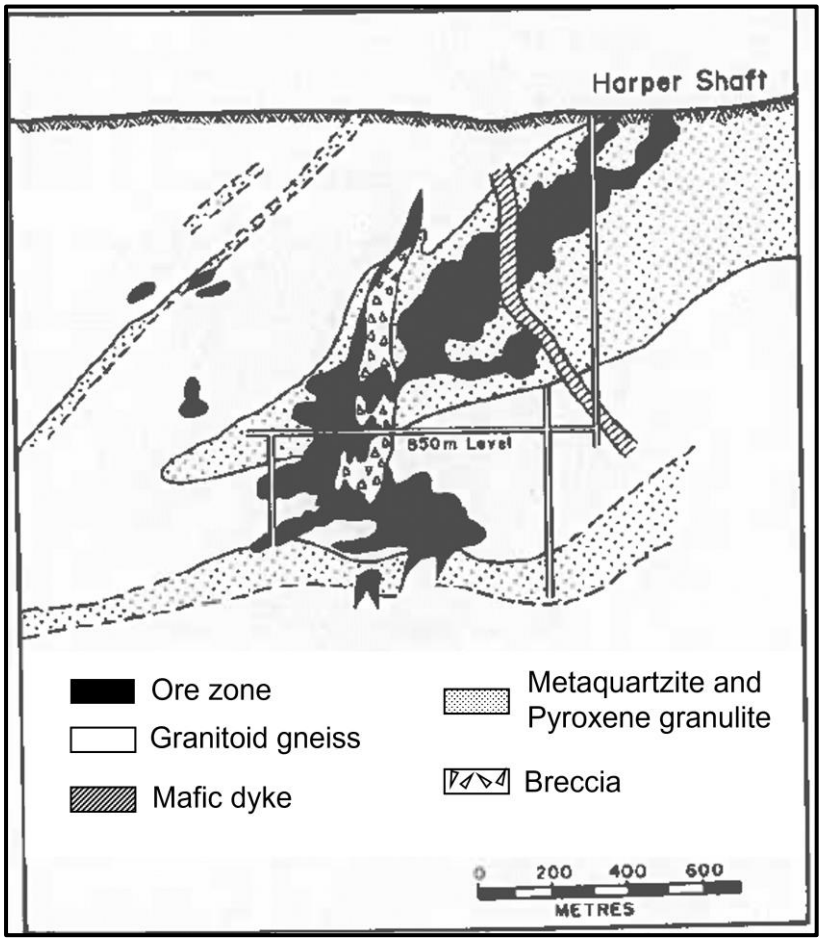


Figure 2: A cross-section showing mineralisation styles within the metamorphic country rocks of Musina area in Harper mine (Bahnemann, 1986).

This unfamiliar and poorly characterised hydrothermal fluid system stimulated interest for this project. The better characterisation and understanding of the overlapping/overprinting, cross-cutting, compositional, and textural relationship between the silicates, sulphides, and iron oxides is expected to

aid in developing a genetic model(s) for the Messina Cu mineralisation. Additionally, the association of hydrothermal alteration zones and sulphide mineralisation will help in understanding the behaviour of the hydrothermal fluids and processes that resulted in the ore formation. The results of this study will present an opportunity for testing the presence of other critical metals, such as Co, Zn, Au, U, or REE for the first time, as potential by-products of Cu mineralisation. These potential critical raw metals are becoming the building blocks for a cleaner and digitized green economy. Thus, their presence in Messina deposit may trigger a new wave of exploration in the area.

2 Geological background

The location of the five mines (namely Campbell, Harper, Messina, Spence, and Artonvilla mine) of the Messina Cu district are interestingly aligned along the east-northeast trending Messina Fault within the Central Zone of the Limpopo Mobile Belt (Figs. 3a and 3b). Some authors believe that the fault controlled the concentration of mineralisation of the Messina Cu deposit (Söhnge, 1946; Jacobsen and McCarthy, 1976; Jacobsen *et al*., 1976; Bahnemann, 1986). However, the Messina Fault intersects the contact between granitic basement rocks and metaquartzite/pyroxenite, and cuts across all the fabrics and structures associated with the Limpopo Mobile Belt event. Thus, it is believed that the fault postdates the metamorphosed sequences of Messina (Bahnemann, 1986).

The basement rocks of the Central Zone consist of a sequence of granodiorite and leucogneisses, overlain by metasediments and metamorphosed igneous rocks composed of metaquartzite, calc-silicates, ferruginous quartzite, pyroxene granulite, cordierite-biotite-garnet-gneiss, and amphibolite (Söhnge, 1945; Bahnemann, 1986; Jaeckel *et al*., 1997; Hofmann *et al*., 1998). These rocks were metamorphosed to granulite-facies during the Limpopo Orogeny (Barton *et al*., 1994; Jaeckel *et al*., 1997; Hofmann *et al*., 1998). The oldest recognised rocks in Musina area include the basement rocks of Sand River Gneiss of >3.3 Ga and the supracrustal rocks of the Beit Bridge Complex dated between 3.25 and 3.35 Ga (Barton *et al*., 1994; Hofmann *et al*., 1998). The Central Zone is reported to have experienced different metamorphic events with a high-grade metamorphic event reported to have occurred at ~2.0 Ga (Barton *et al*., 1994; Jaeckel *et al*., 1997). These metamorphic sequences are overlain unconformably by the post-Karoo sequences (Cox *et al*., 1965).

It was reported that metamorphism was synchronous with folding during the Limpopo Orogeny (Söhnge, 1945; Jacobsen, 1967; Bahnemann, 1986). Three separate deformational events affected the Musina area (Söhnge, 1945; Jacobsen, 1967). The first deformation formed large anticlinal fold northwest of Campbell and Artonvilla and a syncline at other places (Sohnge, 1945; Cox *et al*., 1965; Jacobsen, 1967). These folds were bent and refolded by the second deformational event, causing isoclinal folding (Söhnge, 1945; Cox *et al*., 1965; Jacobsen, 1967; Bahnemann, 1986). The last deformation superimposed on fold limbs of the second fold and developed parallel to the Limpopo Mobile Belt structural trend (Söhnge, 1945; Jacobsen, 1967). The buckling and warping of this fold caused bending of previous folds into a wide arc at their apex like in Artonvilla mine (Fig. 3b; Jacobsen, 1967; Bahnemann, 1986). During folding, old planar and linear structures were deformed into new compositional bands and lineations parallel to the linear fabrics of deformed country rocks. It was postulated that the deformed structures allowed differential movement of hydrothermal mineralising fluids along individual lithological contacts (Jacobsen, 1967; Bahnemann, 1986). Nonetheless, the undeformed nature of the ore bodies implies that they post-date earlier penetrative deformation (Ryan *et al*., 1983).

Söhnge (1945) reported that high-grade regional metamorphism in Messina occurred long before low-grade shear metamorphism. Thus, mineralisation occurred after granulite metamorphism, implying that hydrothermal metasomatism and mineralising fluids are not related to regional metamorphism. However, no reliable age of mineralisation exists (Söhnge, 1945; Jacobsen *et al*., 1976). Nonetheless, Ryan *et al* (1983) characterised mineralising solution of Messina Cu deposit using $^{87}Sr/^{86}Sr$ ratios, K/Rb ratios, and lead isotopic data from albite, quartz, and sulphides of Campbell, Artonvilla and Messina mines respectively. They postulated that the mineralising fluid was emplaced between 1 800 and 1 000 Ma and possibly remobilised during the Karoo age between 300 and 145 Ma. They also compared sulphide lead isotopic data from Messina mine with that of Nuanetsi igneous rocks, and revealed that the lead might be of crustal origin and not related with the Nuanetsi igneous activity (Ryan *et al*., 1983). Jacobsen and McCarthy (1976), Jacobsen *et al* (1976) and McCarthy and Jacobsen (1976) argued that the mineralising solution is related to the intrusive cycle of Nuanetsi Igneous Complex (NIC) and was emplaced during post-Karoo times based on pre- and post-mineralisation dolerite and diabase dykes. On the other hand, other authors are of the view that mineralisation may have been reactivated or remobilised by later faulting events after emplacement during post-Karoo age (Söhnge, 1946; Jacobsen, 1967; Bahnemann, 1986).

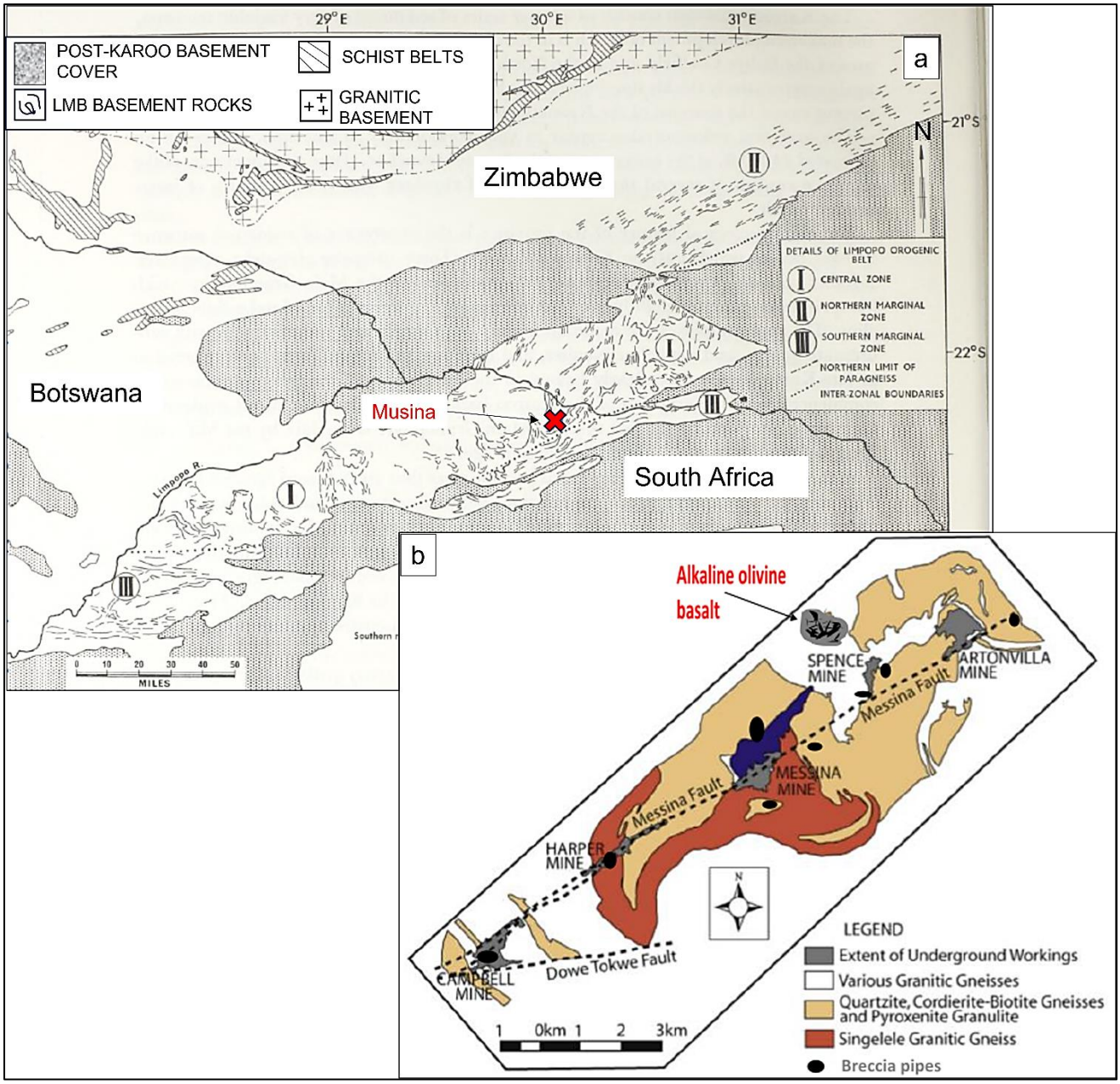


Figure 3: Simplified geology of the location of (a) Musina area within the Central Zone of the Limpopo Mobile Belt and (b) the distribution of mines along the Messina Fault in Messina mining district. Breccia pipes are represented by the small, black circular-like shapes (after Cox *et al*., 1965; Mundalamo, 2019). LMB = Limpopo Mobile Belt.

The sulphides are dominantly hosted within cordierite-biotite-garnet gneiss, pyroxene granulites, and amphibolites (Jacobsen and McCarthy, 1976; Sawkins, 1977). These host rocks were affected by intermediate to intense hydrothermal alteration (as described below in section 3.1.2) and show mineralisation within immediate zones of alteration (McCarthy and Jacobsen, 1976). Gangue mineral assemblages of different alteration zones vary depending on the composition of the original country rocks (e.g., whether it was mafic or felsic, Jacobsen, 1967). The mineralisation appears to be concentrated within strongly deformed fold limbs, fault zones, and fractures along lithological contacts of contrasting rock competency (Jacobsen, 1967; Jacobsen and McCarthy, 1976; Bahnemann, 1986), although most of the ore bodies intercepted in the underground workings do not actually reach the surface (Fig. 4). It was assumed that mineralisation occurred in a closed system where the mineralising fluids were trapped within deformed structures (Jacobsen and McCarthy, 1976; Jacobsen *et al*., 1976;

McCarthy and Jacobsen, 1976). Such a closed system is postulated to have resulted in mineralising fluids not reaching upper levels except where conduits were partly opened (Jacobsen *et al*., 1976; Bahnemann, 1986). Thus, to better characterise the Messina Cu deposit, extensive underground mapping was carried out, because where the ore bodies were partly exposed, the mineralisation was either poorly developed, leached or absent (Söhnge, 1945; Jacobsen, 1967; Jacobsen *et al*., 1976; Bahnemann, 1986).

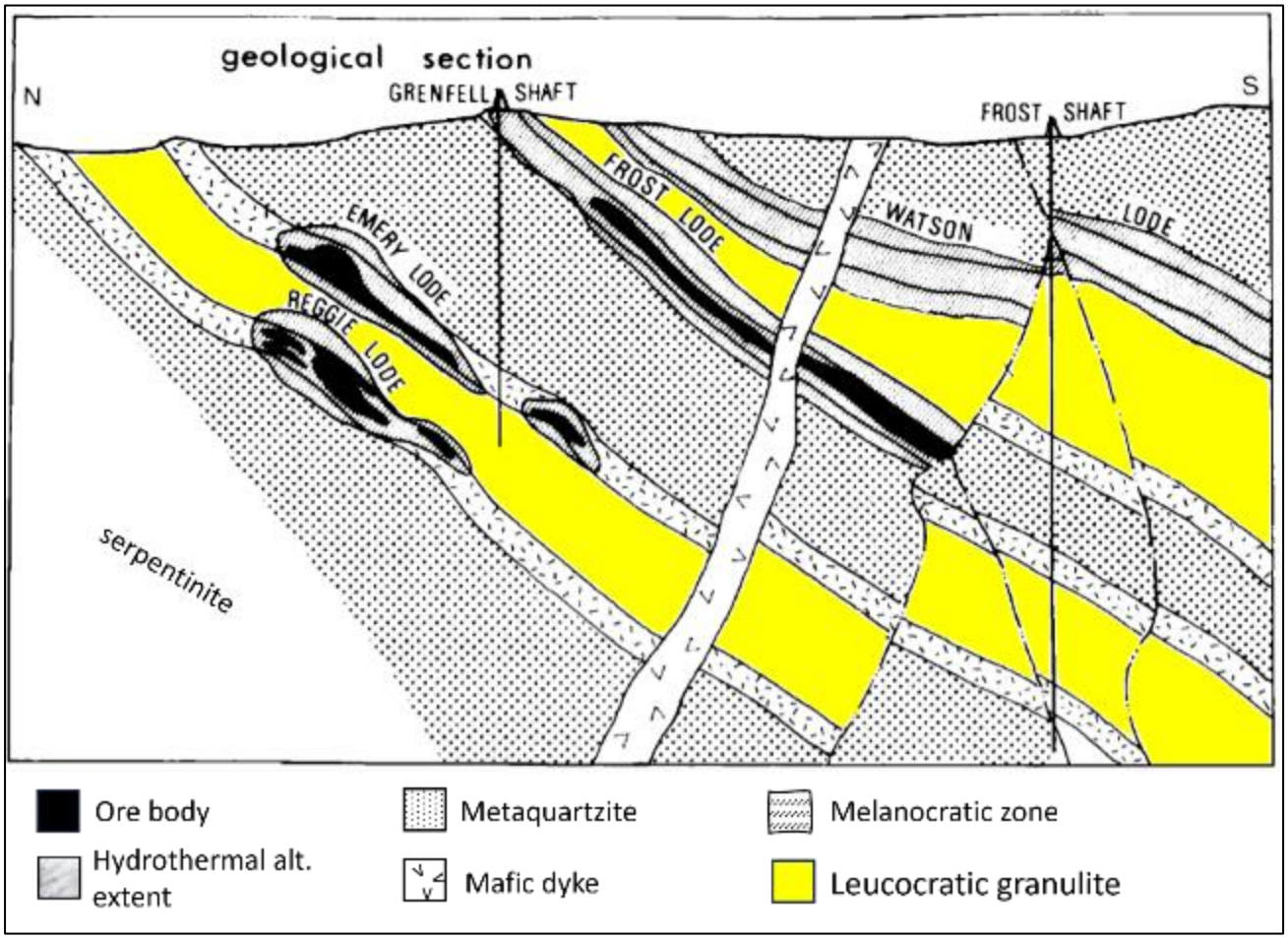


Figure 4: Geological cross-section of Artonvilla mine shafts showing the occurrence of mineralisation within mafic and felsic granulites at Frost Lode, Emery Lode, and Reggie Lode (after Jacobsen and McCarthy, 1976).

3 Previous studies of Messina Cu deposit

3.1 Source of hydrothermal fluids and alteration

There is a contention about the styles of mineralisation of the sulphides in Messina because the ore-forming processes responsible for the ore are poorly understood. The consensus is that: 1. The mineralisation is structurally controlled, as the mining operations occur along the Messina Fault within deformed and faulted rocks; 2. Copper mineralisation is associated with light to pervasive hydrothermal alteration of the country rocks (Jacobsen and McCarthy, 1976; Jacobsen *et al*., 1976; Bahnemann, 1986). It has been postulated that all the mined ore bodies, together with the alteration, formed by similar fluids and belong to the same ore-forming system (Jacobsen *et al*., 1976). Thus, their comparable alteration and mineralogy suggest that the hydrothermal fluids moved over a large distance (Bahnemann, 1986). However, the origin and nature (such as composition and age) of the fluid that caused mineralisation and the associated hydrothermal alteration are debated. Jacobsen and McCarthy

(1976) and Jacobsen *et al* (1976) supported a magmatic origin of the hydrothermal mineralising fluid, which evolved and changed in composition during its ascent to shallower crustal levels. Since there is no apparent coeval and cogenetic magmatic event in the region, Jacobsen and McCarthy (1976) and Jacobsen *et al* (1976) suggested a genetic relationship between the copper mineralisation and the intrusive event of post-Karoo Nuanetsi Igneous Province, exposed in southern Zimbabwe. On the other hand, Sawkins (1977) and Sawkins and Rye (1979) argued for a meteoric source of the mineralising hydrothermal fluids.

Smirnov (1976) reported that ore bodies that originates from magmatic-hydrothermal fluids tend to be disseminated and hosted within hydrothermally altered rocks, where alteration becomes progressively less pervasive towards the edges of the alteration aureole. The formation of hydrothermal sulphide deposits requires vapour-magmatic fluids and are typically associated with alteration zonation in the surrounding country rocks (Smirnov, 1976). Magmatic-hydrothermal fluids tend to follow a cooling trend from hot temperatures of approximately 700^{o}C to 600^{o}C above a magmatic body to lower temperatures below 200^{o}C away from the intrusion (Hemley *et al*., 1992; Seedorf *et al*., 2005). Therefore, magmatic-hydrothermal ore deposits typically show the temperature gradients decreasing from the hot central parts towards colder unaltered outer country rock (Lindgren, 1933; Pirajno, 1992). This typical magmatic-hydrothermal system manifests itself in the field with high-temperature alteration assemblages and ore minerals in the hotter inner parts and progressive colder mineral paragenesis towards the outer edges of the system. However, this typical couple alteration-mineralisation sequence is not observed in Messina deposit. The Messina deposit zonation of alteration and mineralisation appear as reverse and concentric, whereby high-temperature minerals are found at the outer portions, whereas low-temperature minerals are at the core of the ore body (Jacobsen, 1967; Jacobsen *et al*., 1976). This reversed and concentric zonation of Messina Cu deposit was reported to have been caused by neck zones formed by deformed structures, which prevented hydrothermal fluids from migrating further upwards (Jacobsen, 1967; Bahnemann, 1986). As a result, the hydrothermal fluids became trapped and crystallised progressively from the margins inward, causing alteration, replacement, and precipitation of sulphides (Jacobsen, 1967; Jacobsen and McCarthy, 1976; Jacobsen *et al*., 1976; Bahnemann, 1986).

Jacobsen (1967) interpreted this reverse concentric zonation as a retrograde hydrothermal style of mineralisation, characterised by decreasing temperature and increasing CO_2, H_2O, and Cu-sulphides (bornite, chalcocite, native Cu) towards the centre, implying that relatively colder inner parts of the system also represent the last phase of crystallisation of the fluids. Jacobsen and McCarthy (1976) analogue the slow retrogressive cooling of Messina hydrothermal system to fluid temperature gradients typical to pegmatites. They suggested that Messina Cu deposit formed by injection of concentrated magmatic fluids, which reacted completely with the host rock within structural geological traps. This pegmatitic hydrothermal model has been contrasted by Bahnemann (1986), who pointed out that some mines showed poor development of such zonation (e.g., Campbell and Messina mines).

3.1.1 Sulphide paragenesis

The Messina sulphide mineralisation style occurs as mineralised breccias, veins/lodes, and disseminated replacement ore. These ore types vary from one mine to another (e.g., Fig.5 – "L" Lode breccia pipe mineralisation). McCarthy and Jacobsen (1976) reported that ore zones grade from pyrite with magnetite in the outermost zone of the ore body through chalcopyrite – bornite, bornite – chalcocite with specularite in the inner zone, and then chalcocite – native Cu with goethite in the central zone. Other reported sulphides in the inner zone and towards the outermost zone include pyrrhotite, galena,

sphalerite (Jacobsen, 1967; Jacobsen and McCarthy, 1976) with traces of molybdenite, cobaltite, tetrahedrite, and tennantite (Mundalamo, 2019). Cuprite, azurite, and malachite represents secondary copper minerals due to surficial alteration of the main copper minerals (Mundalamo, 2019).

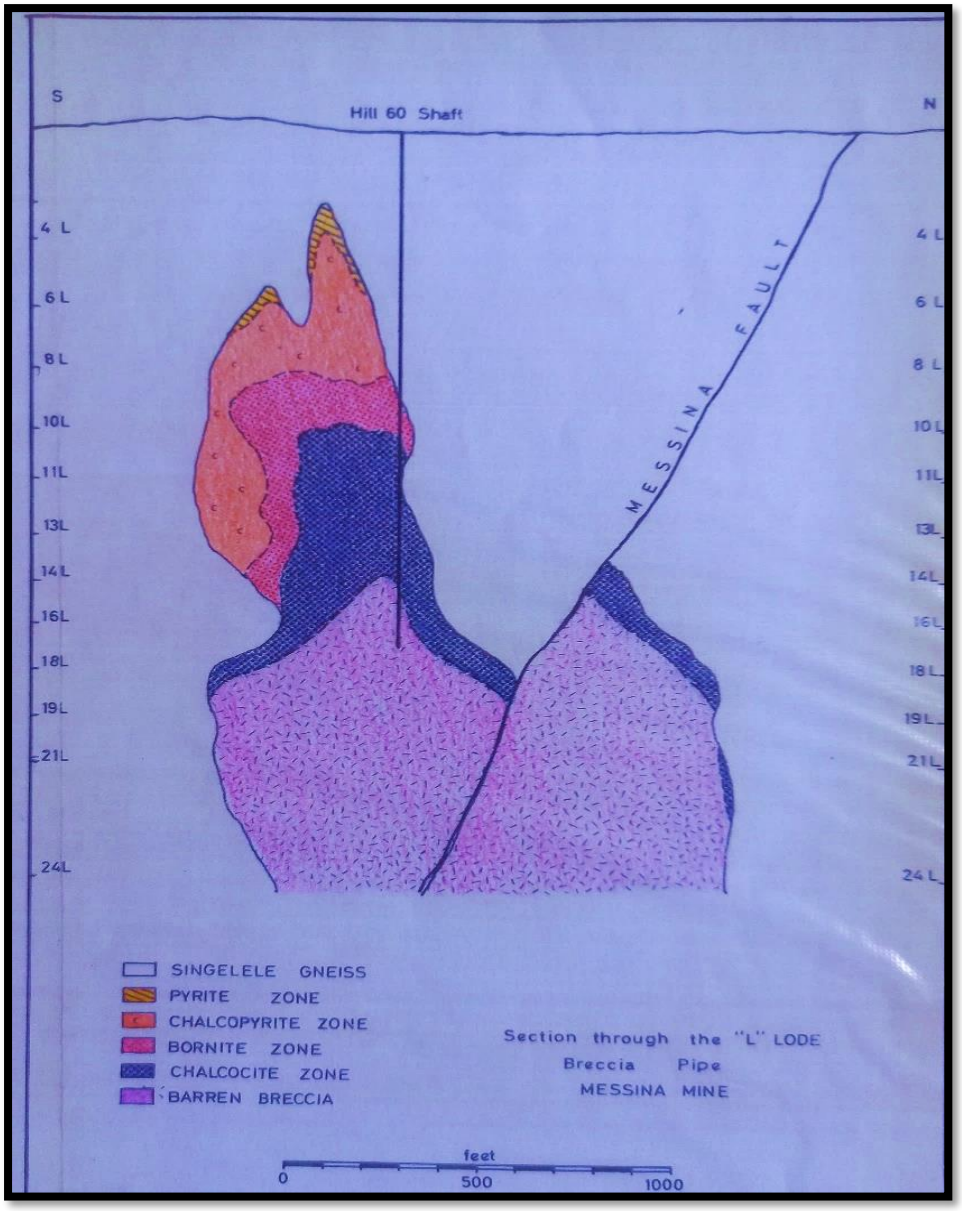


Figure 5: Sketch showing sulphide zonation in the L Lode breccia pipe of Messina mine (from Jacobsen, 1967).

Mineralisation-alteration zonation

In the breccia pipes, sulphide mineralisation shows distinct concentric zonation, which is consistent with the reversed concentric variation in enveloping alteration minerals (Figs. 6a and 6b; Jacobsen *et al*., 1976; McCarthy and Jacobsen, 1976). The outer alteration zone is mostly characterised by sericitisation and pyrite, and towards the inner zones there is an increase of albite and chlorite associated with chalcopyrite and bornite, and then epidote associated with bornite and chalcocite in the central zones (Jacobsen and McCarthy, 1976; Jacobsen *et al*., 1976; McCarthy and Jacobsen, 1976). Whereas the variation in silicate mineral assemblages indicates an increase in H_2O with increasing alteration intensity, the associated changes in sulphide mineral paragenesis indicate progressive decrease in S

content with increasing alteration (Jacobsen, 1967; Sawkins, 1977; Sawkins and Rye, 1979). Mundalamo (2019) described the paragenesis of the ore and associated gangue minerals based on their mineral assemblages, textural relationships, and mutual grain boundary relationships. Other observations revealed different generations of one mineral with increasing alteration. For example, at least two generations of pyrite (early anhedral and late euhedral pyrite) and three distinct quartz generations were reported (Mundalamo, 2019). Two albite generations (hydrothermal anhedral albite and euhedral one lining vugs) were also reported by Jacobsen and McCarthy (1976).

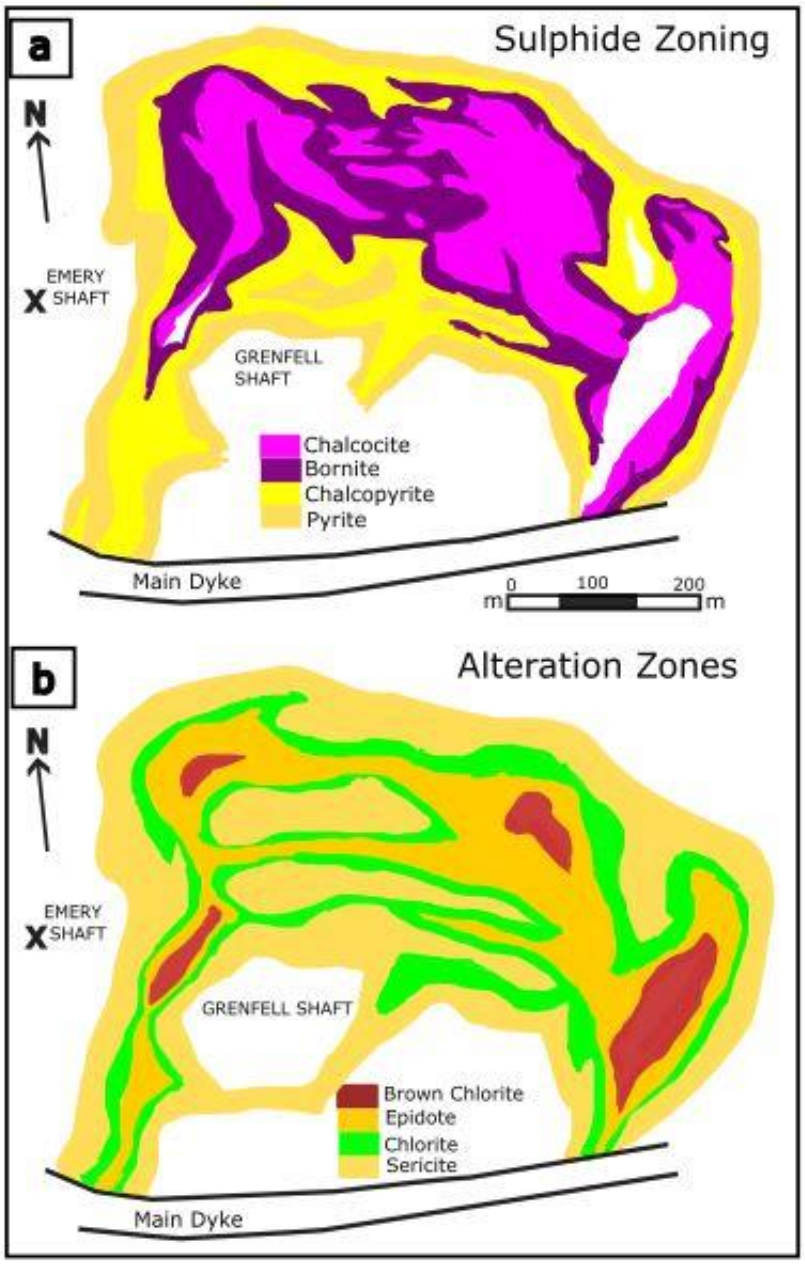


Figure 6: Sketch showing the concentric zonation of (a) the sulphides and (b) associated hydrothermal alteration zones in Emery Lode of Artonvilla mine (after Jacobsen and McCarthy, 1976). The white areas within sulphide zoning represent leached ore.

The Messina deposit is also characterised by iron oxide-rich zones associated with sulphide mineralisation, varying from magnetite to hematite and specularite, and finally goethite towards the central zone of the ore body (Jacobsen and McCarthy, 1976; McCarthy and Jacobsen, 1976). The

relationship between the sulphides and iron oxides is not well-constrained. Jacobsen (1967) suggested that these oxidation zones have no association with sulphide zonation. Mundalamo (2019) interpreted the oxidation zones as a product of metamorphism. On the other hand, McCarthy and Jacobsen (1976) noted that the Fe-oxides show increasing oxidation with increasing intensity of alteration.

Different mineral assemblages were reported by different authors for the three mineralisation types or styles:

i. Breccia pipe ore

Söhnge (1945) and Taylor (2009) define breccia pipes as collapse features associated with inter-fragmental fill by immediate surrounding rocks. Messina breccia pipes commonly occur below the surface and rarely have a surface expression (Jacobsen *et al*., 1976). Their inter-fragmental fill is made of mostly quartz and sulphides in association with albite and chlorite, which increase in abundance towards the centre of the pipe (Jacobsen *et al*., 1976). The margins of the breccia consist of small, rounded grains of quartz, which grade inwards to angular, elongated, coarse-grained, and blocky fragments (Jacobsen *et al*., 1976). These fragments become parallel to equidimensional towards the centre (Jacobsen *et al*., 1976).

The breccia pipes are reported to be associated with contacts of stockwork systems, which represent early regional joint patterns and are enclosed by wall rock hydrothermal alteration (Jacobsen *et al*., 1976). In the pipes, chalcopyrite and bornite dominate the sulphide mineralisation and are associated with quartz, chlorite, epidote, and/or malachite in some places (Mundalamo, 2019).

ii. Vein/fissure ore

Most veined ore in Messina mines is generally found to emerge from the breccia pipes (Söhnge, 1946). The veined ore occurs as quartz veins with mineralisation along stockwork microfractures (Jacobsen *et al*., 1976; Mundalamo, 2019). However, some quartz veins are unmineralised and coated or stained with iron oxides. Fine stockworks occur in contact with unbrecciated altered country rock at upper levels of breccia pipes (Jacobsen *et al*., 1976; McCarthy and Jacobsen, 1976).

iii. Disseminated replacement ore

According to Jacobsen and McCarthy (1976), this ore type is associated with suitable structural traps and exhibits pervasive alteration extending beyond the leucocratic granulite and metaquartzite. It comprises pyrite and chalcopyrite disseminations within quartz veins and the host rocks (Jacobsen and McCarthy, 1976; Mundalamo, 2019). In some places at deeper levels, the ore occurs within vugs or cavities filled with chlorite, quartz, epidote, minor zoisite, and calcite (Jacobsen *et al*., 1976). The vugs are enveloped by specularite or albite (Jacobsen and McCarthy, 1976; Bahnemann, 1986). Replacement is well-developed at the Artonvilla mine and reveal chalcopyrite replacement by bornite, which is in turn replaced by chalcocite then native copper inwards (Jacobsen and McCarthy, 1976; Bahnemann, 1986).

3.1.2 Silicate paragenesis and alteration zones

The zonation of alteration halos around mineralisation is attributed to an increase in hydrous silicate minerals, leaching of silica, and formation of epidote, albite, and zoisite, which resulted in complete alteration and in places to complete destruction (metasomatism) of the original host rock minerals (Jacobsen, 1967; Sawkins, 1977; Cairncross, 1991). Jacobsen and McCarthy (1976) and Jacobsen *et al* (1976) reported sericitisation, albitisation, chloritisation, and epidotisation alteration associated with all

three ore types. Chlorite, prehnite, analcite, and quartz were found to dominate the central alteration zones (Jacobsen *et al*., 1976; McCarthy and Jacobsen, 1976; Mundalamo, 2019). The degree of alteration varies laterally and vertically from minor to pervasive. These lateral and vertical changes in paragenesis is interpreted as evidence of hydrothermal fluids that were rich in Al_2O_3, K_2O, Na_2O, CaO, MgO, and H_2O, and of low pH (Jacobsen *et al*., 1976; McCarthy and Jacobsen, 1976). The hydrothermal fluids circulated within the country rocks, altering the primary rock-forming mineral constituents, and redistributing leached elements into new mineral phases. For example, leached silica from the distal areas of the deposit recrystallised as secondary quartz in vugs within the central parts during final stages of crystallisation (Jacobsen and McCarthy, 1976; Sawkins, 1977; Mundalamo, 2019). Redistributed K and Ca elements also formed new epidote and calcite in the inner alteration zone (Jacobsen, 1967; Jacobsen and McCarthy, 1976; Jacobsen *et al*., 1976; Sawkins, 1977). The occurrence of calcite was interpreted to be synchronous with the final phase of mineralisation (Jacobsen, 1967; McCarthy and Jacobsen, 1976; Sawkins, 1977; Mundalamo, 2019). Jacobsen *et al* (1976) reported late quartz fragments, as well as quartz and albite veins in the innermost zones of the ore body. Retrograde reactions are said to have started after sericitisation, owing to the inward crystallisation of the hydrothermal fluid caused by impervious barrier trapping high temperature solution within the structural traps (Jacobsen, 1967; Jacobsen and McCarthy, 1976; Jacobsen *et al*., 1976).

The close relationship of hydrothermal alteration and the sulphides led Jacobsen (1967) and Jacobsen and McCarthy (1976) to suggest that Cu and S were the primary constituents of the ore-forming fluid, as they do not seem to have been leached from the country rock. During mineralisation, S reacted with the Fe released from mafic minerals of the host rocks to form pyrite (Jacobsen and McCarthy, 1976; McCarthy and Jacobsen, 1976). The Cu carried by the ore-forming fluid sequentially reacted with previously formed sulphides, resulting in concentric zonation of the sulphides (Jacobsen *et al*., 1976).

4 Methodology

A total of 16 samples were studied in this project (Table 2). Five rock samples from the School of Geosciences collection at Wits, and 11 block samples (labelled with letter "P" before a number) from Jacobsen J.B.E. (1967) PhD dissertation collection carried out at the University of the Witwatersrand. The samples are from different lodes in Artonvilla, Messina, and Campbell mines. The samples were selected based on visible mineralogy as some samples were not clear enough to be examined petrographically.

Refer to Appendices (A and B) for more descriptions. For the rock samples, thin sections were prepared and examined petrographically using transmitted and reflected light optical microscopy (Table 2). The block samples of Jacobsen (1967) were thick and rectangular in shape, that when viewed under petrographic microscope, some minerals were difficult to tell what they represent. As a result, new thin sections were prepared for petrographic examination (Table 2). After petrographic examination of all the samples, seven samples with intriguing textural relationships and mineralogical compositions were selected and analysed for secondary minerals using the Tescan Integrated Mineral Analyser (TIMA) in the automated mineralogy lab housed in the School of Geosciences at Wits (Table 2).

Table 1: List of the samples used in this project

Sample ID	**Mineralogy**	**Petrographic observations**	**SEM-EDS (TIMA) analysis**	**Samples chosen for high-resolution mapping**
19077	Quartz-chlorite	✓	✓	✓
19068	Quartz-chlorite	✓	✓	✓
19073	Quartz (Fe-stained)-chlorite	✓		
19078	Quartz-chlorite	✓		
19075	Quartz-chlorite-epidote	✓		
P580	Quartz-epidote	✓		
P579	Plagioclase-orthopyroxene	✓	✓	
P774	Epidote-quartz-chlorite	✓	✓	✓
P814	Plagioclase-quartz-chlorite	✓		
P812	Quartz-sericite	✓		
P782	Quartz-sericite-chlorite	✓	✓	
P817	Quartz-sericite-chlorite	✓	✓	✓
P677	Quartz-sericite-chlorite	✓		
P679	Quartz-biotite-chlorite	✓		
P613	Plagioclase-quartz-epidote	✓	✓	
P740	Epidote-quartz	✓		

The Olympus BX 41 polarising microscope was used for petrographic observations of the polished thin sections, to characterise mineralogy and textures of the samples. Olympus BX 53/41D microscope in the School of Geosciences WIMLab (Wits Imaging and Microscopy Lab) was used to produce full-scan microscopic photomicrographs of the 16 samples.

Automated Scanning Electron Microscope (SEM) coupled with energy dispersive X-ray spectrometer (EDS) was used to analyse secondary minerals and other critical and base metals within the sulphide and Fe-oxide minerals. SEM-EDS examination was performed using TIMA with version 2.4.1 TIMA

software in the automated mineralogy lab. The method uses back-scattered electron spectrometer (BSE) and energy dispersive X-Ray spectrometer signals to measure elemental concentrations and create mineralogy images. The samples were initially coated with carbon to manipulate electron build-up during subsequent analysis. After coating, samples were selected for liberation analysis to characterise individual copper and oxide minerals, and their associated secondary minerals. For acquisition, measurements used for packing ratio and imaging speed are 100 % and 4 µs respectively. Dot mapping X-ray resolution was used to perform a full-section scan for textural data (composition, mineral association, content, spatial relationship) with pixel spacing of 7 µm and a field width of 500 µm. For chosen areas of the thin sections, high-resolution mapping with pixel spacing of 3 µm and field width of 250 µm was used. This high-resolution mapping was performed on samples containing mostly chalcopyrite, bornite, and chalcocite, and for some samples with pyrite. A classification scheme set up in the TIMA software was then used to determine mineralogy of the analysed samples. From TIMA elemental maps, phase maps of primary minerals were obtained, including silicate minerals previously not identified using optical microscopy. The mineralogy of the silicate minerals was used to compare TIMA results with petrographic results. The TIMA raw data was also used to create elemental maps, showing relative variations in individual element concentrations across the analysed areas of the thin sections. The distribution or concentration of the elements associated with the minerals present are represented by the various colours as per the colour code at the bottom of all samples. It must be noted that due to detection limits, metals like gold (Au), platinum-group metals (PGMs), and uranium (U) could not be detected. On the other hand, rare earth elements (REE), lead (Pb), and molybdenum (Mo) reported no concentrations in association with the sulphides and/or iron oxides and were therefore left out. Thus, the metals analysed include cobalt (Co), zinc (Zn), and tin (Sn).

5 Results

The results of this study are reported in two parts. The first part presents petrographic descriptions of the mineralogy of alteration, gangue, and ore minerals, including textures and the type of ore based on the evaluation of the hand specimens (where possible) and optical microscopy (petrography). The abbreviations PPL, XPL, and REF refers to Plane Polarising Light, Crossed Polarising Light, and Reflected Light, respectively. For more descriptions, refer to Appendix A. The second part of the results show the mineral and elemental maps obtained by TIMA on selected samples, displaying the distribution of elements within sulphide and Fe oxide minerals.

5.1 Petrographic descriptions

Sample 19068

The sample consists of discrete sub-rounded and subhedral quartz grains (0.5-1 mm) within massive bornite, representative of a mineralised vein (Fig. 7). Within the massive bornite, light-green fine-grained veins and grains of chlorite can be observed. Other discontinuous thin multiple chlorite veinlets preferentially crosscut massive bornite (Fig. 7a). Iron staining occurs mostly associated with fine-grained chlorite and sometimes as tiny, isolated orange-red spots on quartz and bornite (Fig. 7a red arrow). There are needle-like lead-grey elongated flakes of specularite forming connected grains between massive bornite and fine-grained chlorite (Fig. 7b white arrow).

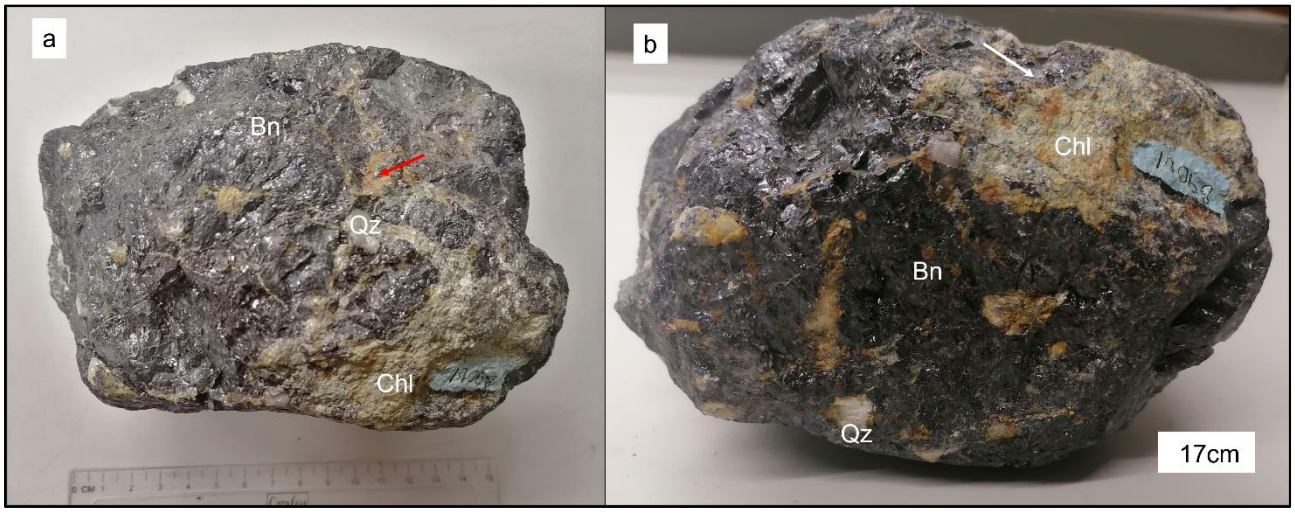


Figure 7: Sample 19068 showing massive bornite (Bn) enclosing discrete subhedral quartz (Qz) fragments and fine-grained irregular chlorite (Chl) veins. Fine-grained multiple chlorite veinlets cut through the massive bornite, whereas another fine-grained chlorite groundmass occurs around it. The chlorite has orange-red iron oxide stains (red arrow in a). White arrow in (b) indicates needle-like specularite between the massive bornite and fine-grained chlorite.

The opaque minerals (sulphides and oxides) occur as interstitial between relatively large subhedral quartz (Qz1) grains (Fig. 8a). Fine-grained chlorite groundmass is not homogeneous in colour: in some parts, the chlorite is green (Figs. 8a, 8b, 8d, and 8f), whereas in other parts it is yellowish-brown (Figs. 8c and 8e). Where the yellowish-brown chlorite is prevalent, thin blades of opaque minerals are visible (Fig. 8e). Chloritic veins and veinlets are visible between and within the opaque minerals (Figs. 8b, 8c, and 8f). Granular chlorite appears to be cementing the opaque minerals (Figs. 8a, 8c, and 8e). Some isolated small grains of chlorite and subrounded-subhedral brecciated quartz are disseminated within the opaque minerals (Figs. 8d and 8e). In Fig 8e, a thin rim of quartz (Qz2) occurs along the contact between massive opaque minerals and chloritic groundmass. Chlorite veins do not cut through quartz 1 grains.

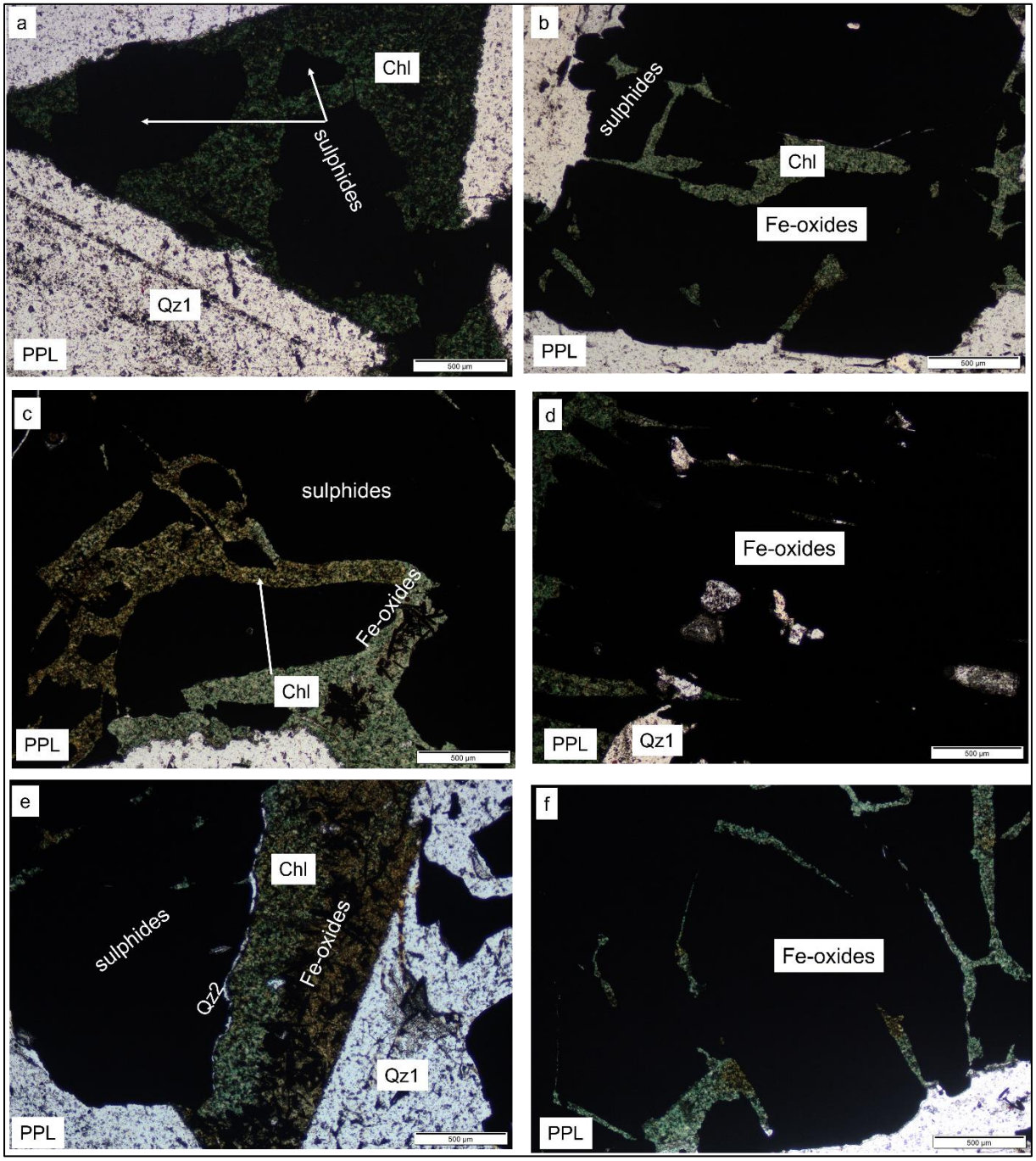


Figure 8: Plane polarised light photomicrographs for sample 19068, showing silicate minerals and their associated opaque minerals. Magnification scale = 500 µm.

The dominant opaque mineral is bornite (Fig. 9), confirming the observations from hand specimens. In places, chalcocite is replacing brecciated bornite as a rim around it (Figs. 9a and 9d). Disseminated bornite grains occur within chlorite groundmass with a single hematite plate (Figs. 9a and 9d). Massive bornite is cut by chlorite veinlets and partially replaced by chalcocite along the boundaries of chlorite veinlets and minor cracks within bornite (Fig. 9b). Relatively big (2 cm), euhedral-subhedral and elongated magnetite laths are cemented by fine-gained chlorite veins, and overprinted by small, brecciated quartz gangue (Figs. 9d and 9f). In hand sample, the laths show specularite characteristics. The chlorite cement also contains inclusions of bornite (Fig. 9f). Hematite plates occur within chlorite veins and show preferential orientation (Figs. 9c and 9e).

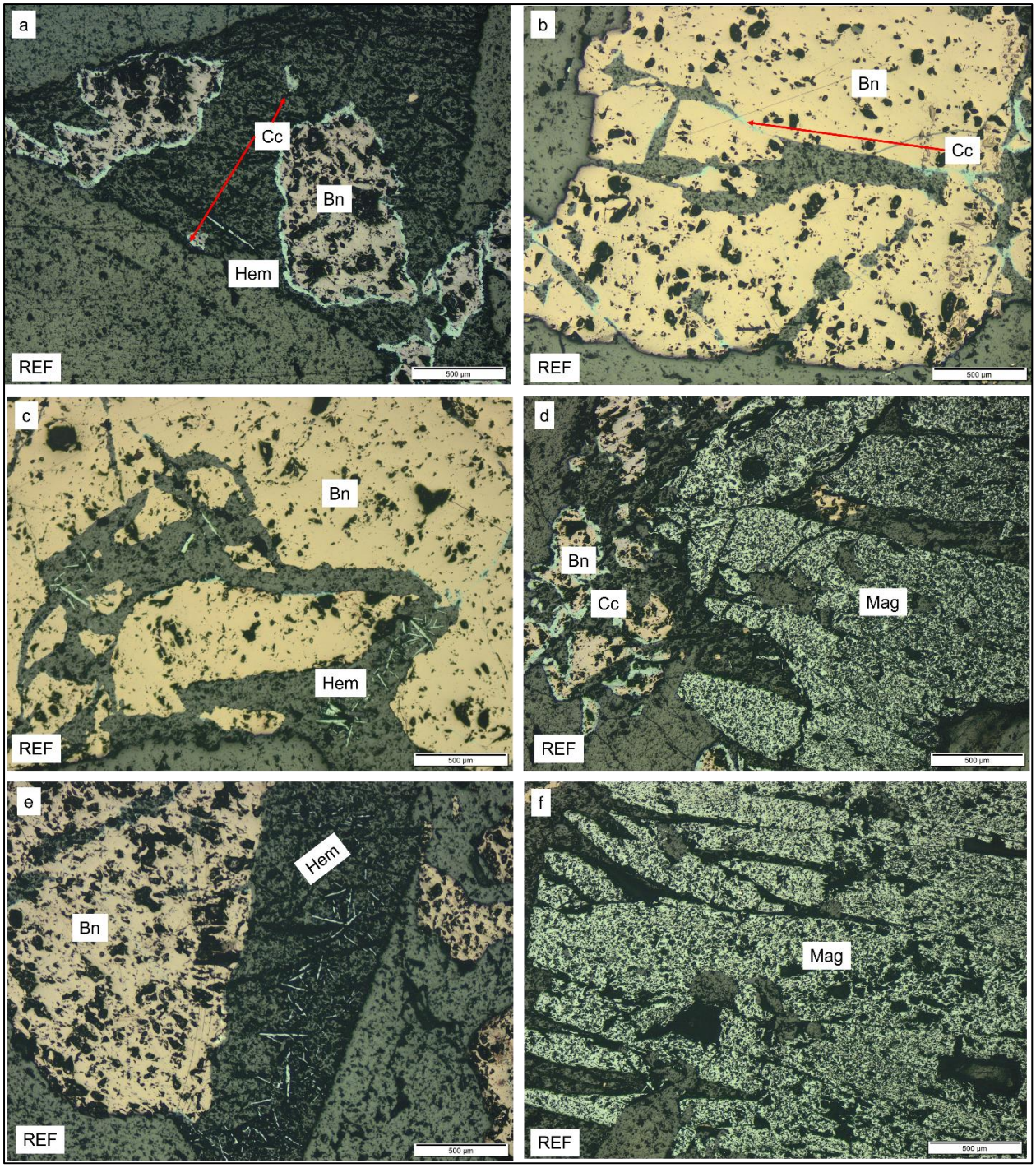


Figure 9: Reflected light photomicrographs showing copper sulphides, mainly bornite (Bn) and chalcocite (Cc), associated with hematite (Hem) and magnetite (Mag). The different colours of bornite are due to different exposures. Some were dark under low exposure and some bright under slightly higher exposure. It is not identified as chalcopyrite because of the absence of chalcopyrite in the hand sample. Magnification scale = 500 µm.

Sample 19077

The sample dominantly consists of massive milky quartz with minor bornite and could represent a piece of a thick quartz breccia vein (Fig. 10). Euhedral and subhedral quartz crystals appear as interconnected, elongated (1-1.5 mm) and sub-horizontal (red arrows, Fig. 10a). The crystals vary in size (0.2 to 1.5 mm) and are coated by red iron oxide stains. Some quartz crystals have angular edges and appear to be brecciated and fractured with fine-grained chlorite grains between them (Fig. 10b). Disseminated bornite occurs between the quartz crystals (Fig. 10b).

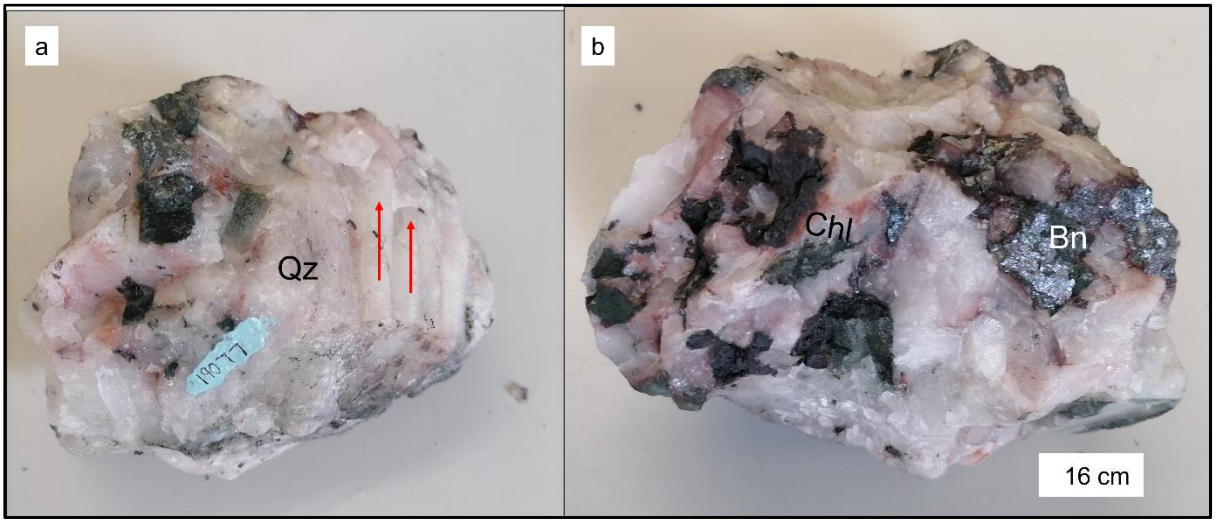


Figure 10: Sample 19077 showing massive interconnected and brecciated quartz crystals (Qz) which contain minor chlorite (Chl) and bornite (Bn). Red arrows in (a) show the elongation of individual quartz crystals, typical of comb veining.

Preferentially oriented subhedral quartz, amphibole, clinopyroxene, and interstitial sulphides are concentrated within fractures of large quartz grains (Figs. 11a and 11b). Interconnected elongated quartz grains are subhedral and have smooth to slightly angular grain boundaries (Figs. 11c and 11d). Minor granular chlorite is present in open spaces between large quartz grains (Fig. 11c). Other small-medium angular and subrounded quartz grains are clustered between large quartz grains and appear to be filling an open space between larger grains (Fig. 11d). Quartz grains show undulose extinction.

The opaque minerals are subhedral and disseminated between brecciated quartz, clinopyroxene (cpx), and amphibole (amp) fragments (Figs. 11a and 11b). Disseminated fine-grained chalcocite occurs between brecciated amp, cpx, and quartz (Fig. 11e). Subhedral bornite is partially replaced by secondary chalcocite and occur between subhedral and angular fragments of quartz, amp, and cpx (Fig. 11f).

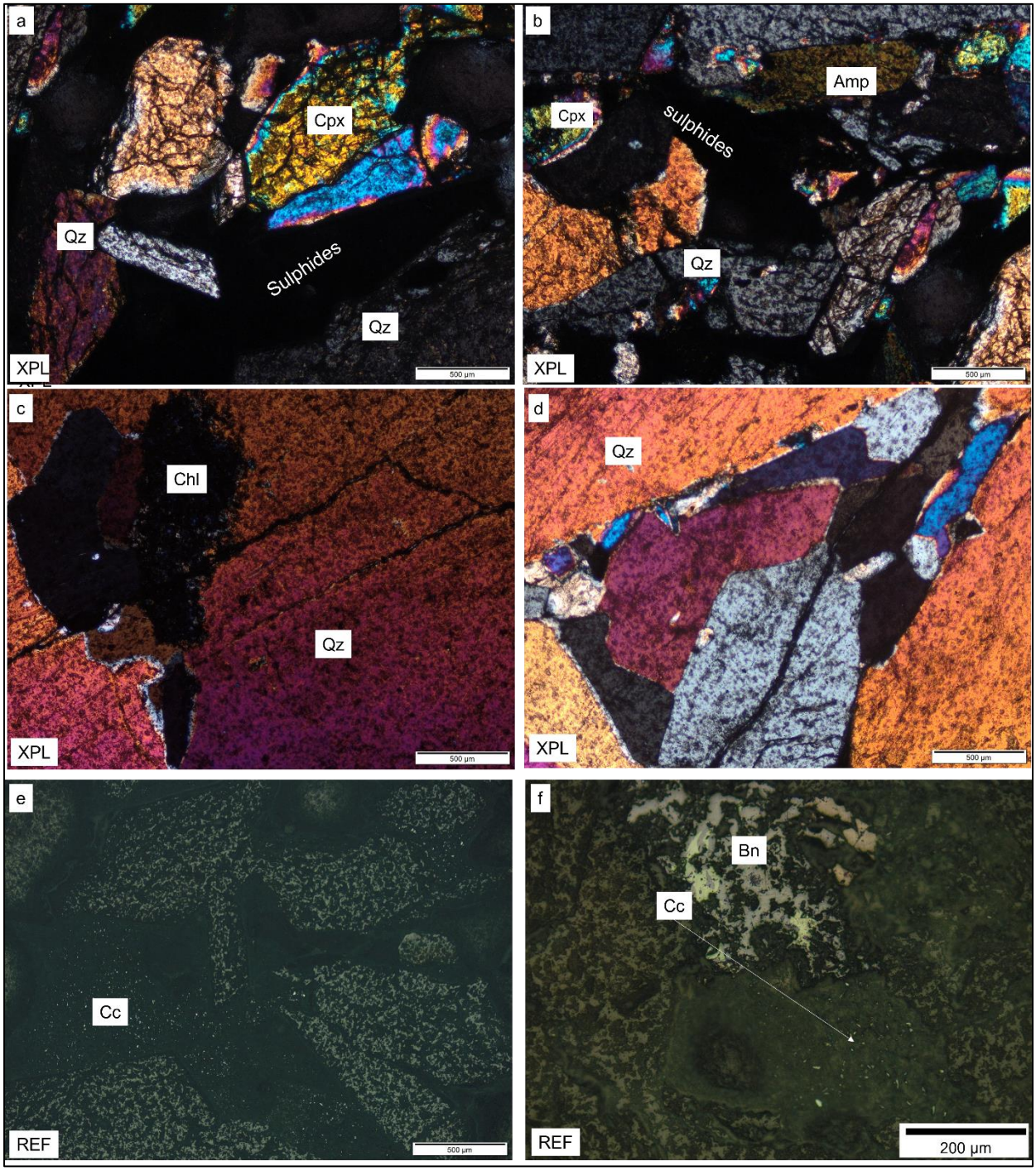


Figure 11: Photomicrographs showing: (a-b) fragments of clinopyroxene (Cpx), quartz (Qz), and amphibole (Amp) concentrated within a fracture; (c) granular chlorite (Chl) with subhedral-subangular quartz grains filling an open space between large quartz grains; (d) small-medium-sized, angular, and subrounded quartz clustered between large quartz grains; (e) disseminated fine-grained chalcocite (Cc); (f) bornite (Bn) blebs partially replaced by Cc and disseminated Cc (white arrow). Magnification scale = 500 µm and 200 µm.

Sample 19073

The hand sample may represent part of a thick vein consisting of very fine-grained groundmass of quartz heavily coated by iron oxide, so far that the quartz is not white but rather pinkish-red in colour (Fig. 12). Within quartz groundmass, subhedral, elongate, and irregular chlorite grains are visible (Fig. 12a). Bornite is interstitial between fine-grained quartz groundmass, and in places is intersected by chlorite (Figs. 12a and 12b). In some parts, subhedral quartz grains are present within interstitial bornite.

Fine-grained brassy yellow chalcopyrite occurs within the iron-stained groundmass. Chalcopyrite also occurs in contact with interstitial bornite (bluish-black; white arrow in Fig. 12b).

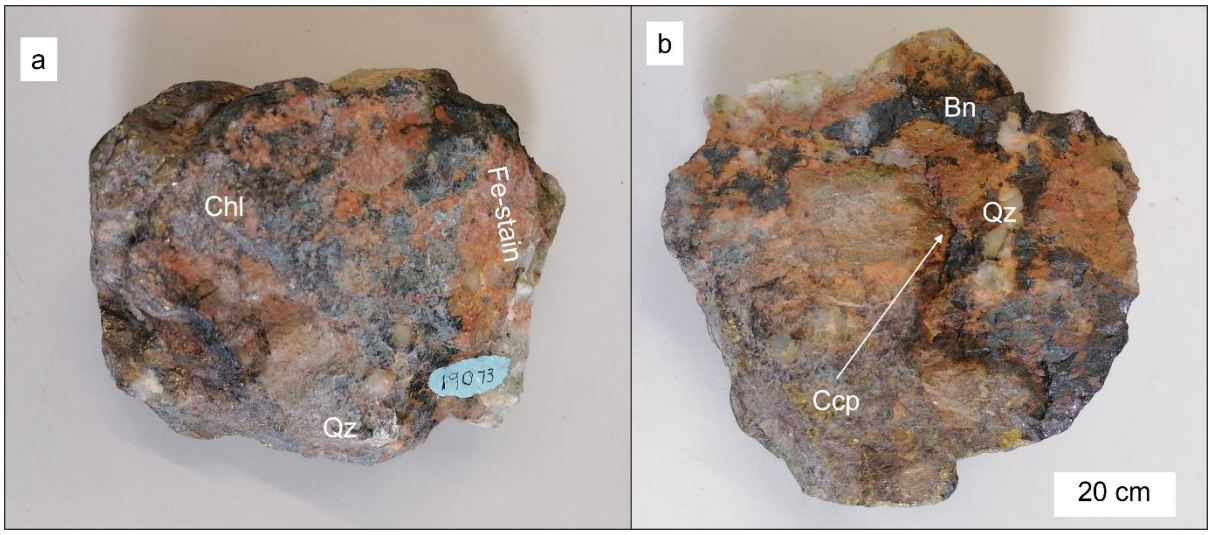


Figure 12: Sample 19073 comprises very fine-grained quartz (Qz) groundmass with subhedral, elongated, and irregular chlorite grains (Chl) in the groundmass. Quartz groundmass is heavily coated by orange-red iron oxide (Fe-stain). Interstitial bornite occurs within the quartz groundmass and is cut by chlorite in places. Some subhedral quartz grains occur within interstitial bornite. Fine-grained chalcopyrite grains (Ccp) are enclosed within the quartz groundmass. Other chalcopyrite (white arrow) is in contact with interstitial bornite (Bn).

The sample is dominated by cryptocrystalline quartz, which is consistent with iron staining, and makes up the sample fine-grained groundmass (Fig. 13a). Small to large (~0.4 to 1 mm) discrete tabular to flaky grains of chlorite are present within iron-stained cryptocrystalline quartz groundmass (Figs. 13a and 13b). The chlorite grains are altered into epidote along their cleavage planes (Fig. 13a). Tiny epidote grains are also visible within cryptocrystalline quartz (Fig. 13a). Iron-stained quartz vein cuts through the cryptocrystalline groundmass (Fig. 13b). In Fig 13c, irregular chlorite-epidote veinlets occur within the opaque minerals. The contact between the silicate and opaque minerals is corroded, whereby the corroded fragments of quartz occur within the opaque minerals (Fig. 13c).

Among the opaque minerals, the major sulphide is coarse-grained and subhedral bornite (pinkish-purple with a violet tint) with minor chalcopyrite, chalcocite, and Fe-oxides. Subhedral massive bornite is enclosed within cryptocrystalline groundmass and cut partly by iron-stained quartz vein (Fig. 13d). Hematite platelets appear to rim the massive bornite along the grain margins (Fig. 13d). Chalcopyrite is completely replaced by bornite, and minor chalcopyrite relics occur within the bornite (Figs. 13d-13f). Isolated, subrounded hematite (bluish-green) which develop into tiny blades occurs within bornite along a fracture (Fig. 13e). High-magnification of Fig. 13e (white square) shows incipient replacement of bornite by chalcocite associated with hematite along minor fractures of the host bornite (Fig. 13f).

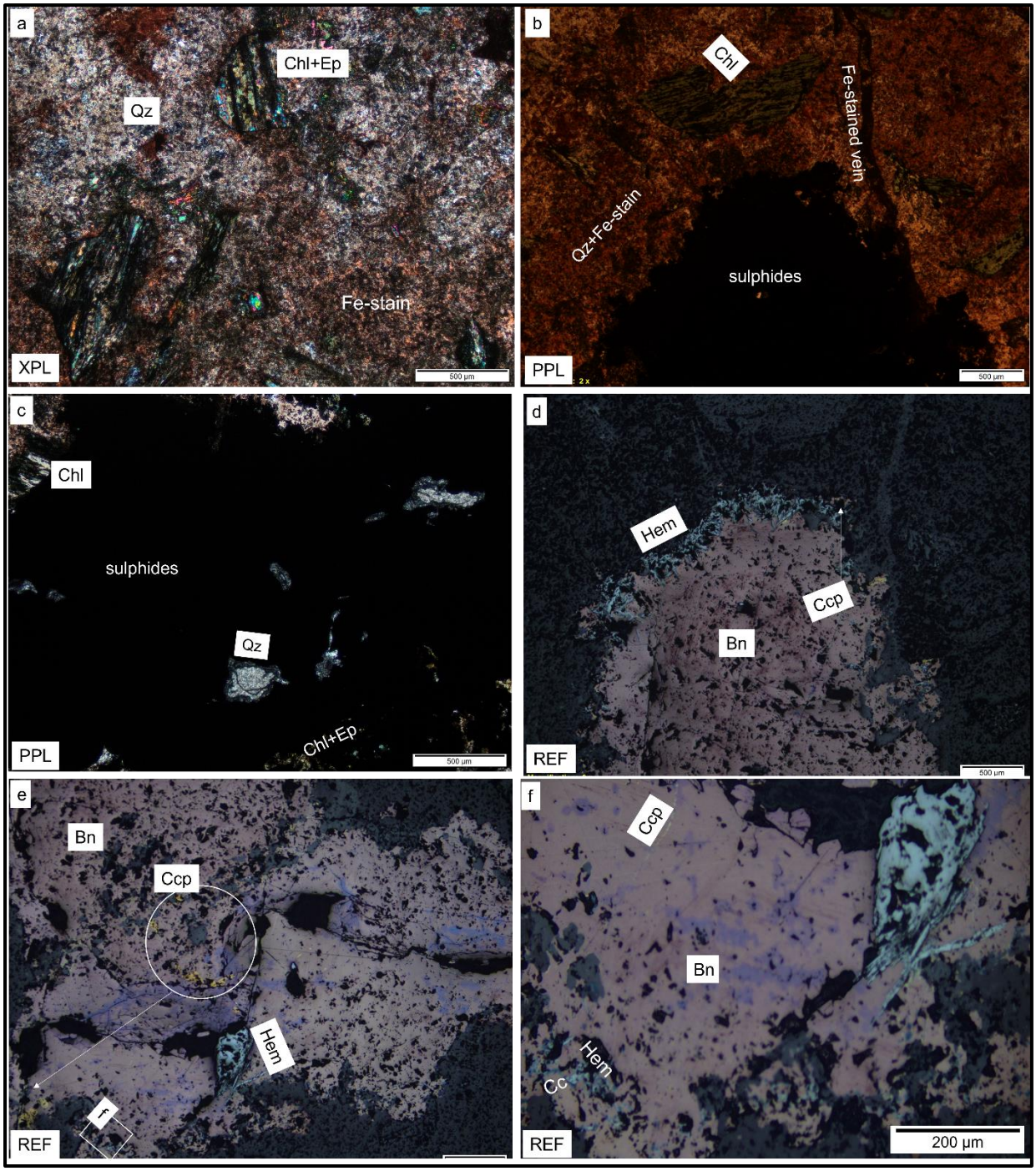


Figure 13: Photomicrographs showing: (a) chlorite (Chl) grains within Fe-stained cryptocrystalline quartz (Qz) are partially altered into epidote (Ep) along cleavage planes; (b) Fe-stained vein cut through cryptocrystalline groundmass and opaque minerals. Irregular grains of green chlorite grains within cryptocrystalline quartz; (c) subhedral quartz and irregular chlorite-epidote veinlets within the opaque minerals; (d) subhedral coarse-grained bornite (Bn) in contact with disseminated chalcopyrite. Hematite platelets rim the bornite along margins; (e) bornite with minor chalcopyrite (Ccp) flame-like relics within bornite. Subhedral hematite developing into elongate blades (light bluish-green) in a fracture in host bornite; (f) tiny blades of hematite and chalcocite along minor fractures of bornite under high-magnification (white square in Fig. 13e). Magnification scale = 500 µm and 200 µm.

Sample 19075

The hand sample represents the contact between the chloritised country rock and a brecciated milky quartz vein hosting massive tarnished bornite (Figs. 14a and b). The bornite contains minor chalcopyrite inclusions in places. Quartz grains in the mineralised vein are subhedral and locally show stains of

orange-red iron oxide (Fig. 14a). The country rock consists of fine-grained quartz and chlorite groundmass (Fig. 14b). The contact between the mineralised vein and chloritic country rock is sharp to irregular with chlorite encroaching into the mineralised vein.

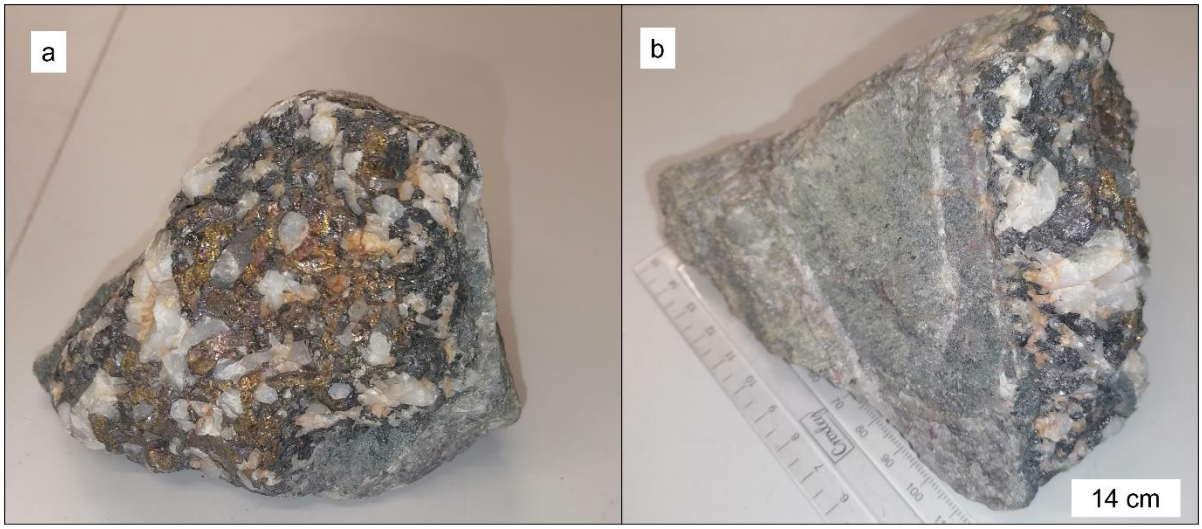


Figure 14: Sample 19075 showing: (a) a mineralised vein of brecciated milky quartz crystals hosting massive tarnished bornite with minor chalcopyrite inclusions. Quartz crystals are coated with orange-red iron oxide stains; (b) contact between fine-grained chloritised country rock with the mineralised vein. Thin veins and discrete quartz crystals also occur within the chloritised country rock.

Granular green chlorite occurs between fragments of quartz and contains inclusions of small, partly isolated, subhedral to angular quartz grains (Figs. 15a and 15b). The chlorite is partially altered into epidote. Subhedral and relatively coarse-grained (about 4 mm) quartz grains with distinct grain boundaries enclose the opaque minerals. Fibrous epidote grains are present between quartz fragments, and where they occur, quartz grains appear brecciated. However, epidote was not observed in the hand specimen. Other fine-grained chlorite aggregates with quartz inclusions invade the opaque minerals as interstitial material (Fig. 15c). The quartz grains are large and interconnected where chlorite and epidote are absent and are brecciated and small-medium sized where they are present.

Bornite dominates the opaque minerals in the sample and occurs as small anhedral lenses and medium-coarse grains disseminated within granular chlorite and quartz grains (Figs. 15d and 15f). Minor chalcopyrite has been completely replaced by bornite along a fracture (Fig. 15d). An irregular convolute-like bluish-green hematite encloses grey magnetite grains and is interstitial between quartz fragments (Fig. 15e). This hematite also cuts through the quartz grains irregularly (Fig. 15e). Coarse-grained bornite is enclosed within granular chlorite gangue and is abutted by irregular to elongated blades of hematite along the margins (Fig. 15f). The elongated hematite blades are overgrown with small hematite blades. The bornite has completely replaced chalcopyrite whereby only minor spots of chalcopyrite are visible (Fig. 15f). Some small blades of hematite are concentrated around open fractures within the host bornite at the contact between bornite and chlorite groundmass (Fig. 15f, top right).

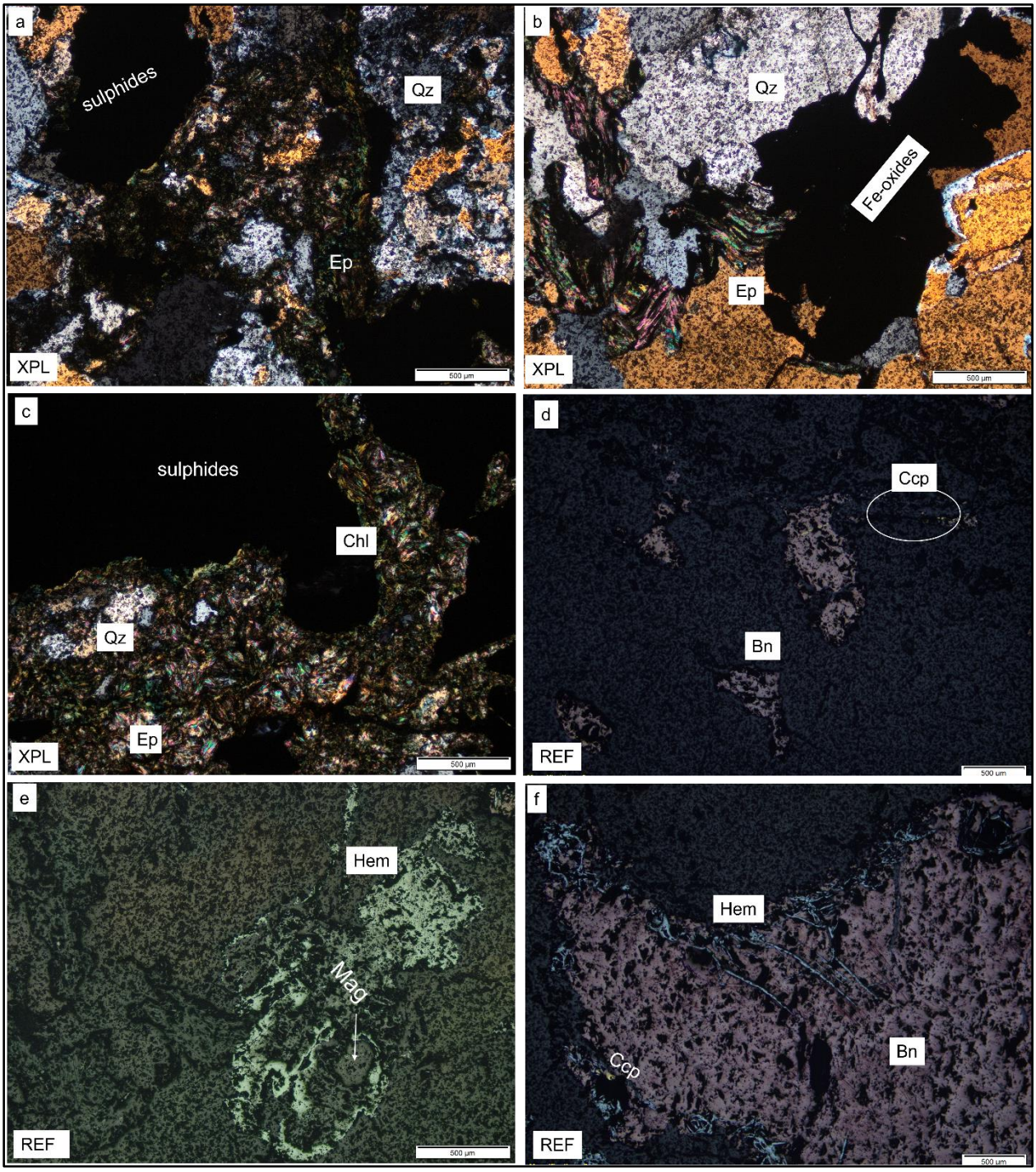


Figure 15: Photomicrographs showing: (a) brecciated quartz (Qz) fragments with interstitial granular chlorite-epidote; (b) quartz fragments with irregular fibrous epidote (Ep) between the fragments; (c) interstitial granular chlorite (Chl) with quartz inclusions invade the opaque minerals; (d) disseminated and anhedral lenses of bornite with minor chalcopyrite replaced by bornite along a fracture; (e) anhedral hematite (Hem) enclosing grey magnetite grains (Mag); (f) coarse-grained bornite (Bn) with minor bright yellow chalcopyrite is abutted by irregular to elongated hematite blades along the margins. Magnification scale = 500 µm.

Sample 19078

The hand specimen represents the contact between altered (epidotised) country rock and a mineralised brecciated milky white quartz vein with interstitial and massive bluish-purple black bornite (Fig. 16). Minor large quartz crystals also occur within the fine-grained light green epidotised country rock. The

epidote appears to have completely altered the country rock and replaced remnants of a mafic country rock. The contact between epidotised country rock and mineralisation is irregular and presents a rim of milky quartz (1 mm). Minor bornite is interstitial between epidotised country rock and quartz crystals. Some parts show bornite in direct contact with the epidotised country rock.

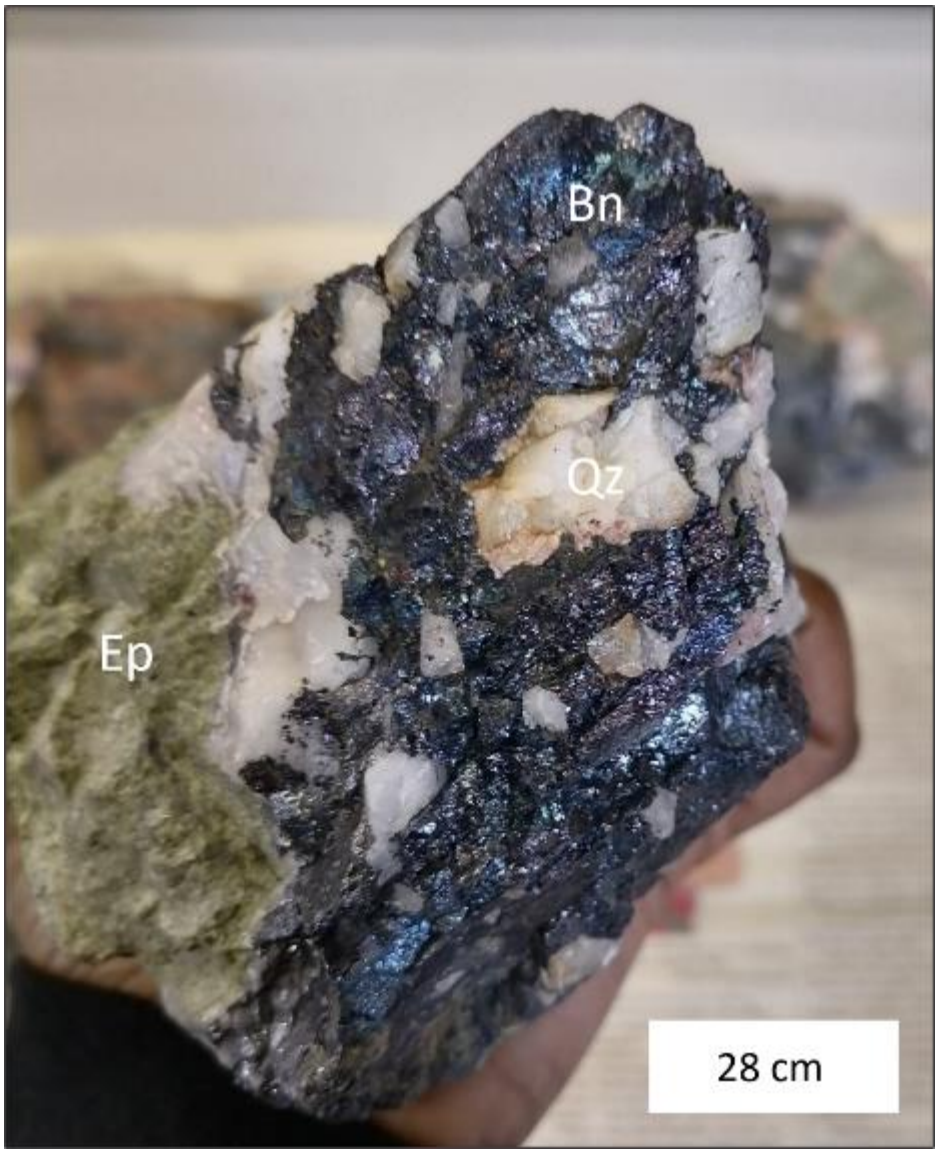


Figure 16: Sample 19078 showing one part representing epidotised (Ep) country rock and the other part representing a mineralised brecciated milky white quartz vein. The contact between them shows irregular quartz (Qz) as a rim. In other parts, bornite is in direct contact with the epidotised country rock. Minor large, subhedral quartz crystals also occur within the epidotised country rock. Fine-grained epidote (Ep) groundmass is also in direct contact with the massive bluish-purple black bornite (Bn).

Epidote aggregates are seen invading the opaque minerals (Fig. 17a). The opaque minerals are also interstitial between large quartz grains and epidote aggregates (Fig. 17b). The large quartz grains within the mineralised vein occur as subhedral grains as observed in hand sample (Fig. 17b). The quartz grains are not transparent, but rather cloudy due to the inclusions (Fig. 17b), as it also has a milky white colour in the hand specimen (Fig. 16). Within the epidotised country rock, opaque minerals are present between epidote aggregates as disseminated grains (Fig. 17c). These epidote aggregates have developed into prismatic bluish-green zoisite grains associated with disseminated opaque minerals (Fig. 17c).

Disseminated mineralisation is mostly concentrated within the epidotised country rock, but not in association with the cloudy quartz.

Bornite is the dominant Cu sulphide in this sample. Coarse-grained, massive tarnished bornite is invaded by epidote aggregates with some disseminations cementing the epidote aggregates in places (Fig. 17d). Other bornite is interstitial between epidote aggregates and quartz grains, and it is partially replaced by chalcocite, which creates rims along the margins of bornite (Fig. 17e). The interstitial bornite confirm the hand sample observation where the Cu sulphides are in contact with altered country rock. Disseminated grains of chalcocite are also present between newly crystallised zoisite gangue and replace bornite (Fig. 17f).

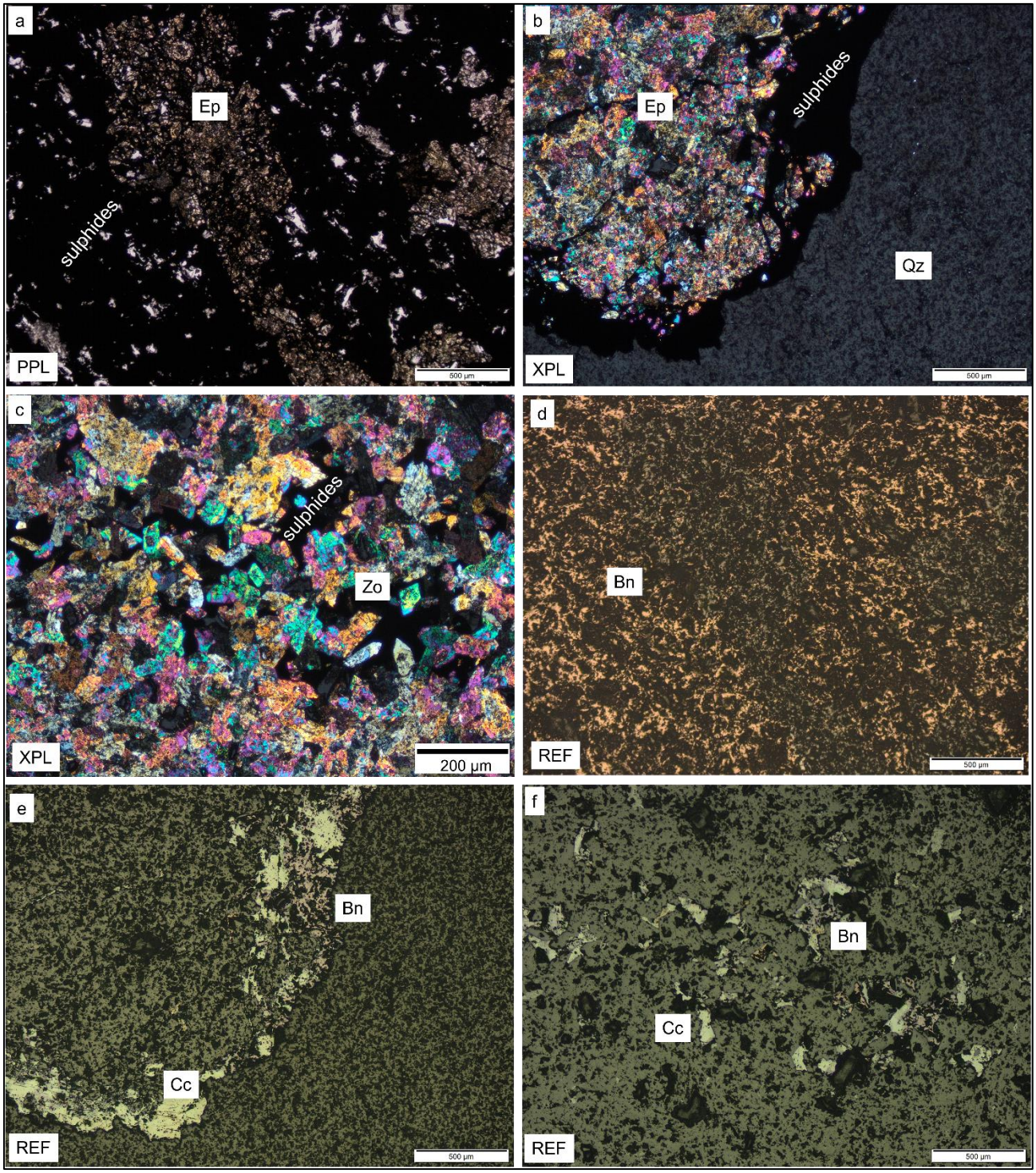


Figure 17: Photomicrographs showing: (a) epidote (Ep) aggregates invading massive opaque minerals. The tiny white and grey grains represent broken material during sample preparation; (b) the opaque minerals are interstitial between large, subhedral cloudy quartz (Qz) and epidote aggregates; (c) epidote aggregates developing into prismatic zoisite (Zo); (d) massive, tarnished bornite (Bn) with minor disseminations cementing epidote aggregates; (e) interstitial bornite replaced partially by chalcocite (Cc) along the margins; (f) disseminated chalcocite. Magnification scale = 500 µm and 200 µm.

Sample P580

The sample consists of massive sulphide mineralisation associated with minor epidote, chlorite, sericite, and quartz grains.

Fine-grained sericite occurs as rims along subhedral quartz grain margins, and it is also enclosed within prismatic epidote grains (Figs. 18a and 18b). The epidote also occurs irregularly within the opaque minerals (Figs. 18a and 18b). Some subhedral to euhedral epidote grains overprint subhedral quartz grains (Figs. 18b and 18c). There are irregular veinlets or aggregates of chlorite occurring within the opaque minerals (Fig. 18b). These aggregates or veinlets of chlorite are partially altered by epidote (Fig. 18b). Other relatively large quartz grains appear intergrown with fine-grained partial rims of sericite along the margins (Fig. 18c). The latter is overprinted by epidote and corroded along the boundaries where it is in contact with the opaque minerals (Figs. 18b and 18c).

Mineralisation is dominated by coarse-grained and massive, tarnished bornite (Figs. 18d-f). Irregular chlorite-epidote veinlets/aggregates and sericite rimmed by epidote invade the massive bornite and contain minor inclusions of bornite (Fig. 18d). Minute grains of chalcocite occur within the host bornite in places and indicate incipient replacement of bornite by chalcocite (white circles in Fig. 18e). An irregular curvilinear bornite occurs between the subhedral quartz grains and fine-grained sericite rim (Fig. 18f).

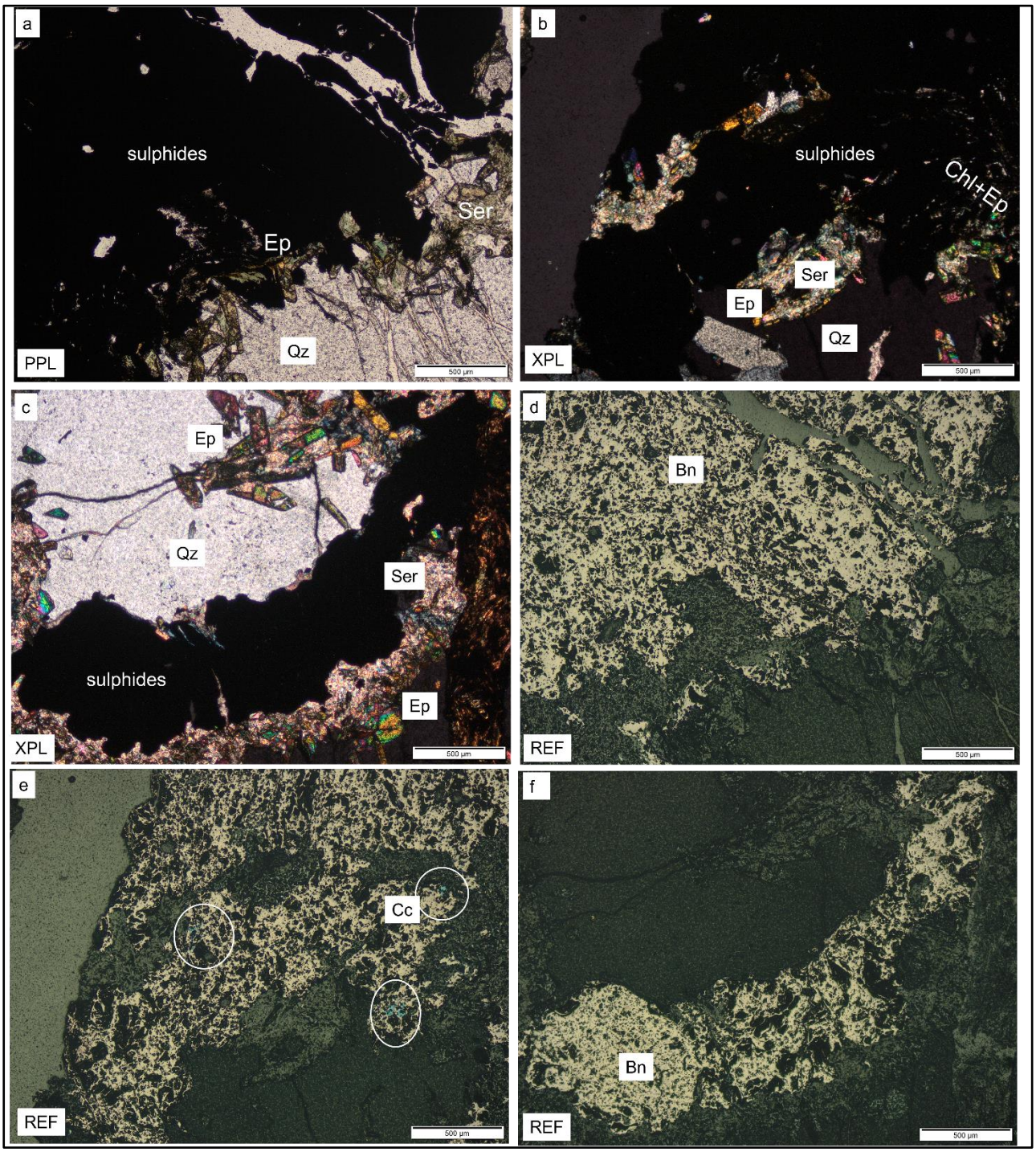


Figure 18: Photomicrographs showing: (a-b) subhedral quartz (Qz) with fine-grained sericite (Ser) rimmed by epidote (Ep) along its margins. Irregular epidote grains also occur within the opaque minerals; Chlorite-epidote (Chl+Ep) veinlets or aggregates occur within the opaque minerals; (c) fine-grained sericite partially rims subhedral quartz grains along the margins and it is overprinted by epidote, where they enclose the opaque minerals. Other euhedral, prismatic epidote grains overprint subhedral quartz grains; (d) massive bornite (Bn); (e) massive bornite with chalcocite (Cc) minute grains in places (white circles); (f) curvilinear coarse-grained bornite between the subhedral quartz grains rimmed by sericite. Magnification scale = 500 µm.

Sample P579

The sample consists of plagioclase (~35 vol%) with orthopyroxene (20 vol%), biotite (less than 5 vol%), chlorite (15%), and the opaque minerals enclosed within plagioclase and orthopyroxene (about 20-25 vol%).

The fractured sub- to rounded albitised plagioclase grains (recognised by multiple twinning) are partially altered by fine-grained sericite (Fig. 19a). Opaque minerals occur as anhedral grains, interstitial between albitised plagioclase and orthopyroxene grains (Figs. 19a and 19b). The opaque minerals also cement the fractured albitised plagioclase grains (Fig. 19a). Chlorite veins form rims around orthopyroxene and albitised plagioclase grains and cut through the opaque minerals (Figs. 19b and 19c). Loose rounded fragments of orthopyroxene and irregular plagioclase are present within the opaque minerals (Fig. 19b). Orthopyroxene also occurs as relatively large and fractured grains associated with a network of chlorite veins filling the fractures (Fig. 19c). Biotite is present as subhedral red-green grains, strongly altered and replaced by chlorite along its margins (Fig. 19c). This chlorite in turn overprints and partially cements albitised plagioclase fragments as veins/interstitial grains (Fig. 19c). The mineral grains of the silicates contain corrosion spaces where opaque minerals occur as disseminations (Figs. 19a-19c).

The main opaque minerals are pyrrhotite, pyrite, and minor chalcopyrite. Anhedral, massive granular pyrrhotite occurs between plagioclase and infills corrosion halos in albitised plagioclase or orthopyroxene as disseminated lenses or tiny grains (Figs. 19d-19f). Anhedral chalcopyrite is also seen between brecciated albitised plagioclase grains and encroaches onto the pyrrhotite (white arrow in Fig. 19d). Massive, granular pyrrhotite is interstitial between orthopyroxene and albitised plagioclase fragments and contains individual euhedral and subhedral creamy yellow pyrite grains (Figs. 19e and 19f). Disseminated pyrrhotite fills the corroded spaces within plagioclase, orthopyroxene and chloritised biotite (Fig. 19f).

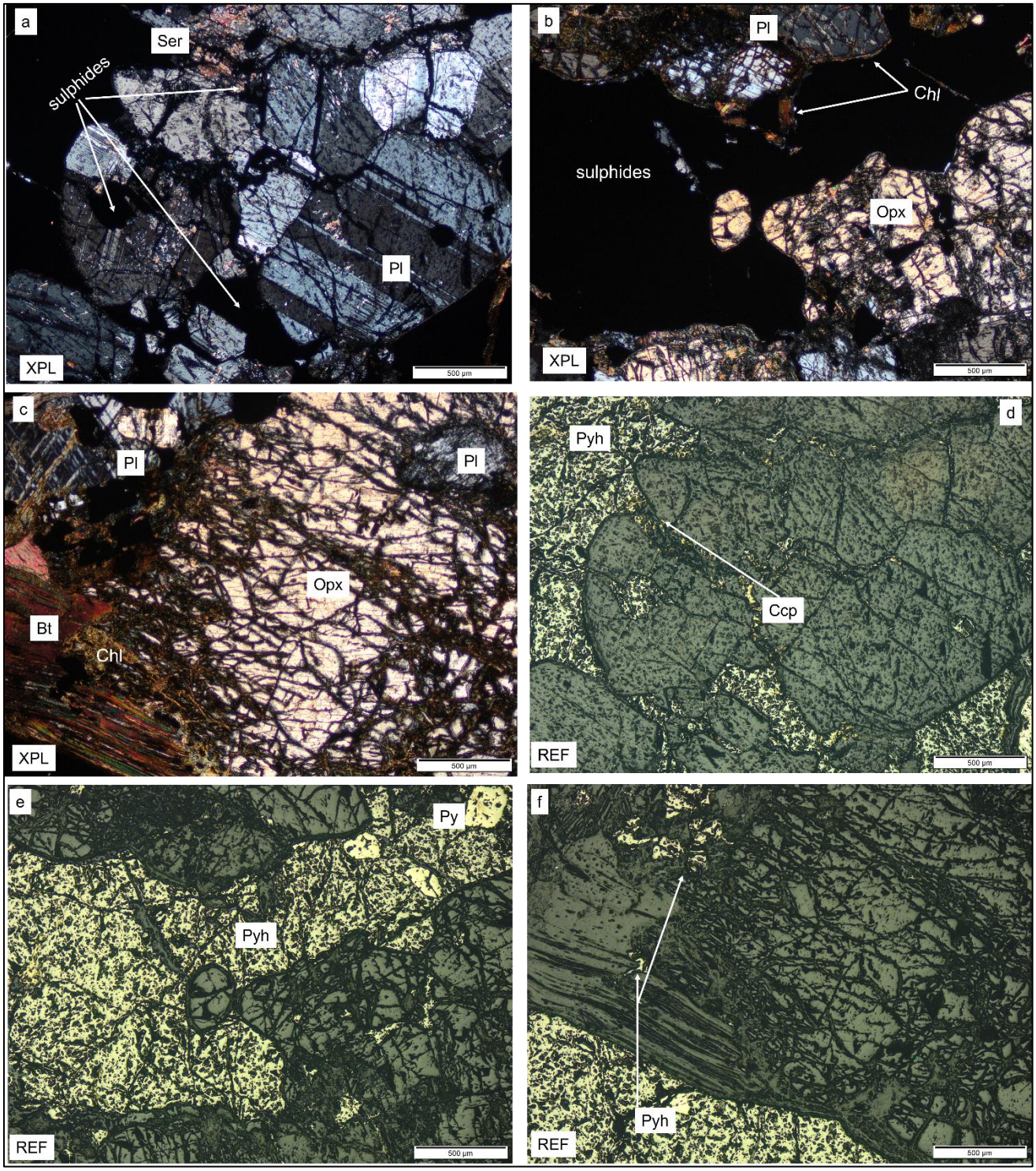


Figure 19: Photomicrographs showing: (a) albitised plagioclase (Pl) partially altered by fine-grained sericite (Ser); (b-c) fractured orthopyroxene (Opx) and plagioclase fragments associated with chloritic (Chl) networks veins filling the fractures, rimming opx and pl, and cementing and overprinting some pl fragments. Some veins occur within the opaque minerals; (d) anhedral pyrrhotite (Pyh) cements albitised plagioclase fragments and is associated with anhedral chalcopyrite (Ccp, white arrow) encroaching onto pyh; (e) massive, granular, interstitial pyh intergrown with individual euhedral and subhedral pyrite (Py) grains; (f) disseminated subhedral and anhedral pyrrhotite filling corroded halos within albitised plagioclase, chloritised biotite and orthopyroxene. Magnification scale = 500 µm.

Sample P679

The sample consists of distinct quartz grains (~50 vol%) with corroded brownish-red biotite (30 vol%) surrounding the opaque minerals (20 vol%) (Figs. 20a-20e).

There are two textural populations of quartz within the sample, here called quartz 1 and quartz 2. Quartz 1 consists of subhedral to sub-angular grains and it is commonly intergrown with irregular biotite grains. It is possible to observe strong and weak corrosion of biotite and quartz 1 grains along the cleavage planes and grain boundaries, respectively (Figs. 20a-20c). Quartz 1 grains are partly fragmented and loose, and some fragments occur within the opaque minerals together with corroded biotite grains (Figs. 20a and 20c). Quartz 2 is observed in veinlets cutting through quartz 1, biotite, and opaque minerals (Fig. 20a). Opaque minerals are enclosed within subhedral quartz grains and corroded cleavage planes of biotite (Figs. 20a-20c). The deep red coloration of biotite on the sample could be iron staining, which under transmitted light microscopy occur as dark brown staining (Figs. 20a to 20c). Biotite grains are seen partially breaking down to chlorite (Fig. 20c).

The opaque minerals consist of iron oxides, such as hematite and magnetite, and Cu sulphides, such as bornite and chalcopyrite. They are interstitial between the silicates, as well as disseminated within corroded halos of quartz and biotite grains (Figs. 20d-20f). Magnetite is intergrown with hematite as exsolution lamellae and occurs irregularly along cleavage planes of biotite-chlorite (Figs. 20d and 20f). Subhedral to interstitial lenses of bornite occur between the quartz grains and contain flame-like lamellae and islands of chalcopyrite (Figs. 20e and 20f). Some bornite and chalcopyrite grains are disseminated within corroded spaces of quartz 1 and biotite (Figs. 20e and 20f). Under high-magnification (area outlined by a white square in Fig. 20e), magnetite-hematite lamellae cut into adjoining bornite and contain inclusions of the host bornite. Irregular subhedral hematite (light bluish-grey) also occur within cleavage planes of biotite grains and enclose chalcopyrite in places (Fig. 20f). Minor chalcocite spots are present in places (white circles) along the margins of subhedral bornite (Fig. 20f).

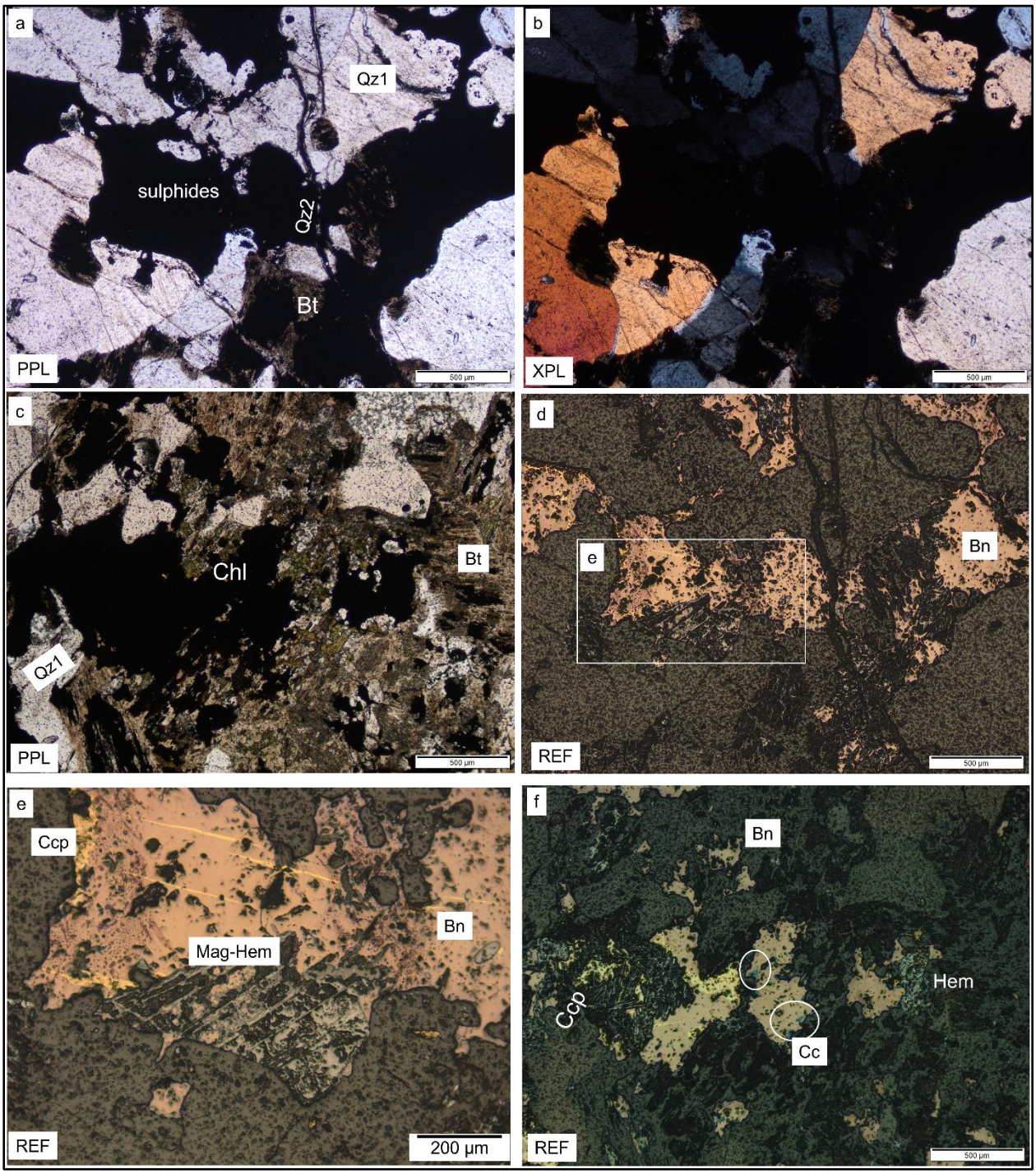


Figure 20: Photomicrographs showing: (a-c) subhedral and subrounded quartz (Qz1) grains intergrown with iron-stained biotite (Bt). Quartz veinlets (Qz2) cut through quartz 1, biotite and opaque minerals. Biotite is partially altered and replaced by chlorite; (d-e) subhedral and anhedral lenses of bornite (Bn) with flame-like lamellae and islands of chalcopyrite (Ccp) occur between quartz and biotite gangue. Hematite-magnetite exsolution lamellae is seen abutting bornite; (f) subhedral disseminations of bornite within corroded spaces of quartz 1 grains. Minor chalcocite spots occur along bornite margins (white circles). Irregular hematite (Hem) grains occur along cleavage planes of biotite and are in places enclosing chalcopyrite. Figure (e) represents a high-magnification image of the area outlined by a white square in Fig (d). Magnification scale = 500 µm and 200 µm.

Sample P774

This sample comprises a thick (~2 cm) vein of epidote aggregates (25 vol%) with small (~1 mm) secondary cloudy, subhedral quartz grains (10-15 vol%) cutting through partly iron-stained, large subhedral quartz grains (30 vol%). The large subhedral quartz grains are interconnected and associated with interstitial fine-grained chlorite (10 vol%) and sericite (10 vol%). Opaque minerals (<10 vol%) are mainly enclosed within the epidote-quartz vein. Thus, the sample comprises country rock matrix and mineralised vein structure.

Epidote aggregates (brownish-yellow in PPL) occur as subhedral, and angular grains cemented by fine-grained secondary quartz 2 grains (Figs. 21a and 21b). Discrete angular amphibole grains (light green) also occur amongst epidote aggregates (Figs. 21a and 21b). Opaque minerals are disseminated between epidote aggregates and secondary quartz 2 (Figs. 21a and 21b). Anhedral, fine-grained sericite (pinkish-brown) is present between relatively large quartz 1 grains (Fig. 21c). Subrounded chlorite also occurs within the fine-grained sericite and between quartz 1 and sericite (Fig. 21c). There appears to be a reaction rim where chlorite is in direct contact with fine-grained sericite grains (dark brown rim around chlorite; Fig. 21c). Subrounded inclusions of quartz 1 occur within sericite, which appears to be partially corroding the margins of quartz 1 grains (Fig. 21c). Some opaque minerals fill anhedral halos within quartz 1 (Fig. 21c).

The sample contains Cu sulphide minerals, such as bornite, chalcopyrite, chalcocite, and iron oxides, such as hematite. Bornite (light pinkish-brown) is replaced by chalcocite (bluish-white) as a rim around it (Fig. 21d). In addition, chalcopyrite is being replaced by bornite and they are both rimmed by chalcocite (Fig. 21d). In turn, a thin rim of greyish-white hematite (Fig. 21d, white arrow) encloses chalcocite. In other parts, subhedral chalcocite grains are disseminated between epidote aggregates and secondary quartz 2 gangue (Figs. 21c and 21d). Small subhedral hematite grains are present within quartz 1 halos (Fig. 21f).

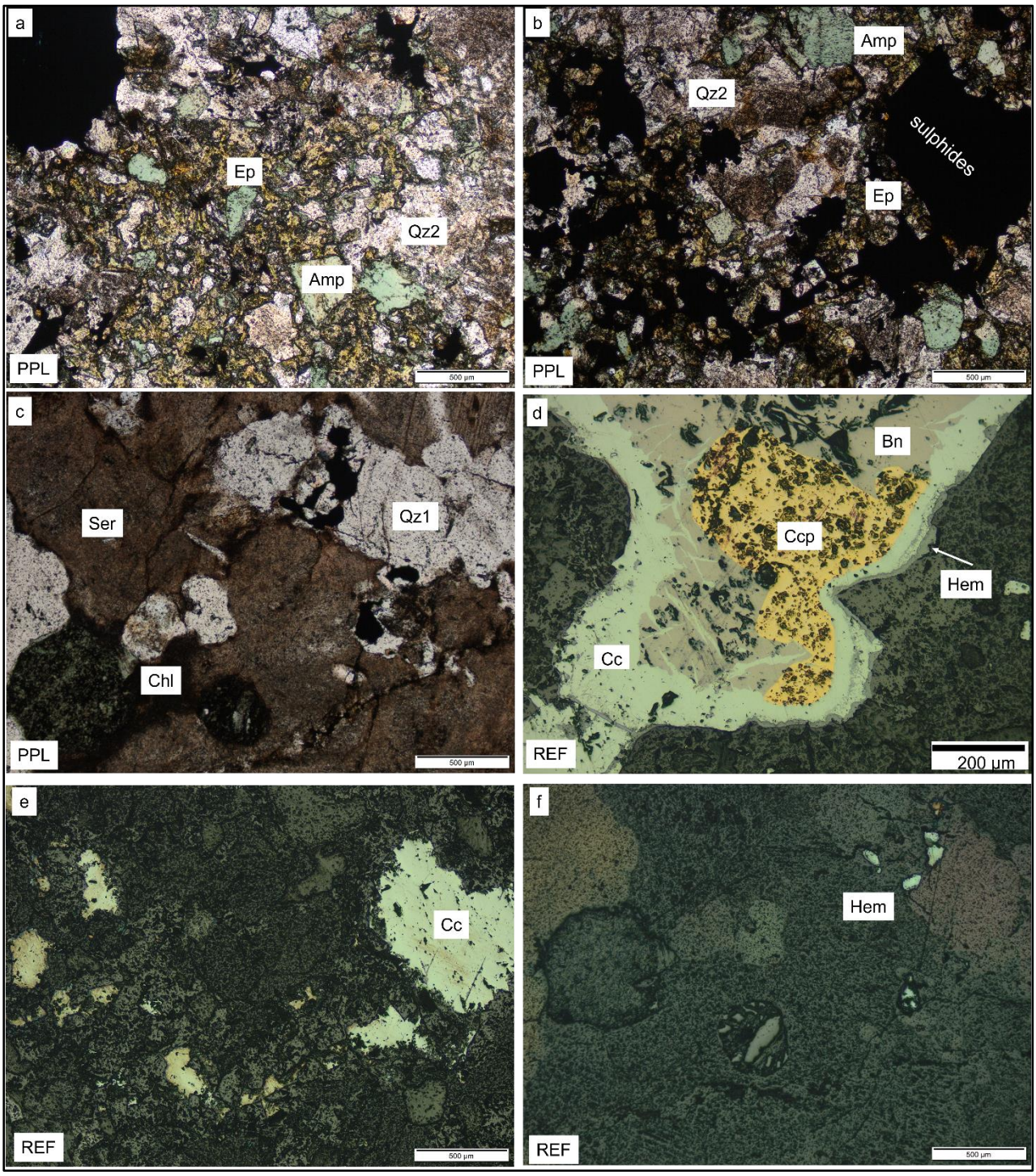


Figure 21: Photomicrographs showing: (a-b) epidote (Ep) aggregates (brownish-yellow in PPL) associated with subangular quartz (Qz2) cement. Light green angular amphibole (Amp) relics occur within epidote aggregates; (c) fine-grained, subrounded chlorite (Chl) between relatively large quartz grains (Qz1) and interstitial sericite (Ser); (d-e) chalcocite (Cc) rims bornite and chalcopyrite (Ccp) and is in turn rimmed by thin hematite (white arrow). Disseminated chalcocite between epidote aggregates and secondary quartz 2 gangue; (f) small subhedral hematite (Hem) grains within quartz 1 halos. The pale colours of the sulphides could be due to polishing. Magnification scale = 500 µm and 200 µm.

Sample P812

This sample is composed of massive, anhedral fine-grained sericite (about 50 vol%) that occurs between medium-large (0.5 to 2 cm) quartz grains (30 vol%). Opaque minerals (5-10 vol%) occur between and within sericite or quartz grains. Minor rock-forming minerals include plagioclase (<5 vol%) and K-feldspar (5%) grains, which also occur in association with the fine-grained sericite.

A large mass of K-feldspar is partially altered and replaced by fine-grained sericite (Figs. 22a and 22b). Subrounded and subhedral quartz grains occur embedded within fine-grained sericite that has altered K-feldspar (Figs. 22a-22c). Anhedral, clear quartz grains are visible between K-feldspar mass (Figs. 22a-22c). Corroded pieces of plagioclase (weak albite twinning), K-feldspar, and sericite occur within the opaque minerals (Figs. 22c and 22d). Quartz grains have varying grain sizes: smaller grains (~0.5 mm) occur embedded within fine-grained sericite whereas large clear grains are invaded and rimmed partially by fine-grained sericite (Figs. 22a-22d). In other parts, subrounded and irregular sericite grains occur along the margins of large clear quartz, where they are in contact with opaque minerals (Fig. 22d). Quartz grains exhibit undulose extinction (Figs. 22c and 22d). Opaque minerals are enclosed within altered alkali feldspars, fine-grained sericite and/or in direct contact with subhedral clear secondary quartz grains (Figs. 22c and 22d).

Pyrite is the dominant sulphide mineral of this sample among the opaque minerals. Pyrite shows varying morphologies and sizes (1 mm to over 2 cm). It occurs as euhedral (almost cubic or pyritohedral) to subhedral, and less commonly anhedral and fairly large, clustered grains (Figs. 22e and 22f). The contact between pyrite and subhedral clear quartz grains is sharp and slightly irregular, whereas the contact between sericite, altered feldspars and pyrite is irregular to corroded (Figs. 22e and 22f). In places, pyrite appears as corroding and replacing sericite, whereby sericite can also be seen as inclusions within the pyrite grains (Figs. 22e and 22f). Smaller pyrite grains are disseminated within fine-grained sericite gangue (Fig. 22e).

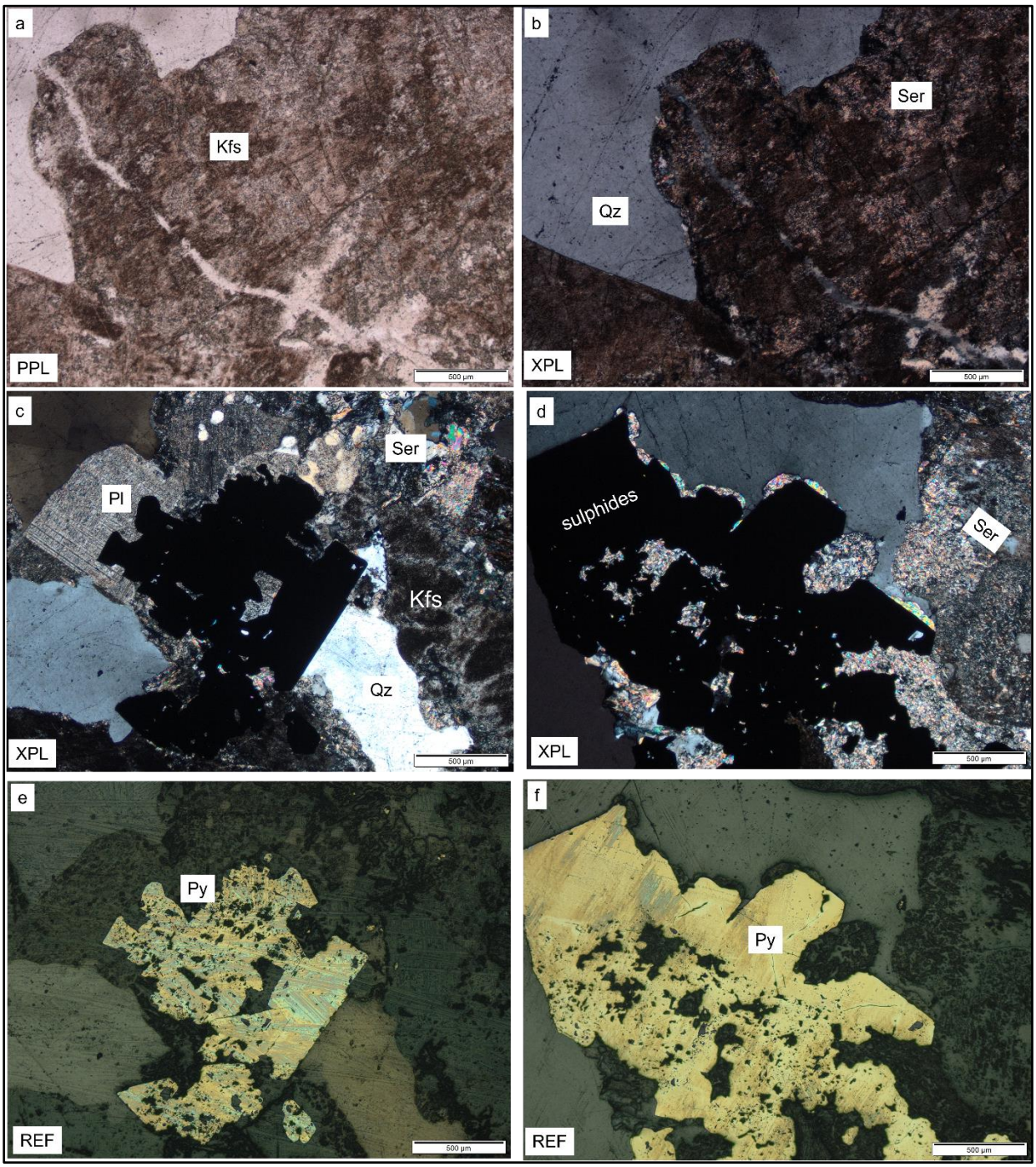


Figure 22: Photomicrographs showing: (a-b) fine-grained sericite (Ser) associated with large, clear quartz grains (Qz) and alters K-feldspar (Kfs, dark brown); (c-d) anhedral quartz grains surrounded by partially sericitised K-feldspar associated with a single plagioclase grain. Sericite partially rims quartz and the opaque minerals. Corroded ser, pl, and kfs occur within the opaque minerals; (e-f) clustered pyrite (Py) grains with inclusions of corroded gangue minerals. Some smaller pyrite grains also occur as disseminated grains within sericite gangue. Pyrite grains are tarnished due to polishing. Magnification scale = 500 µm.

Sample P814

The sample is composed of plagioclase (20 vol%), garnet (<5 vol%), K-feldspar (orthoclase, 20-25 vol%), minor sericite (5-10 vol%), chlorite (15 vol%), and opaque minerals (15 vol%). At least two textural populations of quartz are observed: Primary quartz (Qz) occurs within the brecciated country rock, whereas secondary quartz occurs in a thick vein (quartz 1) together with K-feldspar and plagioclase and as thin veins (quartz 2, 5 vol%) cutting grains within the thick vein.

Dark brown K-feldspar, minor plagioclase, and garnet occur together with primary quartz grains in the brecciated country rock matrix (Fig. 23a). Fine-grained sericite is seen partially altering and replacing K-feldspar and plagioclase (Fig. 23a). Some sericite occurs as irregular anhedral grains between primary quartz and plagioclase grains (Fig. 23a). In the brecciated matrix, biotite has also been completely altered and replaced by chlorite, which is partially altered by tiny epidote aggregates (Fig. 23a). A relict thick vein contains intergrown grains of plagioclase and K-feldspar (Figs. 23b and 23c). Relatively large grains of secondary quartz 1 within the thick vein contain inclusions of K-feldspar and plagioclase (Figs. 23b and 23c). Fine-grained sericite incipiently alters plagioclase grains within the vein along the grain margins, and also occurs in contact with K-feldspar (Figs. 23b and 23c). The alkali feldspars display polysynthetic and simple twinning (Figs. 23b and 23c). The thick vein encloses anhedral and subhedral opaque minerals and is slightly corroded along grain boundaries (Figs. 23b and 23c). Thin stockwork veins of secondary quartz 2 cut through quartz 1 and altered alkali feldspars (Figs. 23b and 23c). These veins also carry fine relics of alkali feldspars together with disseminated opaque minerals (Fig. 23b).

Chalcopyrite is the major copper sulphide of this sample. In the country rock matrix, subhedral and anhedral chalcopyrite grains are disseminated within chlorite-epidote aggregates, garnet fractures, and brecciated quartz grains (Fig. 23d). Irregular molybdenite laths are also seen occurring in association with anhedral sericite (Fig. 23d). Subhedral chalcopyrite is enclosed within the thick vein and cut partly by quartz 2 (Figs. 23d-23f). Chalcopyrite also occurs as disseminated grains within quartz 2 stockwork veins (Figs. 23e and 23f).

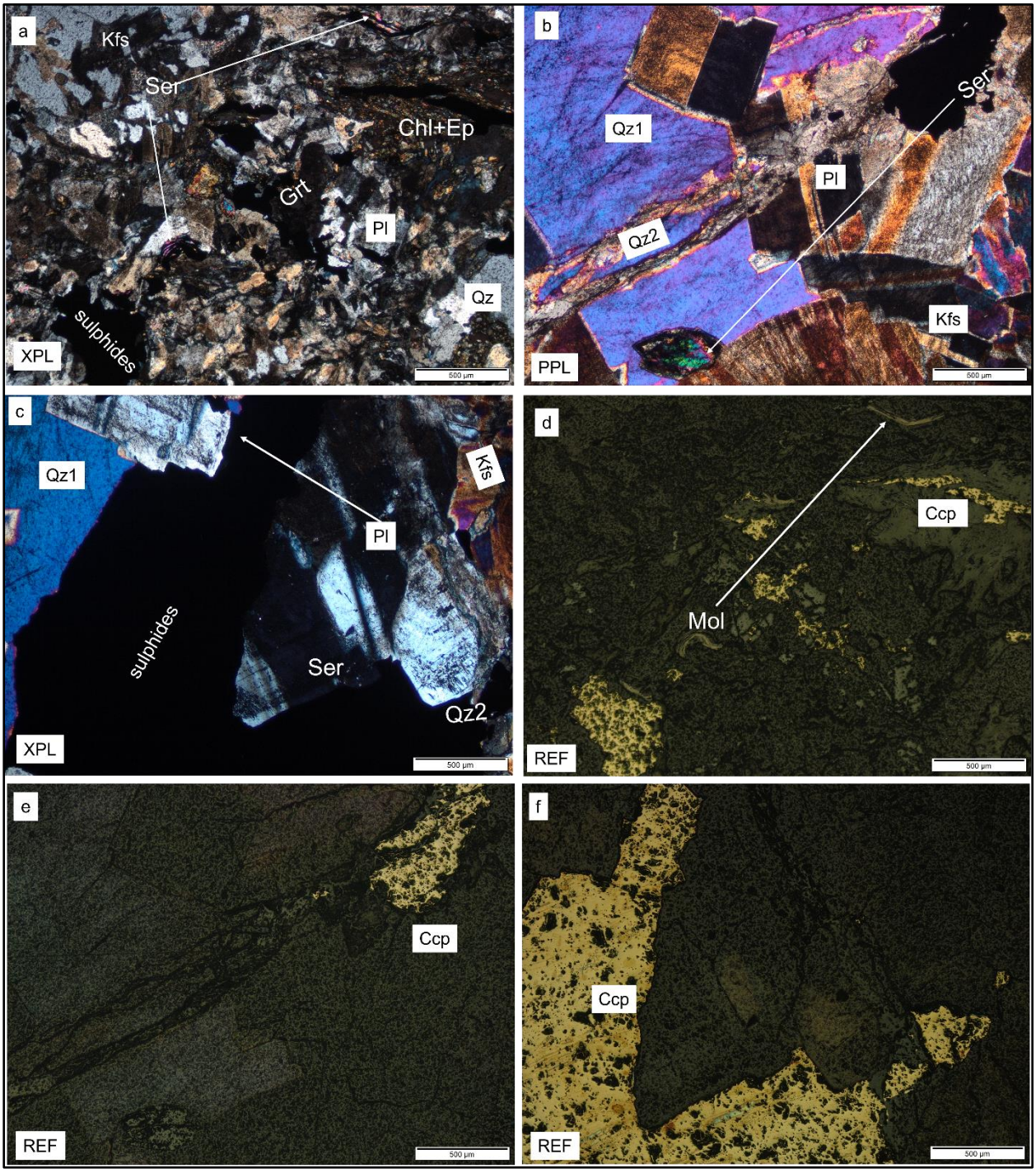


Figure 23: Photomicrographs showing: (a) brecciated country rock matrix of primary quartz (Qz) intergrown with fractured garnet (Grt) and partially altered K-feldspar (Kfs) and plagioclase (Pl) grains. Fine-grained sericite (Ser) partially alters Kfs and Pl. Chlorite (Chl) has completely replaced biotite and it is also altering into epidote; (b-c) irregular stockwork veins of secondary quartz 2 (Qz2) cutting through quartz 1 (Qz1), alkali feldspars, and the opaque minerals within a thick vein. The alkali feldspars also occur as inclusions within quartz 1; (d) subhedral and anhedral disseminated chalcopyrite (Ccp) within the brecciated country rock matrix. Molybdenite (Mol) laths are associated with anhedral sericite; (e-f) subhedral chalcopyrite within the thick vein is cut by quartz 2 veins. Disseminated smaller chalcopyrite also occurs within quartz 2 veins. Magnification scale = 500 µm.

Sample P782

The sample consists of subhedral quartz grains (30 vol%), fine-grained sericite groundmass (40-45 vol%), biotite-chlorite aggregates (10 vol%), garnet (<5 vol%), and opaque minerals (10 vol%).

Fine-grained sericite groundmass encloses large garnet grains that are almost completely altered and replaced by chlorite (anomalous blue) along the cracks (Fig. 24a). Fine-grained sericite groundmass contains inclusions of subrounded, smaller quartz grains and elongated biotite that is also partially altered and replaced by chlorite (deep blue; Figs. 24a-24c). Some partially altered grains of biotite occur between subhedral quartz grains (Fig. 24a). The subhedral quartz grains are cemented by fine-grained sericite groundmass (Figs. 24a-24c). Quartz, sericite groundmass, and some biotite grains are corroded by the opaque minerals and some corroded pieces occur within the opaque minerals as irregular grains (Figs. 24b and 24c). Other subrounded and subhedral opaque minerals are enclosed within the corroded halos of sericite groundmass and quartz grains (Figs. 24b and 24c). Veined opaque minerals also occur between sericite groundmass and quartz grains (Figs. 24b and 24c). The contact between the sericite groundmass-quartz and veined opaque minerals is corroded and irregular. Quartz grains exhibit undulose extinction.

The opaque minerals are pyrite, magnetite, molybdenite, and chalcopyrite. Isolated subhedral and subrounded porous pyrite grains are partly clustered and disseminated within the corroded halos of sericite groundmass, biotite, and quartz grains (Figs. 24d-24f). Minor magnetite lenses occur within the chloritised garnet and some biotite (Fig. 24d). Chalcopyrite occurs as relatively large coarse-grained, irregular vein and thin anhedral grains (Fig. 24e). It is associated with pyrite and is found between quartz-sericite gangue (Fig. 24e). A thick (3-4 cm) pyrite vein also occurs between sericite-quartz gangue and corrodes the silicates along the contact with the vein (Fig. 24f). Minor brownish-yellow, euhedral laths of molybdenite also occur within the gangue and are often in contact with altered biotite grains.

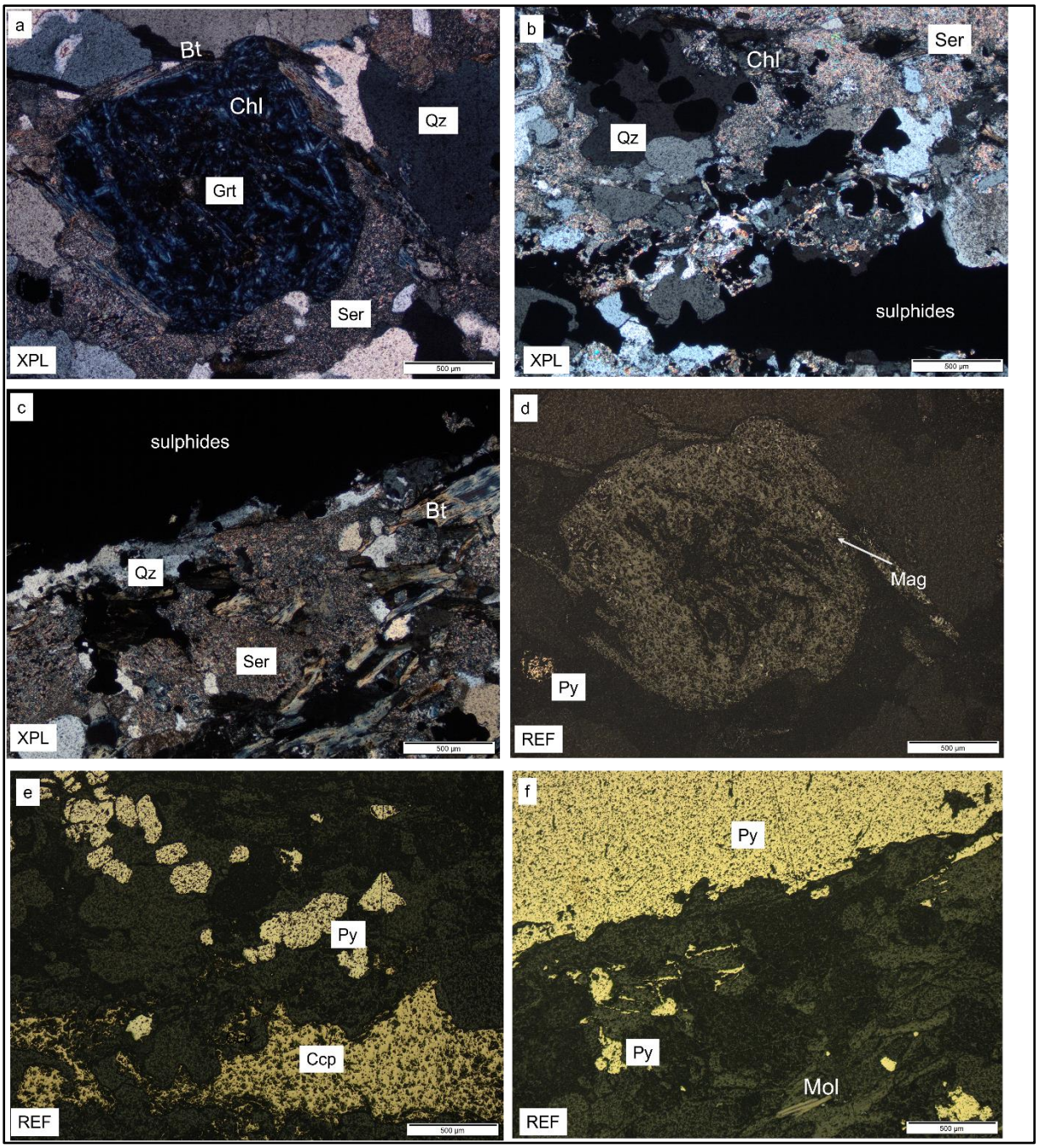


Figure 24: Photomicrographs showing: (a-c) fine-grained sericite (Ser) groundmass encloses altered garnet (Grt) and subhedral secondary quartz (Qz) grains. Elongated biotite (Bt) and subrounded-subangular quartz grains are included within sericite groundmass. Garnet and biotite are altered and replaced by chlorite (Chl). Fine-grained sericite and quartz enclose the opaque minerals and are corroded by opaque minerals; (d) small lenses of magnetite (Mag) within altered garnet and biotite; (e) disseminated subhedral and subrounded grains of pyrite (Py) within corroded spaces of the silicates. Coarse-grained irregular vein and thin anhedral lenses of chalcopyrite (Ccp) between sericite-quartz. Some pyrite grains are partly clustered; (f) thick pyrite vein and irregular lenses of pyrite disseminations. The vein contains sericite-quartz inclusions corroded from the contact between sericite-quartz and vein. Minor molybdenite (Mol) euhedral laths occur within the gangue and are in close contact with altered biotite grains. Magnification scale = 500 µm.

Sample P817

This sample resembles a thick (>5 cm) compacted quartz vein (50 vol%) in contact with brecciated country rock that is altered by chlorite (20 vol%) and sericite (10-15 vol%). The alteration minerals invade the quartz vein in places. Opaque minerals (15 vol%) occur within the quartz vein and brecciated country rock.

Large, interconnected, clear quartz grains, typical of a blocky vein cement trains of subhedral opaque mineral clusters, which occur preferentially around boundaries of quartz grains (Figs. 25a and 25b). Fine-grained sericite is present along grain margins of quartz grains, as well as within the opaque minerals along with green chlorite veins (Fig. 25b). The contact between the quartz vein and country rock is marked by brecciated fragments of amphibole, clinopyroxene, garnet and biotite that are partially altered by green and blue chlorite embedded within plagioclase (Fig. 25c). Irregular brecciated fragments of the altered country rock material penetrate the quartz vein (Fig. 25c). Within the brecciated country rock, plagioclase is partially altered and replaced by minute grains of sericite (Fig. 25c). The sericite also fills irregular fractures within large quartz grains (Fig. 25c). Green chlorite is present along twinning planes of plagioclase as irregular veins (Fig. 25c). Blue chlorite veins cut through the fractured garnet and also occur within plagioclase as minor granular grains overprinting sericite (Fig. 25c). Biotite is stained with brown iron oxide and contains halos of radioactive minerals in places (Fig. 25c).

The dominant sulphide mineral among the opaque minerals is pyrite. Disseminated pyrite grains of varying sizes and morphologies are enclosed within large quartz grains and occur preferentially following distinct grain boundaries (Fig. 25d). The grain size ranges from <1 mm to 2 mm for single euhedral to subhedral grains, whereas clustered grains range from 2 mm to 1 cm (Figs. 25d and 25e). Chlorite and sericite gangue appear to be overprinting pyrite grains (Fig. 25e). Chlorite also contains minor inclusions of tiny, isolated pyrite grains (Fig. 25d). Pyrite clusters are fractured and cemented by thin veins of chlorite and sericite (Fig. 25d). Some fractured pyrite grains are not cemented by any alteration minerals (Figs. 25d and 25e). Porous pyrite grains contain small grey magnetite inclusions (Figs. 25d and 25e). Subhedral greyish-brown magnetite grains are also found within the brecciated country rock (Fig. 25f).

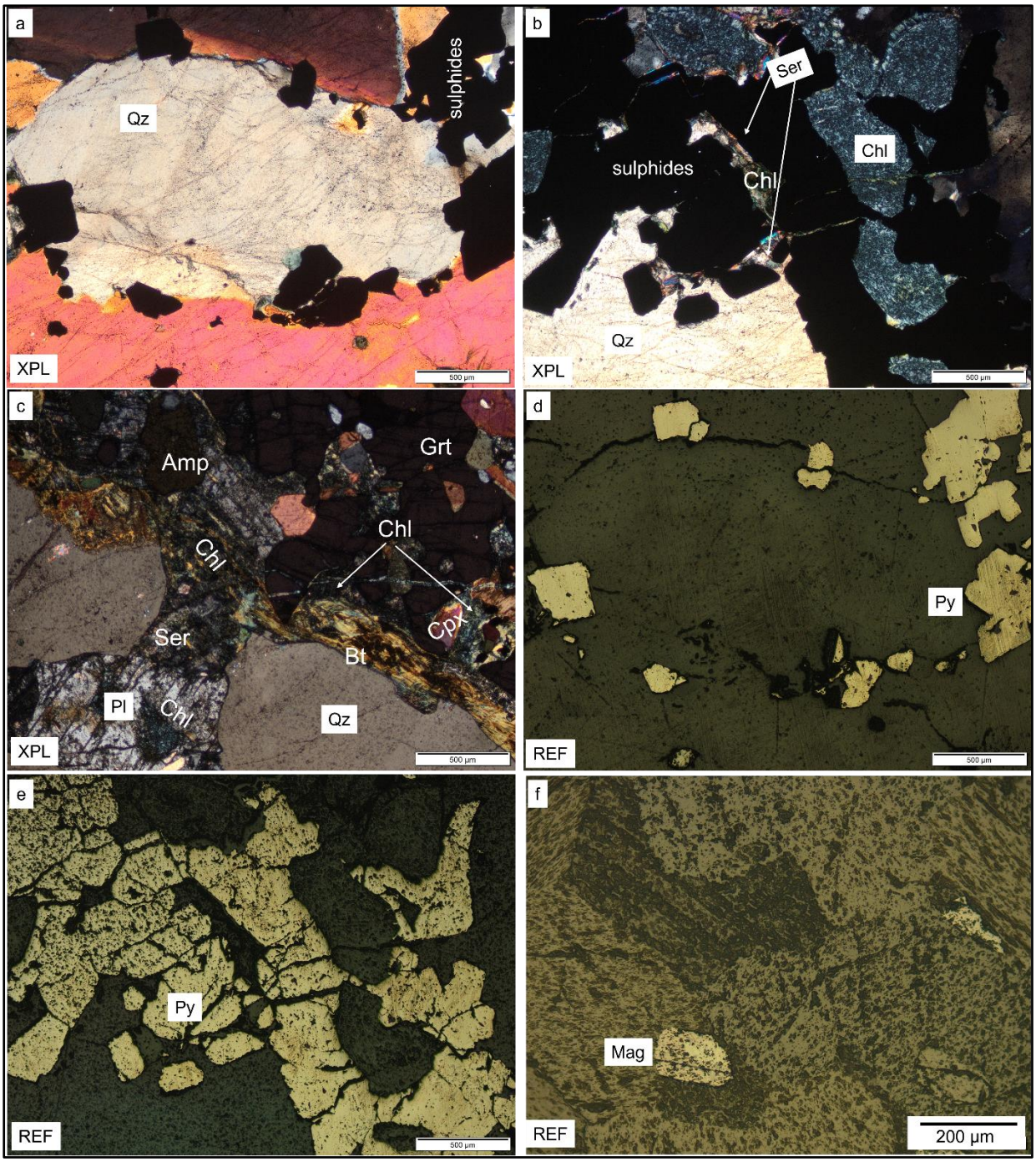


Figure 25: Photomicrographs showing: (a) interconnected, large clear quartz (Qz) grains, typical of blocky vein cementing the opaque minerals; (b) subhedral blue chlorite (Chl) with sericite (Ser) cut through the opaque minerals. Sericite also occurs along quartz margins and granular chlorite; (c) contact between the quartz vein and brecciated country rock. The country rock contains fragments of partially altered garnet (Grt), amphibole (Amp), clinopyroxene (Cpx), and biotite (Bt) embedded within plagioclase (Pl). These fragments penetrate the quartz vein; (d) disseminated pyrite grains preferentially aligned around quartz grain boundaries; (e) fractured and porous clusters of pyrite with inclusions of tiny magnetite grains; (f) subhedral magnetite within the altered country rock. Magnification scale = 500 µm and 200 µm.

Sample P613

This sample is dominated by creamy white plagioclase grains (40-45 vol%), epidote aggregates (15 vol%), green mafic minerals that could be clinopyroxene or chlorite (5 vol%), subhedral quartz grains (20 vol%), and subhedral-anhedral opaque minerals (15%).

Interconnected plagioclase grains (recognised by multiple twinning) surround irregular interstitial opaque minerals (Figs. 26a and 26b). Plagioclase is partly brecciated and cemented by the opaque minerals (Figs. 26a and 26b). A curvy epidote vein cuts through fractured garnet and quartz grains (Fig. 26c). The fractured garnet is brecciated and weakly altered and replaced by pale green chlorite grains in places (Fig. 26c). In other parts, plagioclase grains are associated with brecciated and corroded aggregates of epidote (pale brown to harlequin colours), clinopyroxene (high interference colours with 90^{o} cleavage planes), and subhedral quartz grains (Fig. 26d). Epidote aggregates also occur at the margins of clinopyroxene and within the opaque minerals (Fig. 26d). Some isolated disintegrated quartz grains are present within the opaque minerals (Figs. 26a and 26d). Opaque minerals occur between the quartz and plagioclase as coarse-grained interstitial mass, as well as disseminated grains within corroded spaces of epidote, clinopyroxene, and quartz (Figs. 26c and 26d).

Chalcopyrite represents the opaque mineral in this sample (Figs. 26e and 26f). It occurs as anhedral and subhedral disseminated grains and coarse-grained interstitial mass within the silicates (Figs. 26e and 26f). Anhedral and subhedral disseminated chalcopyrite occurs within clinopyroxene, quartz, epidote, and plagioclase (Fig. 26f). Interstitial chalcopyrite cements brecciated plagioclase (Fig. 26e).

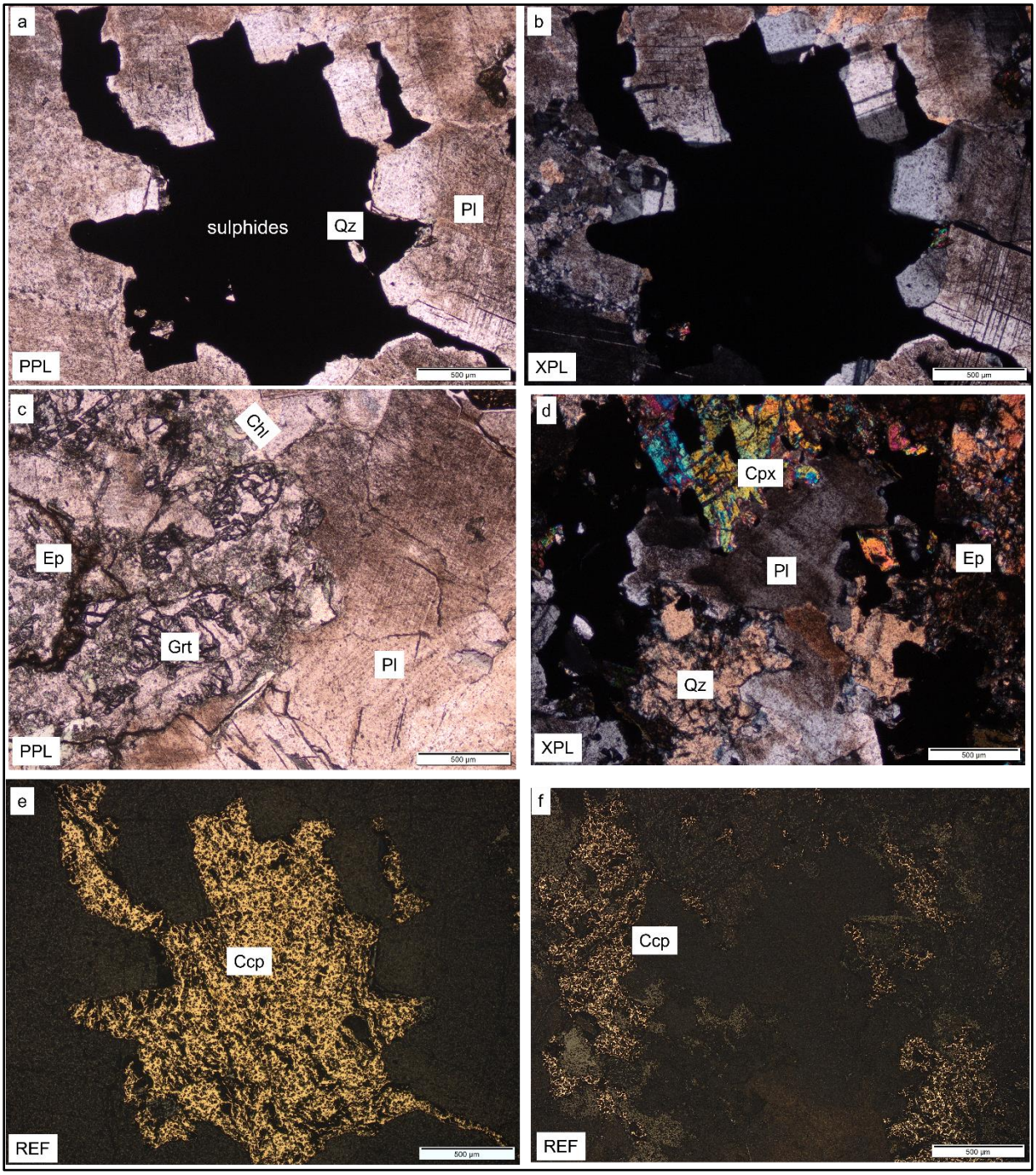


Figure 26: Photomicrograph showing: (a-b) interconnected plagioclase (Pl) grains enclosing interstitial opaque minerals; (c) a curvy epidote vein cuts fractured garnet (Grt) intergrown with plagioclase and quartz. The garnet is weakly altered by pale green chlorite in places; (d) brecciated, corroded, and partially altered clinopyroxene (Cpx) and plagioclase intergrown with quartz. Epidote (Ep) aggregates partially altered and replaced plagioclase and clinopyroxene; (e) interstitial chalcopyrite (Ccp) cementing plagioclase; (f) subhedral and anhedral disseminated chalcopyrite within corroded gangue minerals. Magnification scale = 500 µm.

Sample P677

About 45 vol% of the sample is dominated by clear secondary quartz that occurs as large, elongated, anhedral (slabby), subhedral, and subrounded grains. Plagioclase (20 vol%), elongated biotite (15 vol%), fractured garnet (10 vol%), and amphibole grains (<5%) form the matrix of the sample. Sericite (20%) and chlorite (15 vol%) alters the country rock mineral assemblages. The sample does not contain opaque minerals.

Relatively small (1 mm), clear, subhedral, and subrounded quartz grains are distributed and overprinted on large, fractured garnet (Figs. 27a and 27b). In other parts, plagioclase grains (multiple twinning) are surrounded by elongated biotite and subhedral amphibole grains, which are also overprinted by subrounded quartz grains (Figs. 27c and 27d). Fine-grained sericite partially alters and replaces plagioclase grains (Figs. 27a and 27b). Anomalous blue chlorite also alters biotite grains partially (Figs. 27c and 27d). In Figs 27c and 27d, a thin fracture cut through plagioclase and amphibole grains, and contains no cement. Another anomalous blue chlorite has almost completely altered and replaced garnet grains, which occurs as brecciated inclusions within it (Figs. 27e and 27f). The chlorite also contains inclusions of elongated biotite (Figs. 27e and 27f). Moreover, elongated, anhedral (slabby), and small subrounded quartz grains overprint chlorite (Figs. 27e and 27f).

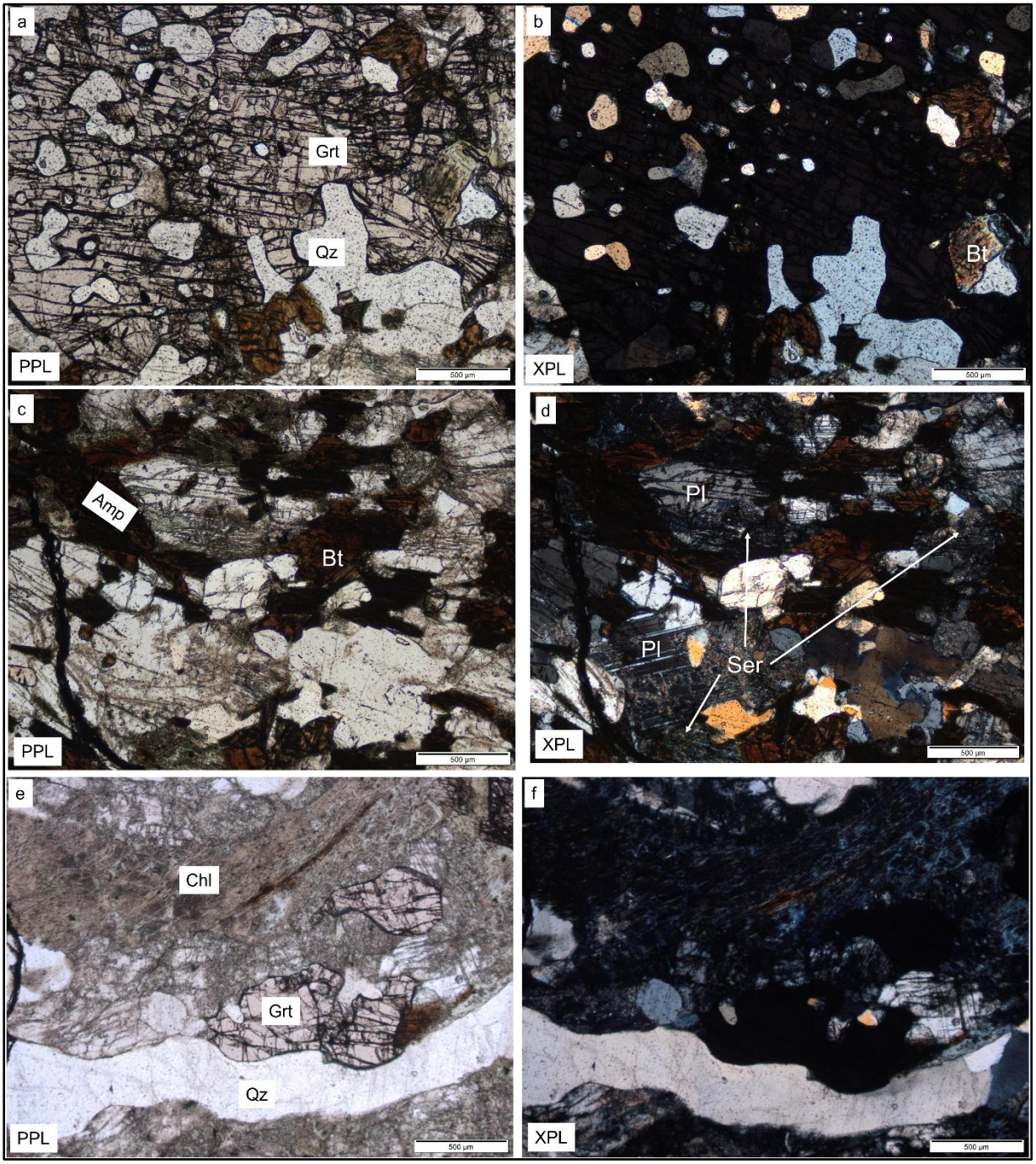


Figure 27: Photomicrographs showing: (a-b) relatively small (1 mm) amorphous and subrounded quartz (Qz) grains overprinting large, fractured garnet (Grt); (c-d) biotite (Bt) and amphibole (Amp) grains surrounding partially sericitized (Ser) plagioclase (Pl) grains. Biotite grains are partially altered and replaced by anomalous blue chlorite (Chl). Subrounded quartz grains overprint altered plagioclase, biotite, and amphibole grains. Uncemented fracture cuts through plagioclase and amphibole grains; (e-f) anomalous blue chlorite mass altered and replaced garnet and contains inclusions of fragmented garnet and biotite. Elongated slabby quartz with smaller subrounded quartz grains overprinting chlorite. Magnification scale = 500 µm.

Sample P740

This sample is dominated by epidote aggregates (45-50 vol%), small-large subhedral quartz grains, thin veins (30 vol%), and elongated prismatic and subhedral amphibole grains (15 vol%) with minor presence of opaque minerals (<5%). The sample represents altered and epidotised country rock.

Epidote aggregates and subhedral amphibole relics are cemented by subhedral secondary quartz 1 (Figs. 28a to 28d). Some epidote grains occur as inclusions within quartz 1 grains and between the elongated prismatic amphibole grains (Figs. 28a to 28d). In other places, thin discontinuous veins of secondary quartz 2 cut through epidote aggregates and occur between elongated amphibole grains (Figs. 28c and 28d). Some amphibole grains are weakly altered and replaced by epidote aggregates (Figs. 28b and 28d). There are subrounded and irregular opaque spots within epidote aggregates and amphibole grains in some parts (Figs. 28a and 28b).

The inclusions of opaque minerals within epidote aggregates and amphibole grains are subhedral magnetite (Figs. 28e and 28f).

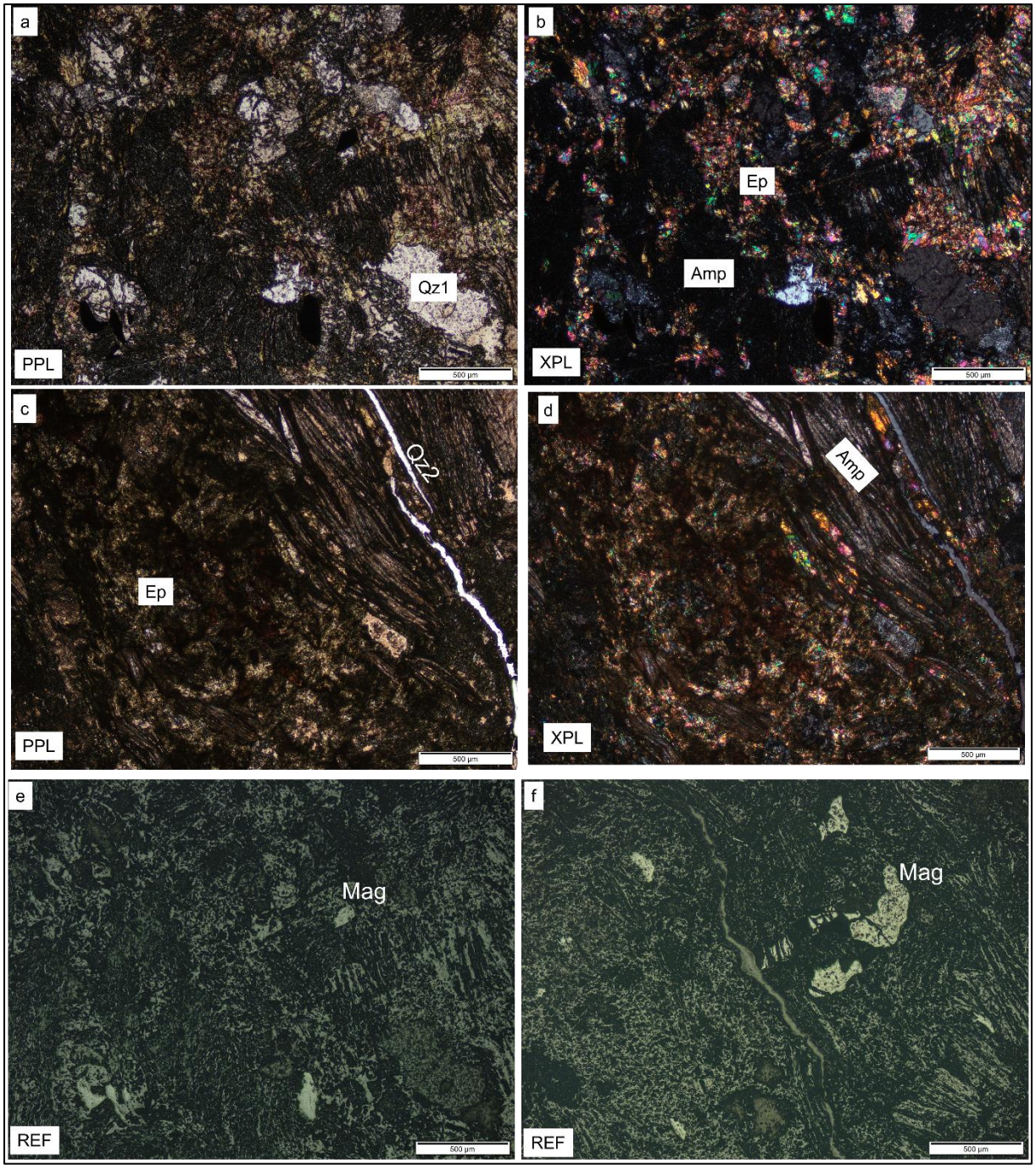


Figure 28: Photomicrographs showing: (a-b) epidote (Ep) aggregates enclose and partially alter subhedral amphibole (Amp) grains. Subhedral secondary quartz 1 cements epidote aggregates and amphibole relics. Some epidote grains are included within quartz 1; (c-d) discontinuous thin veins of secondary quartz 2 cuts through epidote aggregates and occur between elongated amphibole prismatic grains; (e-f) subhedral magnetite grains within epidote and amphibole grains. Magnification scale = 500 µm.

5.2 SEM-EDS (TIMA) analysis

Selected samples were analysed to produce mineral and elemental maps by TIMA (refer to Table 2). This includes trace elements associated with the sulphide and oxide minerals of Messina Cu deposit. Textural, mineralogical, and compositional information varies considerably in the samples. Of particular interest is the ability of TIMA to show clear textural relationships and identify fine textures of composite minerals.

Sample 19068

The distribution of mineral assemblages of this sample shows abundant gangue minerals, such as quartz, chlorite-clinochlore (Mg-rich), and chlorite-chamosite (Fe-rich), associated with massive bornite (Fig. 29). Petrographically, the two chlorite minerals can be distinguished by different colours: Mg-rich chlorite-clinochlore is pale green in PPL, while Fe-rich chlorite-chamosite is brownish-yellow in PPL (e.g., Figs. 8c and 8e). Quartz forms small-large discrete subhedral and angular grains enclosing chlorite and Cu sulphides (Fig. 29a). It also occurs in association with iron oxides as a discontinuous vein cutting through magnetite laths (Figs. 29a and 29b). Kaersutite is designated to amphibole relics that were present within chlorite groundmass using optical microscopy (refer to Appendix A1). Pyrope could be related to the completely altered and replaced garnet by chlorite. The unclassified material could be related to polishing pits seen during petrographic observations (refer to Appendix A3).

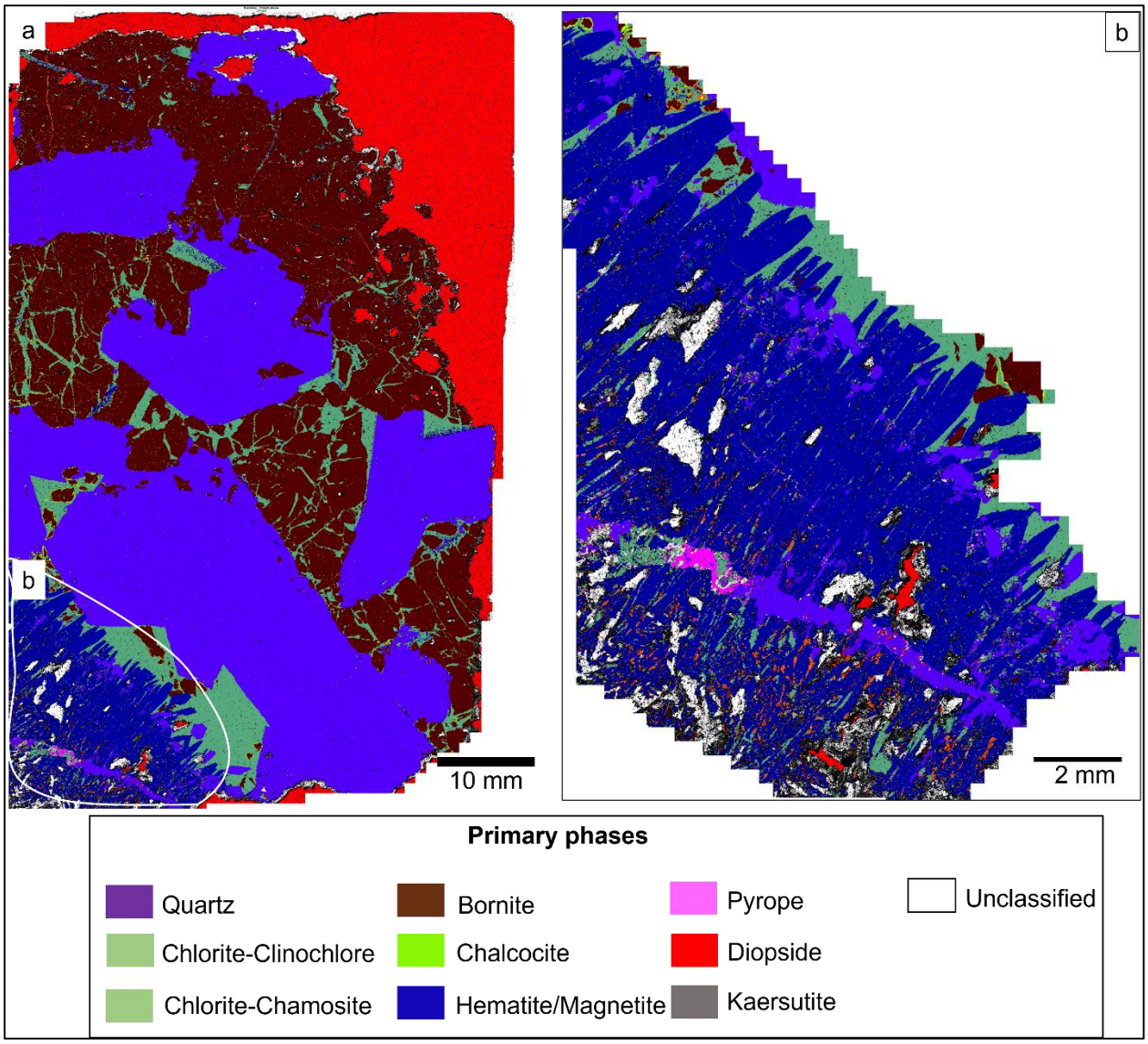


Figure 29: Phase maps showing detected minerals in sample 19068: (a) Full scan phase map; (b) high-resolution phase map.

The high-resolution imaging used in the investigation of trace elements associated with Cu sulphides and iron oxides shows magnetite laths with some intergrown with the Cu sulphides (Fig. 29b). Copper and S are more concentrated in copper sulphides (bornite, chalcocite; Figs. 30b and 30c). On the other hand, high Fe concentrations are associated with Fe-oxides than copper sulphides (Fig. 30b). There also

exists elevated Co content in association with Fe-oxides (Fig. 30e). There is no association of tin (Sn) with Fe-oxides or Cu sulphides (Fig. 30f). Traces of slightly elevated Sn concentration occur within some parts of the quartz vein, where altered pyrope occur and between magnetite laths in chlorite.

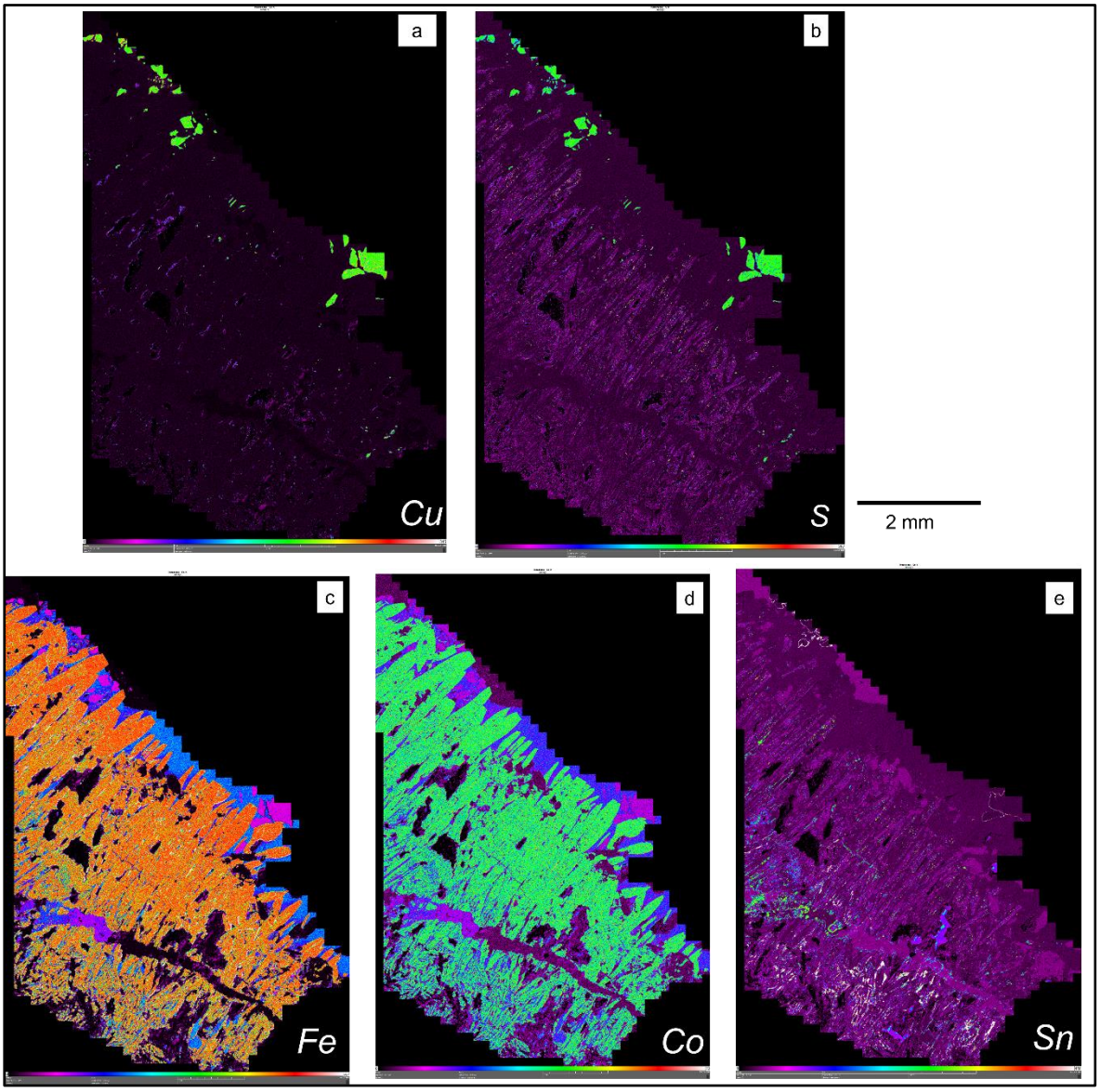


Figure 30: (a-e) Elemental maps of the selected area showing concentrations of Cu=copper, S=sulphur, Fe=iron, Co=cobalt, and Sn=tin in sample 19068 copper sulphides and iron oxides.

Sample 19077

This sample is dominated mainly by quartz associated with chlorite and diopside (clinopyroxene) (Fig. 31b). This corroborates with petrographic observations (Fig. 31a), except that the amphibole observed in petrography (see Fig. 11b) was not identified by TIMA. The interstitial diopside seen intergrown with chlorite was not observed in optical microscopy (Fig. 31b elongated red coloured minerals). Tiny inclusions of pyrope and almandine-spessartine (garnet) occur within granular chlorite. This chlorite also envelopes sulphides in other parts. However, this was not observed in optical microscopy. The unidentified minerals appeared as cloudy and black holes in optical microscopy and were not classified.

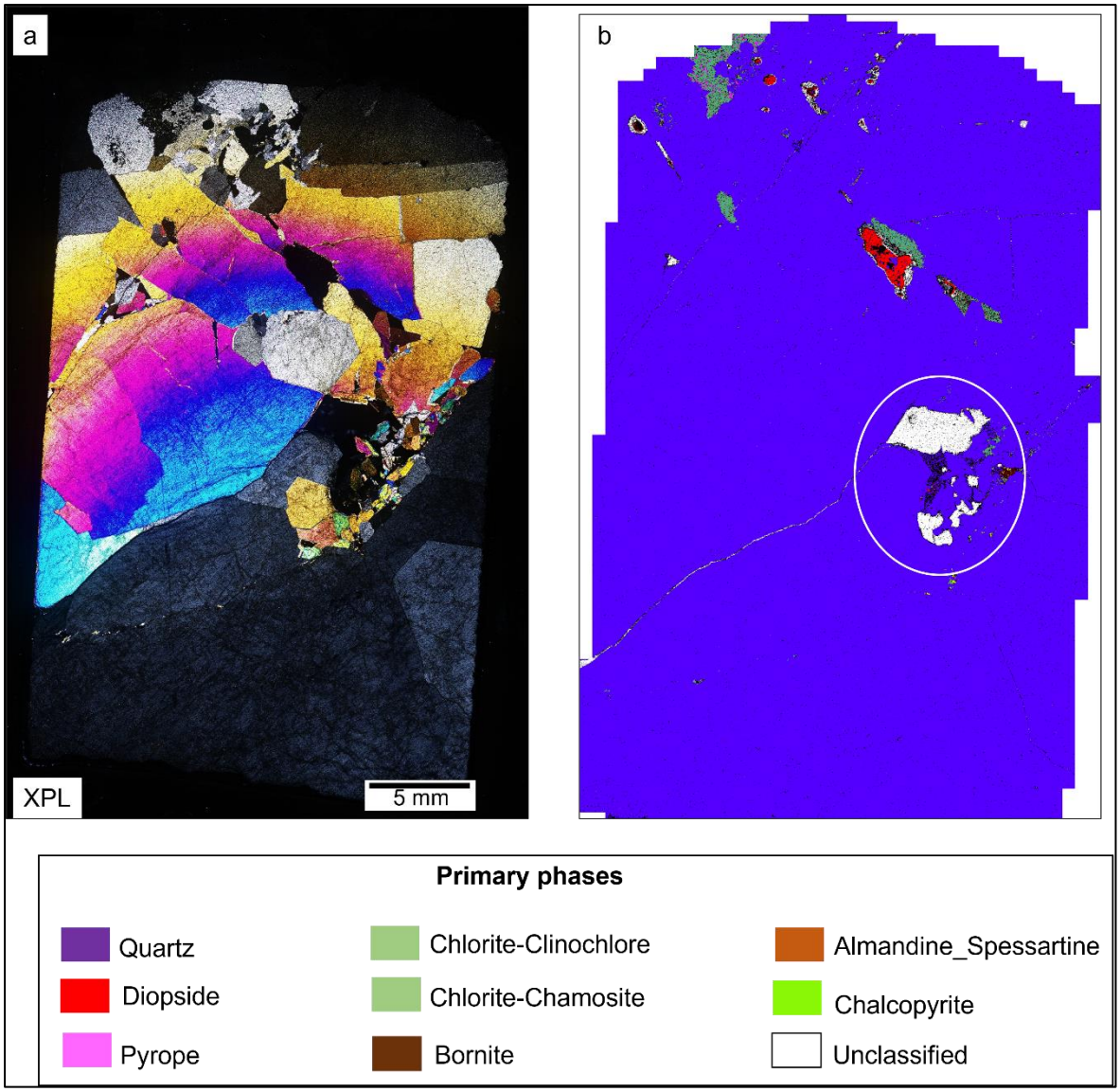


Figure 31: (a) Full scan image for sample 19077 under transmitted light; (b) Phase map showing detected minerals.

A phase map of the selected area for high-resolution imaging (white circle in Fig. 31b) shows presence of bornite and chalcocite closely associated with quartz and chlorite (Fig. 32). The pyrope tiny grains regions that appear like plugged out mineral grains (shades of black) were not observed in optical microscopy. Instead, disseminated chalcocite was observed in this region. Chalcocite also occurs partly within and along margins of bornite suggesting incipient replacement of bornite. These corroborate with optical microscopy observations. It is possible that TIMA was able to detect minute grains of covellite within chalcocite, though they could not be observed using optical microscopy.

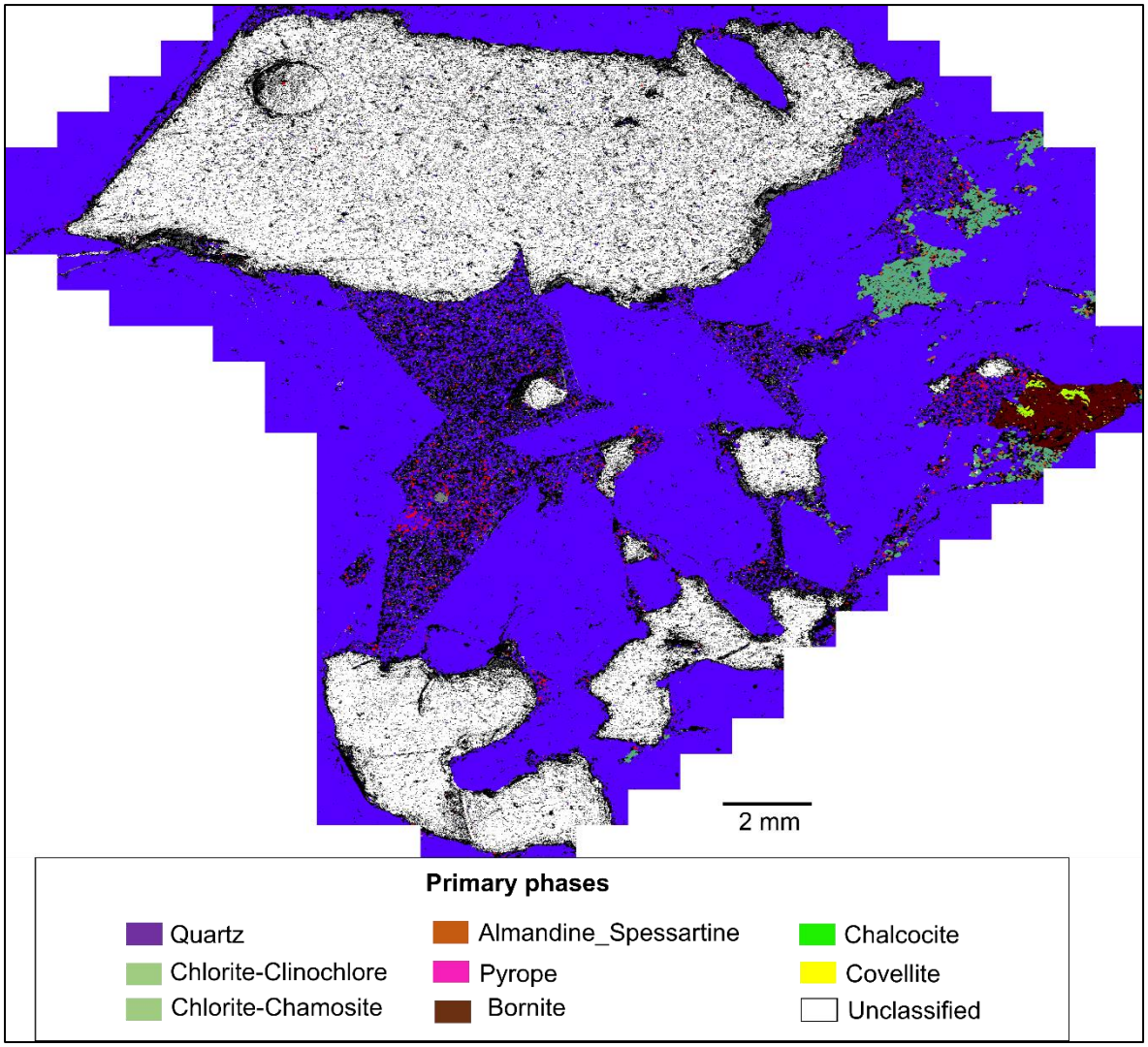


Figure 32: Phase map showing mineralogy of the selected area in sample 19077.

Elements that were detected in high concentrations are Cu and S, with low Fe for the copper sulphides (Figs. 33a, 33b and 33c). Cobalt is poorly associated with the copper sulphides as shown by very low concentrations within bornite and chalcocite (Fig. 33d).

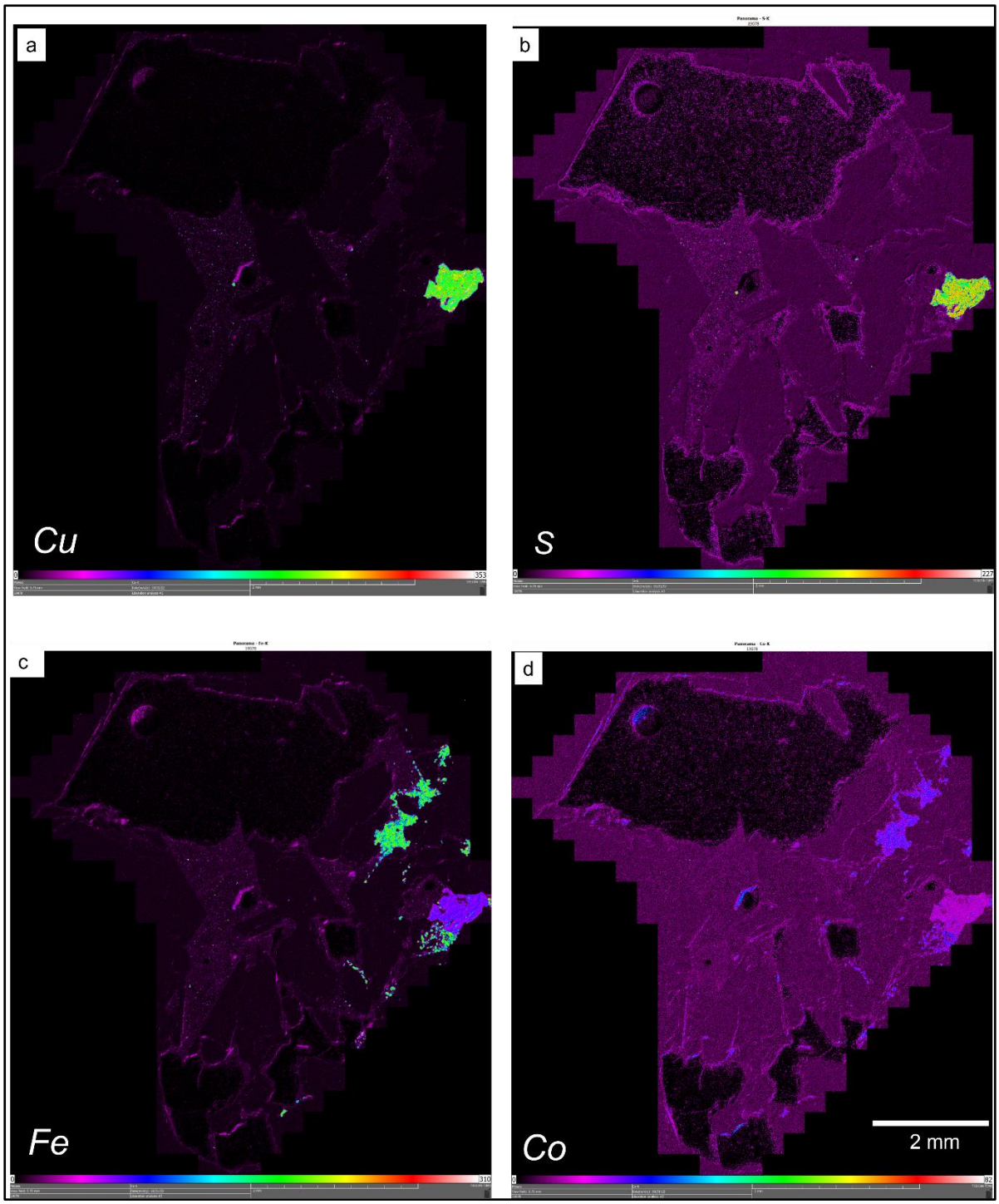


Figure 33: (a-d) Elemental maps showing concentrations of Cu=copper, S=sulphur, Fe=iron, and Co=cobalt in sample 19077 copper sulphides.

Sample P579

Transmitted and reflected light full scan images show abundant hypersthene (orthopyroxene) and subrounded plagioclase in association with massive pyrrhotite, minor pyrite and chalcopyrite (Figs. 34a and 34b), which corroborate with TIMA full scan phase map (Fig. 34c). Quartz was only observed as veins bordered by chlorite under optical microscopy and not grains as identified by TIMA (Fig. 34c, also Appendix B9). Some plagioclase grains contain inclusions of diopside grains (Fig. 34c). Identification of diopside is problematic as it was absent in optical microscopy. The alteration of plagioclase by muscovite (Fig. 34a cloudy plagioclase grains) that was observed under optical

microscopy is absent in TIMA (Fig. 34c). Gangue minerals, sulphides, and oxides consistent with petrographic observations include hypersthene, plagioclase, chlorite, quartz veins, biotite, pyrrhotite, pyrite, chalcopyrite, and magnetite. The latter occurs within chlorite veins that border orthopyroxene and massive pyrrhotite (refer to Appendix B9).

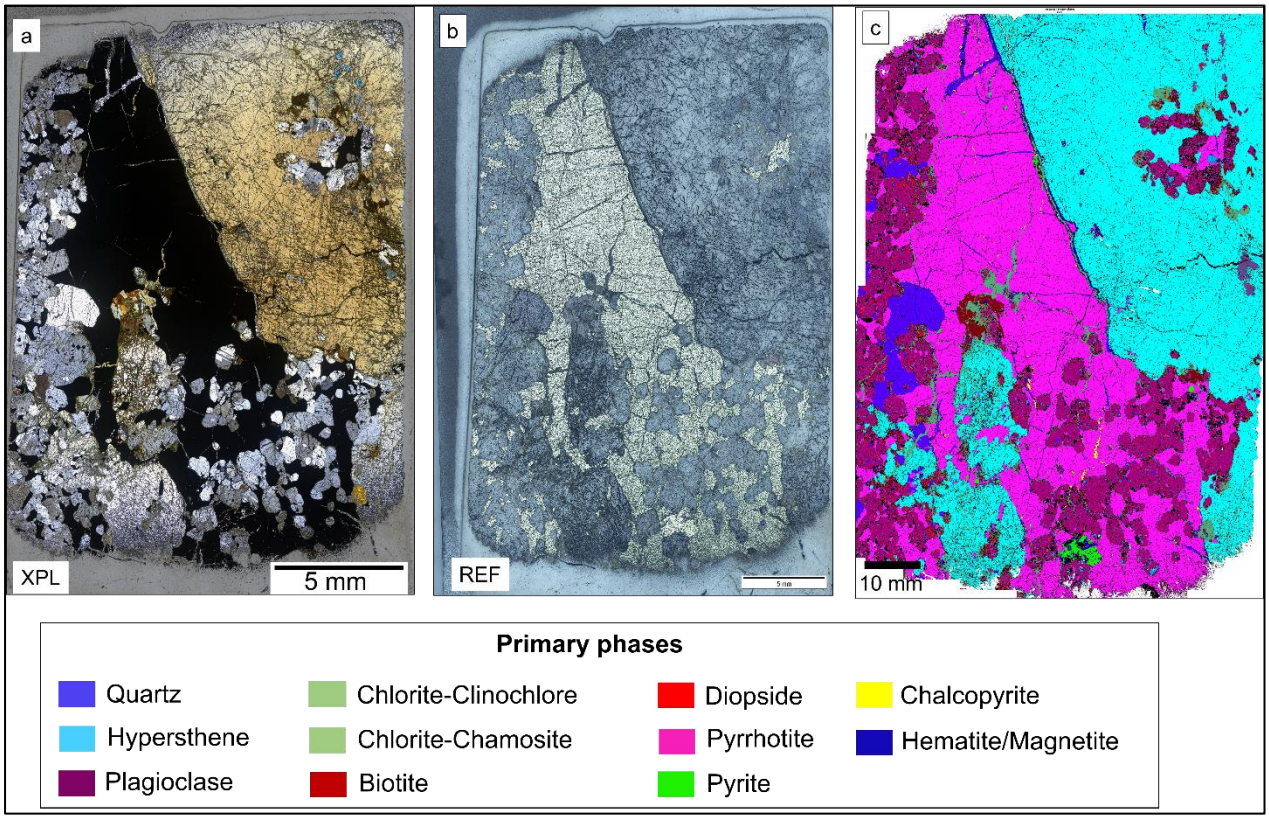


Figure 34: (a-b) Transmitted and reflected light full scan images for sample P579; (c) Phase map showing the detected minerals.

Full scan image under reflected light is shown in Fig 34b and is made up of a thick (~2 cm) vein and disseminated sulphides. For sulphides, Cu is concentrated in interstitial chalcopyrite (Fig. 35a). Sulphur and Fe are strongly concentrated in pyrrhotite and pyrite, and probably magnetite in chlorite veins (Figs. 35b and 35c). No zinc was found to be associated with the sulphides (Fig. 35d). There is elevated Co concentration associated with pyrrhotite and pyrite (Fig. 35e). Figure 35e also shows Co concentration in hypersthene. It is not obvious to see Co concentration in association with magnetite in chlorite veins as they are thin.

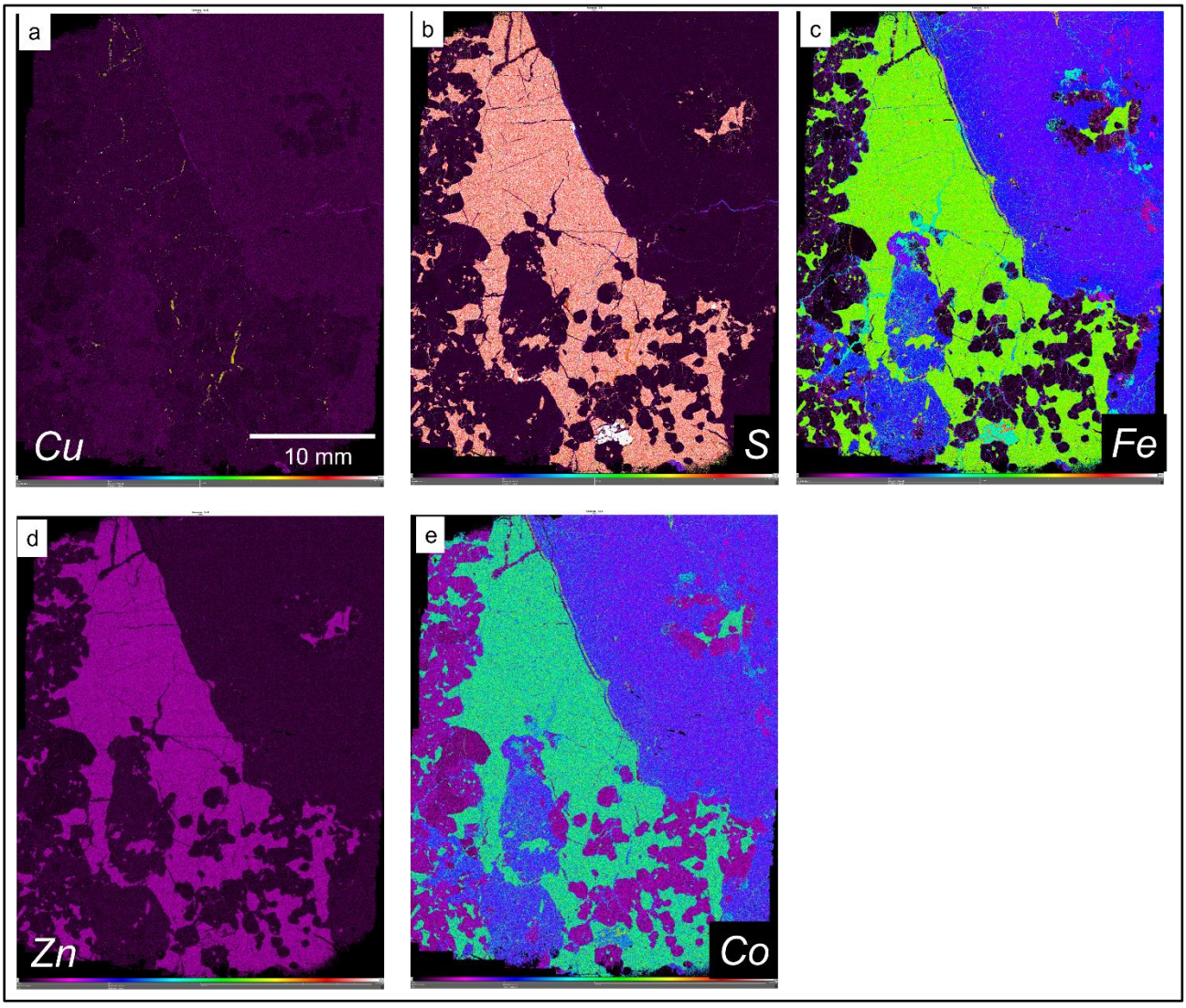


Figure 35: (a-e) Elemental maps showing concentrations of Cu=copper, S=sulphur, Zn=zinc, Fe=iron, and Co=cobalt in sample P579 sulphides and iron oxides.

Sample P774

A full scan transmitted light image shows abundant sub-anhedral quartz grains with interstitial dusty sericite, and dark green chlorite in the country rock and a thick micro-brecciated vein containing mostly epidote, minor quartz, and dark greenish black mafic mineral (probably amphibole) (Fig. 36a). On the other hand, TIMA phase map shows the sample is dominated by albite, quartz, and chlorite cut by a vein of zoisite, quartz, kaersutite, and chlorite (Fig. 36b). Identified muscovite (sericite) inclusions within albite by TIMA do not coincide with optical microscopy observations, as sericite was observed in the region where albite occurs and not as inclusions (Fig. 36a, see Fig. 21c). Additionally, zoisite was detected as the only epidote group mineral, even though epidote was also present in optical microscopy. Covellite was also not observed petrographically. Instead, optical microscopy identified the following minerals: chlorite, quartz, sericite, chalcopyrite, bornite, chalcocite, and hematite. Chlorite only occurred in the country rock and within the mineralised epidote vein in optical microscopy (also Fig. 36a). Kaersutite represents amphibole relics that were present within epidote aggregates using petrographic microscopy.

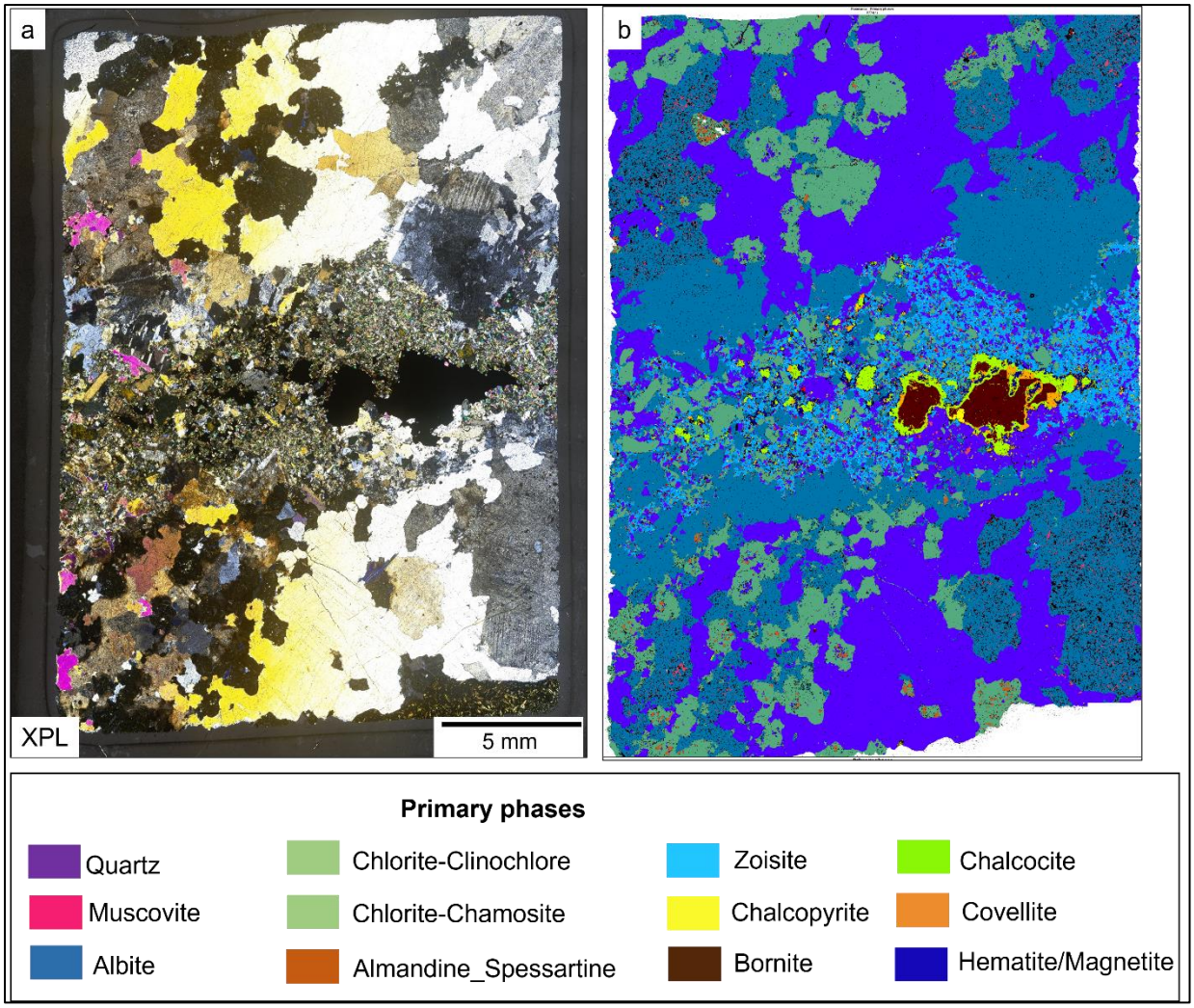


Figure 36: (a) Transmitted light full scan image for sample P774; (b) Phase map showing detected minerals.

Reflected light full scan image shows the selected area for trace elements analysis (Fig. 37a, white circle). Under high-resolution, covellite that was identified in the full scan phase map (Fig. 36b) is not identified (Fig. 37b). Hematite/magnetite is seen along what looks like fractures within chalcocite, as well as around it as a rim. Under optical microscopy, hematite was only seen as a rim around chalcocite (see Fig. 21d). Chalcopyrite replacement by bornite, and chalcocite rim around the Cu sulphides corroborate with optical microscopy observations (Figs. 37a and 37b). However, chalcopyrite disseminations within the epidote aggregates and quartz grains were not observed under optical microscopy (Fig. 37b). Instead, only chalcocite disseminations were observed (Figs. 37a and 37b).

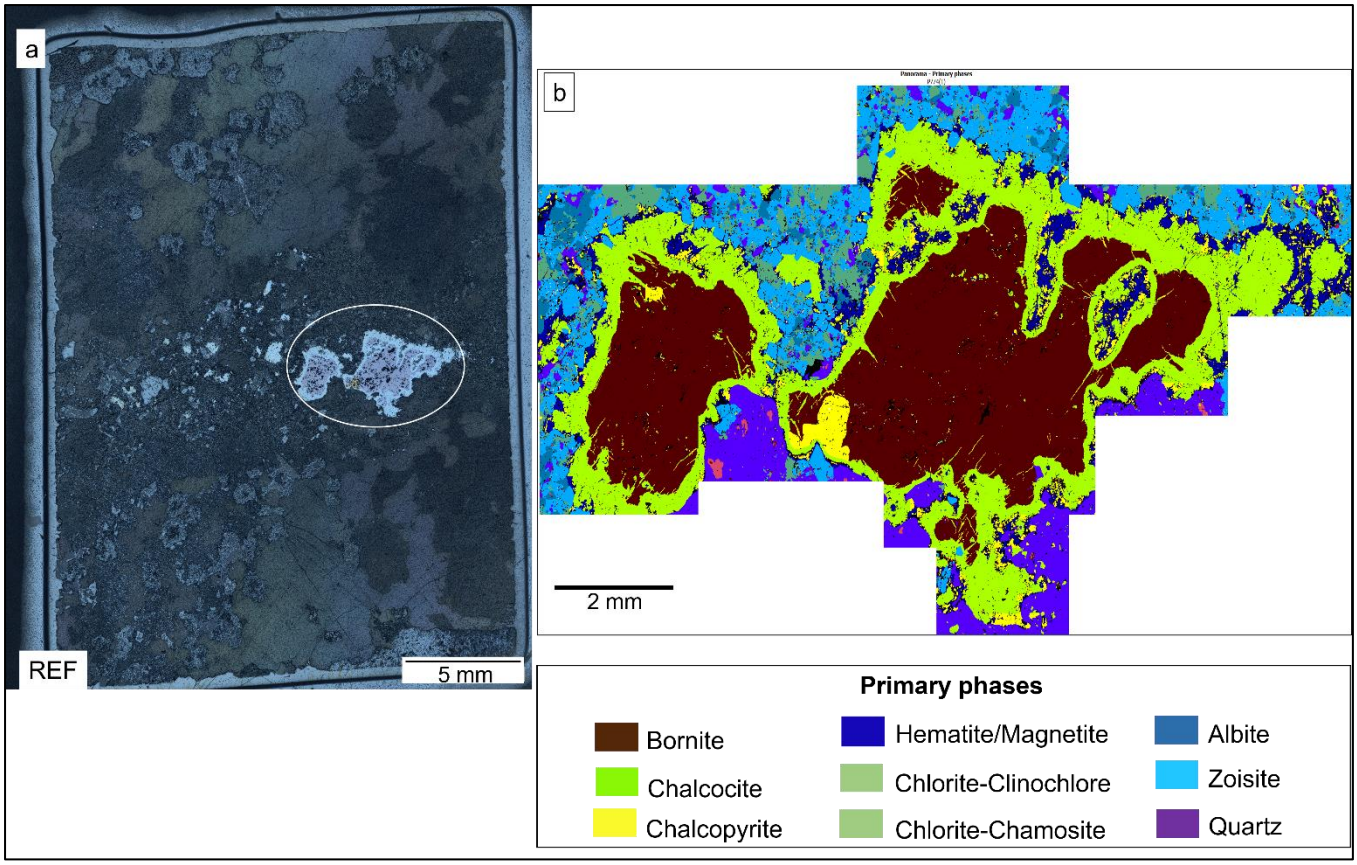


Figure 37: (a) Full scan image under reflected light for sample P774; (b) Selected area (white circle in a) for high-resolution TIMA imaging.

The copper sulphides show inverse relationship for Cu and S concentrations with strong Cu concentrations in chalcocite > bornite > chalcopyrite, and vice versa for S concentrations (Figs. 38a and 38b). These Cu-sulphides also show Fe concentrations inversely related to Cu and S with only chalcopyrite showing slightly elevated concentrations (Fig. 38c). Iron-oxides, on the other hand, have elevated Fe concentration (Fig. 38c). Zinc is poorly concentrated in Cu sulphides and Fe-oxides (Fig. 38d). Distribution of Sn is not associated with Cu sulphides/iron oxides, but gangue minerals within the vein (Fig. 38e). Elevated Co concentration is mostly associated with iron oxides (Fig. 38f).

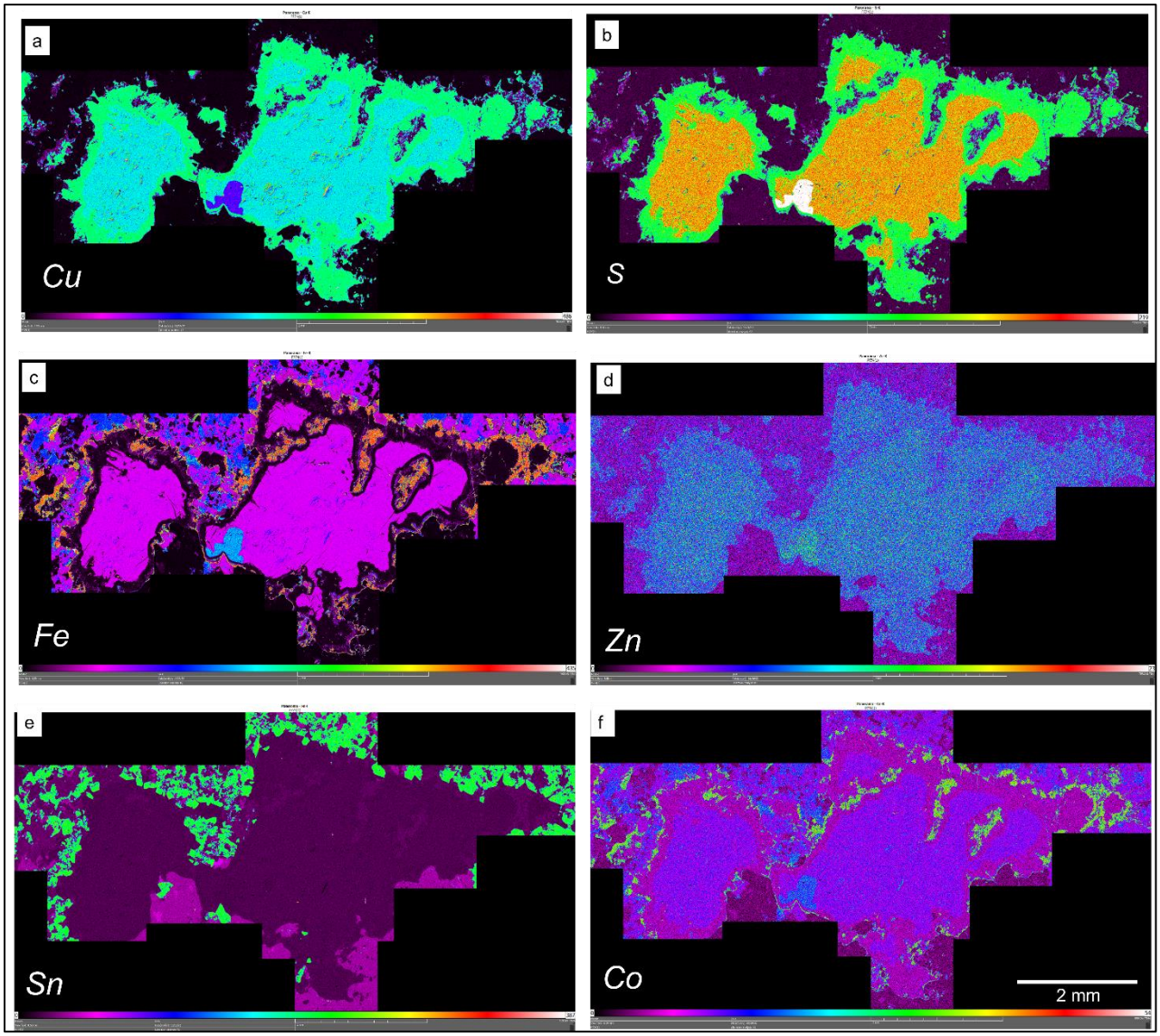


Figure 38: (a-f) Elemental maps showing concentrations of Cu=copper, S=sulphur, Zn=zinc, Fe=iron, Sn=tin, and Co=cobalt in sample P744 sulphides and iron oxides.

Sample P817

Here, a thick quartz vein is in contact with brecciated country rock and is penetrated by irregular grains of the brecciated country rock fragments (Figs. 39a and 39b). For Fig 39a, optical microscopy identified the following country rock mineral assemblages: amphibole, clinopyroxene, garnet, plagioclase, biotite, sericite, and chlorite. TIMA phase map identified kaersutite (amphibole), almandine-spessartine (garnet), grossular (garnet), biotite, diopside (clinopyroxene), chlorite, albite, plagioclase, and zoisite (Fig. 39b). These corroborate with optical microscopy observations, however, zoisite was not observed in optical microscopy and sericite is not prominent in TIMA.

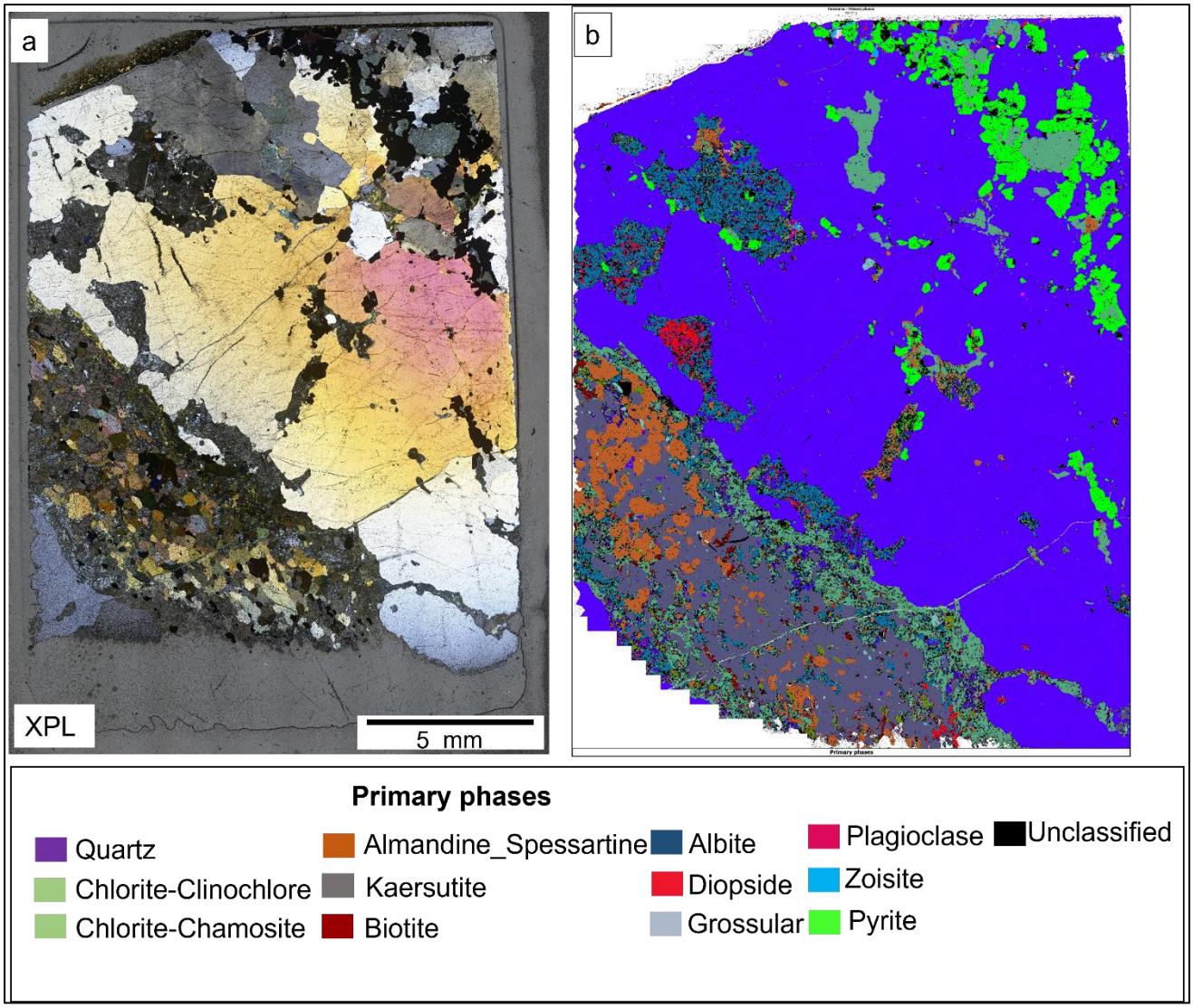


Figure 39: (a) Full scan image under transmitted light; (b) TIMA phase map showing detected minerals in sample P817.

The selected area for trace elements association consists of a train of clustered pyrite (Figs. 40a and 40b). The pyrites are enclosed within the quartz vein and are overprinted by chlorite (Figs. 40a and 40b). Magnetite inclusions within porous pyrite grains were also observed using optical microscopy.

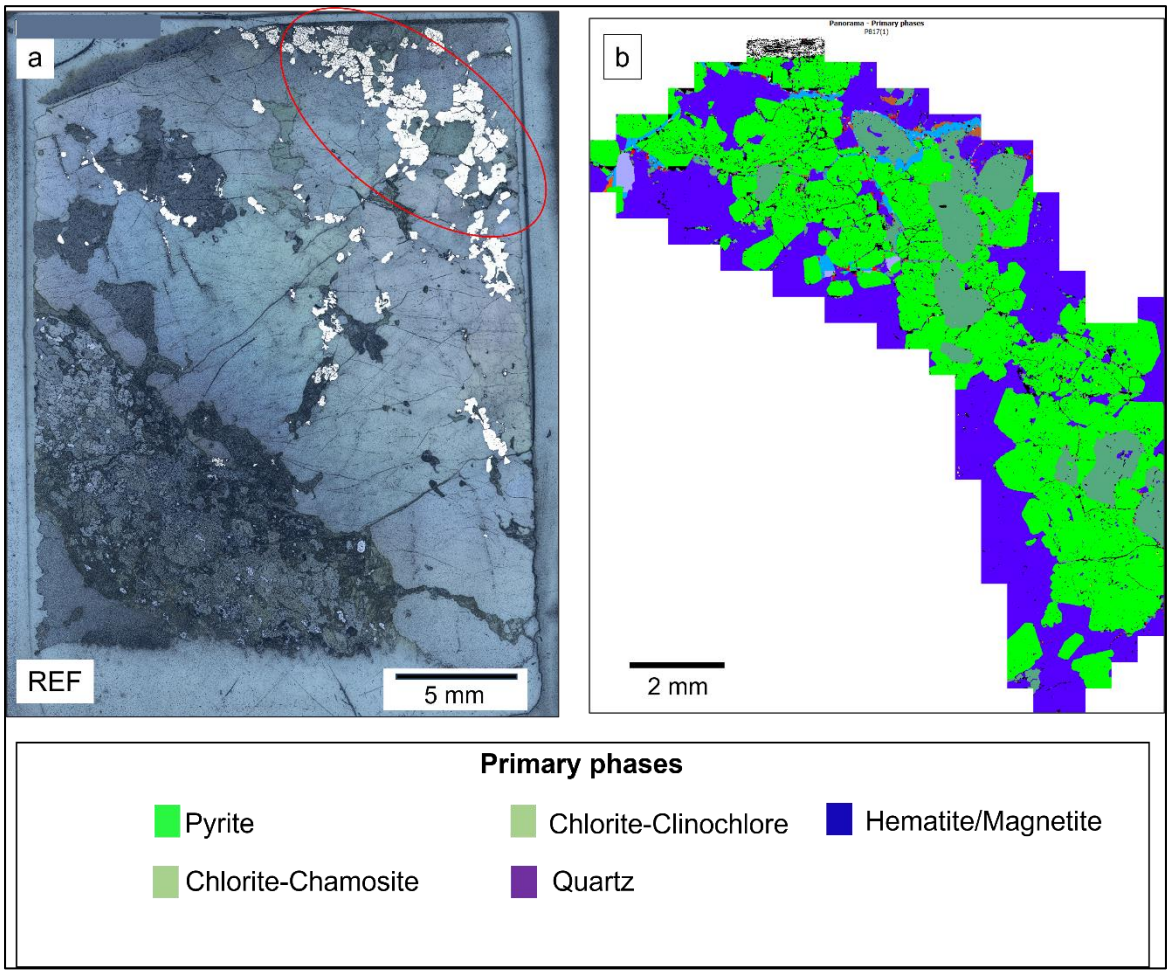


Figure 40: (a) Full scan image under reflected light for sample P817; (b) TIMA phase map showing the selected area for high-resolution imaging (area circled red in a).

The area selected for analysis of trace elements associated with pyrite reveal no Cu concentration as was expected (Fig. 41a). Sulphur and Fe are strongly concentrated within pyrite (Figs. 41b and 41c). It is believed that magnetite inclusions also play a role in the elevation of Fe concentration. There is elevated Zn concentration and low Co concentrations associated with pyrite (Figs. 41d and 41e, respectively).

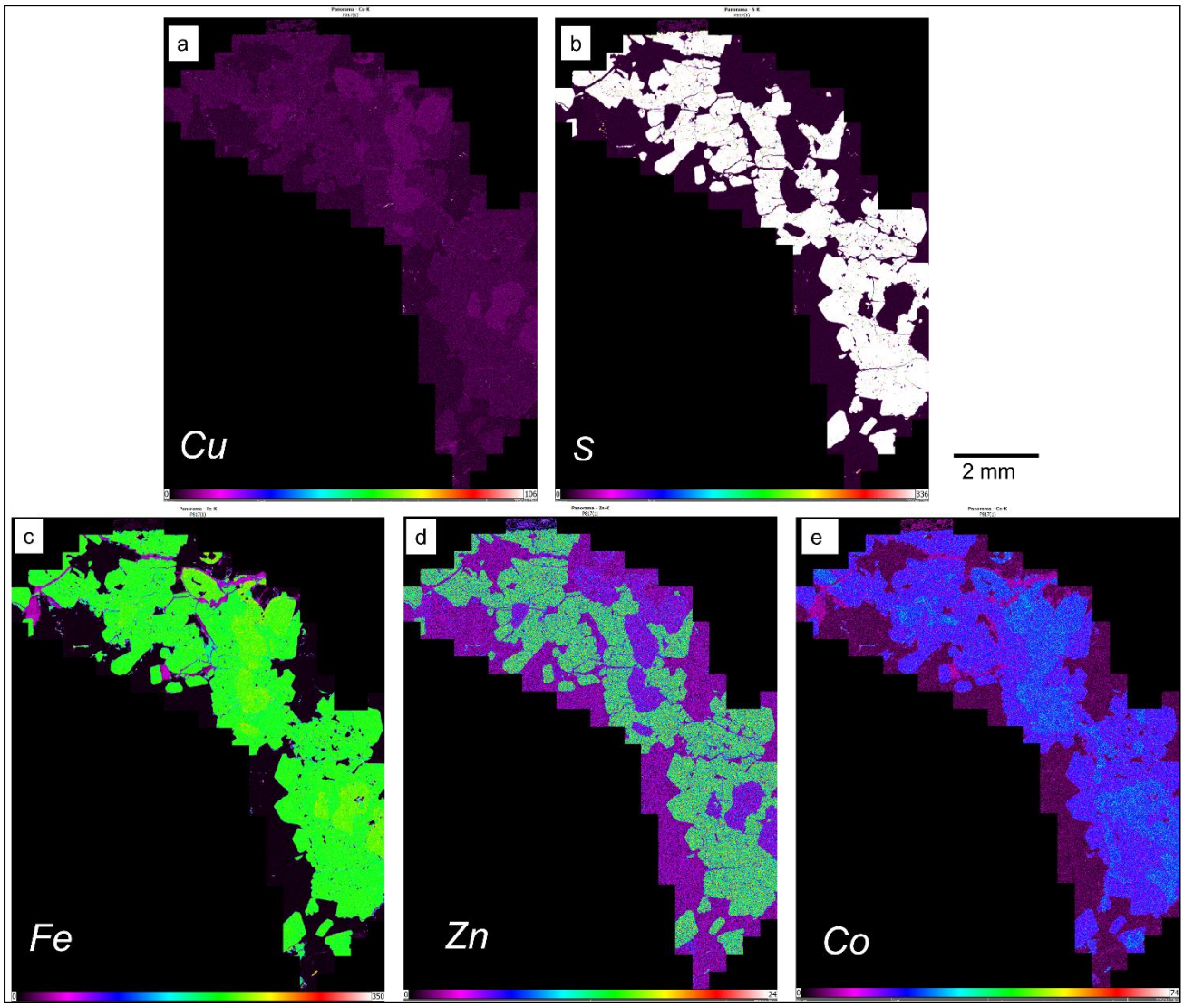


Figure 41: (a-e) Elemental maps showing concentrations of Cu=copper, S=sulphur, Fe=iron, Zn=zinc, and Co=cobalt in sample P817 iron sulphides and oxides.

Sample P782

The silicate minerals in the full scan images under transmitted and reflected light corroborate with those identified by TIMA phase map (Figs. 42a-42c). These include quartz, muscovite (sericite), biotite, almandine-spessartine (garnets), and chlorite (Figs. 42a and 42c). The albite identified by TIMA was found to be sericite and individual albite grains were absent in optical microscopy (not the case in Fig. 42c). Detected sulphides by TIMA imaging (pyrite and chalcopyrite) are also consistent with optical microscopy and reflected light image (Figs. 42b and 42c). However, molybdenite remained undetected by TIMA.

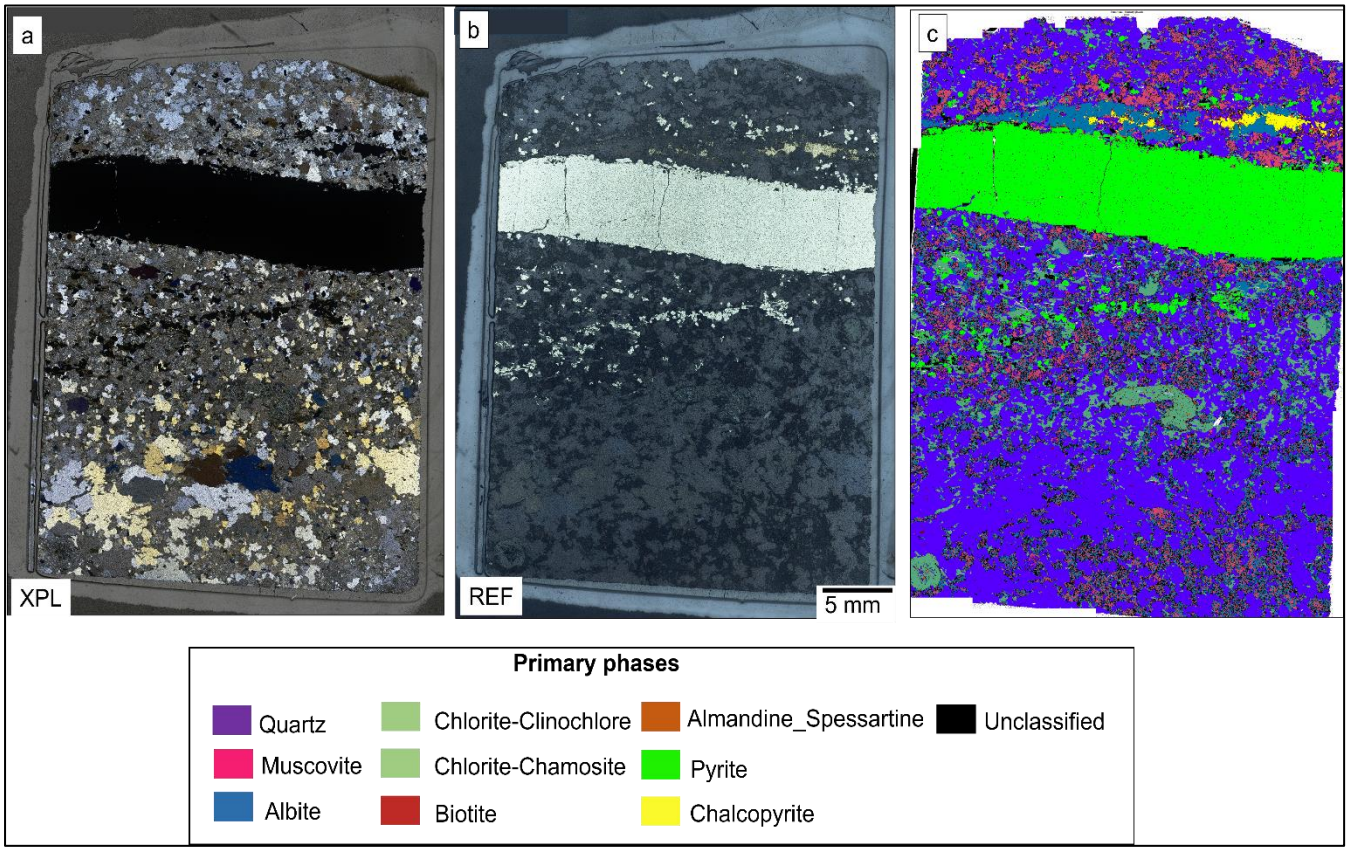


Figure 42: (a-b) Full scan images under transmitted and reflected light for sample P782; (b) TIMA phase map showing detected minerals.

For the sulphides present, Cu is abundant in chalcopyrite (Fig. 43a). Sulphur concentrations vary with respect to chalcopyrite and pyrite, whereby it is concentrated strongly in pyrite compared to chalcopyrite (Fig. 43b). Elevated Fe concentrations are shown in both pyrite and chalcopyrite (Fig. 43c). Both sulphides have no significant association with Zn but show low concentrations of Co (Figs. 43d and 43e, respectively). Figure 43e also shows that Co is poorly distributed within the silicates (especially associated with chlorite).

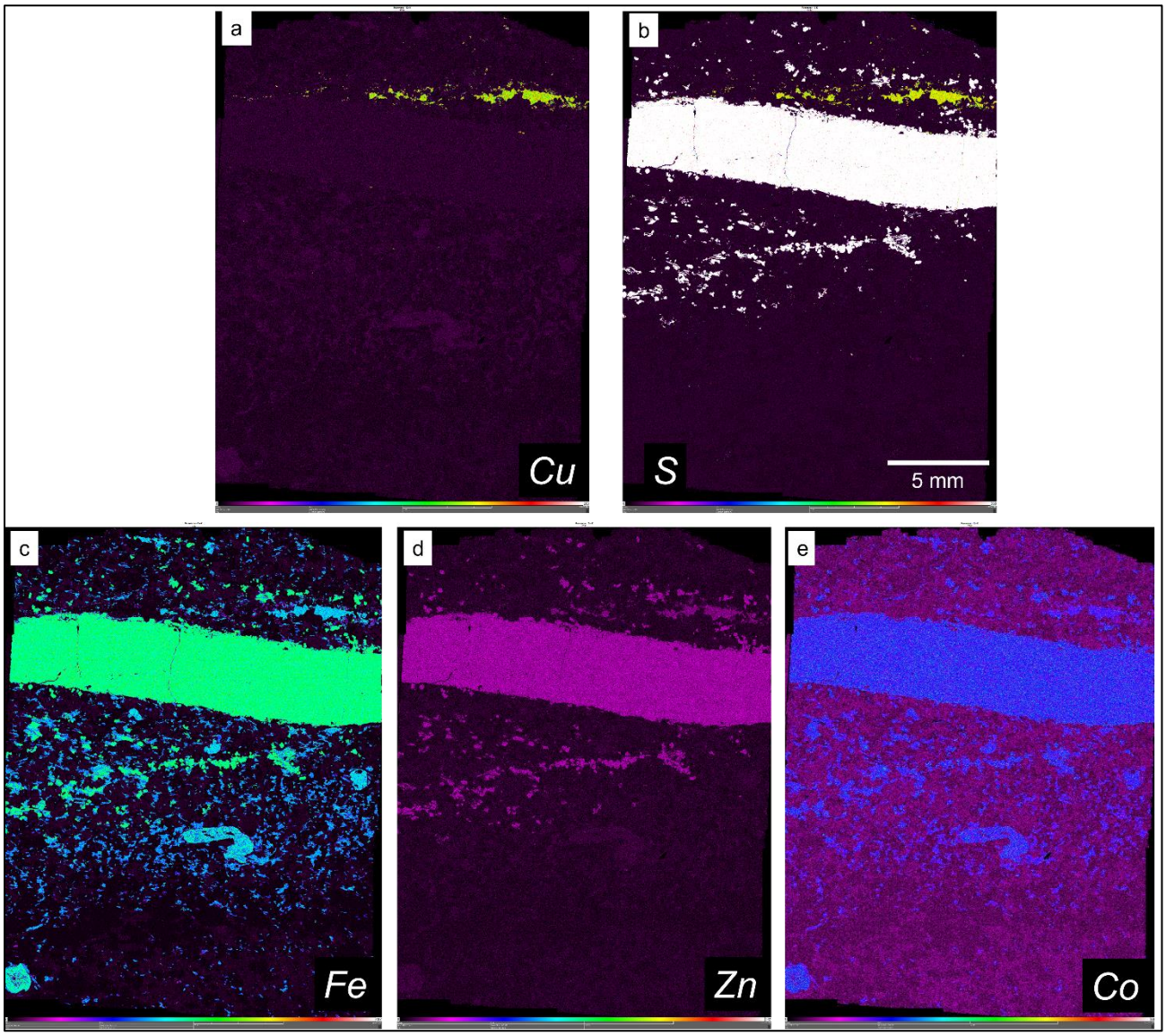


Figure 43: (a-e) Elemental maps showing concentrations of Cu=copper, S=sulphur, Fe=iron, Zn=zinc, and Co=cobalt in sample P782 iron and copper sulphides.

Sample P613

Albite constitute a large portion of this sample (Figs. 50a and 50c). Zoisite textures in association with diopside, albite, and quartz coincide with those observed using optical microscopy, but zoisite was identified as epidote. Chalcopyrite is the only observed Cu sulphide mineral seen in the full scan reflected light image and TIMA imaging (Figs. 44b and 44c).

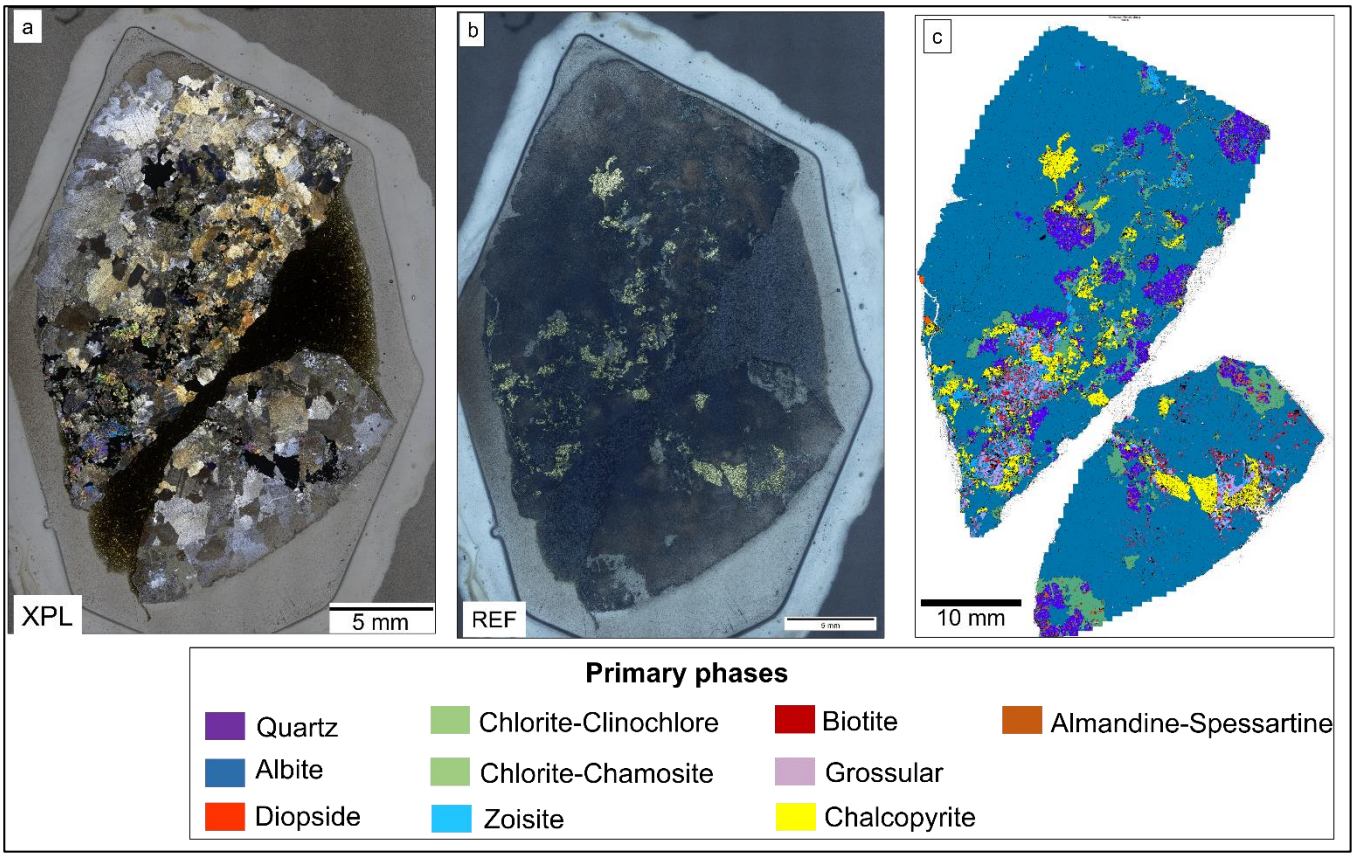


Figure 44: (a-b) Full scan images under transmitted and reflected light for sample P613; (c) TIMA phase map showing detected minerals.

With chalcopyrite being the only Cu sulphide mineral, there are strong concentrations of Cu and S, and moderate Fe (Figs. 45a-45c). Cobalt is poorly concentrated within chalcopyrite and chlorite (Fig. 45d).

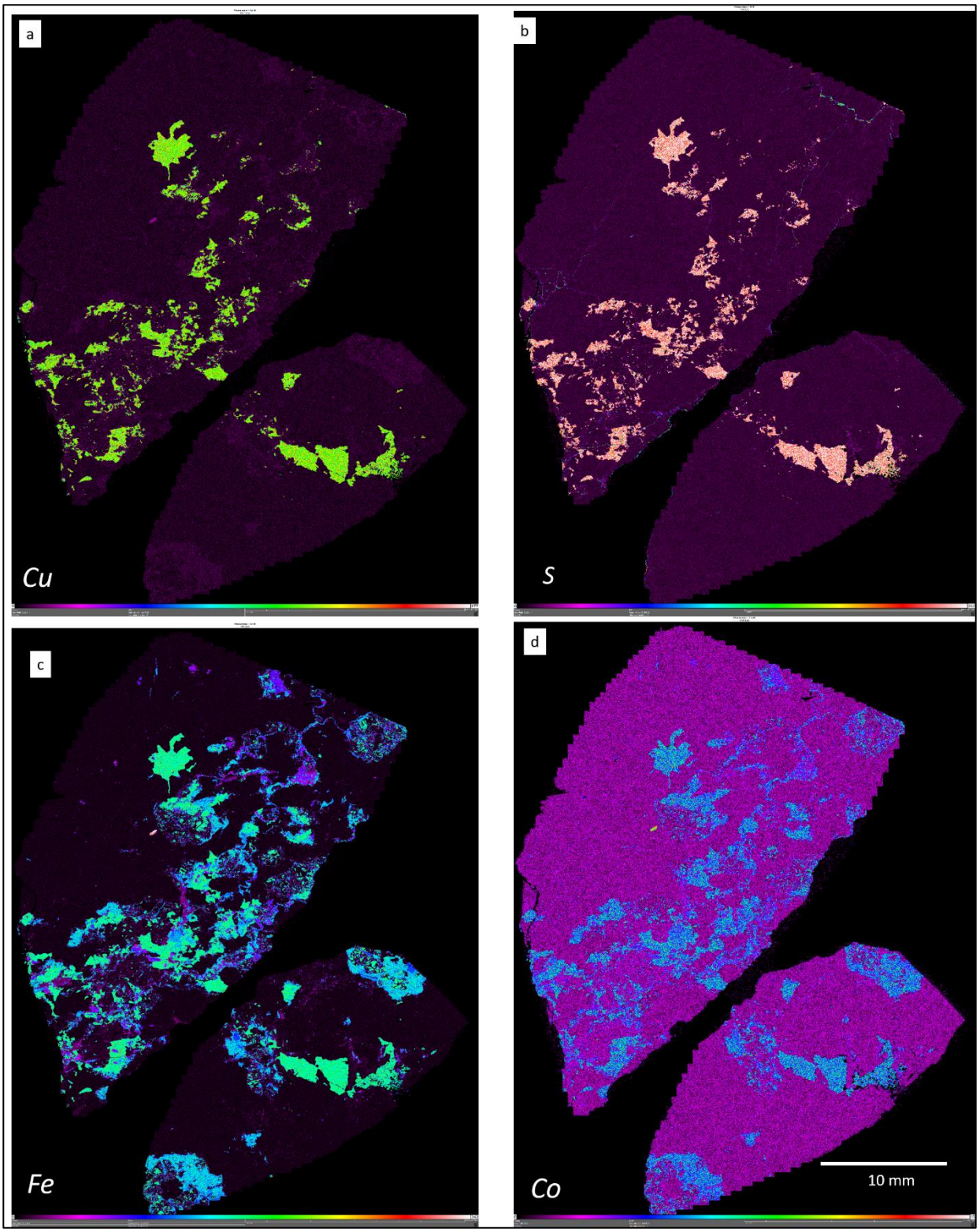


Figure 45: (a-d) Elemental maps showing concentrations of Cu=copper, S=sulphur, Fe= iron, and Co=cobalt in sample P613 copper sulphides.

6 Interpretation of the results

The petrographic observations revealed primary minerals of the country rock and secondary minerals formed by hydrothermal alteration (Table 2), as well as sulphide minerals and their associated iron oxide minerals (Table 3). Most silicate minerals that were detected using TIMA also coincide with petrographic descriptions (Table 4). TIMA was able to identify minerals that were completely altered and replaced by hydrothermal phases as tiny inclusions. In cases where a mineral could not be identified unambiguously due to polishing effects, TIMA assisted in confirming or assigning the correct mineral name (Figs. 29 and 32), as well as identifying end-member minerals (e.g., chlorite-chamosite, chlorite-clinochlore, garnet/epidote group minerals). Moreover, sulphides and iron oxides detected by TIMA were also observed in optical microscopy. However, molybdenite remained undetected by TIMA. Therefore, these results are helpful in understanding reaction processes that produced hydrothermal alteration and ore minerals, and thus, the composition of the hydrothermal fluid.

Table 2: List of the primary and secondary minerals observed in the samples

Sample ID	**Primary minerals**								**Secondary minerals**			
	Qz	Kfs	Bt	Pl	Grt	Amp	Opx	Cpx	Qz	Ser	Chl	Ep
19068									✓		✓	
19077						✓		✓	✓		✓	
19073									✓		✓	✓
19075									✓		✓	✓
19078									✓			✓
P580									✓	✓	✓	✓
P579			✓	✓			✓			✓	✓	
P774						✓			✓	✓	✓	✓
P814	✓	✓	✓	✓	✓				✓	✓	✓	✓
P817			✓	✓	✓	✓		✓	✓	✓	✓	
P782			✓		✓				✓	✓	✓	
P812		✓		✓					✓	✓		
P677			✓		✓	✓			✓	✓	✓	
P679			✓						✓		✓	
P613	✓			✓	✓			✓			✓	✓
P740						✓			✓			✓

Table 3: List of iron oxide and sulphide minerals observed in the samples

Sample ID	**Iron oxides**		**Sulphides**					
	Hem	Mag	Mol	Py	Pyh	Ccp	Bn	Cc
19068	✓	✓					✓	✓
19077							✓	✓
19073	✓					✓	✓	✓
19075	✓	✓				✓	✓	
19078							✓	✓
P580							✓	✓
P579		✓		✓	✓	✓		
P774	✓					✓	✓	✓
P814			✓			✓		
P817		✓		✓				
P782			✓	✓		✓		
P812				✓				
P679	✓	✓				✓	✓	✓
P613						✓		
P740		✓						
P677	No opaque minerals observed							

Table 4: List of silicate minerals detected using TIMA

Minerals	**Sample ID**						
	19068	19077	P579	P774	P817	P782	P613
Chlorite (Clinochlore/chamosite)	✓	✓	✓	✓	✓	✓	✓
Albite				✓	✓	✓	✓
Biotite					✓	✓	✓
Muscovite			✓	✓		✓	
Garnets	✓	✓		✓	✓	✓	✓
Kaersutite	✓			✓	✓		
Zoisite				✓			✓
Diopside	✓	✓			✓		✓
Hypersthene			✓				
Quartz	✓	✓	✓	✓	✓	✓	✓

Relationship between silicates, oxides, and sulphides

Petrographic and TIMA observations reveal that most hydrothermal alteration minerals are closely associated with sulphides and Fe oxides. The observed minerals show that Messina Cu deposit contained some unique minerals and minerals common in other copper deposits such as quartz, chlorite, sericite, and epidote hydrothermal alteration products. Primary minerals mostly represent remnants of the country rock minerals that have been partially altered and replaced by their hydrothermal alteration products. Some primary minerals remained unaltered, indicating that they resisted the effect of the hydrothermal alteration (e.g., Figs. 11, 21, 23, 27, 28). Other unaltered primary minerals were corroded by the mineralising fluids whereby sulphides or iron oxides precipitated within the corroded halos (Figs. 20, 26, 28). Altered minerals were also corroded along their grain boundary contact with the sulphides (Figs. 13, 18, 19, 20, 22, 24).

In most samples, sericite occurs as an alteration product of plagioclase, potassium feldspar and/or quartz (Figs. 19, 21, 22, 23, 24, 25, 27). Some fine-grained sericite partially rims quartz grains along grain margins or occurs as irregular veins/veinlets within the minerals it is altering (Figs. 18, 22, 23, 25). Other fine-grained sericite occurs with inter-fragmental secondary quartz where it cements the quartz (Figs. 21, 22, 24), suggesting that quartz formed before sericite alteration. Often, sericite is found with chlorite, which occurs as fine-grained groundmass, veinlets, and rims around sericite (Figs. 24 and 25), suggesting that chlorite alteration commenced when sericite alteration was still active.

Chlorite mostly alters and replaces biotite and garnet (Figs. 13, 19, 20, 21, 24, 25, 27, 26). Interstitial chlorite occurs between quartz grains, cracks/fractures, and cleavage planes of primary minerals like garnet, orthopyroxene, and biotite (Figs. 13, 15, 19, 20, 21, 25). At least two chlorite end-members were observed: Chlorite-chamosite and chlorite-clinochlore, which represent Fe-rich and Mg-rich end members (Figs. 29, 31, 32, 34, 36, 39, 42, 44; Wu *et al*., 2019). Some chlorite veins/veinlets do not cut through silicate minerals, but sulphide minerals, indicating that they formed after or during latest stage of sulphide crystallisation (Figs. 8, 18, 19, 25). Other chlorite occurs as massive groundmass enclosing the sulphides or granular groundmass/grains between quartz (Figs. 8, 11, 25, 27). Some chlorite veins do not cut through quartz grains (Fig. 8) and are envisaged to have formed before the quartz grains. This is clear in TIMA phase map (Fig. 29) where quartz grains appear to enclose chlorite and sulphides. Where granular chlorite occurs between large quartz grains, it is envisaged that it completely altered and replaced country rock minerals that were incorporated between quartz grains or was remobilised from other parts into open spaces by hydrothermal activity (Fig. 11).

Advanced chlorite alteration coincides with formation of epidote and a shift from chloritisation into epidotisation (Figs. 9, 13, 15, 18, 21, 23, 26, 28). The overlap between chloritisation and epidotisation is associated with epidote and chlorite along cleavage planes of biotite, veinlets of chlorite + epidote within sulphides, and granular epidote within chlorite (Figs. 13, 15, 18). This indicate that epidotisation commenced at least during the latest stages of chloritisation, partially altering chlorite. Epidote alters and replaces mafic and felsic minerals such amphibole, plagioclase, and clinopyroxene/diopside (Figs. 21, 26, 28, 44). A shift into epidotisation is associated with pervasive epidote alteration, where the country rock minerals are completely altered and replaced by epidote aggregates (Figs. 17, 21, 28). Other epidote grains overprint and rim secondary quartz grains, sericite, and chlorite (Fig. 18) and indicate that it formed at a later stage. Two generations of epidote were observed: 1. Occurs as fine grains, aggregates or prismatic crystals; 2. Newly crystallised euhedral, subhedral, and prismatic zoisite grains.

The above-mentioned alteration zones are associated with interconnected, fragmented, cryptocrystalline, and irregularly elongated secondary (hydrothermal) quartz grains. This secondary quartz is present in almost all the samples, and occurs as inter-fragmental grains (Figs. 18, 20, 21, 22, 24), as veins (Figs. 10, 11, 13, 15, 17, 19, 20, 23, 25, 28), irregular grains intergrown with/cementing/enclosing other grains (Figs. 8, 13, 15, 20, 21, 28) or overprinting other grains (Figs. 27 and 28). Inter-fragmental quartz grains are mostly envisaged to have formed before their associated alteration minerals by hydrothermal inter-fragmental filling of open spaces (Figs. 18, 20, 21, 22, 24). Where the quartz encloses/cement altered minerals, it is suggested that hydrothermal alteration occurred before the formation of quartz (Figs. 8, 13, 20, 21), whereas where they overprint altered minerals, they suggest having formed after alteration (Figs. 21, 27, 28). Secondary quartz grains (usually in mineralised veins/quartz breccia veins and inter-fragmental grains) invaded by interstitial alteration minerals suggest that alteration formed during the latest stages of vein formation or after the formation of inter-fragmental quartz grains (Figs. 13, 15, 21, 25, 32, 39, 43). In some samples, two generations of secondary quartz were observed and identified as quartz 1 and quartz 2 (Figs. 8, 20, 21, 23, 28), whereby quartz 2 often cuts through other minerals, suggesting it formed after all the alteration products. Some alteration minerals occurred in conjunction with one another and are assumed to be a result of overprinting of late phases on earlier-formed phases. For example, epidote rims around sericite and chlorite (Fig. 18). Secondary quartz grains and veins overprint/cut through sulphide and alteration minerals, and it may represent the last stage of hydrothermal activity for Messina deposit (Figs. 8, 13, 20, 23, 28).

The sulphides and iron oxides are enclosed within the silicates as disseminations or occur as interstitials between aggregates/fragmented grains/corroded spaces (Figs. 17, 19, 20, 21, 22, 23, 24, 26, 28), disseminations in mineralised veins (Figs. 9, 11, 13, 15, 23, 25), as veins (Figs. 18, 19, 24), and/or massive ore (Figs. 9, 15, 17, 18, 19). The latter is mostly associated with mineralised breccia veins, especially quartz breccia veins.

Sericite alteration occurs mostly in association with pyrite/pyrrhotite and minor chalcopyrite (Figs. 19, 22, 24, 25). Pyrite grains observed disseminated within sericitised feldspars, while also corroding and replacing the sericite in a quartz vein, are suggested to have formed during or at the late stages of sericitisation but after vein formation (Fig. 22). Some grains overprint the quartz grains and are rimmed/cut by sericite veins along fractures (Fig. 25), suggesting that they formed after vein formation but before sericite alteration. However, some fractures did not contain any alteration minerals, suggesting that some fracturing occurred after alteration. Where pyrrhotite grains occur between and within sericitised grains, it is envisaged that they formed during the latest stages of sericitisation (Figs. 20 and 36b). This pyrrhotite contained subhedral grains of pyrite and was encroached by chalcopyrite, indicating formation of pyrite by exsolution, followed by incipient replacement of pyrrhotite by chalcopyrite. Pyrite and chalcopyrite grains completely enclosed/cemented by sericite indicate they formed before sericite alteration, whereby chalcopyrite formed when Cu precipitated from the mineralising fluids after pyrite formation (Fig. 24). A thick pyrite vein was observed cutting through sericite and quartz while corroding them, suggesting that the vein formed after sericitisation (Figs. 24 and 47). The sericite alteration is also associated with minor magnetite within pyrite grains, which suggests it formed by oxidation of pyrite (Figs. 25 and 45).

Where sericite and chlorite alteration coincide, chlorite cut pyrite/pyrrhotite grains as veinlets (Fig. 20) and overprint pyrite grains (Fig. 25), suggesting that chlorite formed later than the sulphides. This overlap is also associated with molybdenite and magnetite. Magnetite mostly occurs within altered

mafic minerals, implying that it formed by Fe-release from the mafic minerals during hydrothermal alteration (Figs. 24, 25, 34). Molybdenite occurs along cleavage planes of altered minerals such as chloritised biotite (Fig. 24) in samples where pyrite or chalcopyrite also occur. It is envisaged that it formed during the early stages of chlorite alteration, perhaps before the crystallisation of the sulphides as the chloritised biotite occurs between inter-fragmental quartz and sericite groundmass.

Chlorite alteration is often associated with Cu sulphides and iron oxides (Figs. 8, 9, 11, 13, 15, 19, 20, 23) and marks the transition from iron sulphides ± chalcopyrite towards more chalcopyrite and bornite in association with hematite and magnetite (Figs. 8, 9, 11, 13, 15, 19, 20, 23). This shift in alteration zone is accompanied by replacement of chalcopyrite by bornite. In this zone, secondary quartz veins rim/cut through the Cu sulphides and magnetite (Figs. 8, 13, 20, 29) and in other places host chalcopyrite disseminations (Fig. 23), suggesting that the vein formed after mineralisation and incorporated the sulphides within the vein. In most samples, the general crystallisation order of the Cu sulphides was found to be chalcopyrite – bornite – chalcocite and magnetite – hematite for the iron oxides. Chlorite veins cement and cut through bornite grains rimmed by chalcocite (Fig. 8) and also cement magnetite laths (Figs. 8 and 29). This indicates that the Cu sulphides and magnetite formed before/during the early stages of chlorite alteration. This zone is also associated with the formation of magnetite-hematite within host bornite (Fig. 20), hematite within chlorite veins (Figs. 9), and along bornite margins and fractures (Figs. 13 and 15). It is possible that the hematite plates in the centre of chlorite veins formed after chlorite alteration. Hematite and magnetite abutting bornite exhibit exsolution lamellae texture, indicating replacement exsolution between the Fe-oxides at the latest stage of bornite crystallisation. The formation of hematite along bornite margins and fractures suggests that it followed the crystallisation of Cu sulphides by precipitating along bornite fractures and margins. Chalcopyrite and bornite also exhibit replacement exsolution lamellae texture (Figs. 13, 15, 20), and indicate replacement exsolution between chalcopyrite and bornite. Replacement of chalcopyrite by bornite overlaps with incipient bornite replacement by chalcocite (Figs. 11, 13, 18, 20).

A shift into epidote alteration is accompanied by complete replacement of chalcopyrite by bornite and minor chalcocite replacing bornite (Figs. 13, 15, 18). Advancement of epidote alteration and formation of zoisite corresponds with pronounced bornite replacement by chalcocite and crystallisation of disseminated chalcocite between epidote/zoisite aggregates (Figs. 17 and 21) or minor magnetite (Fig. 28). These disseminations appear to be filling spaces between the altered minerals and suggest they formed after hydrothermal alteration. Disseminated chalcocite is mostly concentrated between epidote-zoisite and not quartz, suggesting that mineralisation occurred in close relation to epidotisation. Magnetite grains between aggregates of epidote and amphibole grains suggest that they formed by release of Fe from primary mineral assemblages during hydrothermal alteration and epidotisation. Other epidote alteration is associated with chalcopyrite and molybdenite (Figs. 23 and 26), where molybdenite is envisaged to have formed before chalcopyrite crystallisation during hydrothermal alteration. This zone is also associated with strong hematitisation, where hematite rims chalcocite (Fig. 21). This indicates that hematite formed after the Cu sulphides. Fe-oxides also account for the iron staining observed in quartz, biotite, and chlorite (Figs. 7, 9, 12, 13, 20, 21).

Alteration minerals and their associated oxides/sulphides provide information on compositional changes during hydrothermal activity. The corrosive nature between sulphide and silicate minerals could suggest selective reactions caused by mineralising fluids upon contact with the silicate minerals, subsequently causing precipitation of sulphides. Mineralisation-alteration invasive relationship could suggest that their timing is closely related. Some textures showed preferential alignment of the altered minerals and sulphides and could be related to the texture of the country rock (e.g., a gneissic rock, Fig.

47, also Appendix A14, B15, B21, 25). This illustrates that the mineralising fluids moved within deformed structures along compositional bands as suggested by Jacobsen (1967) and Bahnemann (1986).

Critical and base metals/trace elements associations

Cobalt was found to be strongly concentrated in hematite/magnetite compared to pyrite and pyrrhotite, and in general surprisingly very low in copper sulphides (Figs. 30, 33, 37, 40, 43, 45). No significant concentrations of Zn were found in Cu sulphides; but were elevated in association with pyrite (Figs. 37, 40, 43). Low concentrations of Co were also detected in gangue minerals such as chlorite and hypersthene (Figs. 37 and 45). Likewise, Sn was detected in only two samples (Figs. 30 and 40), especially where silicate minerals like epidote/zoisite and quartz were present. These gangue minerals, however, rarely host critical, base, or trace elements, therefore, their concentrations are ambiguous.

Observations from previous studies

Mundalamo and Ogola (2012) and Mundalamo (2019) reported the following mineral associations:

- Bornite with pyrite
- Chalcopyrite and sphalerite replacement
- Chalcopyrite replacement by malachite
- Bornite with azurite and malachite
- Chalcocite between pyrite grain boundaries
- Cuprite with malachite, azurite, and native copper
- Anhedral pyrite cutting across magnetite
- Hematite/magnetite in quartz
- Galena associated with pyrite and sphalerite
- Calcite associated with pyrite filling microfractures of hematite (replaced by goethite)
- Hematite replacement by ankerite.

Jacobsen (1967) reported the following occurrences:

- Pyrrhotite along pyrite fractures
- Replacement of pyrite by hematite
- Pyrite islands in chalcopyrite cutting garnet
- Crystalline quartz/calcite along pyrite cracks
- Magnetite rimmed by chalcopyrite
- Two generations of chalcocite (white Cc with grated texture and blue irregularly banded myrmekite) associated with chalcopyrite, goethite, and covellite
- Transformation of covellite to native copper.

Some minerals observed by Jacobsen (1967), Mundalamo and Ogola (2012) and Mundalamo (2019) were identified by TIMA imaging, however, they were absent under optical microscopy (e.g., calcite, ankerite, cuprite, goethite, covellite). In addition, the ore textures reported by the above authors are also different from the observations of this report, including chalcopyrite replacement by sphalerite, chalcocite between pyrite grains, magnetite rimming chalcopyrite, malachite replacing chalcopyrite, pyrite in microfractures of hematite associated with calcite, and pyrrhotite along pyrite fractures. Instead, in this report, pyrite was found associated with pyrrhotite where it occurred as replacement exsolution lamellae and with chalcopyrite and magnetite in brecciated altered country rock. Pyrite grains were also observed along quartz cracks (Fig. 45). Comparing observations of this study with

Mundalamo and Ogola (2012) and Mundalamo (2019), the only mineral associations that are similar are hematite/magnetite occurrence in quartz grains/fragments. Chalcocite and bornite were never observed occurring with pyrite. Thus, the results of this study do show some associations with the results of Jacobsen (1967), Mundalamo and Ogola (2012) and Mundalamo (2019). However, the varying observations may be attributed to the use of different methods and interpretation analysis or the location/site from which the ore samples were collected due to the complexity of the mineralogy of Messina ores. Thus, some mineral associations/textures/zonation prominent in some mines, do not occur at all or are poorly developed in other mines (Jacobsen, 1967; Bahnemann, 1986). For example, clear zonation of sulphides and associated alteration was found to be absent in Harper mine, absence of pyrite in Campbell mine, unaltered marble in Spence mine. Therefore, it is speculated that textural, mineralogical, and compositional information varies considerably across the mines.

This work acknowledges concentration of sulphide mineralisation within immediate zones of alteration as discussed by Jacobsen and McCarthy (1976). The sulphide minerals cementing altered brecciated fragments indicates they formed after alteration of the country rock (e.g., Figs. 17, 20, 21, 23, 26). On the other hand, sulphides are also enclosed, cut, and overprinted by alteration minerals, suggesting they formed before alteration (e.g., Figs. 9, 11, 13, 15, 18, 22, 24, 25). As a result, it is presumed that the hydrothermal activity involved episodic compositional changes during the evolution of the hydrothermal fluids.

7 Discussion

The country rocks of Messina copper deposit comprise granulite, metaquartzite, amphibolite, granitoid gneiss, biotite-rich garnetiferous schist, and pyroxene amphibolite, which have been partly and extensively altered by hydrothermal activity related to mineralisation (Bahnemann, 1986). The country rocks have been exposed to different alteration types, which in this study have been observed as:

- Sericitisation, with the formation of sericite (muscovite) as a product of alteration of plagioclase and K-feldspar (Figs. 19, 21, 22, 23, 24, 25, 27).
- Chloritisation, with the formation of chlorite by alteration and replacement of garnet, biotite, and/or amphibole (Figs. 8, 9, 11, 13, 15, 19, 20, 21, 23).
- Epidotisation, with the formation of epidote as a product of alteration of amphibole, chlorite, garnet, diopside, and plagioclase (Figs. 9, 13, 15, 18, 21, 23, 26, 28).
- Zoisitisation, as overgrowth of zoisite aggregates on previously formed epidote (Figs. 17 and 21).
- Hematitisation, as a rim around chalcocite (Fig. 21), blades/platelets along bornite fractures (Figs. 13 and 15), at the centre of chlorite veins (Fig. 9), exsolution lamellae with magnetite within bornite (Fig. 20) or with magnetite between quartz grains.
- And silicification as the formation of secondary quartz grains and veins cross-cutting and overprinting early formed phases (Figs. 8-18, 20-25, 27-28).

The main Cu-ore body, chalcopyrite-bornite-chalcocite in association with magnetite and hematite is closely related to chlorite-epidote-zoisite alteration zones. These orebodies are also associated with brecciated fragments/veinlets/veins of quartz within and around mineralisation.

7.1 Ore types

At least four types of ores were observed in the studied samples: 1. Brecciated ore; 2. Veined ore; 3. Disseminated ore; and 4. Massive ore. Different ore types may occur in one sample (e.g., veined and

disseminated). Thus, there is no general sequence regarding the ore types as they occur in conjunction with one another.

1 Brecciated ore

The morphology and estimated depth of breccia pipes have been well documented by Jacobsen *et al* (1976), reporting about 9 breccia pipes extending to over 700 m depth. Most breccia pipes are identified as blind as they do not reach the surface. The exposed breccia pipes were discovered during Cu exploitation (Jacobsen *et al*., 1976). Some breccias can be surficial outcrops for the altered country rocks (Bahnemann, 1986). In fact, hydrothermal alteration envelopes the breccia pipes with zonation grading from the outward sericite zone, inner albite-chlorite, and central epidote-zoisite and quartz (Jacobsen *et al*., 1976). However, it is not clear whether alteration occurs within or outside the breccia pipe. Breccia pipes hosted the richest ore exploited at Messina (Jacobsen, 1967; Jacobsen *et al*., 1976; Jacobsen and McCarthy, 1976; Sawkins, 1977; Mundalamo, 2019) and some authors (Jacobsen *et al*., 1976; Mundalamo, 2019) believe that other ore types (e.g., vein/fissure and disseminated ore) emerge from the breccia pipe. Although the breccia pipes are important for their association with mineralisation, previous studies did not detail the brecciation characteristics in Messina Cu deposit (e.g., Sawkins, 1977; Mundalamo, 2019). Mundalamo (2019) discussed that brecciated ore is coarse-grained and characterised by sulphides surrounding quartz and amphibole breccias, with mineralisation accompanied by chloritization.

Quartz makes up most gangue minerals of the breccia pipes, occurring as inter-fragmental grains, brecciated fragments/breccia veins invaded by alteration minerals, and as brecciated fragments intergrown with altered minerals and within mineralisation. Observed fragments in brecciated zones include distributed subrounded, subhedral, and subangular grains of varying sizes (0.5 mm-2 cm). Localised brecciation of primary and altered minerals could suggest fluid-aided brecciation during movement of hydrothermal fluids within the breccia. The coarse grain nature of brecciated fragments in some samples obscure early formed textures and minerals (Figs. 17, 18, 23, 27, 28). All brecciated minerals are associated with altered minerals, sulphides or iron oxides filling open spaces between the grains, cementing loose fragments, and/or cutting through fragments as veinlets (e.g., Figs. 8, 9, 11, 13, 15, 17, 18, 21, 23, 26). The sulphides themselves are not brecciated, except in one sample (Fig. 9) where bornite grains appear to be subangular. Therefore, defining this ore type as brecciated does not properly describe other observed occurrences of mineralisation. From the results of this study, the Messina Cu deposit is rather characterised by “mineralised breccias”. Thus, brecciation is a texture of the host rock and gangue minerals, whereas sulphides are found in fractures and/or cementing fractures and/or disseminated between brecciated fragments.

The observations also revealed that not all the breccias are mineralised. Barren breccias are associated with pervasive alteration (Figs. 27 and 28) and Fe-sulphides, while mineralised breccias are associated with chalcopyrite, bornite, and chalcocite between altered fragments. Barren breccias are characterised by vein quartz in contact with brecciated country rock (Fig. 25), brecciated quartz grains cemented by sericite and chlorite (Figs. 22 and 24), as well as brecciated plagioclase/orthopyroxene grains cemented by pyrrhotite or alteration veins (Fig. 19). The occurrence of fragmented altered country rocks associated with ore minerals implies that they occur within the breccia pipe as discussed by other researchers (McCarthy and Jacobsen, 1976; Chaumba *et al*., 2016). The observed features suggest that the breccia pipe formed by over-pressured hydrothermal fluids, which led to the filling of the void by country rock brecciated fragments. The fragments were altered when the hydrothermal fluids migrated within the breccia, corroding, and reacting with the host rocks while leaching and transporting some material and elements to other parts. The corrosion of fragments created more space for the fluid to pass

and slumping of fragments within the pipe. Some quartz veins and inter-fragmental quartz grains within the breccia were locally rebrecciated/refractured by migrating hydrothermal fluids and filled by altered minerals from the country rocks (Figs. 11, 15, 25). Blocky, equidimensional, macro-breccias reported to occur at deeper levels of the breccia (Jacobsen *et al*., 1976) were not observed in this study. However, blocky, large quartz fragments were observed, and some are reported to represent secondary quartz veins (e.g., Fig. 25).

2 Veined ore

This ore type is characterised by mineralised veins of brecciated quartz grains enclosing altered gangue minerals (Figs. 7, 8, 9, 10, 14, 15, 16, 17, 21). The ore is dominantly represented by sulphides that are hosted between brecciated quartz, chloritised, epidotised, and zoisitised grains as interstitial mass and disseminated grains. Some quartz grains in this ore are coated by Fe-stains (Figs. 7, 10, 12, 14). In Figs 12 and 13, the mineralised vein comprises microcrystalline quartz groundmass heavily coated by Fe-oxides and enclosing altered grains of chlorite and epidote. The mineralised veins contain either disseminated or massive ore. The sulphide minerals also occur as veins or veinlets within host country rocks. Pyrite veinlets associated with inter-fragmental quartz grains, sericite cement, and Fe-rich chlorite (Fig. 24) were observed. A thick pyrite vein (~4 cm) and slightly aligned euhedral-subhedral pyrite grains associated with magnetite inclusions also occur (Figs. 24 and 25). Copper sulphide minerals in veins are mostly associated with irregular chalcopyrite veins or disseminations in a vein (Figs. 23 and 24). Less frequently, curvilinear bornite occurs between the quartz grains rimmed by sericite (Fig. 18). Massive, granular pyrrhotite vein was also observed between plagioclase and orthopyroxene fragments and dissected and rimmed partly by quartz and chlorite veins (Fig. 19). Other pyrite veinlets occur in open spaces of large, interconnected quartz grains (part of Fig. 25 in Appendix B46). Mineralised quartz veins forming stockwocks as reported by Mundalamo (2019) and Jacobsen *et al* (1976) were not observed in this study. The observed veins were dominantly discontinuous and irregular. Veined ore was reported to occur within quartz veins with mineralisation along microfractures forming ore stockworks with quartz stringers (Mundalamo, 2019). Mineralised stockworks were observed in this study, but they appear as secondary veins within the brecciated country rock carrying disseminated mineralisation and remobilising primary mineralisation (e.g., Fig. 23). Some veins were unmineralised but contained altered minerals or secondary quartz 2.

3 Disseminated ore

Disseminated ore was reported to be characterised by pyrite and chalcopyrite disseminations within quartz veins and amphibole host rock, as well as chalcopyrite disseminations replaced by malachite or bornite (Jacobsen and McCarthy *et al*., 1976; Mundalamo and Ogola, 2012; Mundalamo 2019). In this study, disseminated sulphides were observed within altered country rock and gangue minerals. This includes mostly disseminated pyrrhotite (Fig. 19), pyrite (Figs. 24 and 25), chalcopyrite (Figs. 23 and 26), and chalcopyrite–bornite (Figs. 11, 15, 17, 20). The disseminated sulphides often occur as replacement minerals where one is being replaced by another sulphide. Small blebs of bornite rimmed by chalcocite were observed within fine-grained chlorite groundmass surrounded by large quartz grains (Fig. 9). In other places, bornite disseminations were abutted by magnetite and hematite aggregates or magnetite-hematite exsolution lamellae and contained relics of chalcopyrite and minor chalcocite (Fig. 20). Chalcocite disseminated grains were observed between epidote and newly crystallised zoisite aggregates in a mineralised vein (Fig. 21). Disseminated pyrite grains were observed enclosed by large quartz grains of the vein quartz (Fig. 25). Some disseminations occurred as irregular grains cementing brecciated fragments (Figs. 20, 23, 24, 26). Other disseminations of sulphide minerals and Fe-oxides

occurred within corroded halos of quartz grains or altered country rock minerals (Figs. 19, 20, 21, 22, 24, 28).

4 Massive ore

A massive mineralisation has not been reported in previous studies, but it is worth to be noted. In the present study, presence of coarse-grained ore (exceeding 1 cm) was observed associated with pervasive alteration. The ore comprises coarse-grained tarnished bornite associated with magnetite/hematite grains/platelets in open fractures within host bornite (Fig. 15); and/or massive bornite adjoined by hematite platelets as a rim or in fractures, tiny chalcocite spots, and flame-like lamellae of a bright yellow chalcopyrite (Figs. 13, 15, 18). These massive ores are hosted within mineralised veins. Moreover, massive bornite was observed between subhedral quartz grains associated with irregular grains of chlorite, sericite, and epidote (Fig. 18). Other occurrences include massive granular pyrrhotite containing subhedral pyrite grains and encroached by minor chalcopyrite (Fig. 19).

7.2 Messina hydrothermal fluid processes

Hydrothermal ore deposits do not have a universally accepted genetic model for their classification, because they are believed to have formed by the combination of more than one fluid (Kelly and Rye, 1979). Hence, they are often classified on the basis of their dominant valuable mineral/commodity (e.g., Cu-Mo deposits).

Previous studies have shown that the fluids responsible for the Messina Cu mineralisation contained H_2O, SiO_2, K_2O, Na_2O, Al_2O_3, MgO, FeO/Fe_2O_3, and CaO elements, which were exchanged, added or remobilised during hydrothermal activity and the interactions between country-rocks and mineralising fluids (McCarthy and Jacobsen *et al*., 1976). During the early stages of alteration, the hydrothermal fluids reacted with the country rock, altering plagioclase into sericite, dissolving primary quartz and albitising feldspars and plagioclase (Jacobsen and McCarthy, 1976; McCarthy and Jacobsen, 1976). With cooling of the fluids, retrogressive reactions initiated, followed by pyrite, pyrrhotite and magnetite formation, and disappearance of free quartz (McCarthy and Jacobsen, 1976; Mundalamo, 2019). On the contrary, Sawkins (1977) reported that the hydrothermal replacement of host rocks led to the dissolution of silica and formation of albitised rock in the central core surrounded by sericitic alteration. Pyrite occurrence was reported to be absent in some breccias in Messina deposit (Jacobsen and McCarthy, 1976).

Further cooling and decrease in pH of the fluid, formed chalcopyrite when Cu reacted with Fe followed by chloritisation of garnet and hydrobiotite in association with epidote formation (Jacobsen and McCarthy, 1976; Mundalamo, 2019). An increase in CaO in the fluid led to the fixation of epidote as zoisite, together with further decrease in pH and temperature, and the formation of bornite. Extensive epidotisation formed in association with chalcocite and Fe oxidation, resulting in loss of S and formation of native copper and sulphate ions by replacing chalcocite (Jacobsen and McCarthy, 1976). Intense alteration is postulated to have been followed by red colouration enhancement by hematite and conversion of country rock to a grey-green clay (Jacobsen and McCarthy, 1976; Bahnemann, 1986).

At lower temperatures and pH, dissolved quartz was then re-distributed extensively in quartz veins and vugs with minor albite and analcite associated with the release of CO_2 and calcite formation. In addition, the breccia periphery is characterised by micro-brecciation, whereas inner zones show macro-brecciation (equidimensional and blocky) (Jacobsen and McCarthy, 1976; Jacobsen *et al*., 1976; McCarthy and Jacobsen, 1976). The formation of younger quartz replacing altered minerals is the

evidence of a late stage of alteration and silicification (Jacobsen *et al*., 1976). The source of the hydrothermal fluids is not known for sure. It has previously been suggested that hydrothermal fluids were sourced from an alkaline magma that ascended towards the surface and descended through faults and joint intersections (Cox *et al*., 1965; Jacobsen e*t al*., 1976). However, there is no evidence for ejection of magma-derived material in Messina. On the contrary, Sawkins (1977) proposed a supergene nature of the ore, due to interaction of meteoric source of the fluids.

Based on the mineralogical and petrographical observations of this study, we are proposing an idealised hydrothermal activity of the Messina Cu deposit. Pressurised hot hydrothermal fluids penetrated and brecciated the country rock, creating fracture systems and open spaces for the fluids to pass. The contact of the hydrothermal fluids with the cold country rocks caused episodic cooling of the fluids. Hydrothermal fluids reacted with the country rock causing alteration of primary plagioclase and K-feldspars, remobilising K_2O and Al_2O_3, and forming sericite. Initial formation of hydrothermal quartz commenced in open spaces and large veins. Sericite cemented inter-fragmental quartz and invaded the quartz veins (Figs. 22, 23, 24, 25). Quartz inclusions occur within the sericite cement, suggesting they formed prior to sericitisation (Figs 22 and 24). Partial to pervasive sericite alteration as fine-grained mass, irregular veins and grains within altered grains and opaque mineral, rims around quartz and opaque minerals occurred (Figs. 18, 19, 22, 23, 24, 25, 27). Primary biotite and garnet minerals within the sericitised country rock were altered into chlorite (Figs. 23, 24, 27). Albitisation of plagioclase grains is not clear whether it was a product of hydrothermal reactions or preserved metamorphic grains. However, it is treated as a product of preserved metamorphic grains as it is not consistent in samples that contain plagioclase and K-feldspar. This contrasts with the findings of Jacobsen and McCarthy (1976) and Jacobsen *et al* (1976), who reported albitisation as a hydrothermal alteration that followed sericitization.

As the fluid moved through the breccia, it locally rebrecciated (fluid-aided brecciation) the country rock minerals further (garnet, biotite, orthopyroxene, quartz, and plagioclase), while altering them and filling the spaces with hydrothermal quartz, alteration minerals and sulphides. The progressive loss of K_2O in the fluid due to pervasive sericitisation, was paralleled by a progressive increase in MgO and FeO by transformation of biotite, amphibole and garnet, leading to the formation of Mg-rich and Fe-rich chlorite. The hydrothermal activity transported this newly formed chlorite further during localised brecciation into open spaces of large grains as fine-grained groundmass, anhedral material between quartz grains and veins, carrying with it inclusions of brecciated country rock (Figs. 8, 11, 15, 21, 25, 26). Other chlorite formed irregular veinlets and grains within the sulphides with brecciated quartz and as inclusions within cryptocrystalline quartz groundmass (Figs. 8, 13, 15, 18, 19, 26, 27). Some chlorite veins appear to be multi-compositional, containing fine-grained sericite, quartz, and chlorite outer rim between pyrrhotite and around primary country rock grains (Figs. 19 and 36).

As the fluid evolved further, gradual depletion of MgO and exchange of MgO with CaO, FeO or Al_2O_3 led to the formation of epidote by replacing chlorite, aided by the release of Ca from garnet/plagioclase and diopside, during fluid interaction with the country rock minerals (Figs. 13, 18, 23, 26).

Some epidote grains were observed rimming fine-grained sericite, which could be a result of Al_2O_3 exchange and selective replacement and/or epidote overgrowing on sericite (e.g., Fig. 18). More epidote formed as more Ca was released during amphibole alteration, of which, intense alteration resulted in crystallization of zoisite in other parts (Figs. 21 and 17). Further evolution of the metasomatising fluids resulted in precipitation of secondary quartz as veins, subrounded, subangular, amorphous, and elongated slabby grains cementing and overprinting other minerals (Figs. 21, 22, 27, 28). Quartz veins

cut through and overprint altered grains and the sulphides (Figs. 23, 28 and Figs. 17, 24 in Appendix B). The overprinting and dissecting nature of the grains and veins in other zones suggest that this silicification stage terminated alteration and mineralisation. These findings contrast previous models of Jacobsen *et al* (1976) and Mundalamo (2019), which proposed the release of CO_2 during late stages to form calcite, which terminated mineralisation and alteration.

Furthermore, the findings of Jacobsen and McCarthy (1976), Jacobsen *et al* (1976), and Mundalamo (2019) reported that SiO_2 and albite were redistributed to the inner parts of mineralisation in vugs and cavities. However, in the samples observed, secondary quartz occurred in both mineralised and unmineralised zones (e.g., Figs. 23 and 28). For example, in the epidote zone, secondary quartz cements brecciated epidote aggregates, while the chlorite zone contains medium-sized inter-fragmental quartz grains, cryptocrystalline quartz with chlorite inclusions, and quartz veins (e.g., Figs. 13, 15, 17, 20, 21, 23, 25, 26, 28). Sericite-chlorite zone contains interconnected, large clear quartz grains invaded by fine-grained sericite groundmass or interstitial chlorite, and irregular/discontinuous quartz veins (Figs. 22, 24, 27). Equidimensional-like, macro-breccias were observed in sample 19077 hand specimen and other samples that contained brecciated large grains (Figs. 19, 20, 22, 23, 25).

It is thus suggested that the breccia pipe/s of Messina Cu deposit are characterised by macro-brecciation at depth or early stages of brecciation, micro-brecciation in inner zones and outward, as well as mixing of fragments due to slumping of loose fragments and localised rebrecciation (Fig. 46). The presence of secondary quartz in most samples may suggest that the hydrothermal fluids were saturated with silica, as suggested by Sawkins and Rye (1979). The crystallisation order of alteration minerals cannot be established unequivocally because the zones overlap with or overprint one another indicating complex fluid movement and mineral transformation (e.g., epidote-sericite association). Although the alteration zones appear as concentric, the irregular nature of the zones and the co-existence of the alteration minerals imply that episodic changes in hydrothermal fluid's composition occurred upon reaction with the primary minerals (e.g., Figs. 13, 15, 18, 23, 24, 25, 26, 27). In other parts, the country rock was completely altered, so that primary minerals could not be identified using the optical microscopy (e.g., Figs. 11, 17, and 28). An idealised sequence of alteration and associated sulphides and iron oxides is presented in Fig 47. The increase in occurrence of hydrous minerals towards the central zone of the ore body is suggested to indicate increasing hydration with increasing alteration (Jacobsen and McCarthy, 1976).

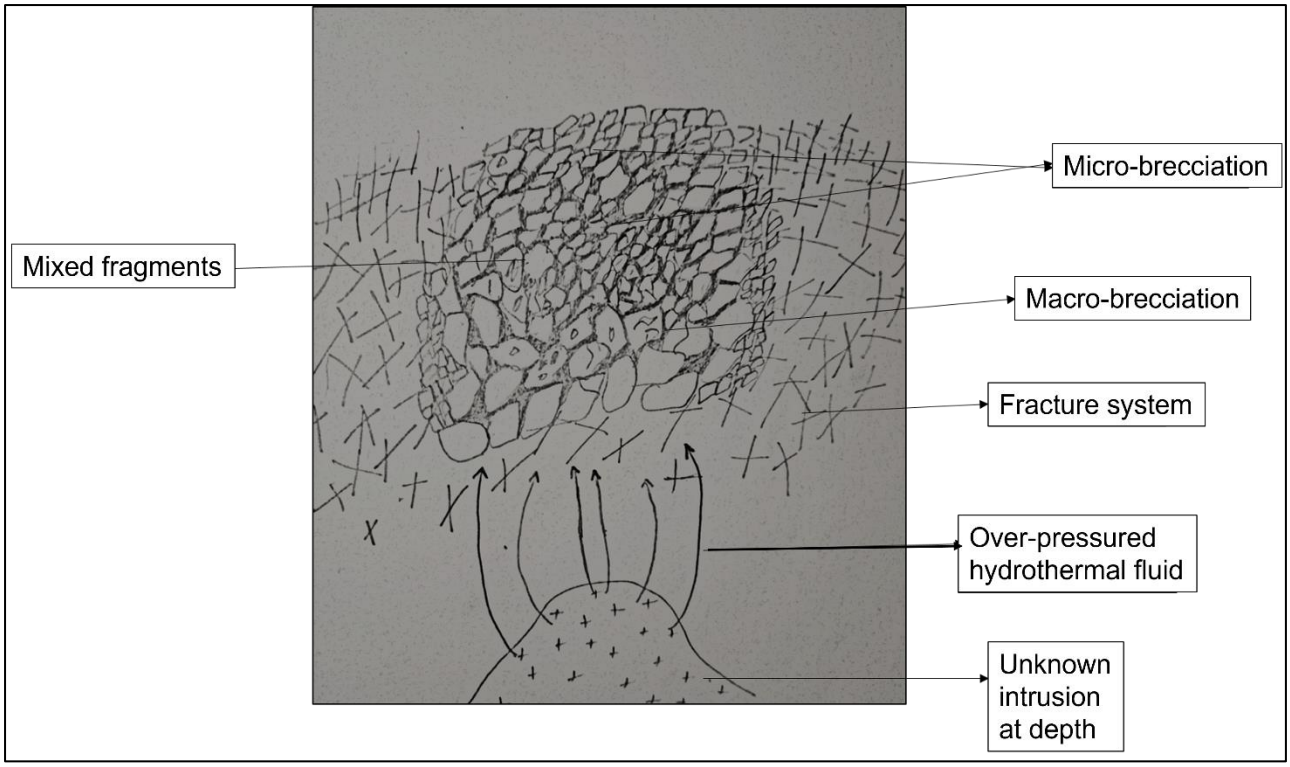


Figure 46: Sketch showing characteristics of Messina Cu deposit breccia pipe(s). Black fillings between fragments are alteration minerals, quartz, and sulphides.

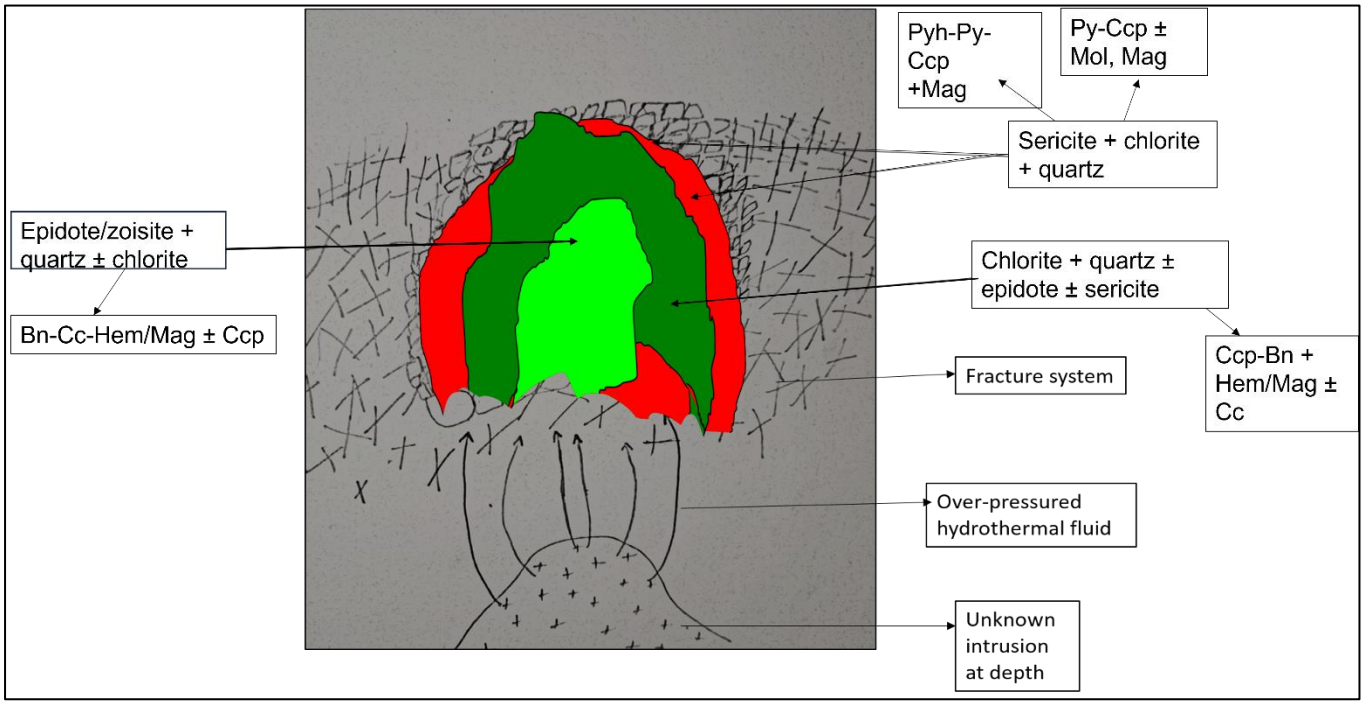


Figure 47: Idealised sketch of the concentric zonation of alteration and associated sulphides and iron oxides of the Messina Cu deposit. The overlapping sequences of mineral crystallisation due to alteration and metasomatism is shown by irregular shapes of alteration zones. The red zone is evident in samples P817, P812, P782, P814, P579, dark green zone in samples 19075, 19077, 19068, P679, P613, and lime-green zone in samples 19078, 19073, P744, and P580.

The observed association of sulphides and oxides in different samples reveal that during the early mineralising phases, Fe-sulphides such as pyrrhotite and pyrite precipitated from the hydrothermal fluids. Pyrrhotite crystallised between sericitised plagioclase and orthopyroxene (Fig. 19). It coincided with pyrite formation as subhedral grains within pyrrhotite, and minor chalcopyrite encroaching onto it (Fig. 19). The continuous release of more Fe and S with minor Cu from the hydrothermal fluids led to the formation of more pyrite in quartz veins and open spaces, together with irregular chalcopyrite within the sericite-chlorite country rock (Figs. 22, 24, 25). In this sericite-chlorite alteration outer zone (red zone in Fig. 47), poorly distributed minor molybdenite laths also crystallised (Figs. 23 and 24). The inclusions of magnetite in some pyrite grains may suggest that the hydrothermal fluids contained oxidising species (Fig. 25). However, some of the observed magnetite grains associated with iron staining of quartz, biotite, and chlorite grains did not crystallise from the hydrothermal fluids, but rather reflect the release of Fe from Fe-bearing minerals during sericitic and chloritic alteration (e.g., Figs. 24, 25, 28). The gradual release of Cu and S from the fluids resulted in abundance of chalcopyrite forming between plagioclase, chlorite, quartz, and epidote (Figs. 23 and 26).

In chlorite-rich zones associated with brecciated quartz (dark green zone in Fig. 47), chalcopyrite dominates among the ore minerals (Figs. 23 and 26). Chalcopyrite is seen cementing country rock minerals as irregular interstitial minerals or disseminations between the grains and within thin quartz veins. It also occurs as disseminated grains between quartz and chloritised biotite grains associated with bornite (Figs. 15 and 20). Where bornite occurs, it is associated with magnetite and hematite, where hematite occurs between bornite and chlorite and at the centre of chlorite veins, indicating it followed sulphides formation (Fig. 9). Magnetite-hematite aggregates also occur enclosed within quartz and chlorite or between fractures in host bornite (Fig. 15). Hematite is also observed rimming the edges of bornite adjoining it or as exsolution lamellae with magnetite abutting the bornite and containing inclusions of bornite and chalcopyrite (Figs. 15 and 20). The host bornite also contains small chalcocite spots and thin flame-like relics of brighter yellow chalcopyrite (Figs. 9, 15, 20). Such occurrence of chalcopyrite within bornite suggests replacement exsolution lamellae between the two minerals (Craig and Vaughan, 1994).

Advanced evolution of the hydrothermal fluids with decreasing Fe and S, and increasing Cu, resulted in formation of more bornite and chalcocite in open spaces between chlorite and epidote grains (Figs. 8, 9, 11, 17, 18, 20, 21), characteristic of samples from the inner alteration zone shown in lime green in Fig 54. The release of more Cu led to the formation of massive bornite and pronounced replacement of bornite by chalcocite (Figs. 17, 18, 21). In some samples chalcocite was also observed rimmed by hematite (as previously seen for bornite), indicating that the Fe-oxides (especially hematite) formation accompanied Cu-sulphides (Fig. 21). This zonation from chalcopyrite to bornite/chalcocite implies progressive reduction of sulphur in the mineralising fluids and increasing oxidation within the ore body (Sawkins and Rye, 1979, 1980). This finding contrasts Mundalamo (2019) statement that attributes the formation of hematite to regional metamorphism. It is speculated that the evolution of the mineralising fluids was controlled mainly by oxygen and sulphur fugacity (O_f & S_f), temperature, and/or pH during formation of the sulphides (Barton and Skinner, 1979; Seedorff *et al*., 2005; Robb, 2005). For example, pyrite-chalcopyrite assemblages are typically stable at higher temperatures whereas chalcopyrite-bornite with/without oxides prevail at lower temperatures in most hydrothermal deposits (Craig and Vaughan, 1994; Seedorff *et al*., 2005).

7.3 Critical and base metals associated with sulphides and Fe oxides

Elemental mapping revealed the presence of Co, Zn, and Sn within the sulphides and Fe-oxides of Messina Cu deposit.

The observed enrichment of critical element Co in hematite/magnetite in the Messina samples indicates that this element was readily partitioned into iron oxides during crystallisation (Figs. 30 and 38). Stergiou *et al* (2021) reported Co concentrations in magnetite a common phenomenon occurring as nano-particle inclusions in magnetite in Vathi porphyry Cu-Au±Mo deposits of Northern Greece. In the analysed samples, slightly elevated Co concentrations were also found in pyrite and pyrrhotite, but interestingly low for copper sulphides (Figs. 33, 35, 38, 41, 43, 45). Pyrite is known for its ability to incorporate abundant critical and precious metals (Velasquez *et al*., 2020; George *et al*., 2016; Stergiou *et al*., 2021). Chalcopyrite grains in Fig 45 show moderate concentrations of Co, compared to other chalcopyrite grains with no significant Co concentrations. Usually, Co concentration in chalcopyrite is accommodated in solid solution (Stergiou *et al*., 2021). In Cu-Co deposits in Zambia, Co enrichment in pyrite/pyrrhotite occurs by isomorphism within Fe-sulphides or as a metallic Co-bearing mineral associated with copper sulphides (Yiguan *et al*., 2021). However, in the samples of Messina deposit, no Co-bearing mineral was observed using optical microscopy and TIMA, therefore it is suggested that Co could be present as nano-particle inclusions in the described minerals. Thus, advanced trace element analysis is still needed for further research in Messina to explore the potential for future exploration.

Base metal concentrations of Zn and Sn were also observed. Zinc was enriched in pyrite (Fig. 41). No elevated Zn concentrations were observed in pyrrhotite and iron oxides (Figs. 35, 38, 43). Chalcopyrite grains contain moderate Zn concentrations, which are assumed to be related to Zn-bearing minerals like sphalerite (Figs. 38 and 45). Mundalamo (2019) reported high levels of Zn using X-Ray Fluorescence in Artonvilla mine ore and concluded that the ore is sphalerite-rich. However, the same cannot be said in the present report because sphalerite was not observed using optical microscopy and TIMA. Rather, the enriched Zn concentrations in pyrite could be attributed to the ability of pyrite to scavenge critical metals from hydrothermal systems (Velasquez *et al*., 2020), whereas concentrations in chalcopyrite could be due to the presence of sphalerite inclusions which could not be identified using optical microscopy.

Tin was found concentrated in gangue minerals, such as chlorite/epidote and quartz (Figs. 30 and 38). This base metal commonly occurs in granite-associated mineralisation as cassiterite mineral in association with sericite and quartz or in hydrothermal veins of greisen deposits (Robb, 2005). Robb (2005) also reported the occurrence of cassiterite disseminations in Zaaiplaats granite deposits associated with epidote-chlorite-sericite greisens. Its concentration here, especially in association with epidote requires further geochemical investigations to understand its association because cassiterite was not observed using optical microscopy and TIMA or in previous studies.

7.4 Comparison of Messina Cu deposit with other hydrothermal copper deposits

The definition of a genetic model that can best explain the formation of the Messina Cu deposit is problematic because a simple model cannot account for all the features of the deposit. With the consensus that the deposit is buried and the source of the hydrothermal fluids unknown, it is difficult to characterise the processes that led to mineralisation and alteration.

The concentric mineralisation and alteration styles have similarities with greisen deposits and porphyry copper systems as shown in Fig 48. For example, the zonation idealised in Fig 47 shows that:

- Sericite – chlorite ± quartz outer zone of the Messina deposit is similar to the quartz + chlorite zone in greisen deposits and the sericitic zone in the porphyry deposits.
- Chlorite – quartz ± epidote ± sericite inner zone is similar to the deep qz–ser–chl–ep–mag zone in the porphyry deposits.
- Epidote – zoisite – quartz ± chlorite central zone is similar to the propylitic zone in the porphyry deposits, except carbonates were not observed in Messina samples using optical microscopy, but were reported by Jacobsen (1967) and Mundalamo (2019).

The zoning patterns in porphyry copper deposits where each alteration zone comprises sulphide and oxide assemblages, are similar to mineral associations observed in the Messina deposit. However, the crystallisation-alteration processes of the Messina Cu differ from traditional copper deposits. For example, the analogue of the porphyry propylitic zone in Messina deposit does not extend far outside the ore body, but is closely associated with the ore body in the central zone.

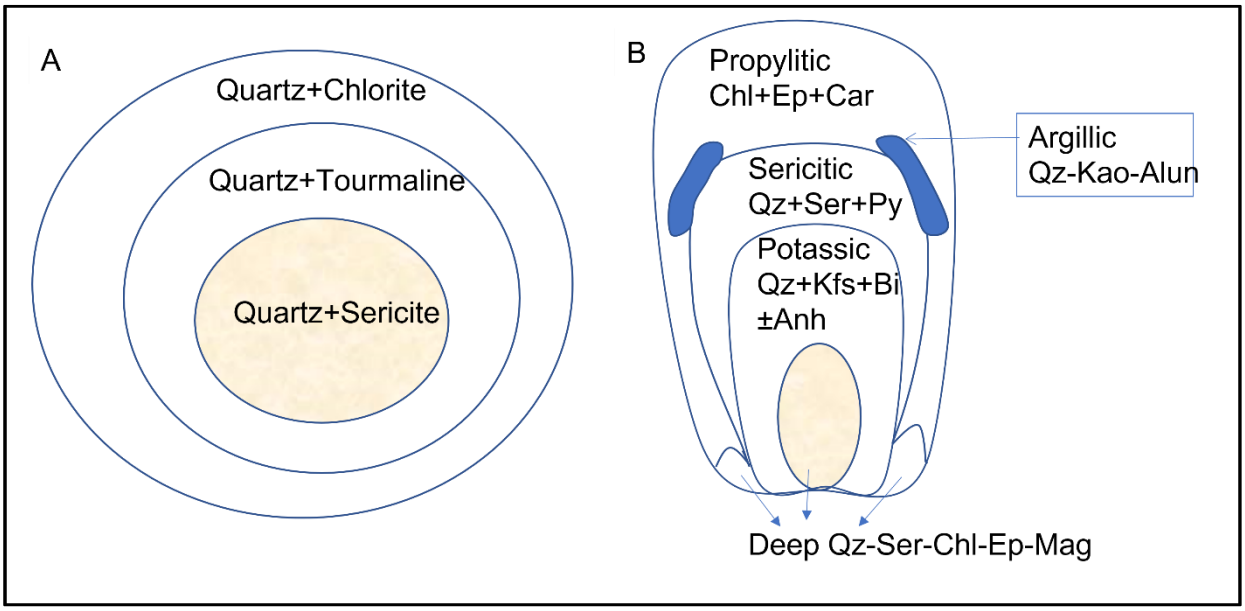


Figure 48: Zonation of hydrothermal halos in (A) Greisen deposits (from Elliot *et al*., 1995) and (B) Porphyry copper systems (Lowell and Guilbert, 1970). Kao=Kaolinite, Alun=Alunite, Anh=Anhydrite, Car=Carbonates.

Burt (1981) suggests that greisen and porphyry deposits have a similar formation process in that they involve the separation of a vapour phase from magma or aqueous brines. Sawkins (1977) suggested that mineralising fluids of Messina were derived from mixing of groundwater with magmatic fluids. At the moment, there is no sufficient geological and structural data to support groundwater circulation. The absence of an advanced sericite-argillic alteration zone common in porphyry deposits also contests the effects of groundwater circulation in Messina. Moreover, clay minerals like kaolinite and smectite were not observed in both optical microscopy and automated mineralogy. This also averts the possibility of groundwater circulation. However, Messina deposit still lends support for meteoric water circulation to account for Fe-rich zones associated with Cu-sulphides.

The observed features and idealised zonation proposed in this study (Fig. 47) are in agreement with the retrogressive cooling of the hydrothermal fluids inwards, where common low-temperature minerals occur in the central mineralised zone, and common high-temperature minerals in the outer parts. This zonation is reported to be a result of retrogressive slow cooling, with initial temperature gradient

decreasing from the centre outward, followed by continued falling temperature inwards by trapped fluids in the same fashion as pegmatite deposits (Jacobsen *et al*., 1976; Jacobsen and McCarthy, 1976; Sawkins, 1977). This retrogressive zonation is different from porphyry and greisen deposits, where zonation involves high-temperature minerals at depth and low-temperature minerals outwards and upwards (Titley and Hicks, 1966; Burt, 1981; as shown in Fig. 48). Porphyry systems are characterised by H_2O and saline magmatic fluids which separate into vapour and hypersaline brine upon second boiling and are localised along subduction zones (Pirajno, 2010). The alteration zonation is interpreted as a continuous, time-staged process associated with the intrusion of porphyry stocks rather than a single event (Guilbert and Park, 1989: p199). Greisen deposits are localised within granitic intrusions, whereas in this report, the mineralisation occurs in the country rocks. However, exo-greisens show comparable alteration zonation where quartz and sericite form by alteration of feldspars. These greisens occur outside the granitic intrusion via sheeted veins, unlike breccia-hosted Messina deposit. Also, granitic intrusions associated with mineralisation were not reported in Musina area. Felsic melts were also not reported, therefore, ruling out the comparison of Messina to pegmatite deposits as other reporters suggested. Brecciation and formation of ore within the host rocks of Messina suggest that the pipes formed by mechanical energy release during subsequent hydraulic fracturing or fluid flow (Sun *et al*., 2015).

Another recognised world's deposit comparable to Messina copper deposit is the iron oxide-copper-gold (IOCG) mineralisation and alteration events. Richards and Mumin (2013) regard IOCGs as low sulphur (S) version of porphyry Cu-Au deposits due to their loosely related characteristics. Most of them lack evidence for their genetic link with the igneous intrusion like Messina Cu deposit (Real *et al*., 2023). They are regarded as Cu-rich deposits overprinting the early iron oxide-gold deposit (Real *et al*., 2023; Haynes *et al*., 1995). The high-temperature event (IOA) was followed by the low-temperature event (IOCG), whereby copper concentrated in the low-temperature stage. The mineralisation is hosted by volcanic-sedimentary rocks of uniform composition. The textural changes of mineral assemblages are mainly attributed to temperature changes during hydrothermal activity in the host rock (e.g., Candelaria deposit in Chile). On the other hand, Messina deposit is hosted by country rocks of heterogeneous composition (e.g., pyroxene granulite, cordierite-biotite-garnet-gneiss, or amphibolite) or occur in quartz breccia veins (Bahnemann, 1986).

Olympic Dam is another renowned breccia-hosted Cu (-Au)-rich deposit that is hematite-rich and dominated by low-temperature sericitic alteration (Fabris *et al*., 2015). Figure 49 shows a sketch of Olympic Dam IOCG breccia pipe-associated mineralisation-alteration. Pervasive deep magmatic alteration is mostly present in the early high-temperature zone and not in the low-temperature sulphide-rich zone. Unlike in Messina, Olympic Dam IOCG contains abundant chalcopyrite which precipitated by replacing early magnetite and not pyrite. Hematite formed during the mixing of magmatic-hydrothermal fluid with oxidized groundwater (Belperio and Freeman, 2004). On the other hand, in Messina Cu deposit, hematite is mostly formed by transformation of magnetite minerals.

Olympic Dam alteration zones are dominated by sericite and hematite with less magnetite, silica, carbonates, and chlorite, unlike the varying alteration zones of Messina (Belperio and Freeman, 2004; Real *et al*., 2023). Moreover, the concentric sulphide zonation from pyrite outer zone to central bornite-chalcocite with hematite and less magnetite is discussed in Messina, whereas in Olympic Dam, the interpreted sulphide zonation involves vertical and lateral zonation of hematite-pyrite ± chalcopyrite with bornite and chalcocite in upper parts and chalcopyrite-pyrite in central parts. The occurrence of bornite and chalcocite in Olympic Dam were reported to have formed by supergene processes (Pirajno, 2010). The breccia characteristics of IOCGs range from simple jigsaw-like clast-supported breccia, to heterolithic matrix-supported breccia, and mixed breccia clasts associated with disseminated

mineralisation (Belperio and Freeman, 2004). These breccia features are partly similar to those described in Messina deposit (refer to Fig. 46). It has been reported that the intensity of alteration is closely associated with the degree of brecciation for Olympic Dam (Belperio and Freeman, 2004), whereas in Messina the intensity of alteration is associated with increasing oxidation of Fe oxides, increasing hydration of silicate minerals, and decreasing S content.

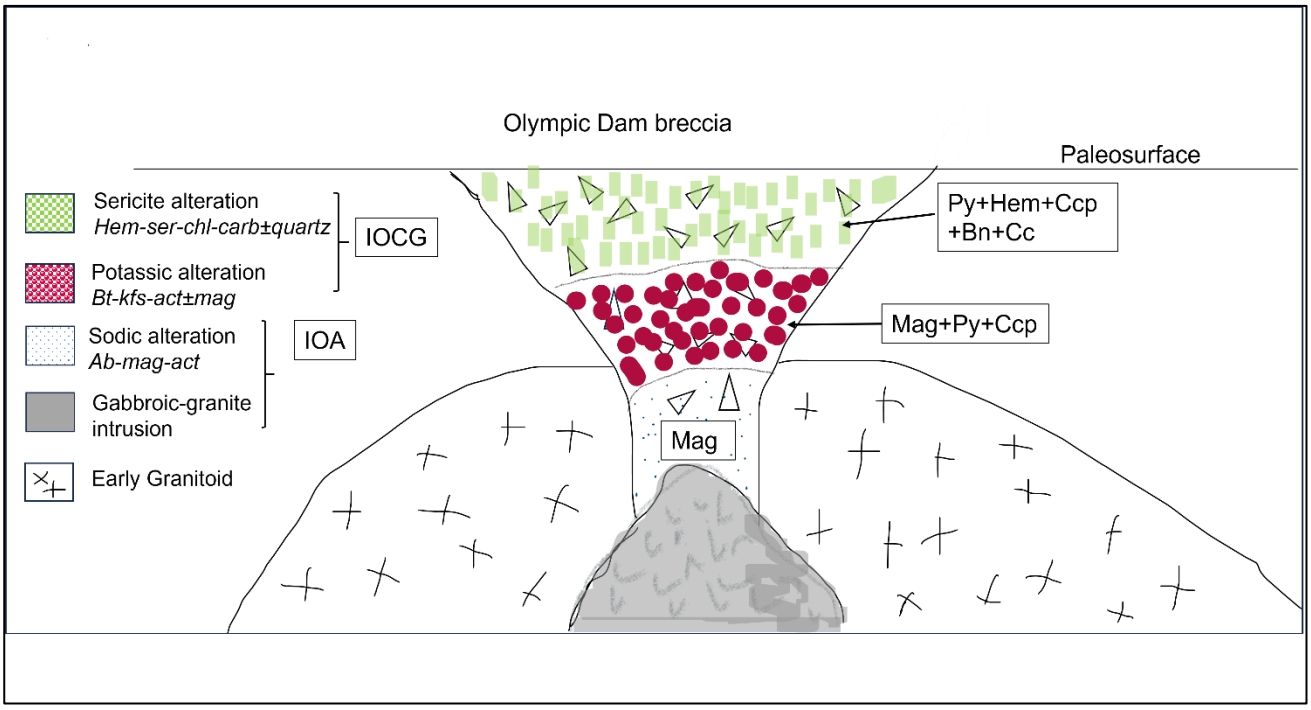


Figure 49: A sketch of the Olympic Dam IOCG breccia complex intrusion into early granitoid rocks showing mineralisation and the associated alteration within the breccia (after Reid, 2019 and Skirrow, 2022).

The alteration zonation styles of Messina Cu deposit suggest that it experienced more than one hydrothermal episode. The unusual hydrothermal fluid system in Messina is postulated to correlate with drastic compositional changes during fluid-rock interaction to produce the retrograde zonation, such that the episodic cooling of the hot hydrothermal fluids as they interacted with the cold country rock initiated retrogressive cooling. The mineralisation in the Messina deposit is suggested to be controlled by several phenomena's rather than a single magmatic-hydrothermal system. Messina breccia-hosted Cu-deposit is unique in that, unlike the traditional intrusive-related hydrothermal breccias that occur in contact with their host rocks, they occur within the host rocks, with ore minerals within brecciated altered fragments.

Messina is regarded as a blind ore, however, the passageways in and out of the pipes are still ambiguous as the formation of the blind ore is not well-documented. Nonetheless, Sillitoe (2010), discusses that a breccia pipe becomes a blind ore once the void ceases to develop upwards. This seems probable for Messina blind ores as the hydrothermal fluids circulated towards the central core, suggesting they became trapped within the breccia pipe and cooled inwards. That is, movement/circulation of the hydrothermal fluids within the breccia caused partial to strong dissolution of minerals and cementation by quartz, sulphides and/or remobilised hydrothermal alteration minerals. This dissolution may have resulted in further collapse of the breccia materials downwards, mixing fragments within the breccia body, and leading to filling of the breccia pipe. The filled breccia pipe then trapped the hydrothermal solution, preventing it from migrating further upwards and interacting with cold meteoric water. As a result, the trapped hydrothermal solution cooled laterally and inwardly resulting in the reversed zonation reported for the Messina Cu deposit. Localised brecciation resulted in continuous fluid movement within the breccia pipe. It is therefore proposed that Messina Cu deposit is controlled by hypogene processes and has both porphyry-type and IOCG affinities,

although it is not known currently whether it contains gold, opening an opportunity for further research in the Musina area.

8 Conclusion

According to the discussed mineralisation-alteration zonation, it is suggested that during ascent, the hydrothermal fluids were trapped within the breccia pipes and crystallised inwards. This resulted in retrogressive cooling, producing high-temperature minerals in the outer zones and low-temperature minerals in the inner zones. This supports Jacobsen *et al* (1976) report about decreasing temperature inwards. In this report, it was found that the ore body (chalcopyrite-bornite-chalcocite) is closely associated with chlorite-epidote-zoisite alteration zones. Alteration zones overlap with one another, suggesting that the hydrothermal fluids experienced episodic compositional changes during different stages upon reaction with the cold country rock. The findings also reveal that early stages of alteration involved sericitisation in association with pyrrhotite, accompanied by initial quartz veins and pyrite-rich zone. Evolved hydrothermal fluids involved chloritisation-epidotisation + minor zoisitisation associated with chalcopyrite-bornite-chalcocite. This implies that low-temperature alteration minerals formed predominantly in the inner zones of the ore body. This stage is also associated with strong hematitisation, indicating increasing oxidation with increasing alteration and mineralisation. The stages coincide strongly with late stage silicification by formation of quartz grains and veins that cement, overprint, and cut through earlier-formed alteration zones. The secondary quartz veins also cut through copper sulphides and some incorporates the copper sulphides, indicating the late stage of the hydrothermal activity for the Messina deposit. This observation contrasts previous studies that proposed that calcite formation by release of CO_2 represents the late stage of the Messina hydrothermal activity. Though the initial composition of the hydrothermal fluid is unknown, the alteration zones revealed that Si, Al, Fe, Mg, Ca, and K were exchanged during the hydrothermal activity. Exchange, reaction, and remobilisation of these elements during hydrothermal activity resulted in the formation of the observed alteration zones of the Messina Cu deposit.

The breccia textures reveal that migration of the hydrothermal fluid through the breccia caused localised brecciation/rebrecciation (fluid-aided) in places, where larger fragments were further fragmented into smaller pieces and mixing the fragments. Ore types reported in this work are mineralised breccias, veined ore, disseminated ore, and massive ore. These ore types often occur concurrently with one another. Thus, the consistent occurrence of ore minerals within and between brecciated altered grains suggests that the hydrothermal breccia pipe acted as a feeder for mineralisation of the Messina deposit (Chaumba *et al*., 2016). The occurrence of secondary quartz in most samples implies that the hydrothermal fluid was saturated with silica (Sawkins, 1977), however, a deep source of the hydrothermal fluid remains unknown.

Alteration zonation of the Messina deposit shows similarities with greisen and porphyry copper deposits. Consistent association of the alteration zones with sulphide-oxide assemblages also show similarities with porphyry copper systems. Nonetheless, they differ regarding hydrothermal processes and the chemical nature of the hydrothermal fluids, as seen by some different mineral assemblages. Furthermore, the retrogressive zonation of the Messina deposit is different to greisen and porphyry deposits, where high-temperature minerals occur at the core and grade outwards and upwards to low-temperature minerals. Messina is thus considered a unique copper deposit on the basis that the ore and brecciation occur within the country rocks unlike breccia-hosted hydrothermal deposits that occur in contact with their country rocks. Iron oxide-copper deposits also share similarities with the Messina Cu deposit regarding the breccia characteristics. However, IOCGs hematite formation by mixing of fluids differs to that of Messina deposit that formed by transformation of magnetite. Since the drill-hole data is not available, this work acknowledges that differences between observations with previous studies are attributed to the different methods or techniques used during interpretation analysis or the chosen location/site which the samples were collected from, and/or the complexity of the mineralogy across different mines.

Critical element Co was found to be strongly concentrated in magnetite and hematite, and slightly elevated in pyrrhotite and pyrite. Lower concentrations were found within copper sulphides. Cobalt concentrations in iron oxides are common in Vathi porphyry Cu-Au±Mo deposits of Northern Greece (Stergiou *et al*., 2021), whereas Co concentrations in pyrrhotite and pyrite are common in Cu-Co deposits of Zambia (Yiguan *et al*., 2021). This presents an opportunity for future geochemical research to explore the economic potential of Messina Cu deposit. Zinc concentrations in chalcopyrite and bornite are suggested to represent inclusions of sphalerite that could not be identified under petrographic microscopy, as Zn-bearing mineral was found to be abundant in Artonvilla mine by Mundalamo (2019). Similarly, Sn concentrations in gangue minerals are commonly associated with greisen-associated mineralisation, such as Sn-bearing cassiterite (Robb, 2005). As a result, the absence of cassiterite in both optical microscopy and TIMA observations renders an opportunity for further geochemical analysis of Messina deposit to understand the complex chemical changes within alteration and mineralisation zones.

9 Limitations

Mineral identification using TIMA software was not always consistent with petrographic observations, as some minerals that were prominent or absent in optical microscopy appeared to be prominent in TIMA or vice versa (e.g., Figs. 34, 39, 42). TIMA identified individual quartz grains where it only occurred as veins (Fig. 34). It was not always possible to distinguish between different generations of minerals (e.g., quartz 1/quartz 2 where they both occurred as grains in Fig. 36). This could be because when they both occur as grains, the texture looks closely the same unlike when they occur as grains and veins. Alteration minerals like sericite were also incorrectly identified as albite (Fig. 36). Some minerals were distributed where they were not observed using optical microscopy. For example, chlorite with epidote (Fig. 36), chalcopyrite disseminations between epidote-zoisite aggregates (Fig. 41), and hematite/magnetite along fractures of chalcocite (Fig. 37). This could be due to systematic/human error during mineral matching. Thus, TIMA requires careful interpretation as mineral identification is not always unambiguous. It was also observed that TIMA could not distinguish between hematite/magnetite due to their similar backscattered electron signal. It can be a hurdle to distinguish between composite minerals petrographically. Also, thin section thickness or polishing may affect interference colours of minerals, making them appear brighter or dull and thus, may be misinterpreted. However, TIMA was able to assign the correct mineral names and their end-members. In samples that contained only pyrite using optical microscopy, TIMA detected the co-occurrence of hematite/magnetite, pyrrhotite, and chalcopyrite, even though this finding did not apply to most samples (Figs. 39 and 44). Additionally, samples containing chalcopyrite, bornite, and chalcocite were found to be associated with covellite, but this phase was never observed using optical microscopy or high-resolution imaging (Figs. 45 and 37). However, covellite occurrence with copper sulphides is consistent with the petrographic findings of Jacobsen (1967), Jacobsen and McCarthy (1976), and Mundalamo (2019). It is therefore important that optical microscopy be used before using TIMA, unless minerals have been sheared beyond recognition and cannot be identified using optical microscopy.

Elemental concentrations were also not entirely consistent with identified minerals. For example, molybdenite concentrations remained undetected by TIMA, although the mineral was present in optical microscopy. Ce-bearing mineral (alanite) was listed in the phase map of sample P782; however, no significant (Cerium) Ce concentrations were detected. Hence, it was not included in the descriptions. This illustrates the necessity of using optical microscopy and TIMA in combination to compare and confirm the mineralogical compositions.

10 Recommendations for future work

Future research should aim at fluid inclusion studies to assist in establishing the genesis and formation temperatures of the deposit. This study sees the need to obtain bulk rock/in situ geochemical data from drill-hole material, to clearly describe processes involved in the formation of alteration and ore minerals. This will

enable improved understanding of the hydrothermal fluid composition. Additionally, the generation of a numerical reactive transport model will aid in better understanding of mineral zonation, the sequence of crystallisation, and path controls for Messina hydrothermal fluids. Detailed mapping of the area in the vicinity of the mines is also suggested in order to obtain geological and structural data to better constrain aspects of groundwater circulation. Coupled with geophysical data, gravity anomalies could aid in determining extent of the inferred NIC intrusion to establish the source of hydrothermal fluids. The tailings could be reworked for iron and copper recovery and should be analysed further for the potential of Co and other metals. A study of Cu isotopes using copper sulphides of Messina such as chalcopyrite or chalcocite is also suggested to unravel the ore genesis processes of the deposit.

11 Reference list

Bahnemann, K.P. (1986) A review of the geology of the Messina copper deposits, Northern Transvaal. *Mineral Deposits of Southern Africa*, pp. 1671-1688.

Barton, J.M., Jr., Holzer, L., Kamber, B., Doig, R. Kramers, J.D. and Nyfeler, D. (1994) Discrete metamorphic events in the Limpopo belt, southern Africa: implications for the application of P-T paths in complex metamorphic terrains. *Geology*, 22, pp. 1035-1038.

Barton, P.B., and Skinner, B.J. (1979) Sulphide mineral stabilities. In Barnes, H.L. (Eds.), *Geochemistry of hydrothermal ore deposits*. 2nd Edition. J. Wiley and Sons, pp. 278-485.

Belperio, A. and Freeman, H. (2004) Common geological characteristics of Prominent Hill and Olympic Dam – implications for iron oxide–copper–gold exploration models. In: PACRIM 2004 Congress, Adelaide, 2004. Proceedings. *Australian Institute of Mining and Metallurgy*, Melbourne, pp. 115-125.

Burt, D.M. (1981) Acidity-salinity diagrams – Application to Greisen and Porphyry deposits. *Economic Geology*, 76, pp, 832-843.

Cairncross, B. (1991) The Messina District, South Africa, *Mineralogical Report*, vol. 22, pp. 187-199.

Chaumba, J.B., Mundalamo, H.R., Ogola, J.S., Cox, J.A., and Fleisher, C.J. (2016) Petrography, sulfide mineral chemistry, and sulfur isotope evidence for a hydrothermal imprint on Musina Copper deposits, Limpopo province, South Africa: Evidence for a breccia origin. *Journal of African Earth Sciences*, 120, pp. 141-159.

Cox, D.P., Lindsey, D.A., Singer, D.A., Moring, B.C., and Diggles, M.F. (2007) Sediment-hosted copper deposits of the world: Deposit models and database, *Open File Report* 03-107, Version 1.3, pp. 1-53.

Cox, K.G., Johnson, R.L., Monkman, L.J., Stillman, G.J., Vail, J.R., and Wood, D.N. (1965) The geology of the Nuanetsi Igneous Province. *Philosophical Transactions of the Royal Society of London*, Series A, Mathematics and Physical Sciences, vol. 251, no.1078, pp. 71-218.

Craig, J.R., and Vaughan, D.J. (1994) Ore microscopy and ore petrology, 2nd edition, Chapter 7, pp. 120-161.

Elliot, J.E., Robert, J., William, R.M. and Kurt, L. (1995) Vein and greisen Sn and W deposits. *Geology*, Environmental Science, pp. 62-69.

Fabris, A., Van der Wielien, S., Keeping, T. and Gordon, G. (2015) Geochemical footprints of IOCG deposits beneath thick cover: insights from the Olympic Cu-Au Province, South Australia. *International Applied Geochemistry Symposium*, pp. 1-9.

George, L.L, Cook, N.J, and Ciobanu, C.L. (2016) Partitioning of trace elements in co-crystallized sphalerite–galena–chalcopyrite hydrothermal ores. *Ore Geology Reviews*, 77, pp. 97-116.

Guilbert, J.M., and Park, C.F. (1986) The Geology of Ore Deposits. Freeman, San Francisco, pp. 985.

Haynes, D.W., Cross, K.C., Bills, R.T. and Reed, M.H. (1995) Olympic Dam ore genesis: A fluid mixing model. *Economic Geology*, 90, pp. 63-74.

Hofmann, A., Kroner, A., and Brandl, G. (1998) Field relationships of mid-to late Archaean high-grade gneisses of igneous and sedimentary parentage in the Sand River, Central Zone of the Limpopo Belts, South Africa. *South African Journal of Geology*, 101(3), pp. 185-200.

Hemley, J.J., Cygan, G.L., Fein, J.B., Robinson, G.R., and d'Angelo, W.M. (1992) Hydrothermal ore-forming processes in the light of studies in rock-buffered systems; I, Iron-copper-zinc-lead sulfide solubility relations. *Economic Geology*, 87(1), pp. 1–22.

Jacobsen, J.B.E. (1967) The geology of the Artonvilla mine, Messina district. Unpublished Ph.D. Thesis, *University of Witwatersrand*, pp. 1-115.

Jacobsen, J.B.E., and McCarthy, T.S. (1976) An unusual hydrothermal copper deposit at Messina, South Africa, *Economic Geology*, vol. 71, pp. 117-130.

Jacobsen, J.B.E., McCarthy, T. S., and Laing, G. J. (1976) The copper-bearing breccia pipes of the Messina district, South Africa, *Minerallium Deposita*, vol. 11, pp. 33-45.

Jaeckel, P., Kroner, A., Kamo, S.L., Brandl, G., and Wendt, J.I. (1997) Late Archaean to Early Proterozoic granitoid magmatism and high-grade metamorphism in the central Limpopo belt, South Africa, *Journal of Geological Society*, London, 154, pp. 25-44.

Kelly, W.C., and Rye, R.O. (1979) Geologic, fluid inclusion, and stable isotope studies of the tin-tungsten deposits of Panasqueira, Portugal. *Economic Geology*, 74(8), pp. 1721–1822.

Lindgren, W. (1933) Mineral deposits. 4th edition, New York and London, McGraw-Hill Book Company.

Lowell, J.D., and Guilbert, J.M. (1970) Lateral and vertical alteration-mineralisation zoning in porphyry ore deposits. *Economic Geology*, 65(4), pp. 373-403.

McCarthy, T.S., and Jacobsen, J.B.E. (1976) The mineralizing fluids at the Artonvilla copper deposit: an example of a silica-deficient, alkaline hydrothermal system, *Economic Geology*, vol. 71, pp. 131-138.

Mundalamo, H.R. (2019) Investigation of the geology, structural setting and mineralisation of the copper-sulphide deposits in the Musina area, Limpopo Mobile Belt, South Africa. Unpublished Ph.D. Thesis, *University of Venda*, pp. 1-381.

Mundalamo, H.R., and Ogola, J.S. (2012) Messina copper sulphide deposits revisited: geological and structural study of the deposits. *International Multidisciplinary Scientific GeoConference: SGEM*, *1*, pp. 399-406.

Pirajno, F. (2010) Hydrothermal processes and mineral systems. *Geological Survey of Western Australia*, Springer, 100 Plain St, East Perth WA 6004.

Pirajno, F. (1992) Hydrothermal Mineral Deposits, Principles and Fundamental Concepts for the Exploration Geologist. Springer-Verlag, Berlin, pp. 709.

Real, I., Reich, M., Simon, A.C., D A., Barra, F., Rodriguez-Mustafa, M.A., Thompson, J.F.H. and Roberts, M.P. (2023) Formation of giant iron oxide-copper-gold deposits by superimposed episodic hydrothermal pulses. *Scientific Reports*, 13, no. 12041, pp. 173.

Reid, A. (2019) The Olympic Cu-Au Province, Gawler craton: A review of the lithospheric architecture, geodynamic setting, alteration systems. Cover successions and prospectivity. *Minerals*, 9(6), pp. 1-37.

Richards, J.P. and Mumin, A.H. (2013) Magmatic-hydrothermal processes within an evolving Earth: iron oxide-copper-gold and porphyry Cu ± Mo ± Au deposits. *Geology*, 41(7), pp. 767–770.

Robb, L.J. (2005) Introduction to ore-forming processes. *Blackwell Science Ltd*, 1st Edition, pp. 98-145.

Ryan, B.D., Kramers, J.D., Stacey, J.S., Delevaux, M., Barton, J.M., Jr. and Fripp, R.E.P. (1983) Strontium and lead isotopic studies and K/Rb ratio measurements relating to the original emplacement of the copper deposits near Messina, South Africa. *Special Publication of the Geological Society of South Africa*, 8, pp. 47-53.

Sawkins, F.J. (1977) Fluid inclusion studies of the Messina Copper deposits, Transvaal, South Africa. *Economic Geology*, vol. 72, pp. 619-631.

Sawkins, F.J., and Rye, R.O. (1979) Additional geochemical data on Messina Copper deposits, Transvaal, South Africa. *Economic Geology*, pp. 684-688.

Sawkins, F.J., and Rye, R.O. (1980) Additional geochemical data on the Messina copper deposits, Transvaal, South Africa-A reply. *Economic Geology*, 75, pp. 481-482.

Seedorff, E., Dilles, J.H., Proffett Jr., J.M., Einaudi, M.T., Zurcher, L., Stavast, W.J.A., Johnson, D.A., and Barton, M.D. (2005) Porphyry deposits: characteristics and origin of hypogene features. In: Hedenquist, J.W., Thompson, J.F.H., Goldfarb, R.J., Richards, J.P. (Eds.), Economic Geology 100th Anniversary Volume, pp. 251-298.

Sillitoe, R. H. (2010) Porphyry copper systems. *Economic Geology*, 105, pp. 3-41.

Skirrow, R.G. (2022) Iron oxide copper-gold (IOCG) deposits – A review (part 1): Settings, mineralogy, ore geochemistry and classification. *Ore Geology Reviews*, 140, pp. 1-36.

Smirnov, V.I. (1976) Geology of mineral deposits. *Moscow*, MIR publishers, 520 pp.

Söhnge, P.G. (1945) The geology of the Messina Copper mines and surrounding country rocks. *Geological Survey of South Africa*, Government Printer, Pretoria, *Memoir* no.40, pp. 272.

Söhnge, P.G. (1946) The geology of the Messina copper mines and surrounding country: *South African Geology Survey Memo*, 40, p. 280.

Stergiou, C.L., Melfos, V., Voudouris, P., Papadopoulou, L., Spry, P.G., Peytcheva, I., Dimitrova, D., Stefanova, E., and Giouri, K. (2021) Rare and Critical Metals in Pyrite, Chalcopyrite, Magnetite, and Titanite from the Vathi Porphyry Cu-Au±Mo Deposit, Northern Greece. *Minerals*, 11(630), pp. 1-28.

Taylor, R. (2009) Ore Textures - Recognition and Interpretation. Springer, Dordrecht, pp. 288.

Warr, L.N. (2021) IMA - CNMNC approved mineral symbols. *Mineralogical Magazine*, 85, pp. 291-320.

Titley, S. R., and Hicks, C. L. eds. (1966) Geology of the porphyry copper deposits. *Southwestern North America*, 287 Tucson, AZ: University of Arizona Press, pp. 143-150.

Valásquez, C., Carrizo, D., Salvi, S., Vela, I., Pablo, M., and Pérez, A. (2020) Tracking cobalt, REE, and gold from a porphyry-type deposit by LA-ICP-MS: A geological approach towards metal-selective mining in tailings. *Minerals*, 10(109), pp. 1-17.

Warr, L.N. (2021) IMA – CNMNC approved mineral symbols. *Mineralogical Magazine*, 85, pp. 291-320.

Whitney, D.L., and Evans, B.W. (2010) Abbreviations for names of rock-forming minerals. *American Mineralogist*, 95, pp. 185-187.

Wu, D., Pan, J., Xia. F., Huang, G., and Lai, J. (2019) The mineral chemistry and its relationship with Uranium mineralisation from Huangsha Uranium mining area in the middle Nanling Range, South East China, *Minerals*, 9(13), pp. 199-214.

Yiguan, L.U., Jiarun, T.U., Kai, S.U.N., Peng, Q.I.N., Huaqing, W.A.N.G., Shangfei, H.E., Hang, Z.H.A.N.G., Penghui, G.O.N.G., Ke, F.E.N.G., and Wenyan, N.E. (20210 Cobalt occurrence and ore-forming process in the Chambishi depositin the Zambian Copperbelt, Central Africa. *Earth Science Frontiers*, 28(3), pp. 338-354.

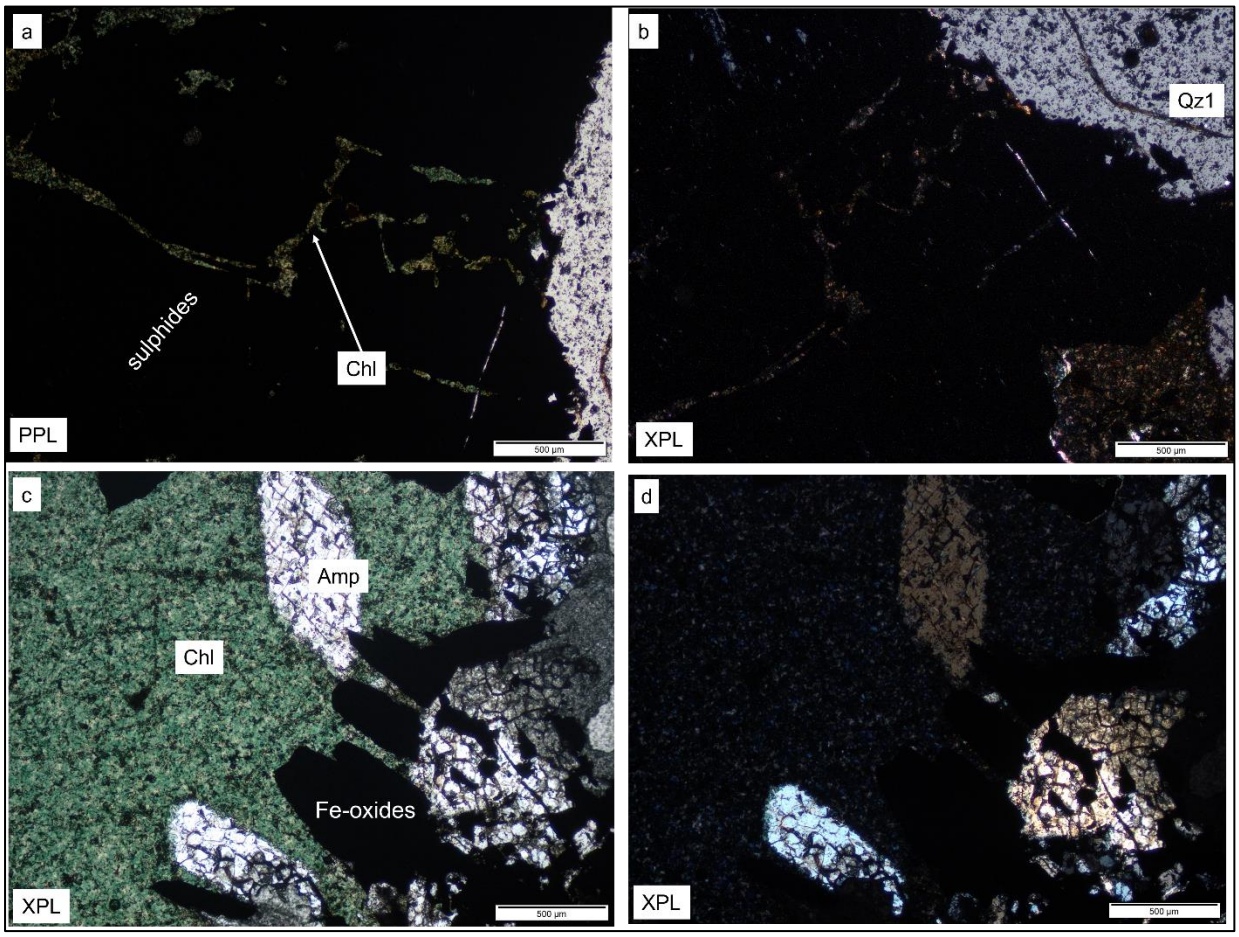
Appendix A

Petrography

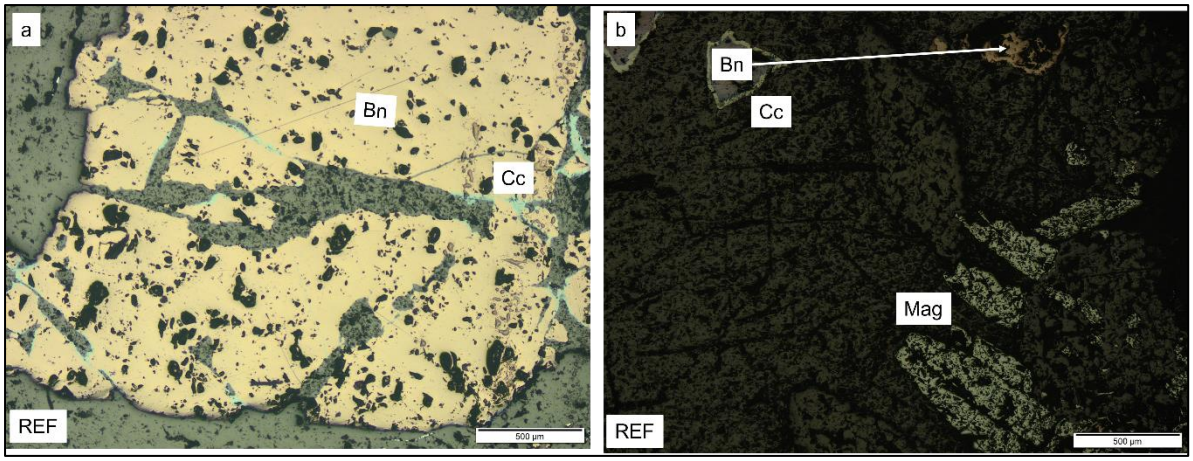
These samples are the collections from the School of Geosciences at the University of the Witwatersrand. Magnification scale = 500 µm and 200 µm (where stated).

Sample 19068

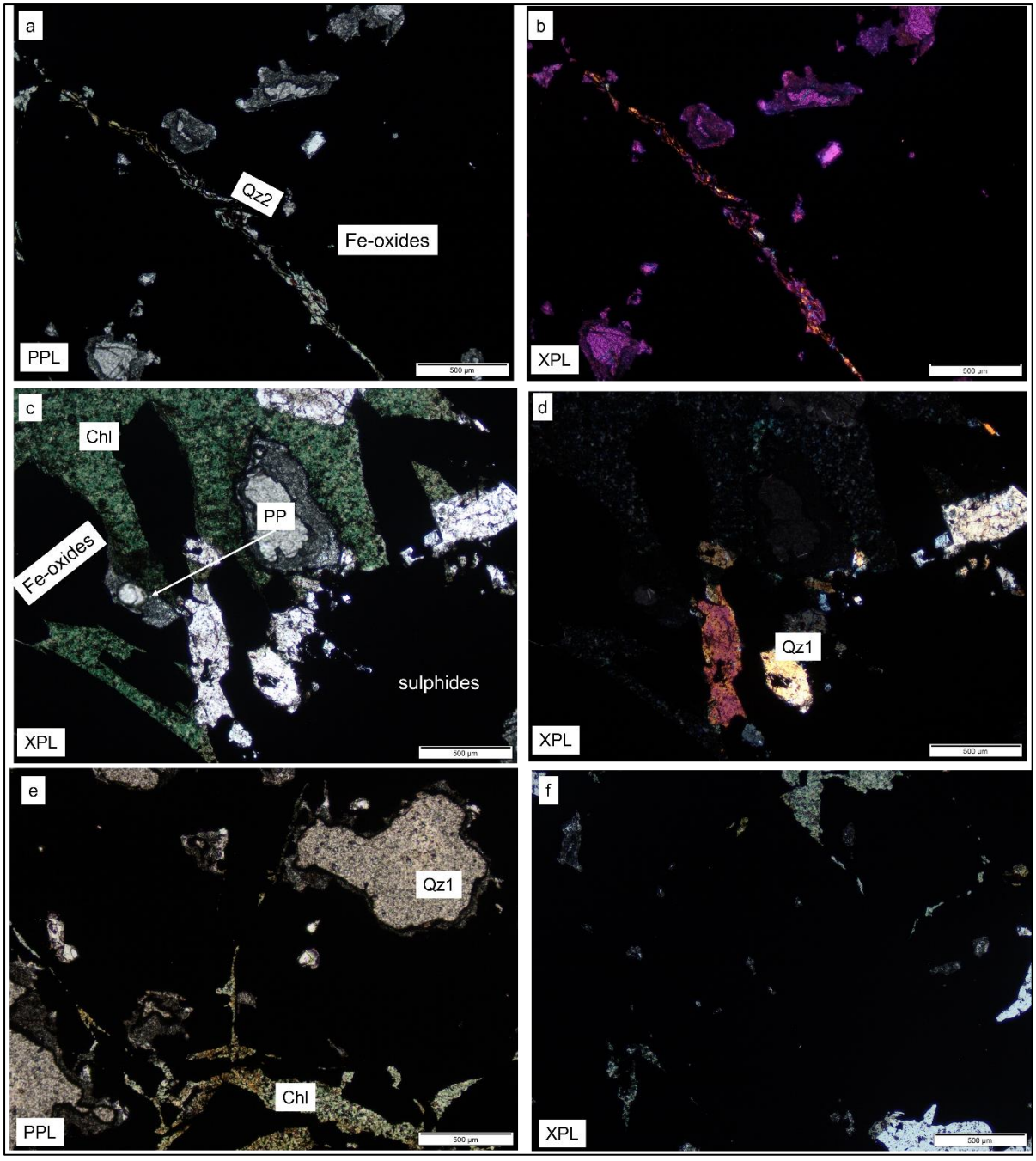
Full scan images of the thin section for sample 19068 could not be produced due to technical issues with the Full-scanning microscope in the WITS Imaging Lab (WIMLab).



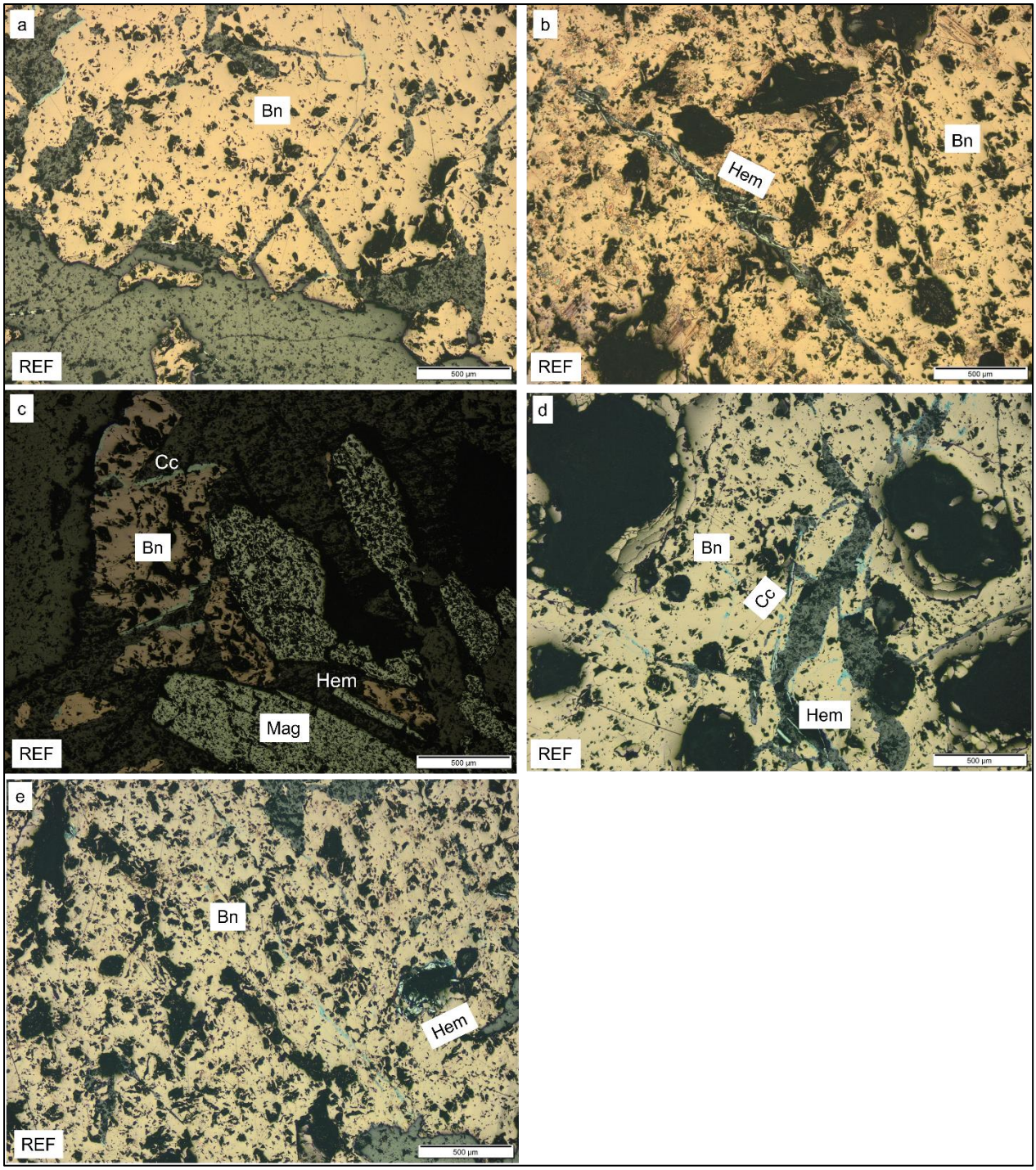
A1: (a-b) fine grained brown and green chlorite occurs as irregular veinlets within the opaque minerals and as subhedral fine grains in contact with or bordered by large quartz grains; (c-d) remnant fractured amphibole grains occur within the chlorite groundmass that encloses the opaque minerals.



A2: (a) subhedral massive bornite is surrounded by chlorite groundmass and other chlorite veinlets cut across it; (b) magnetite laths are surrounded by fine-grained chlorite groundmass which also occurs between the laths. The remnant gangue is seen being corroded by the magnetite in some parts. The bright colour of the bornite is due to reflected light exposure/reflectance.

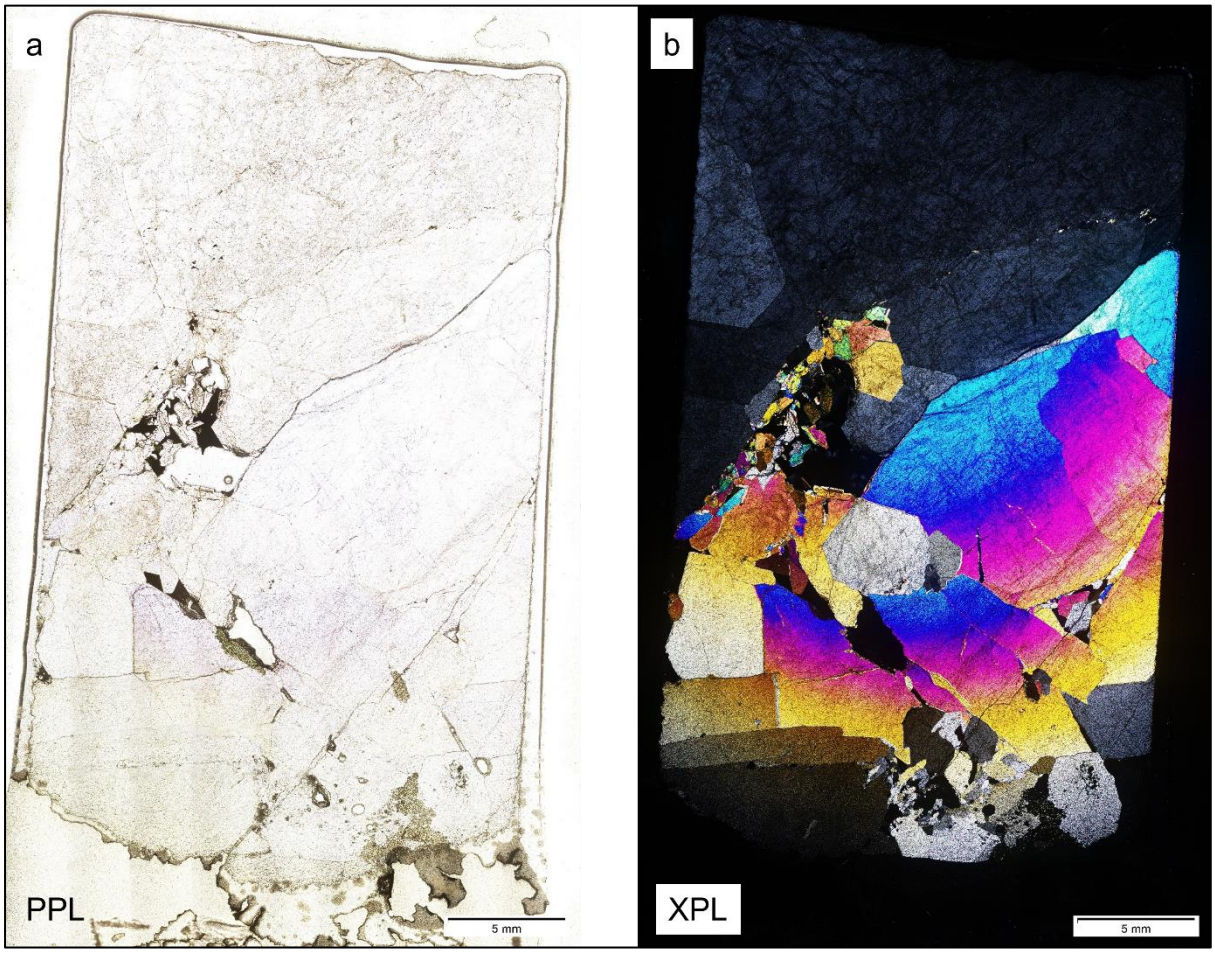


A3: (a-b) a thin quartz vein cut across the opaque minerals. Other subhedral to subrounded quartz grains are distributed within the opaque minerals. In XPL the chlorite is deep blue; (c) green fine-grained chlorite cements the opaque minerals. Quartz angular fragments occur within the opaque minerals and chlorite groundmass; (e) irregular medium to thin chlorite veinlets are present within the opaque minerals and also occur around angular quartz grains.

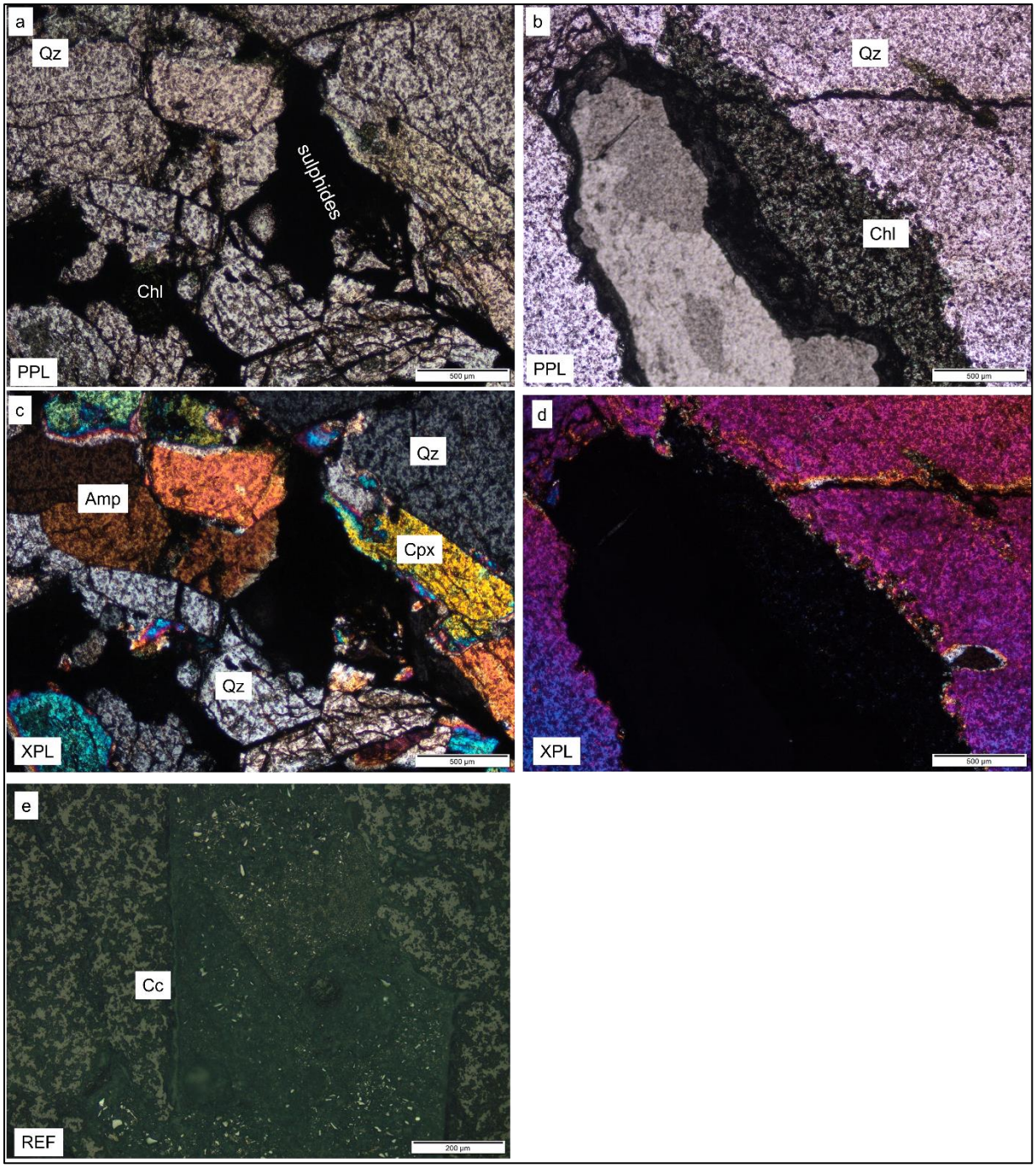


A4: (a-b) tarnished bornite is invaded and bordered by the chlorite gangue. Other isolated bornite grains occur within the surrounding quartz gangue. Small, bladed hematite grains occur within the chlorite vein cutting through the massive bornite. The change in colour of bornite could be due to oxidation or reflected light exposure effect because no chalcopyrite was observed in the hand specimen; (c) subhedral and tabular magnetite laths occur in association with bornite that is rimmed by chalcocite. A single hematite platelet occurs between the magnetite and is hosted by chlorite veins/interstitial gangue; (d) hematite platelets are embedded in chlorite gangue that cuts across the coarse-grained bornite. Irregular blue chalcocite occurs within the bornite and along the contact between bornite and chlorite. The black holes are polishing pits; (e) in other parts, coarse-grained massive bornite occurs with inclusions of subrounded and angular quartz and chlorite gangue. Hematite grains are present in fractures within the host bornite.

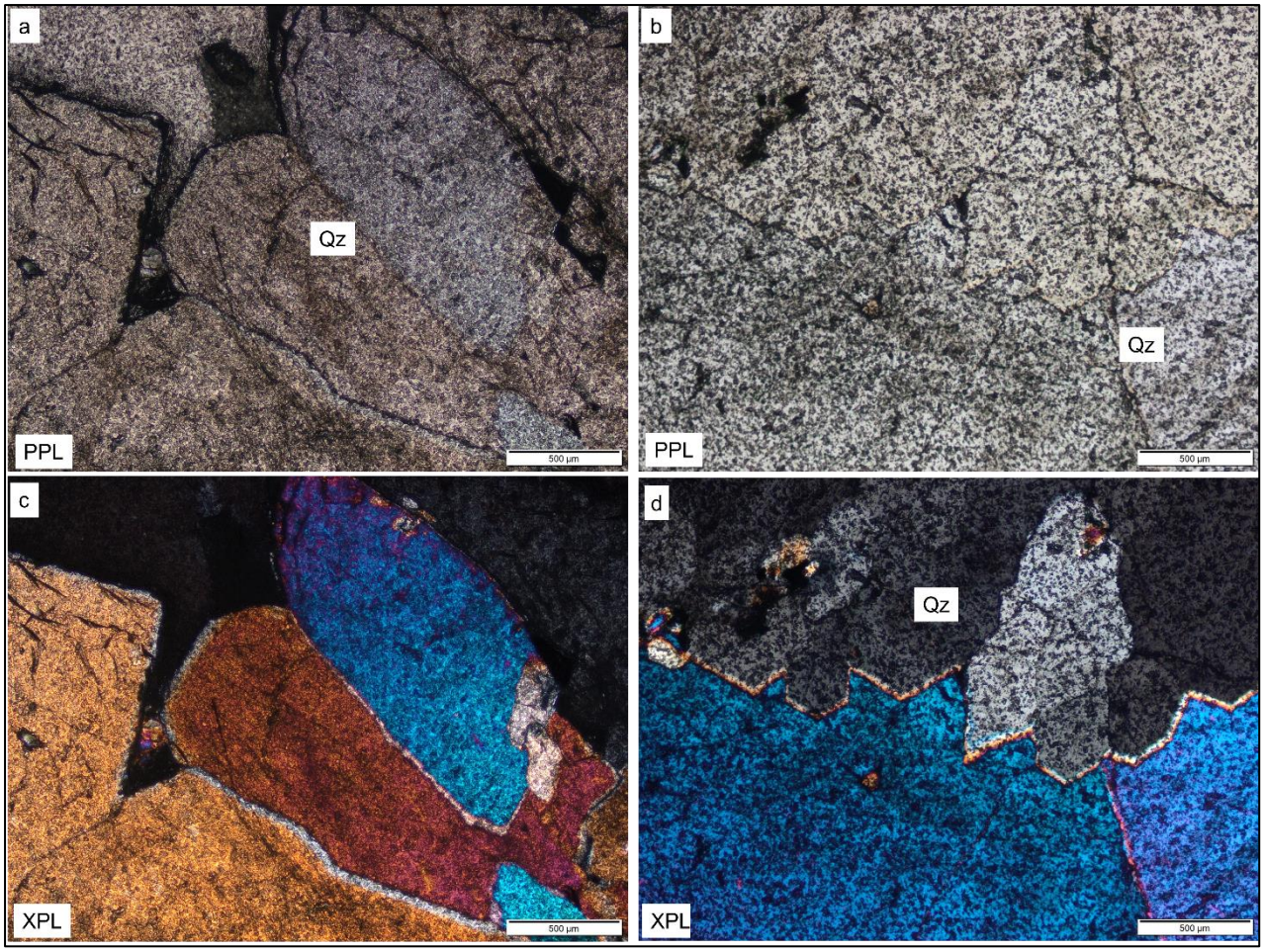
Sample 19077



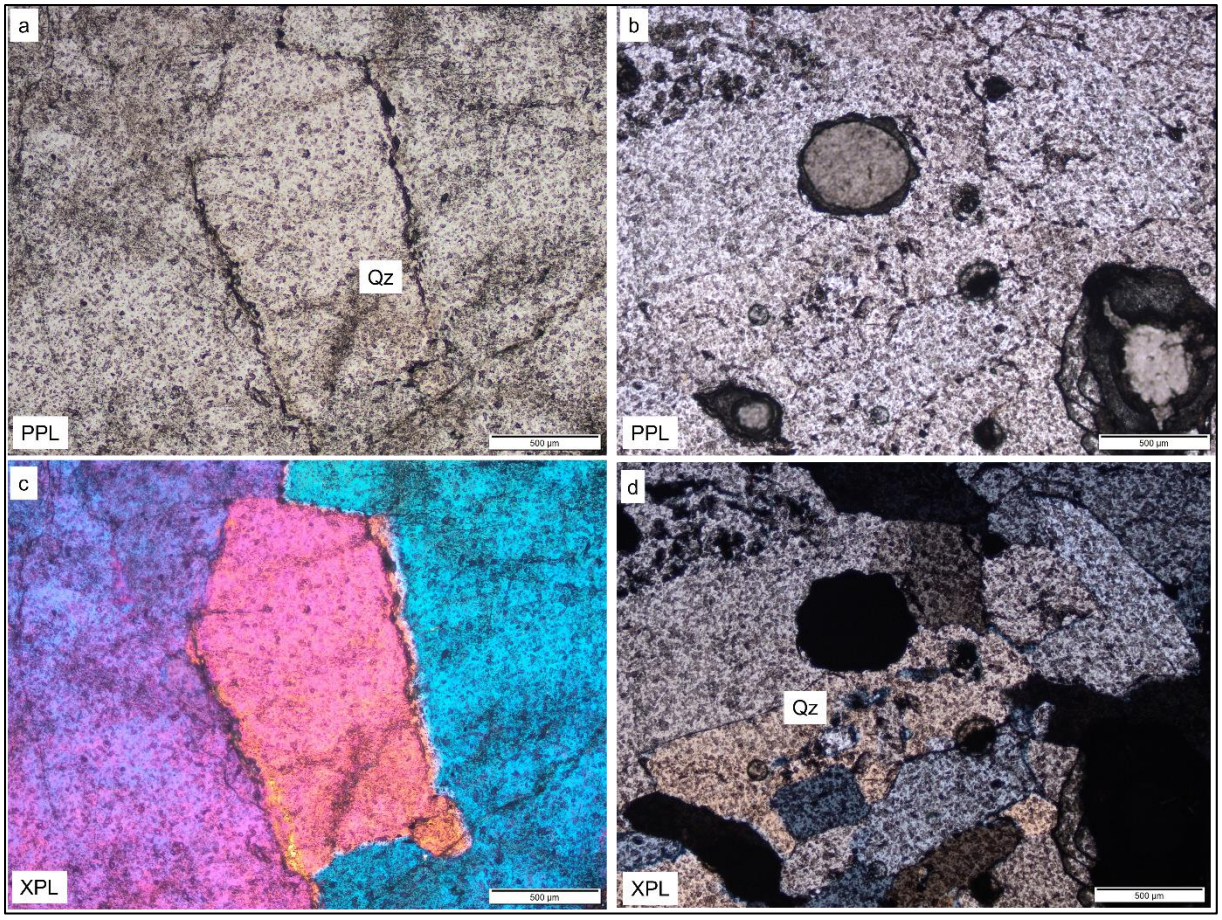
A5: Full-scan photomicrographs for sample 19077 in (a) PPL and (b) XPL. The sample is dominated by quartz grains. Other silicate minerals and the sulphides are concentrated in open spaces/fractures between the large quartz grains. The thin section size = 5 mm.



A6: (a) medium to large, fractured quartz grains surround granular chlorite and the opaque minerals; (b) large, fractured quartz grains are associated with the granular chlorite that appear to be filling an open space between the quartz grains; (c) angular, fractured, small-medium quartz and remnant cpx and amphibole grains occur within an open space between large quartz grains surrounding them. The grains appear to be partly dismembered and could represent localised brecciation. Opaque minerals occur between the grains in the open space; (d) XPL photomicrograph of (b) shows the deep blue granular chlorite within the open space of quartz grains; (e) the fractured silicates surround tiny chalcocite (Cc) disseminations.

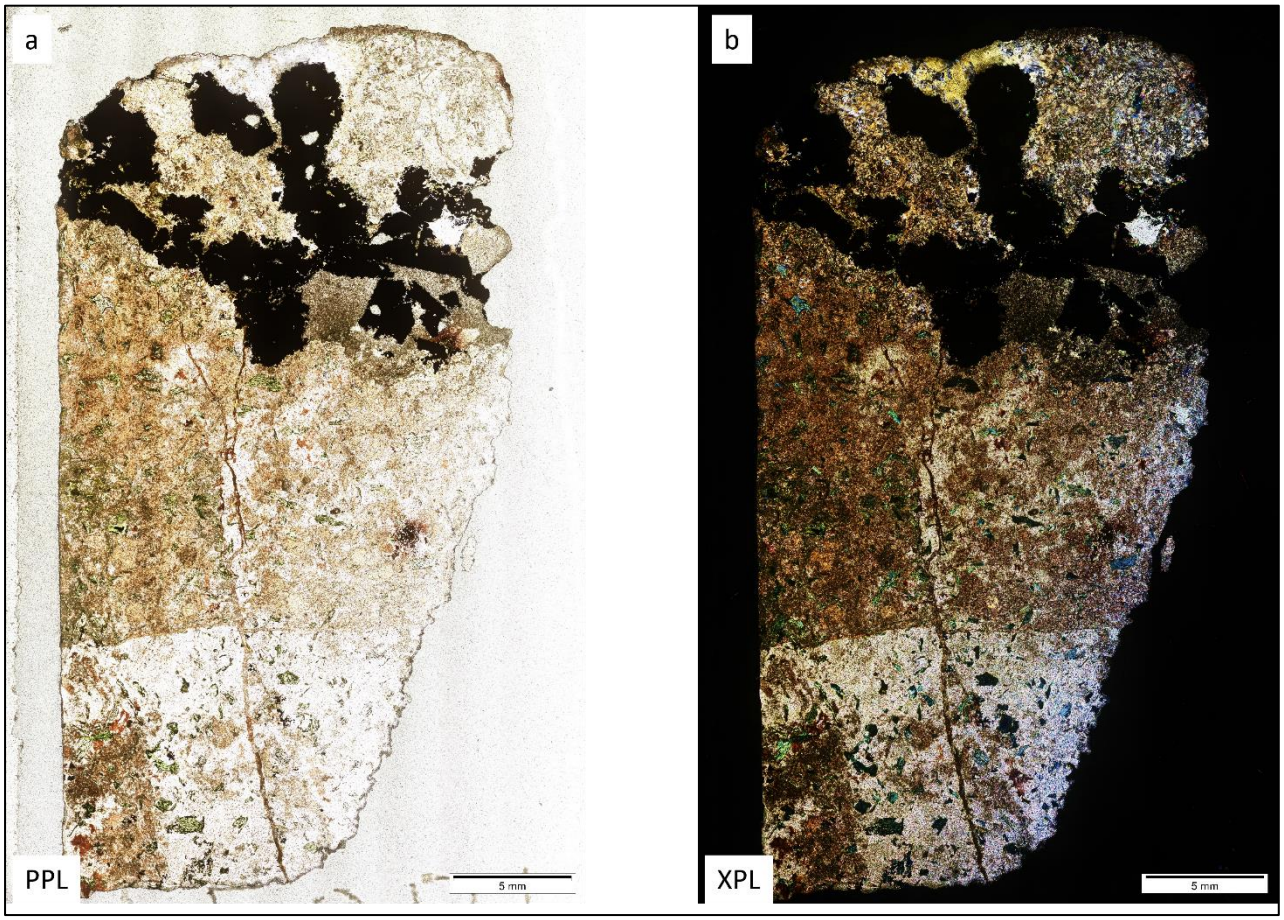


A7: Different morphologies of small to large quartz grains occur in contact with one another. The quartz grains are intergrown together and are subhedral, angular and sub-rounded. In XPL (c-d) the quartz grains show sharp, irregular and sutured grain boundaries. Minor fractures or open spaces between large quartz grains are filled with small subrounded and angular quartz grains, representative of remobilization of grains and localised brecciation.

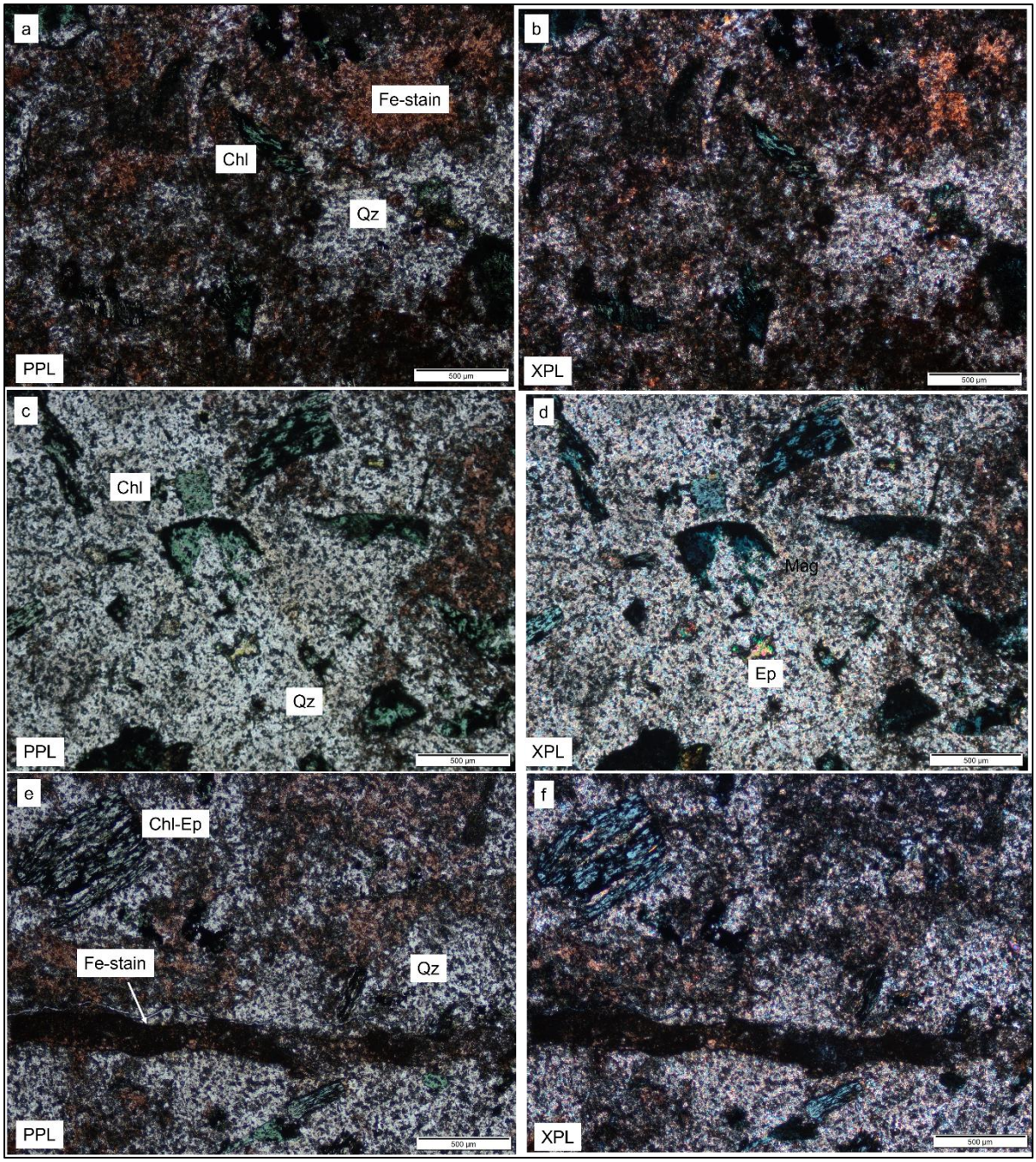


A8: (a-c) interconnected quartz grains with irregular-smooth grain boundaries. The rounded dark grey grains represent polishing pits; (d) subhedral and sub-rounded quartz inclusions also occur between large grains. The grains appear to be partly brecciated though still in contact with one another. The black areas within the grains are polishing pits.

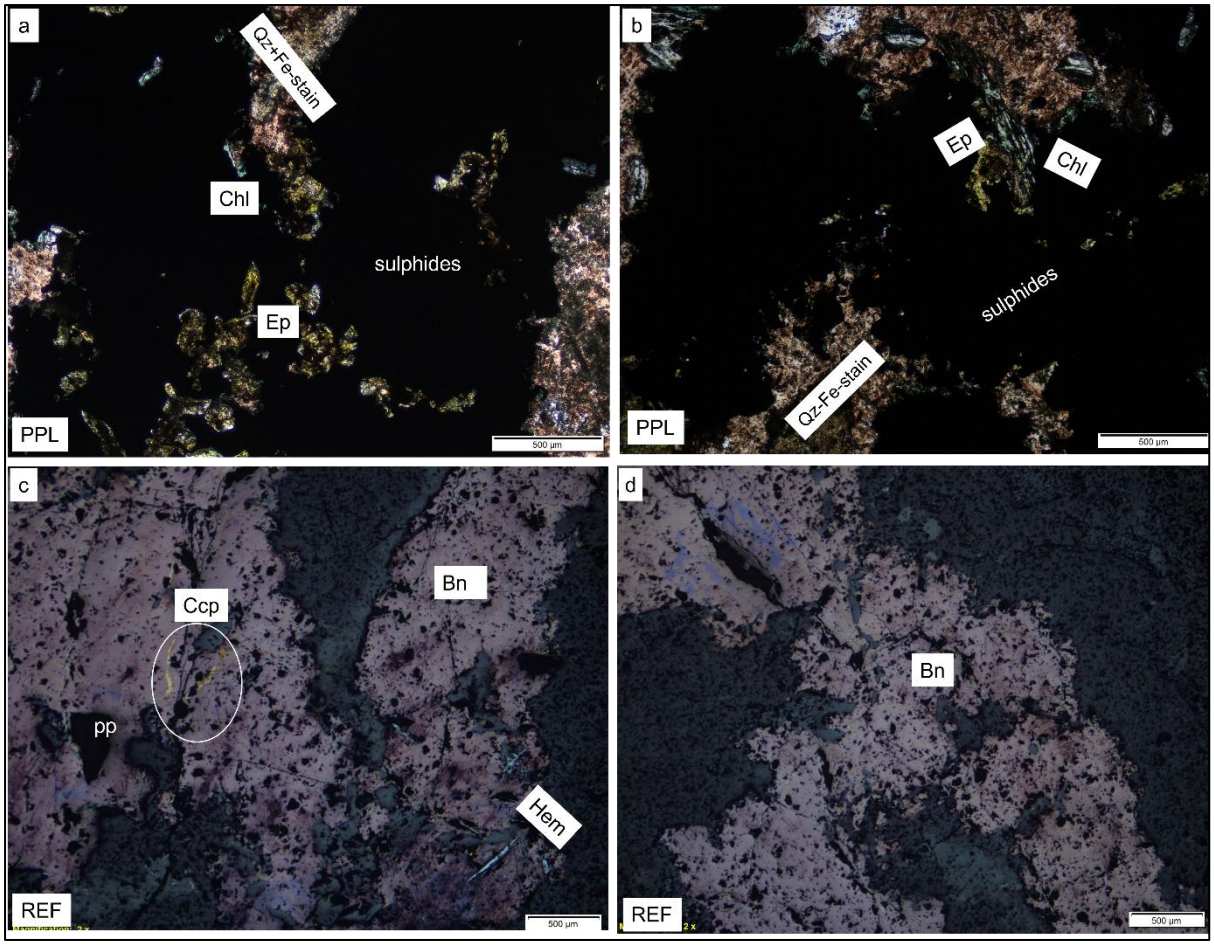
Sample 19073



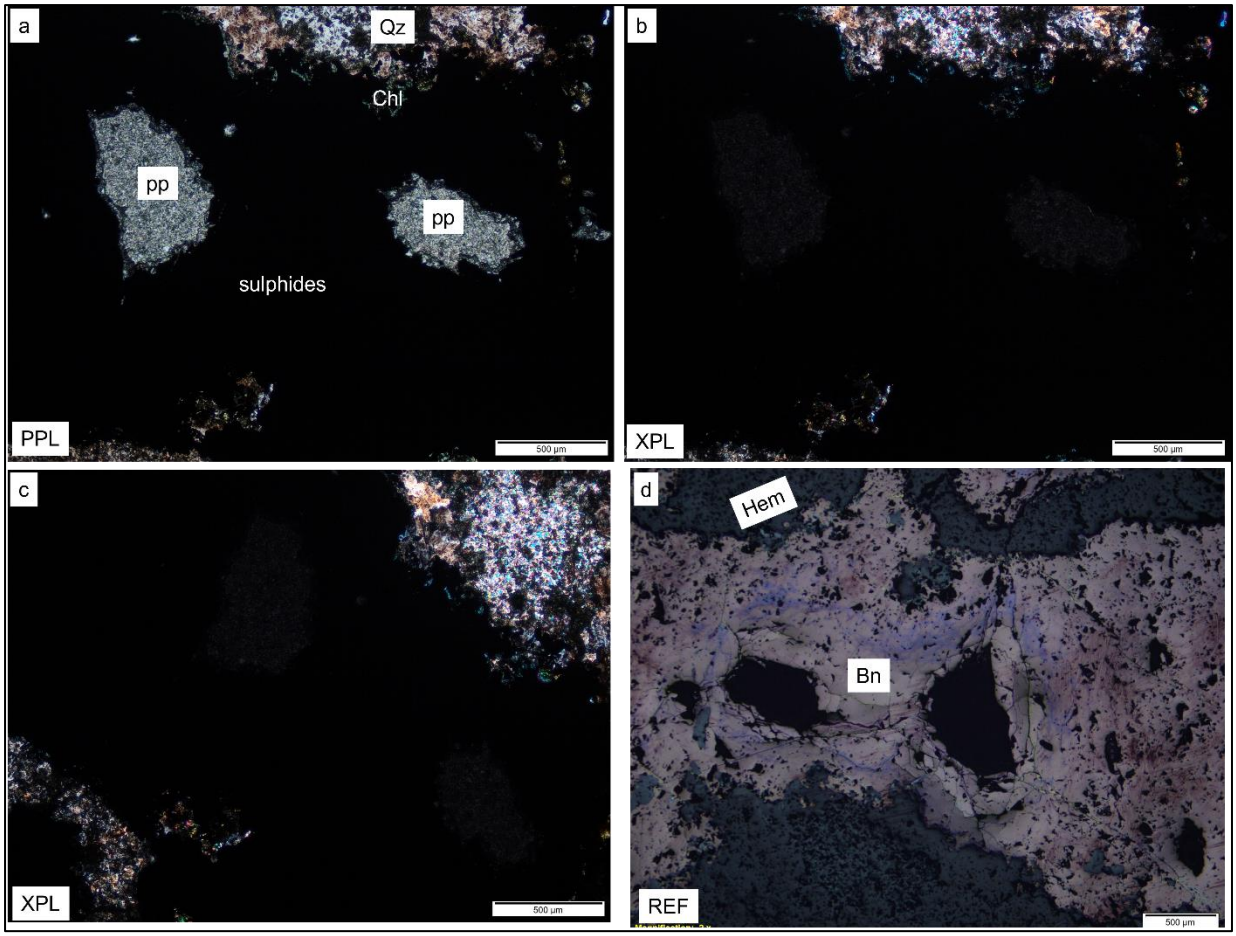
A9: Full-scan photomicrographs for Sample 19073 in (a) PPL and (b) XPL. Microcrystalline quartz makes up the groundmass for this sample. It is heavily coated by Fe-staining such that the quartz appears brown red. Small, elongated and subhedral grains of green-blue chlorite and harlequin epidote are embedded within the microcrystalline quartz groundmass. Fe-stained quartz veins cut through the groundmass and not the opaque minerals. Subhedral to irregular opaque minerals are surrounded by the microcrystalline groundmass and also contain irregular grains of quartz, chlorite and epidote. Sample size = 5 mm.



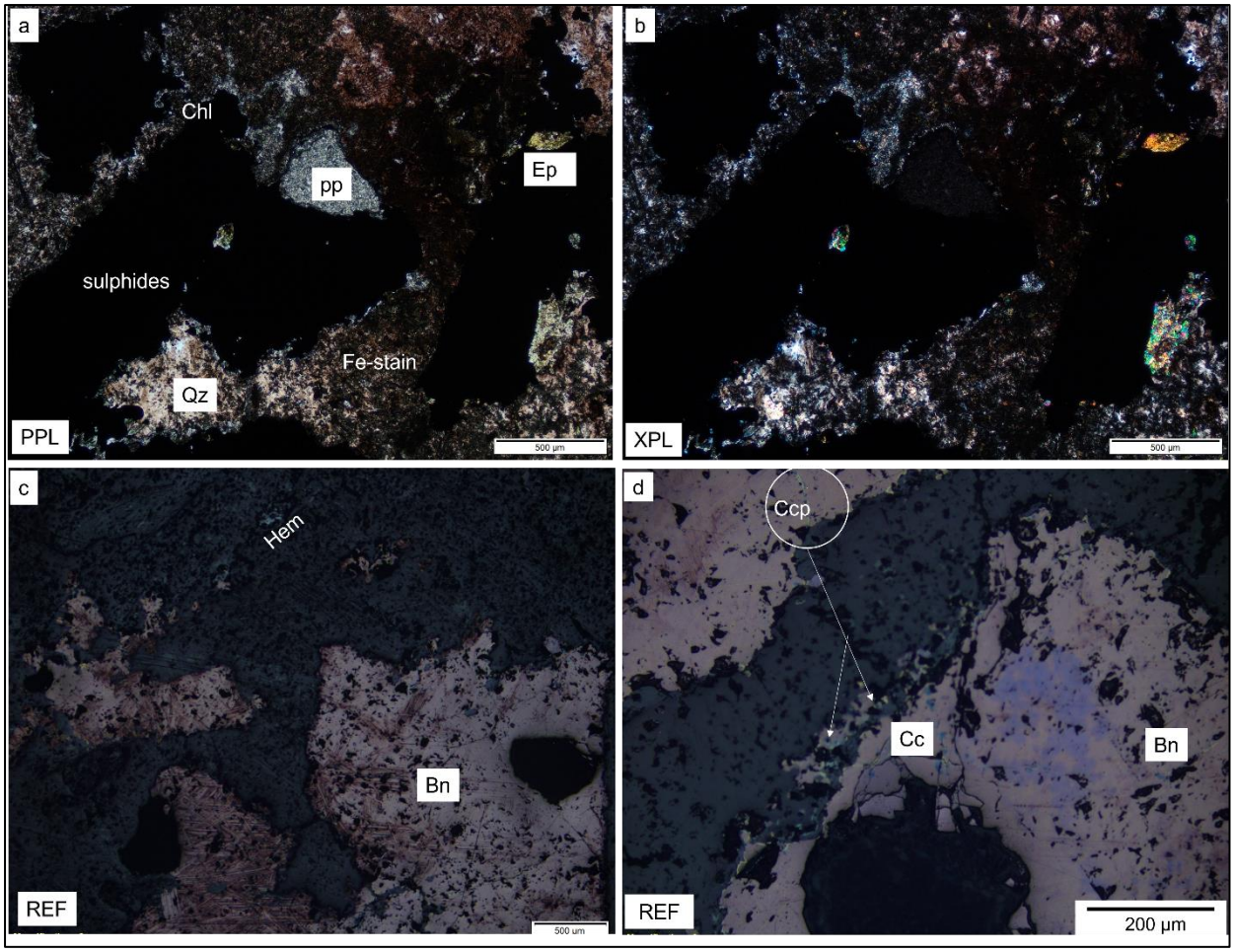
A10: (a-b) cryptocrystalline quartz groundmass with iron staining and inclusions of green chlorite; (c) irregular and elongate green chlorite and minor epidote within the cryptocrystalline quartz groundmass that is stained with brownish-red iron; (d) blue-green chlorite and harlequin-colored epidote occur within the white cryptocrystalline quartz groundmass; (e) tabular chlorite grains are present within the iron-stained cryptocrystalline quartz groundmass and have completely altered biotite along cleavage planes. Iron-stained vein cut the section E-W and contains tiny chlorite grains; (f) impurities of epidote occur along the chlorite cleavage plane.



A11: (a) cryptocrystalline quartz groundmass is extensively stained with iron oxides. Brownish-yellow euhedral to irregular epidote occurs within the opaque minerals and at the edges of cryptocrystalline quartz; (b) chlorite is partially altering into epidote grains along margins of the iron-stained cryptocrystalline quartz groundmass. Chlorite is in contact with cryptocrystalline quartz and the opaque minerals. It is also present within the opaque minerals as small irregular grains; (c) bright-yellow flame-like relics of chalcopyrite (white circle) occur within the subhedral bornite. Elongated and tiny hematite blades occur within the host bornite and are in contact with epidote gangue. Black holes represent polishing pits; (d) coarse-grained subhedral bornite cut by quartz, chlorite-epidote gangue.

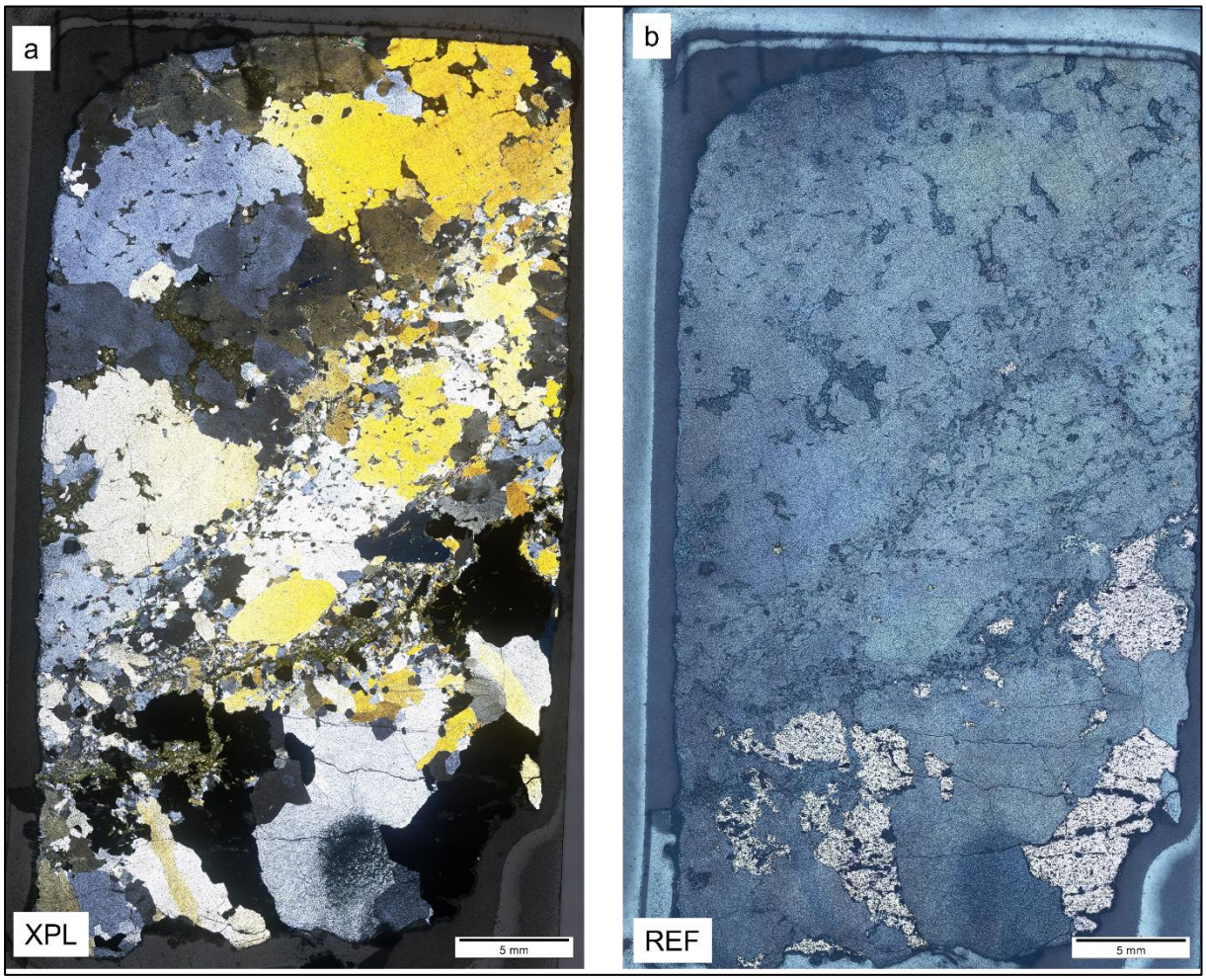


A12: (a) isolated cryptocrystalline quartz grains are present within the opaque minerals as well as irregular chlorite rim along quartz margins. The chlorite rim is partly corroded and in contact with the opaque minerals; (b) in crossed polarising light, the quartz grains appear dark grey and indicate lost material during polishing. The colourful material on cryptocrystalline quartz represents fine-grained epidote; (c) fine-grained epidote occurs in close contact with the opaque minerals at margins of cryptocrystalline quartz; (d) subhedral mass of bornite with purple coating is surrounded and cut by the cryptocrystalline quartz gangue. Epidote gangue occurs within bornite. Tiny hematite platelets occur along the margins of the host bornite.

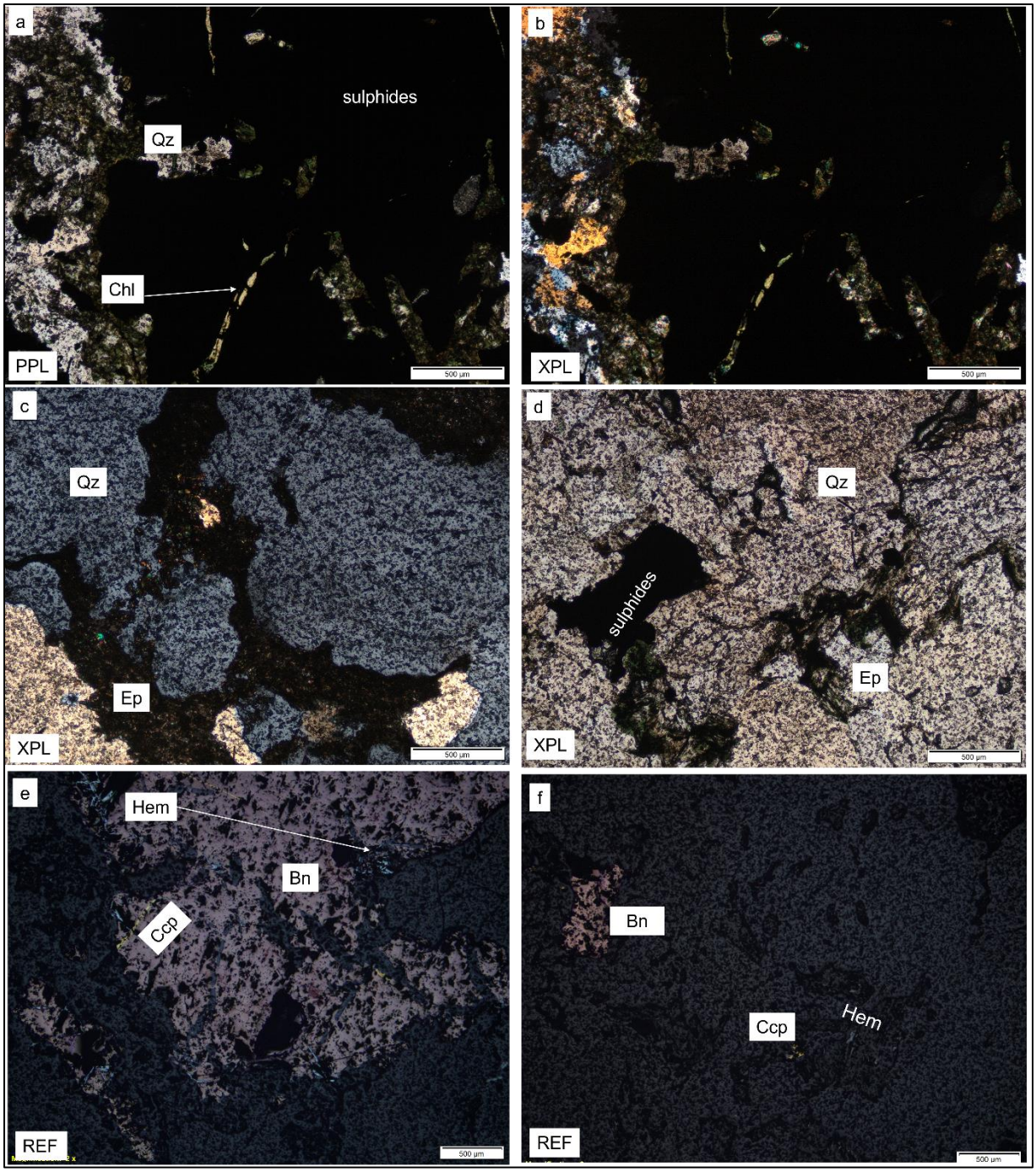


A13: (a-b) heavily iron-stained cryptocrystalline is intergrown with irregular chlorite that is partially altered into epidote and enclose the opaque minerals; (c-d) coarse-grained subhedral bornite is enclosed by quartz and chlorite-epidote gangue. Bornite contains tiny spots of a blue chalcocite (white circle and arrows) and yellow chalcopyrite relics.

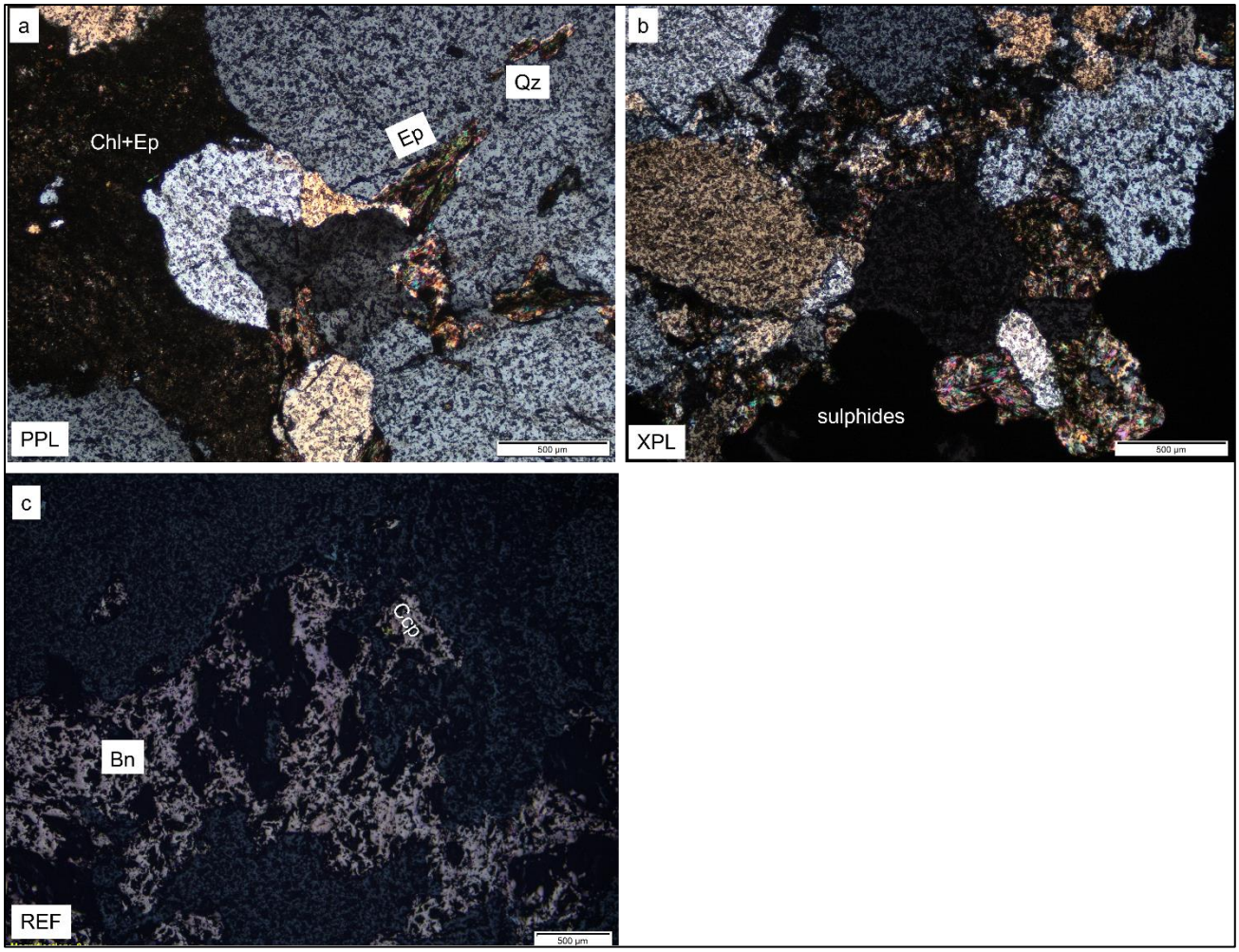
Sample 19075



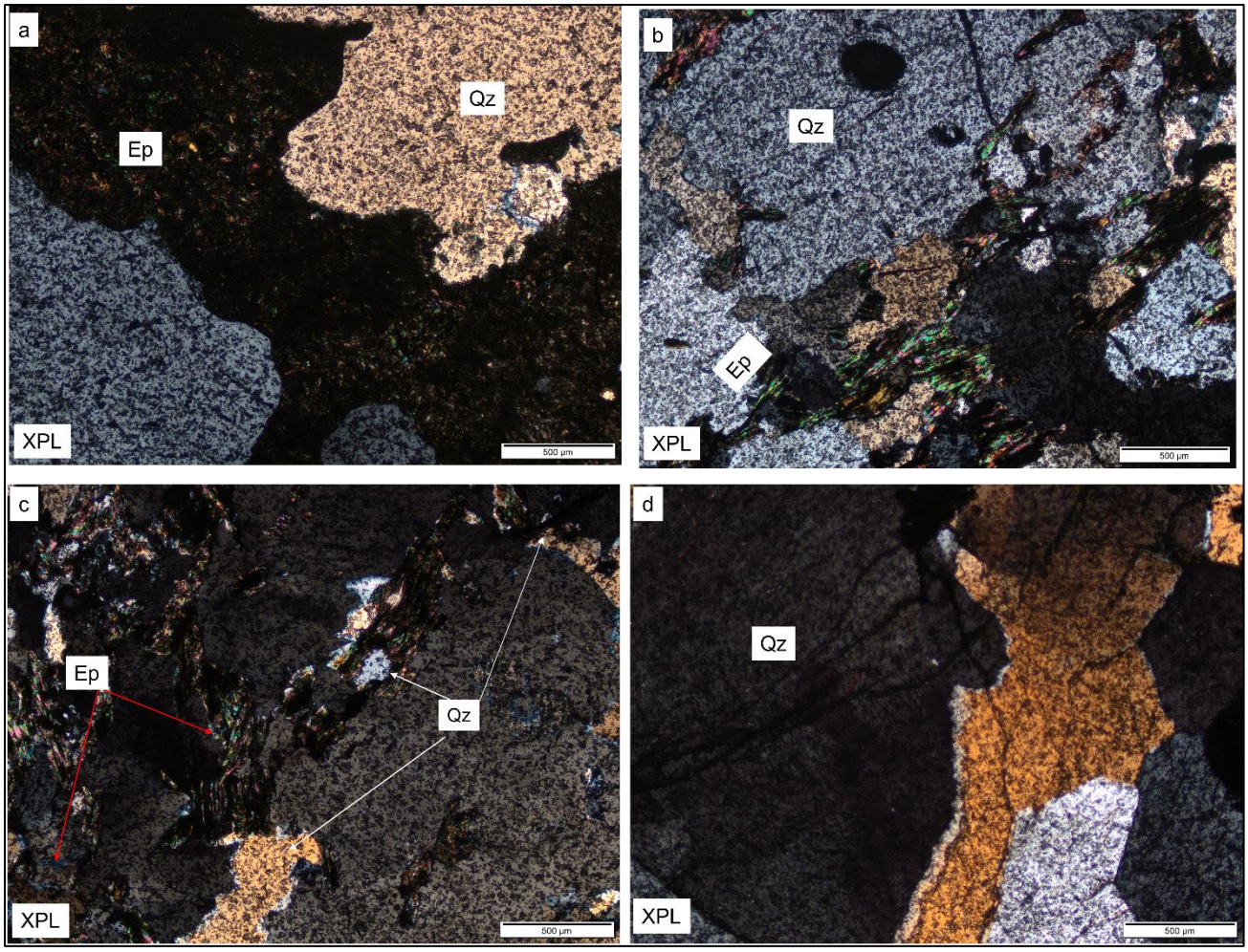
A14: Full-scan photomicrographs for Sample 19075 in XPL and REF: (a) large subhedral quartz grains are partly interconnected and in contact with micro-brecciated quartz grains that are preferentially aligned between the large quartz grains. Granular brownish-green chlorite-epidote is interstitial between the quartz grains; (b) reflected light microscopy shows that the sample is dominated by bornite that occurs as subhedral to anhedral grains between quartz grains. Small bornite and yellow chalcopyrite disseminations also occur. Sample size = 5 mm.



A15: (a-b) Elongated flakes of chlorite occur within the opaque minerals and appear to be growing from the granular chlorite at the margins of quartz grains; (c-d) intergrown quartz grains with distinct grain boundaries are invaded by granular interstitial chlorite that is partially altered into epidote. The granular chlorite-epidote contains inclusions of micro-brecciated quartz grains. The opaque minerals are enclosed within the quartz grains and partly in contact with interstitial chlorite: (e) tiny Hem platelets occur along the margins of tarnished bornite in places. Relics of bright-yellow chalcopyrite occur within the host bornite; (f) Bn occurs between quartz grains, as well as chalcopyrite as disseminations. Tiny bluish-grey hematite occurs within the interstitial chlorite between quartz grains.

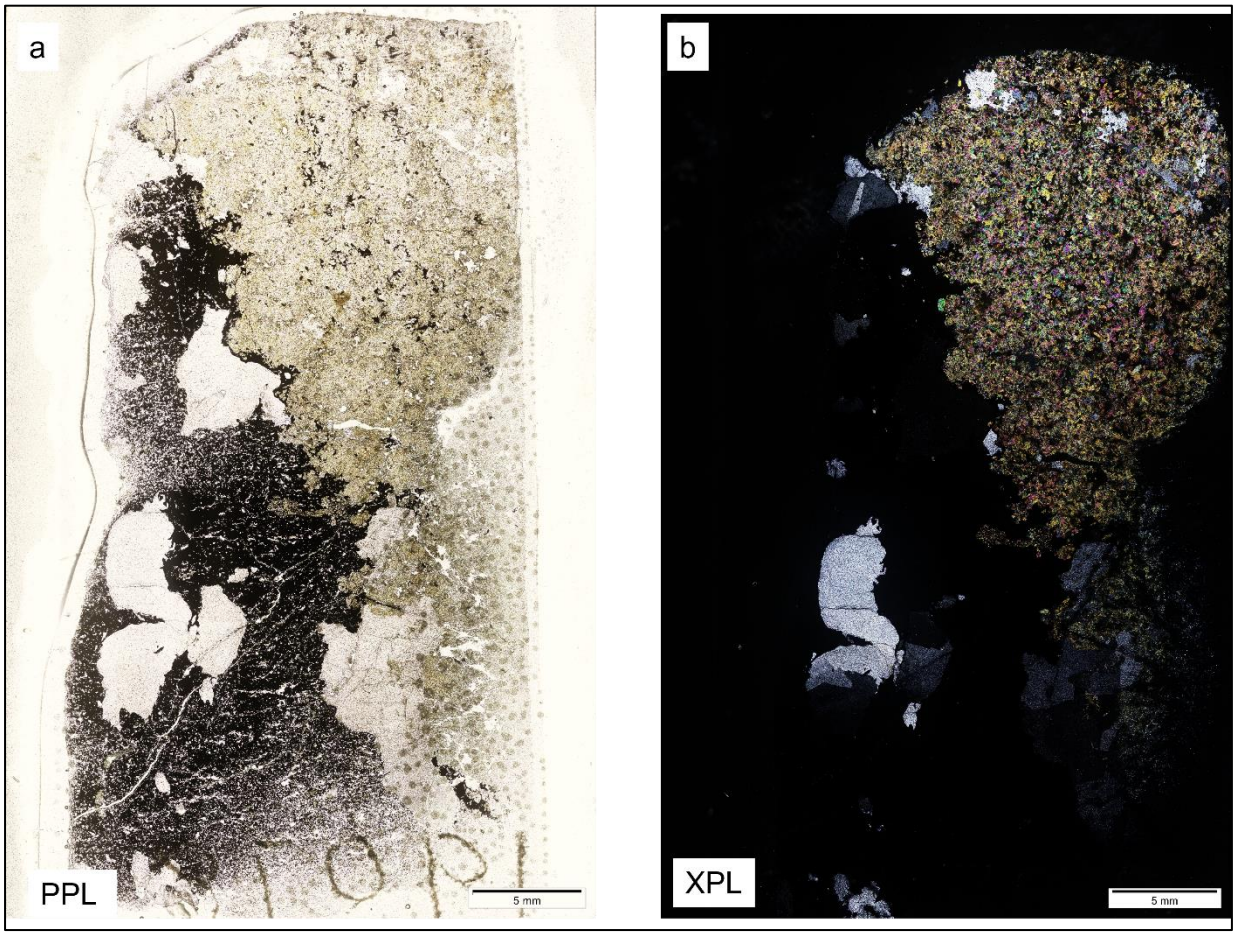


A16: (a-b) epidote flakes occur between the quartz grains. In other places, the epidote appears granular and represents complete alteration of the chlorite. Subhedral small-medium quartz is intergrown with large quartz and some are included within the granular epidote between the grains. Where the interstitial chlorite-epidote or epidote flakes occur the quartz grains appear micro-brecciated and where they are not present, they are interconnected and large. The opaque minerals are enclosed within the silicates; (c) coarse-grained subhedral bornite occurs between the quartz and chlorite+epidote gangue. Some grains occur as disseminations between small spaces of quartz grains. Chalcopyrite is completely altered by bornite and appears as relics within the host bornite.

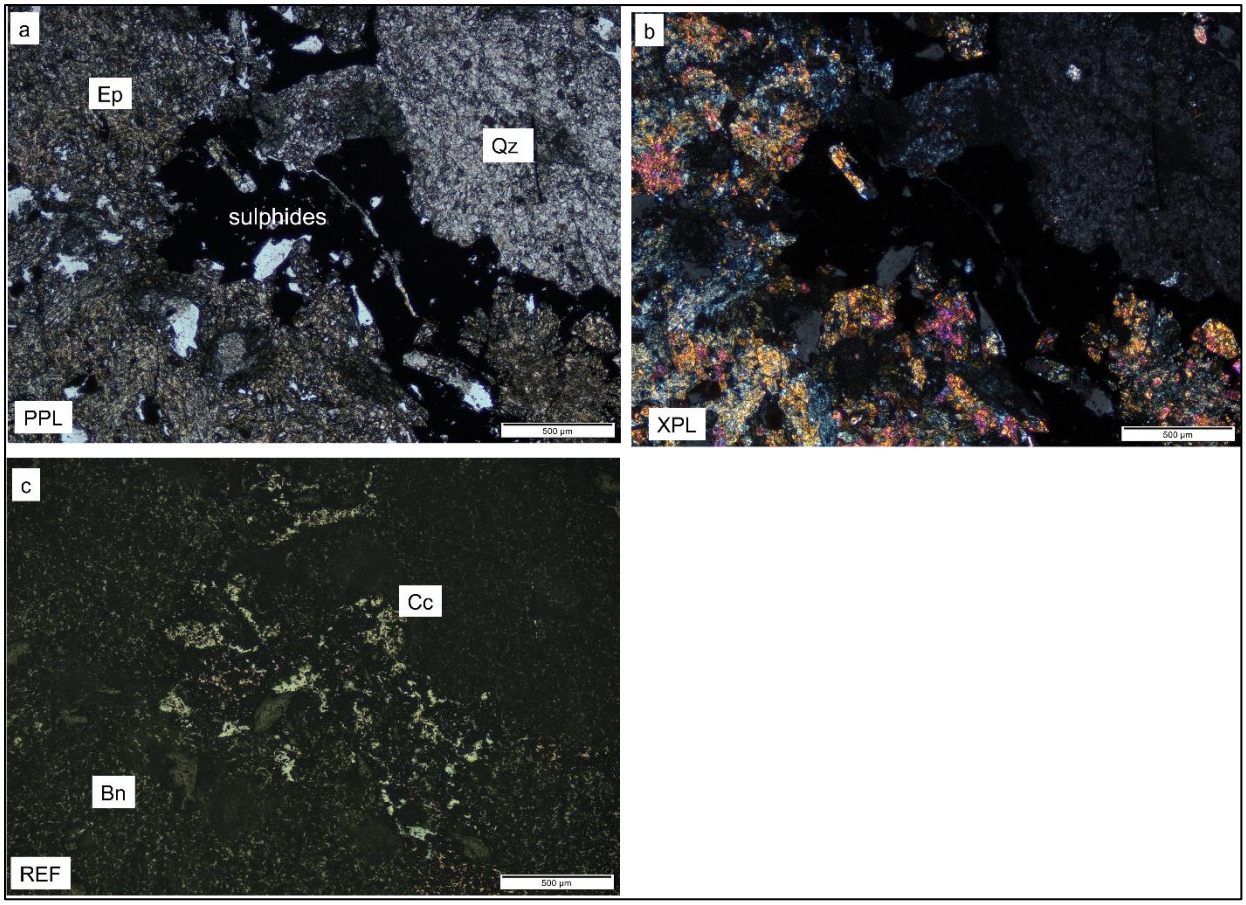


A17: (a) subhedral, large quartz grains invaded by interstitial epidote that has completely altered chlorite; (b-c) fibrous epidote grains also occur between the grains and where they occur the quartz grains appear micro-brecciated; (d) large, interconnected quartz grains that are fractured and have sharp to smooth grain boundaries.

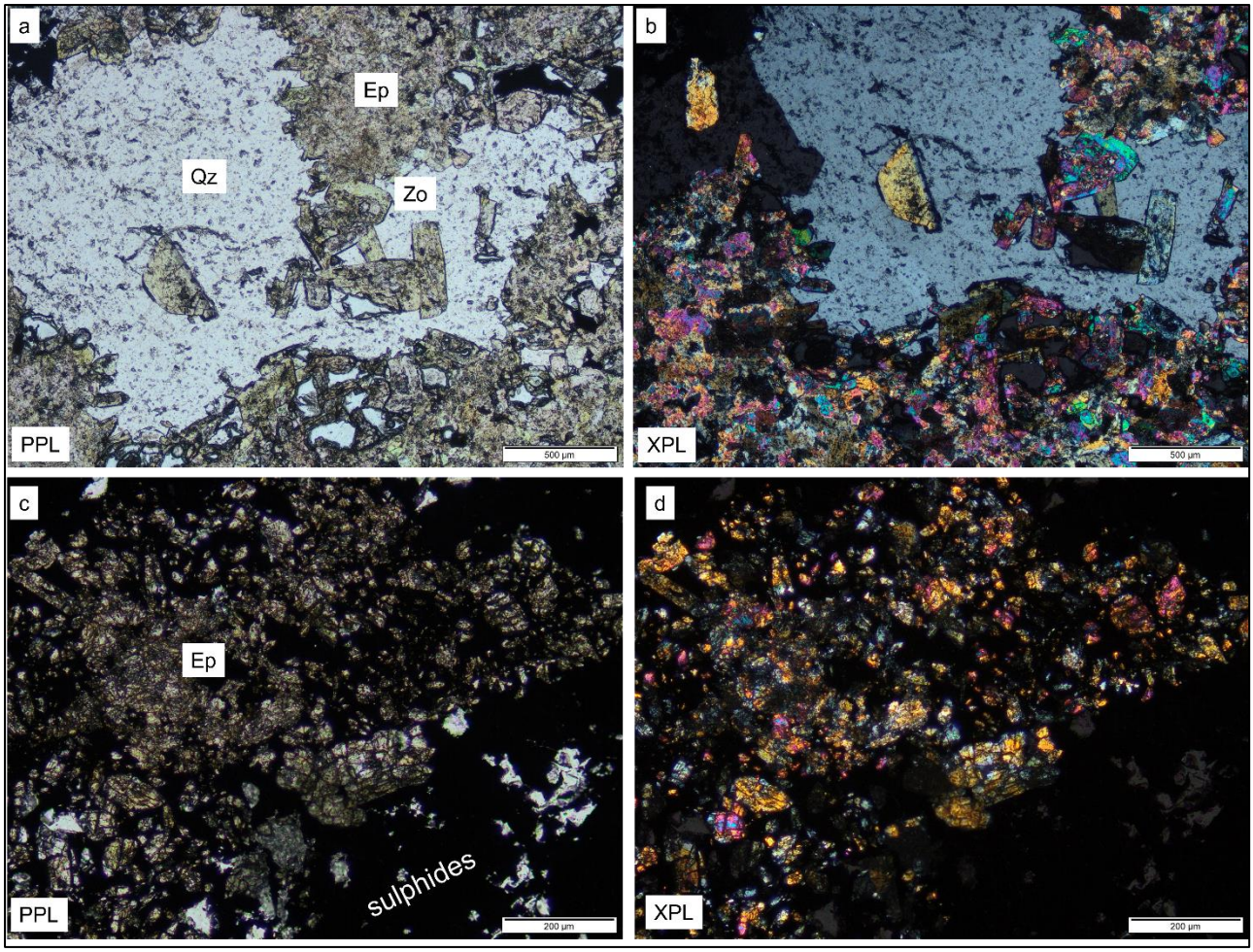
Sample 19078



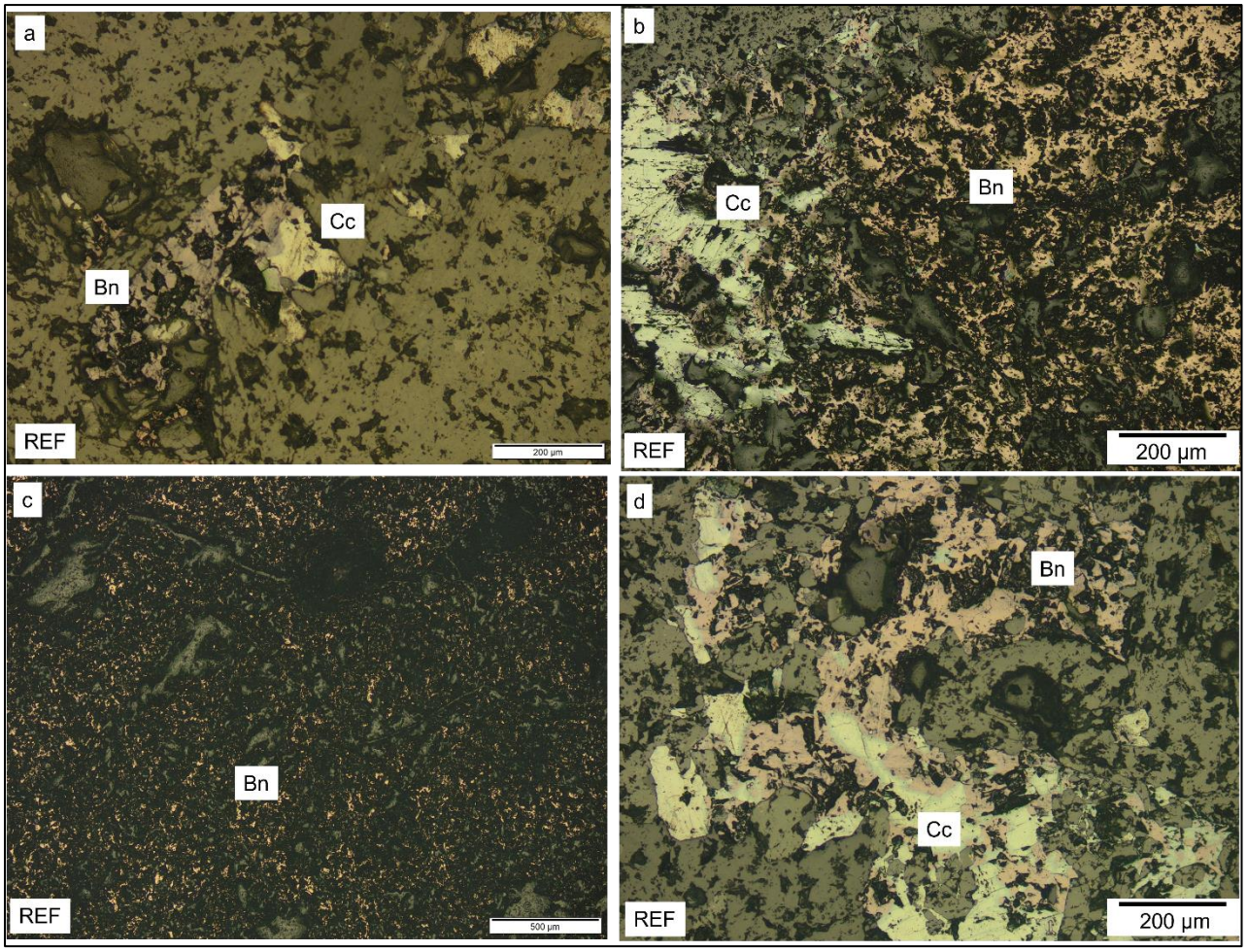
A18: Full-scan photomicrographs for Sample 19078 in PPL and XPL: (a) brownish-yellow granular aggregates of epidote surround the opaque minerals. Subhedral and angular quartz grains occur within the opaque minerals. Other opaque minerals are disseminated within the granular aggregates; (b) epidote granular aggregates show high reflectance in XPL and angular greyish-white quartz appears to occur within and in contact with epidote aggregates in places. Sample size = 5 mm.



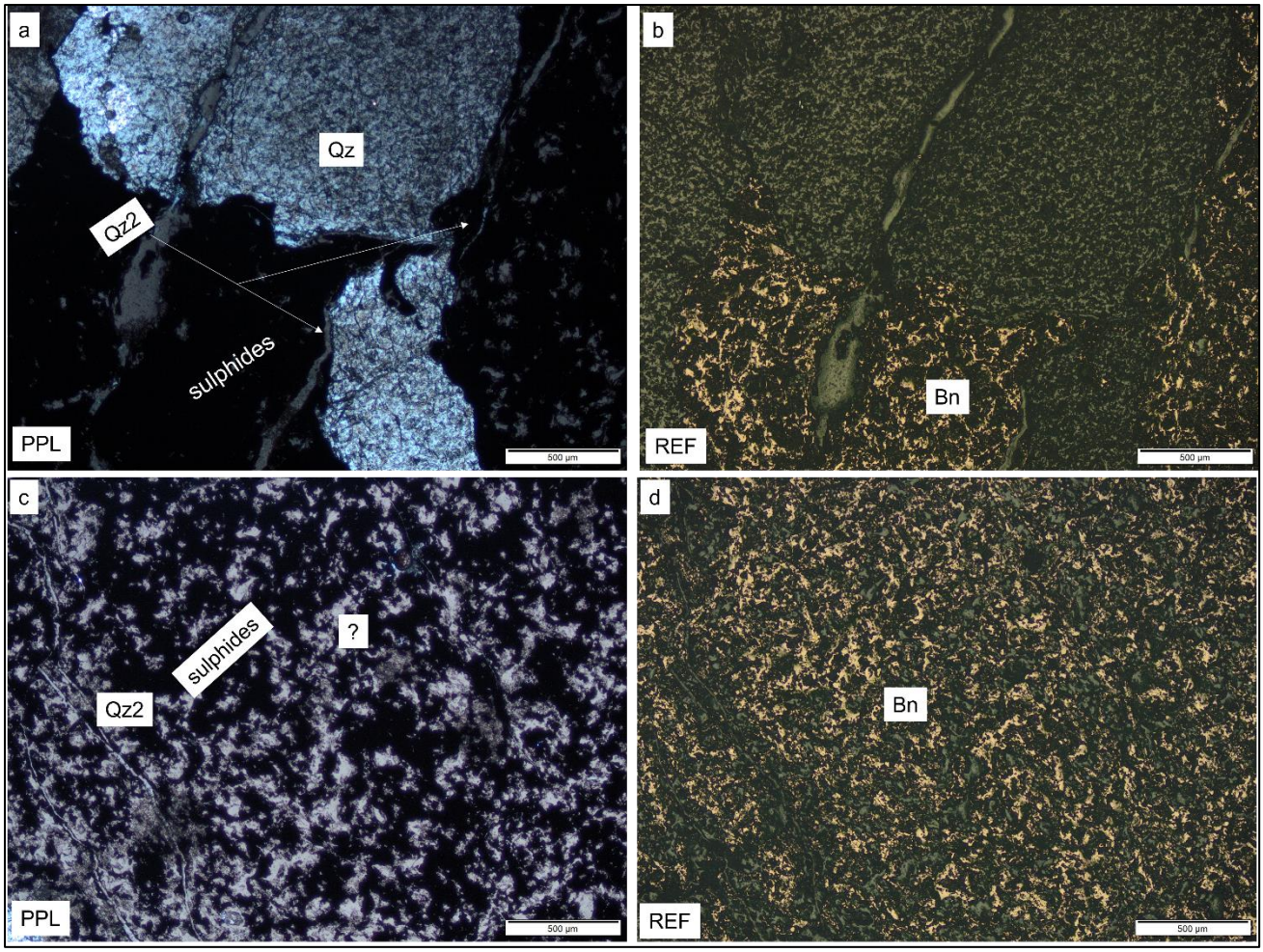
A19: (a) small irregular secondary clear quartz grains occur within the granular brownish-yellow epidote aggregates. The epidote aggregates surround the opaque minerals, which are also disseminated between the aggregates; (b) blue chlorite is altering into epidote. Minor epidote aggregates occur within the opaque minerals in other places; (c) tarnished bornite is anhedral between primary cloudy quartz grains and epidote aggregates and is being replaced by chalcocite along margins.



A20: (a-b) subhedral, large, secondary clear quartz grains are surrounded by brownish-yellow epidote aggregates which also occur as tabular to irregular grains overprinting quartz; (c) micro-brecciated fragments of brownish-yellow epidote occur within the opaque minerals; (d) high birefringence of brecciated epidote. The opaque minerals are disseminated between the aggregates.



A21: (a) irregular tarnished bornite disseminations are partially being replaced by chalcocite; (b) coarse-grained tarnished bornite being replaced by chalcocite along the margins; (c) coarse-grained, massive, tarnished bornite contains elongate and angular fragments of quartz gangue; (d) interstitial tarnished bornite with chalcocite replacing it along the margins.

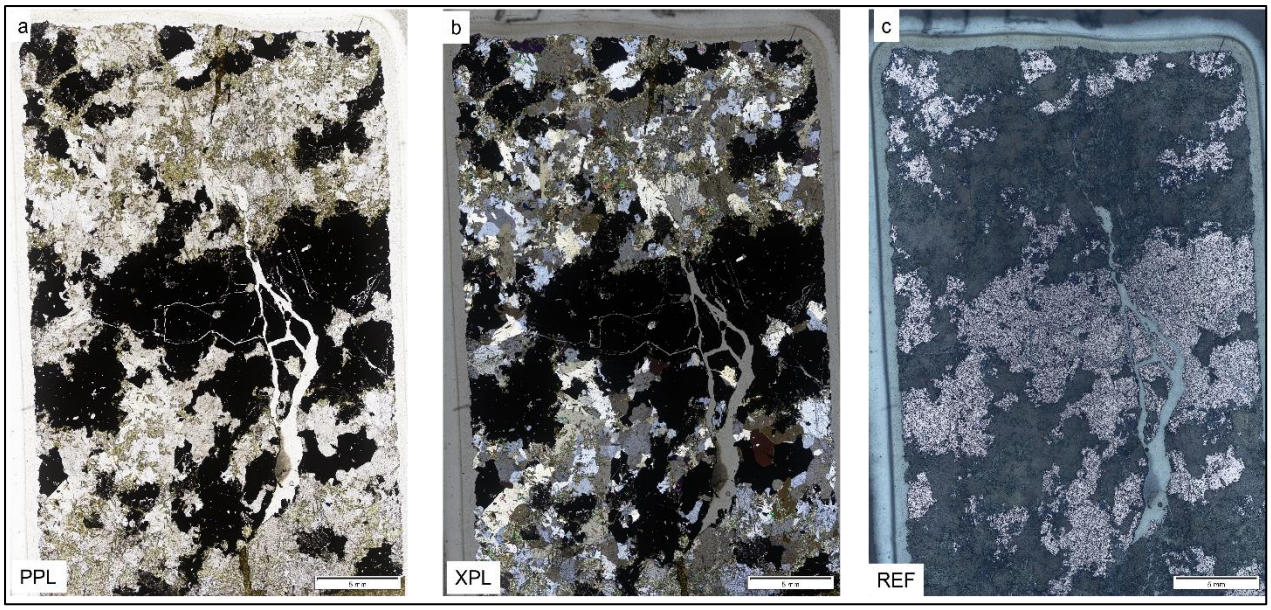


A22: (a) secondary veinlet of clear quartz cuts through the opaque minerals and large primary cloudy quartz; (b) coarse-grained tarnished bornite represent the opaque minerals. The large quartz encloses the bornite; (c) thin discontinuous secondary quartz veins cut through the opaque minerals. The micro-brecciated spots represent broken material during sample preparation; (d) coarse-grained, massive, tarnished bornite.

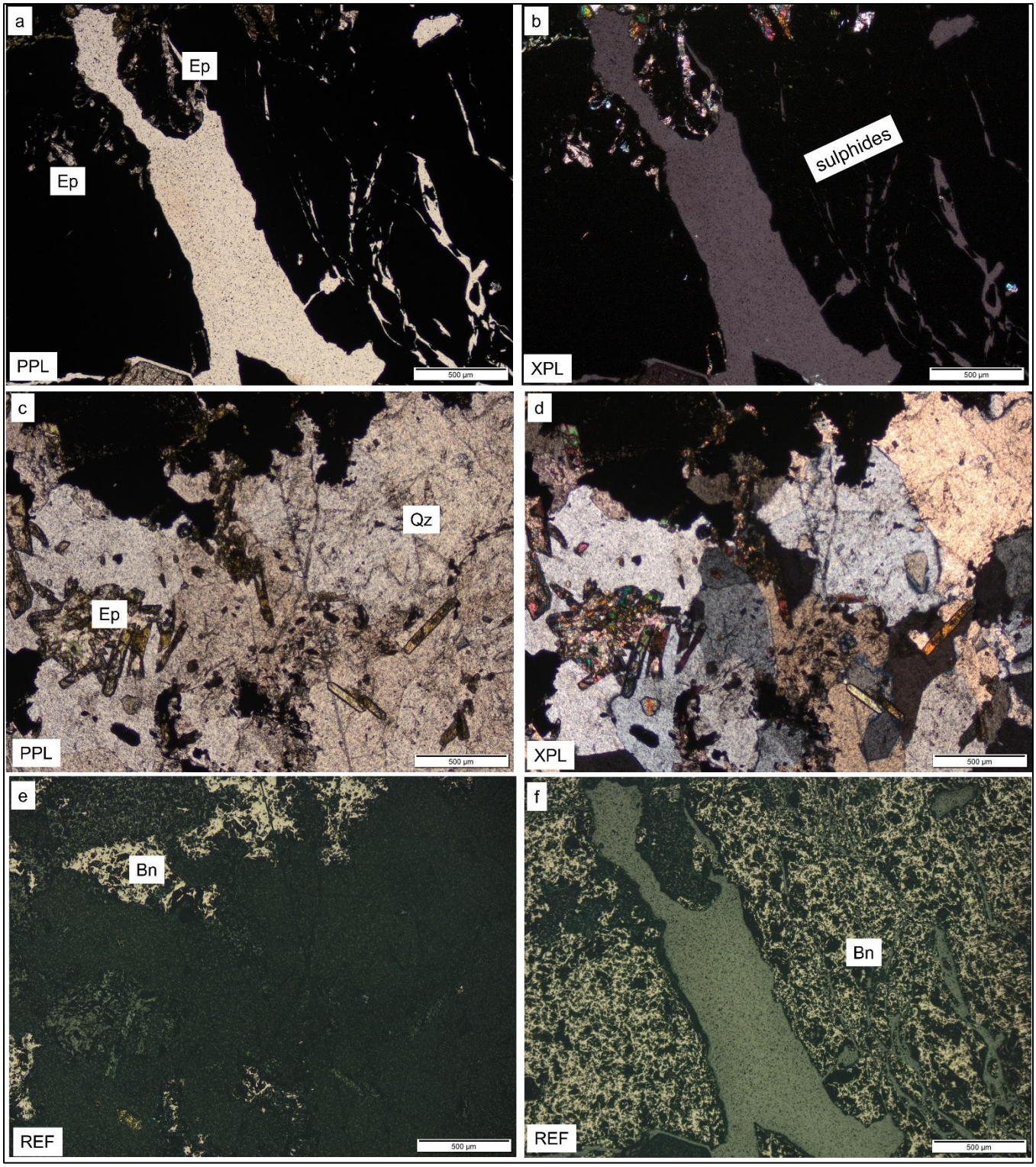
Appendix B

Samples from Jacobsen (1967) collections. Magnification scale = 500 µm and 200 µm (where stated).

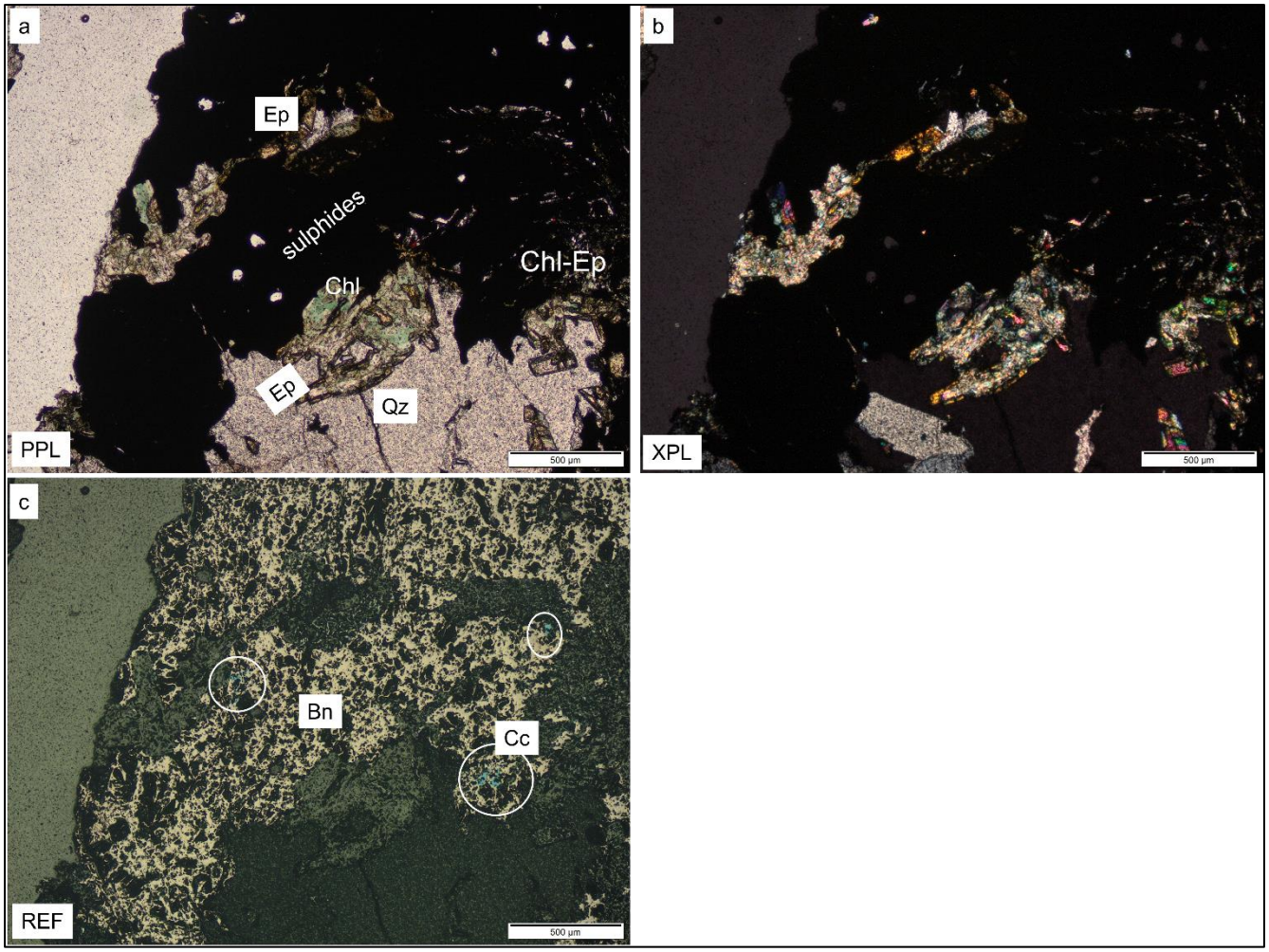
Sample P580



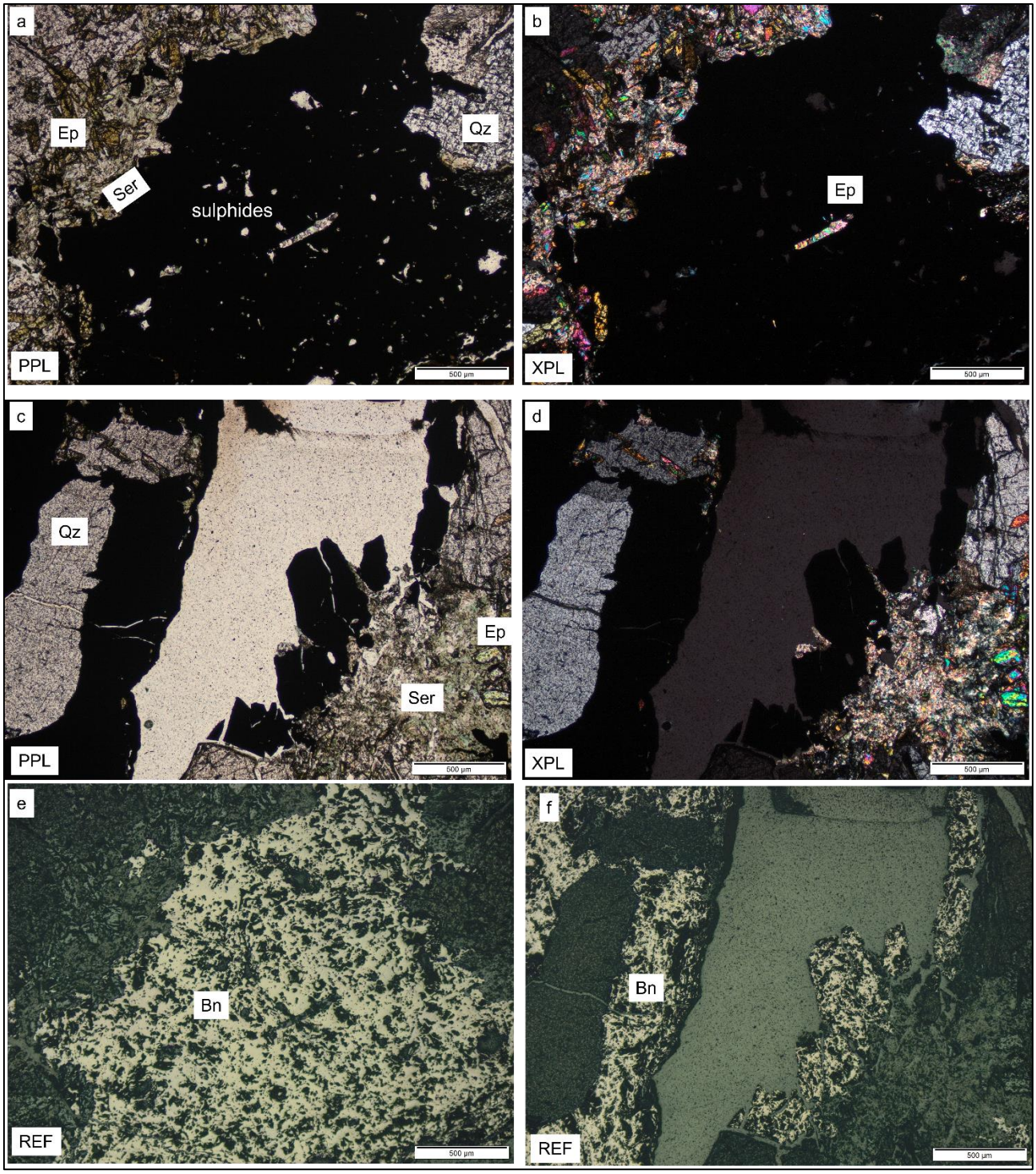
B1: Full-scan photomicrographs for Sample P580 in PPL(a), XPL (b), and REF (c). The sample contains quartz, sericite, chlorite, and epidote. Under reflected light, massive coarse-grained bornite represent the dominant opaque mineral with minor chalcocite. The elongated thin vein-like features represent resin and not an actual vein. Sample size = 5 mm.



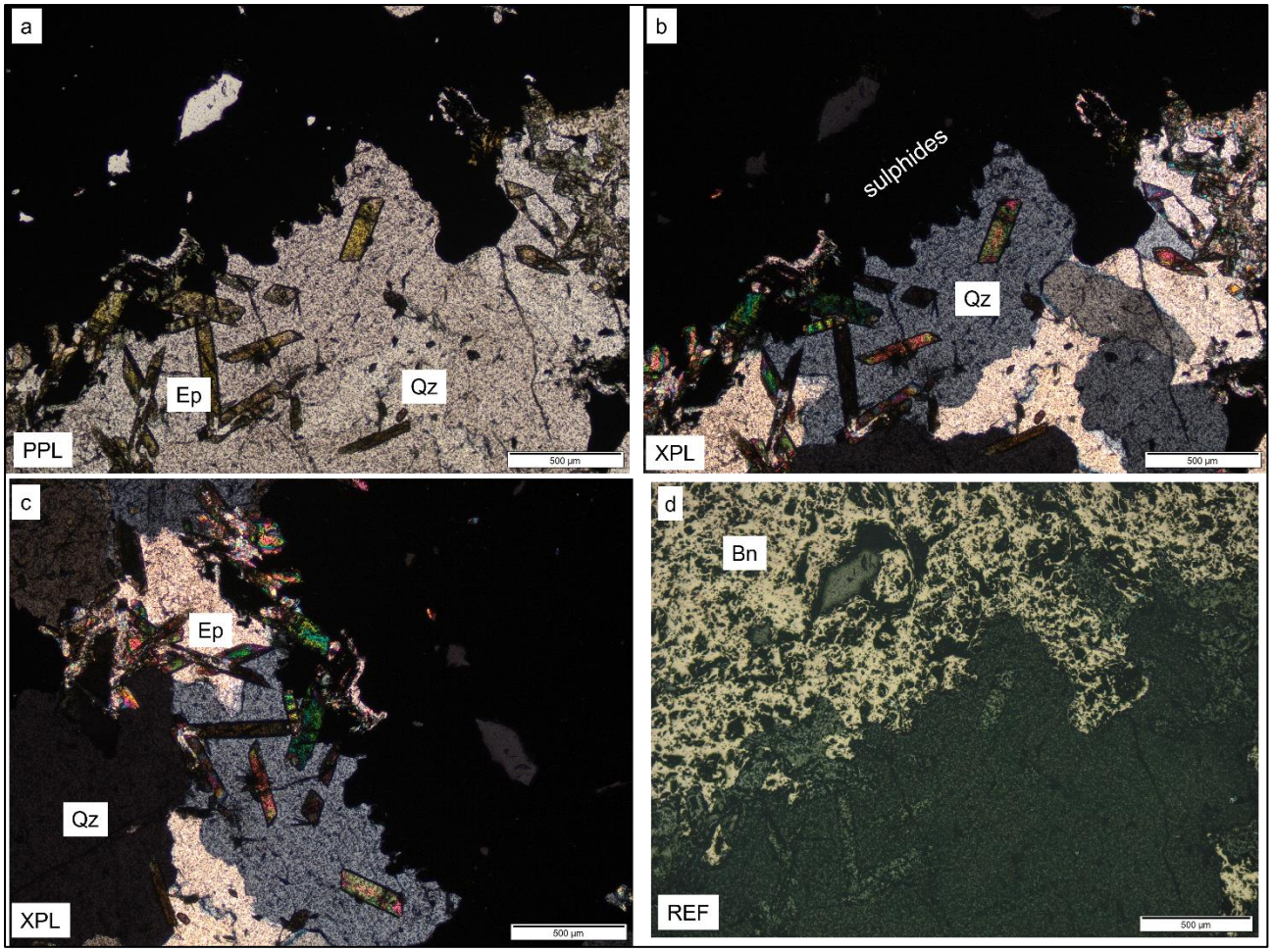
B2: (a-b) the thick creamy pink vein and veinlets are a cut on the sample and not a mineral (grey in XPL with no extinction and remain the same when the stage is rotated). Irregular epidote aggregates and veinlets occur within the opaque minerals; (c-d) elongate, prismatic epidote grains occur overprint the subhedral quartz grains. The quartz grains have irregular grain boundaries. Fine-grained sericite (lower interference colours than epidote) is enclosed by the epidote grains; (e) subhedral tarnished Bn (brownish-purple) blebs and minor disseminations occur enclosed within the quartz grains. In some parts, the bornite grains occur in halos/corroded spaces within the subhedral quartz grains; (f) coarse-grained, massive bornite associated with irregular epidote aggregates and veinlets.



B3: (a-b) euhedral to subhedral epidote grains occur with interstitial chlorite along margins of subhedral quartz grains and within the opaque minerals. Epidote also appears as a rim around chlorite and fine-grained sericite (lower reflectance than epidote). Small irregular disintegrated chlorite-epidote grains occur within the opaque minerals. The quartz grains show undulate extinction; (c) minor tiny chalcocite grains are present within the massive tarnished bornite (white circles) and indicate incipient replacement of bornite by chalcocite.

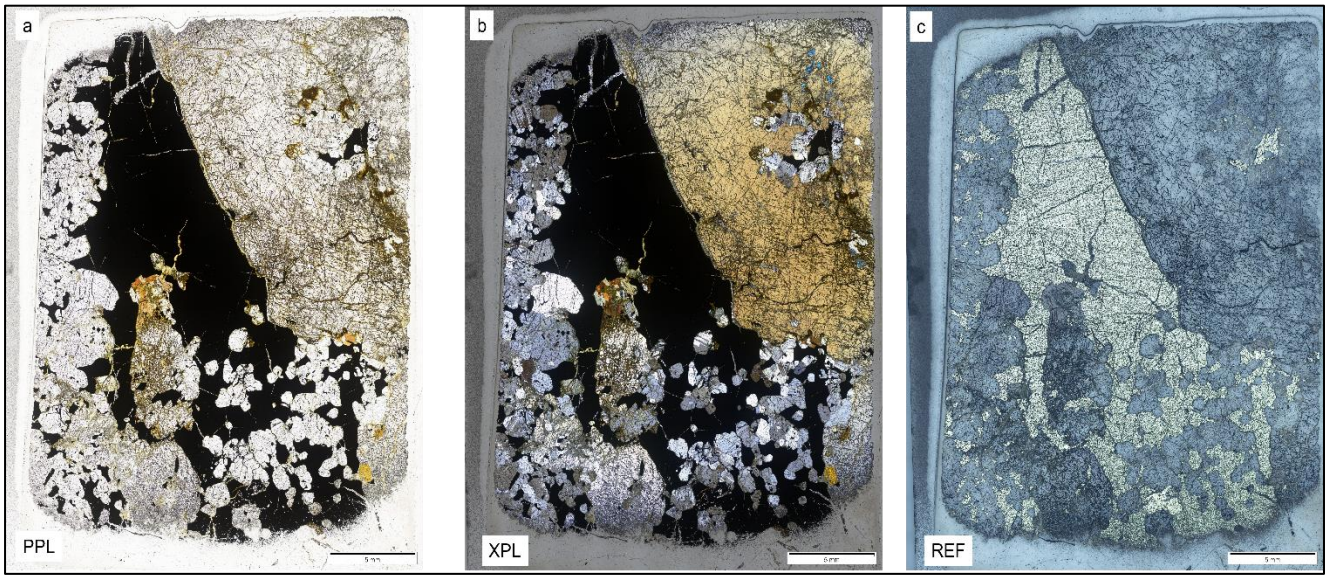


B4: (a-b) euhedral, prismatic, and subhedral epidote grains with fine-grained sericite occur along the margins of subhedral quartz grains that are partly fractured. Some epidote grains are distributed within the opaque minerals. Epidote grains appear to be overprinting the fine-grained sericite and are closely associated with the opaque minerals; (c-d) subhedral quartz grains occur within the opaque minerals. Small epidote grains enclose fine-grained sericite at the margins of subhedral quartz grains; (e-f) coarse-grained, massive, tarnished bornite (pinkish brown) occurs between the sericite-epidote and quartz gangue and some are partly disseminated as small grains within the fine-grained sericite and epidote grains.

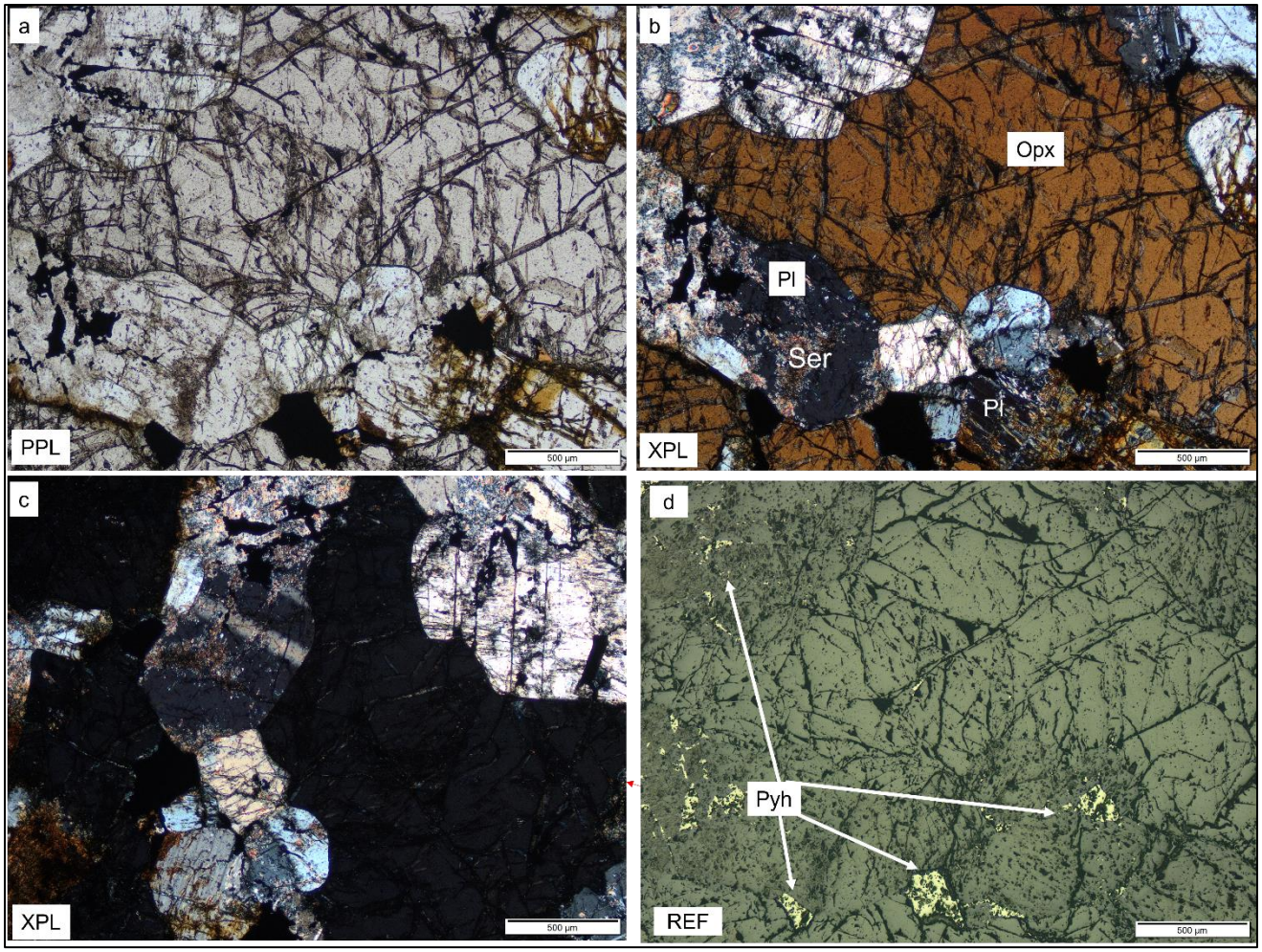


B5: (a-b) euhedral prismatic epidote grains are overprint the quartz grains (are intergrown in XPL and have distinct grain boundaries). The white (grey in XPL) grains within the opaque minerals are not minerals but rather unidentified material of the sample. Fine-grained sericite also occurs along the margins of the quartz grains with the epidote grains; NS extinction (b) and parallel extinction (c). Euhedral epidote grains do not show replacement relationship with the sericite, but rather occur around it; (d) coarse-grained, massive bornite is enclosed by the quartz and contain epidote-sericite gangue.

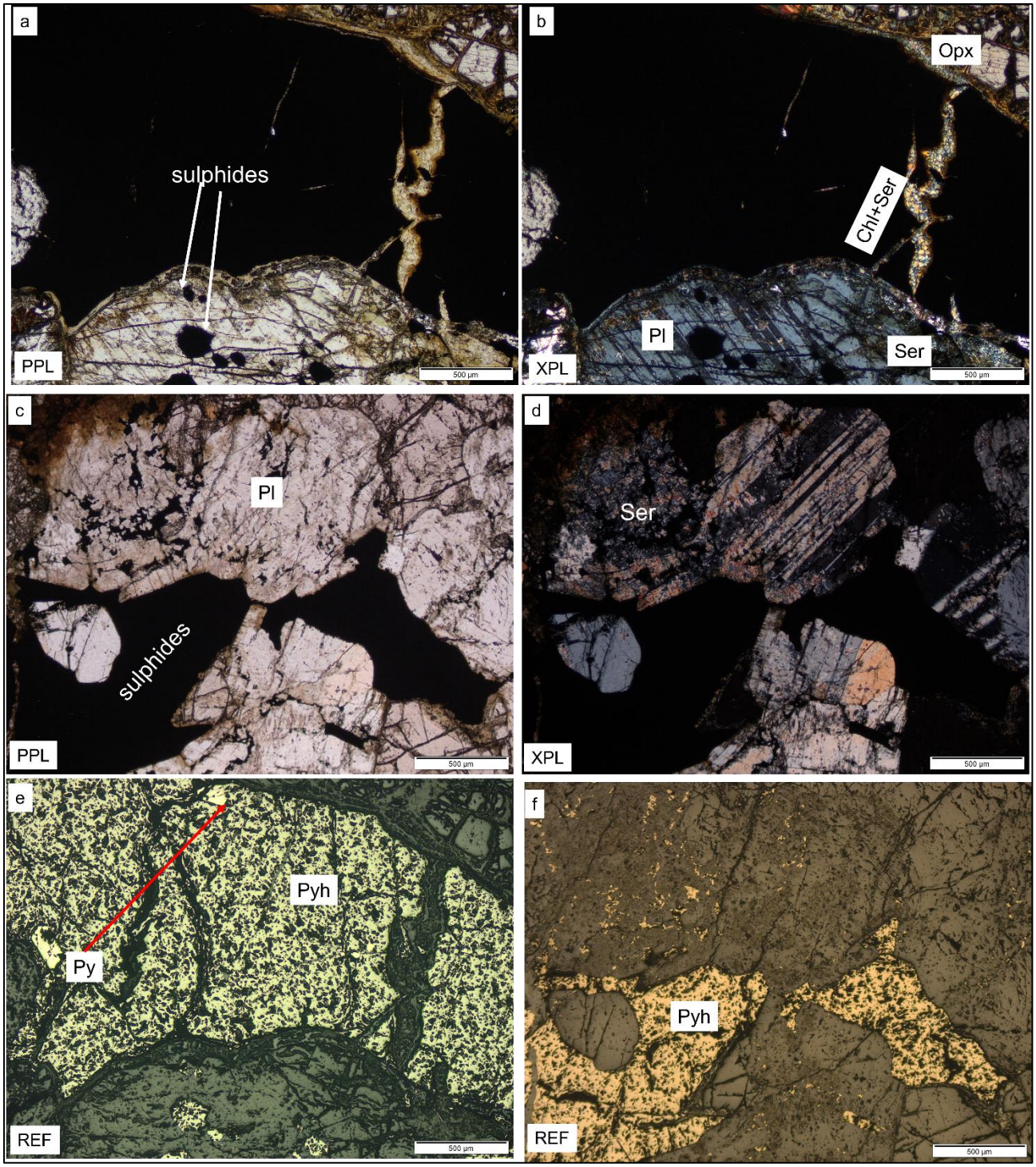
Sample P579



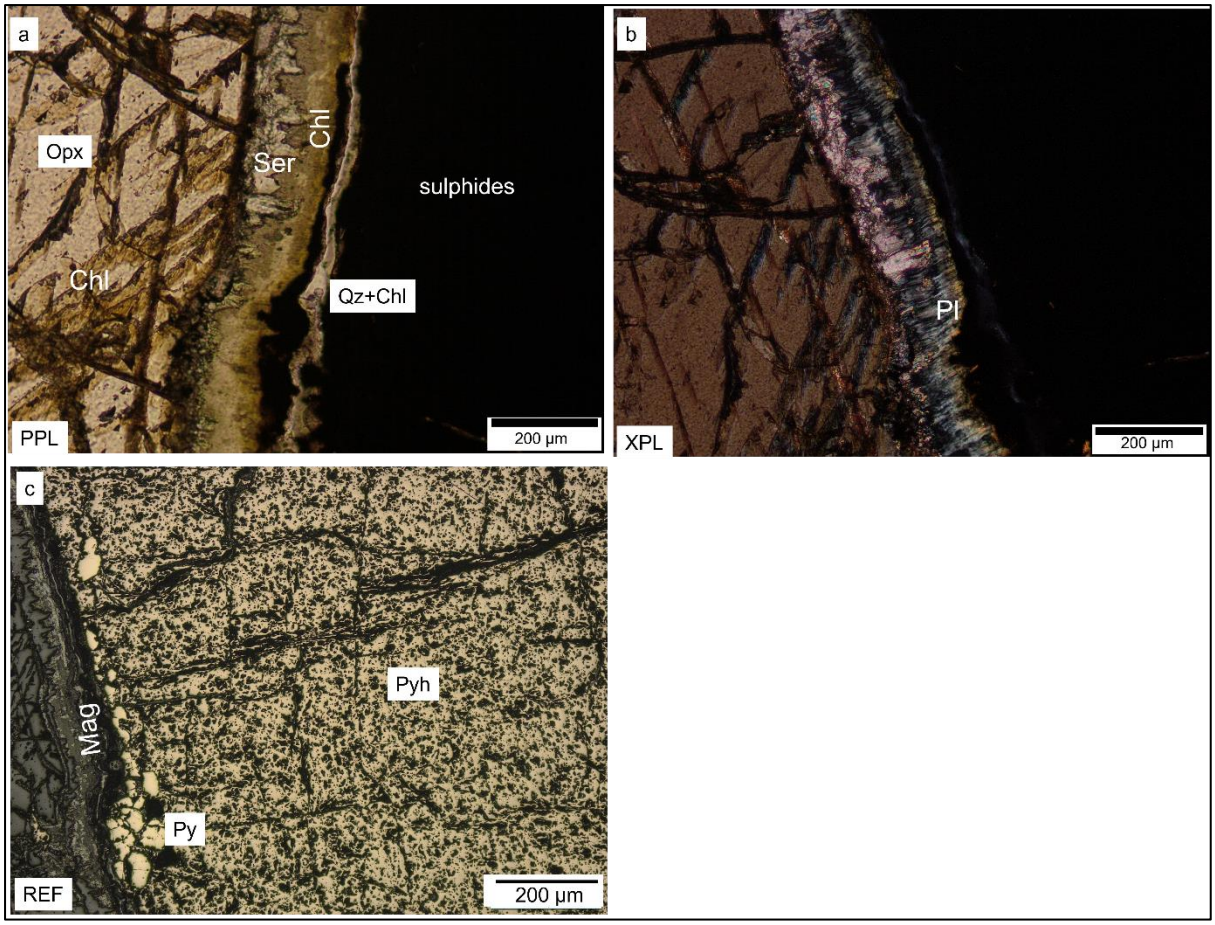
B6: Full-scan photomicrographs for Sample P579 in PPL (a), XPL (b), and REF (c). A large, fractured orthopyroxene and brecciated subhedral and subrounded grains of plagioclase enclose the opaque minerals. Some plagioclase grains occur within open spaces within fractured orthopyroxene. Dismembered plagioclase grains also occur within the opaque minerals. Pyrrhotite dominates the opaque minerals and contains small euhedral pyrite grains. Sample size = 5 mm.



B7: (a-b) large, fractured orthopyroxene occurs with brecciated plagioclase grains. The plagioclase grains show albite twinning and have corrosion halos filled by the opaque minerals. Fine-grained sericite appears to be corroding the plagioclase grains while partially replacing them; (c) NS extinction for (a-b); (d) pyrrhotite grains are disseminated within the corroded spaces of plagioclase grains. The Opx grains are unaltered.

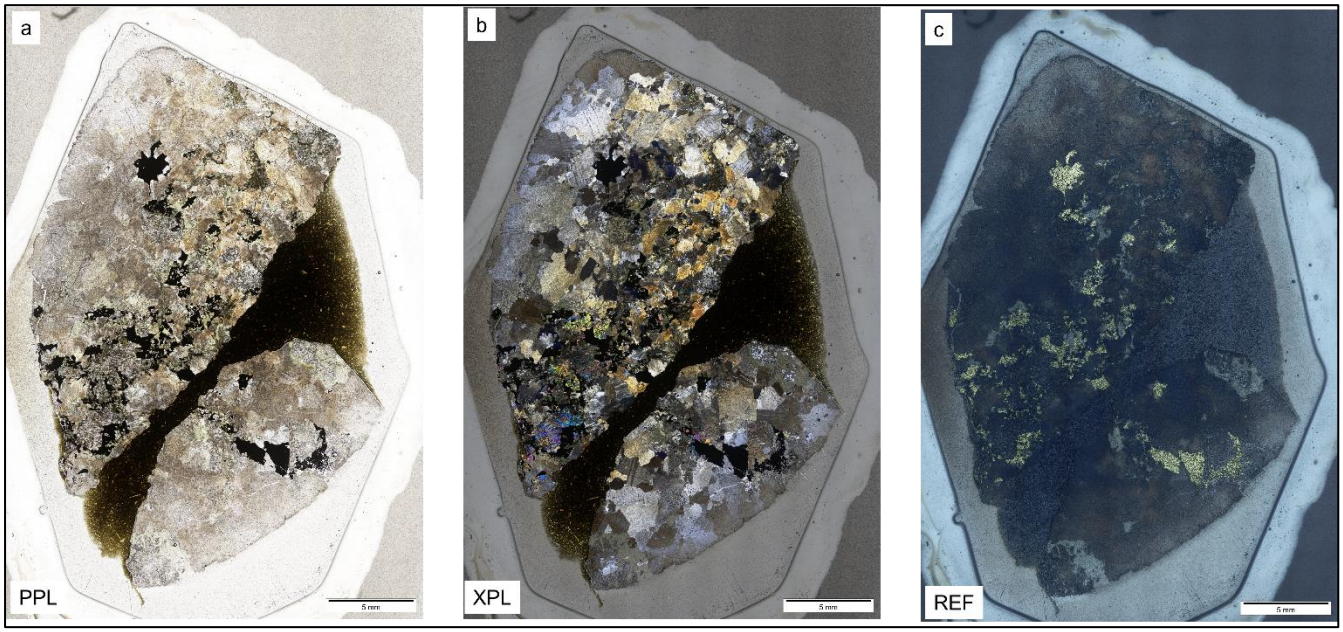


B8: (a-b) plagioclase (multiple twins) and opx are bordered by multi-compositional rim of cryptocrystalline sericite and chlorite. The multi-compositional rim also occurs as a vein cutting across the opaque minerals. The opaque minerals are disseminated (white arrows) within corroded halos of plagioclase grains; (c-d) anhedral opaque minerals occur between the brecciated, corroded plagioclase grains and within the corroded spaces; (e) coarse-grained yellow pyrrhotite occurs between the rimmed opx and plagioclase and contains discrete euhedral pyrite grains (white arrow) at margins. Other subhedral pyrrhotite grains fill halos within plagioclase grains; (f) anhedral pyrrhotite fills corrosion spaces within plagioclase grains and occurs as cement between brecciated plagioclase grains.

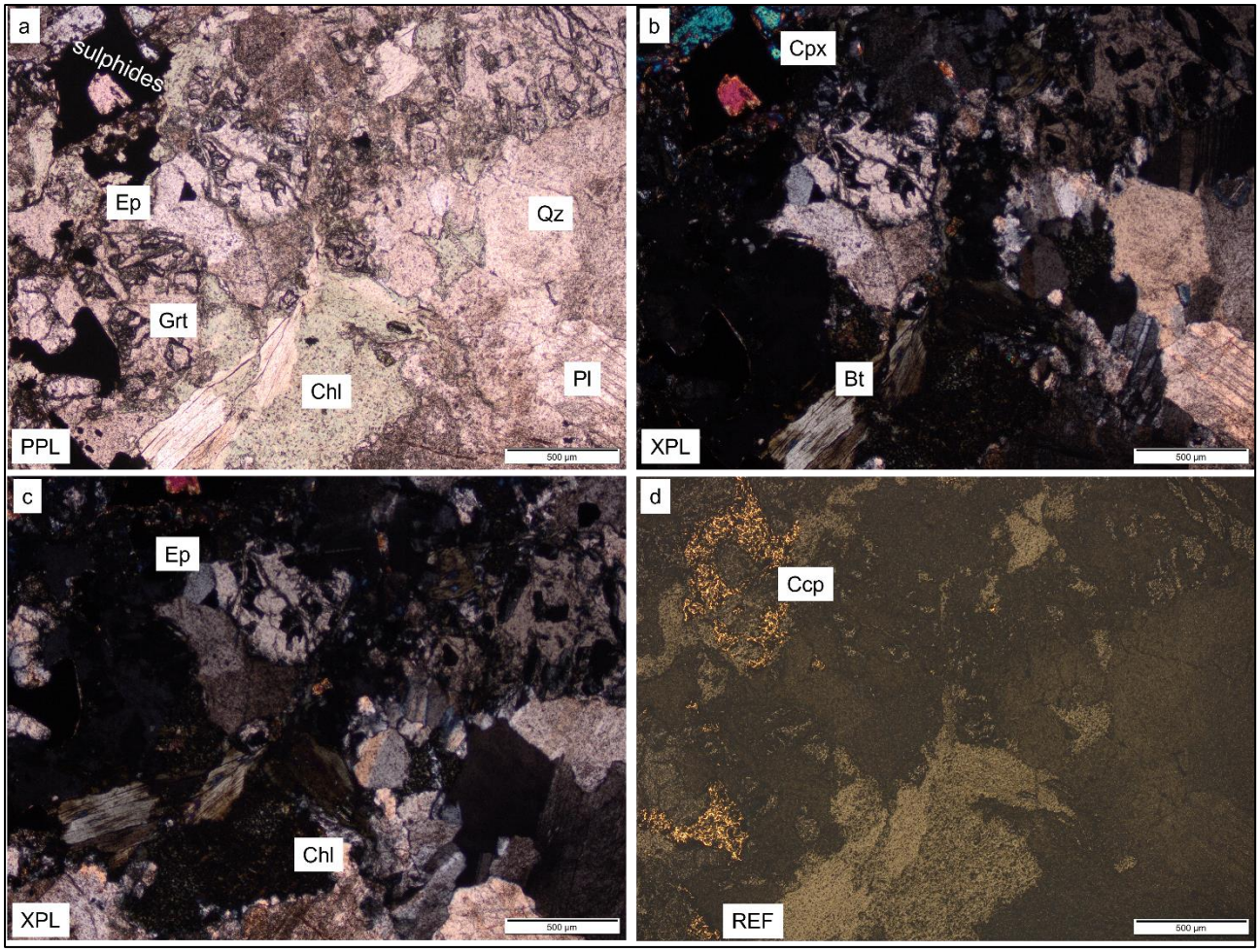


B9: (a-b) fractured opx bordered by multi-compositional vein of sericite-chlorite. Chlorite vein networks also fill the fractures within opx. An irregular quartz vein cuts across the opaque minerals and makes contact with the multi-compositional vein of sericite-chlorite. Sericite alters and replaces relict plagioclase (multiple twins can still be seen within the vein); (c) The multi-compositional vein hosts magnetite as elongate anhedral grains within the vein. Subrounded pyrite grains are present along the margins of the coarse-grained pyrrhotite.

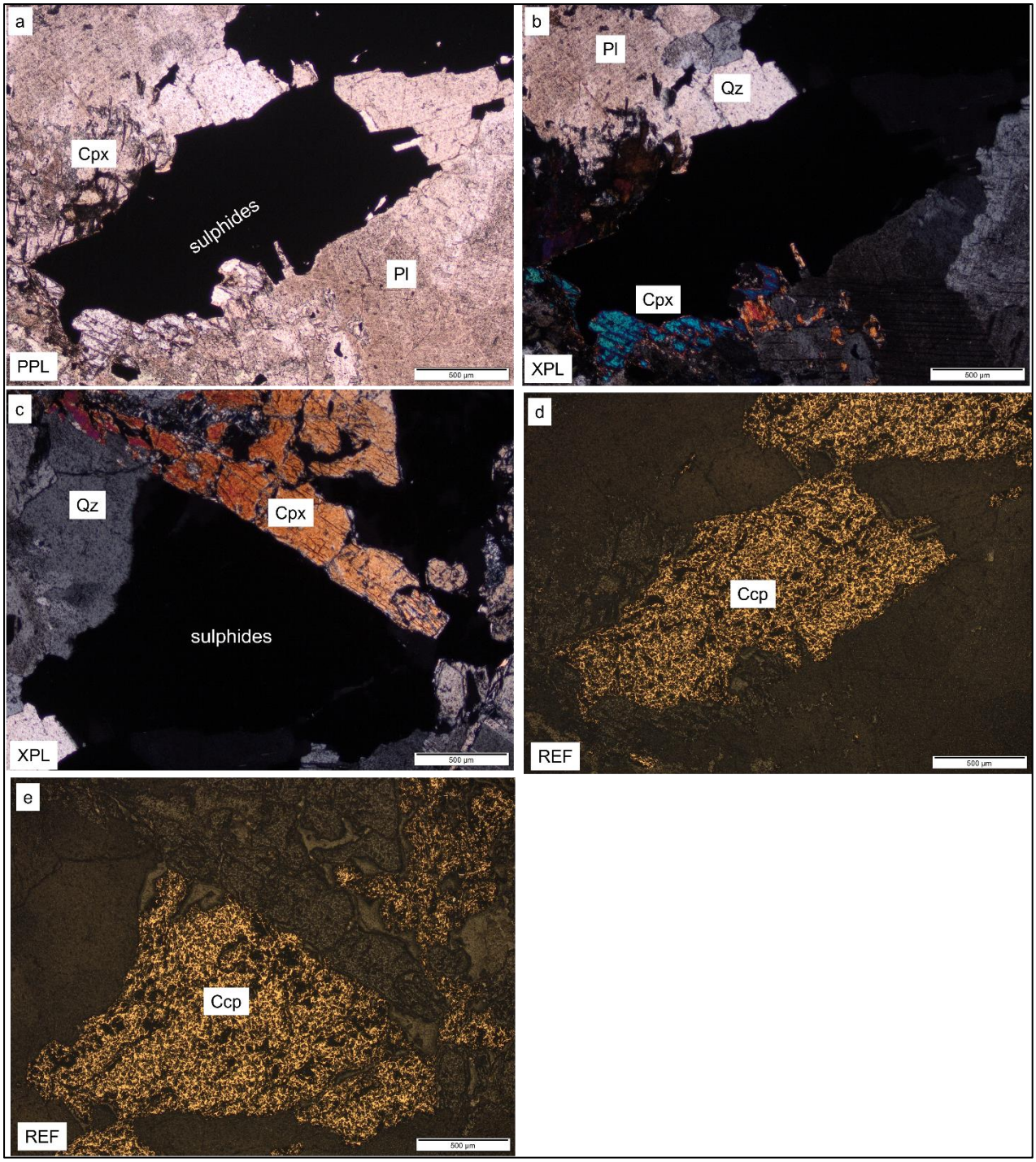
Sample P613



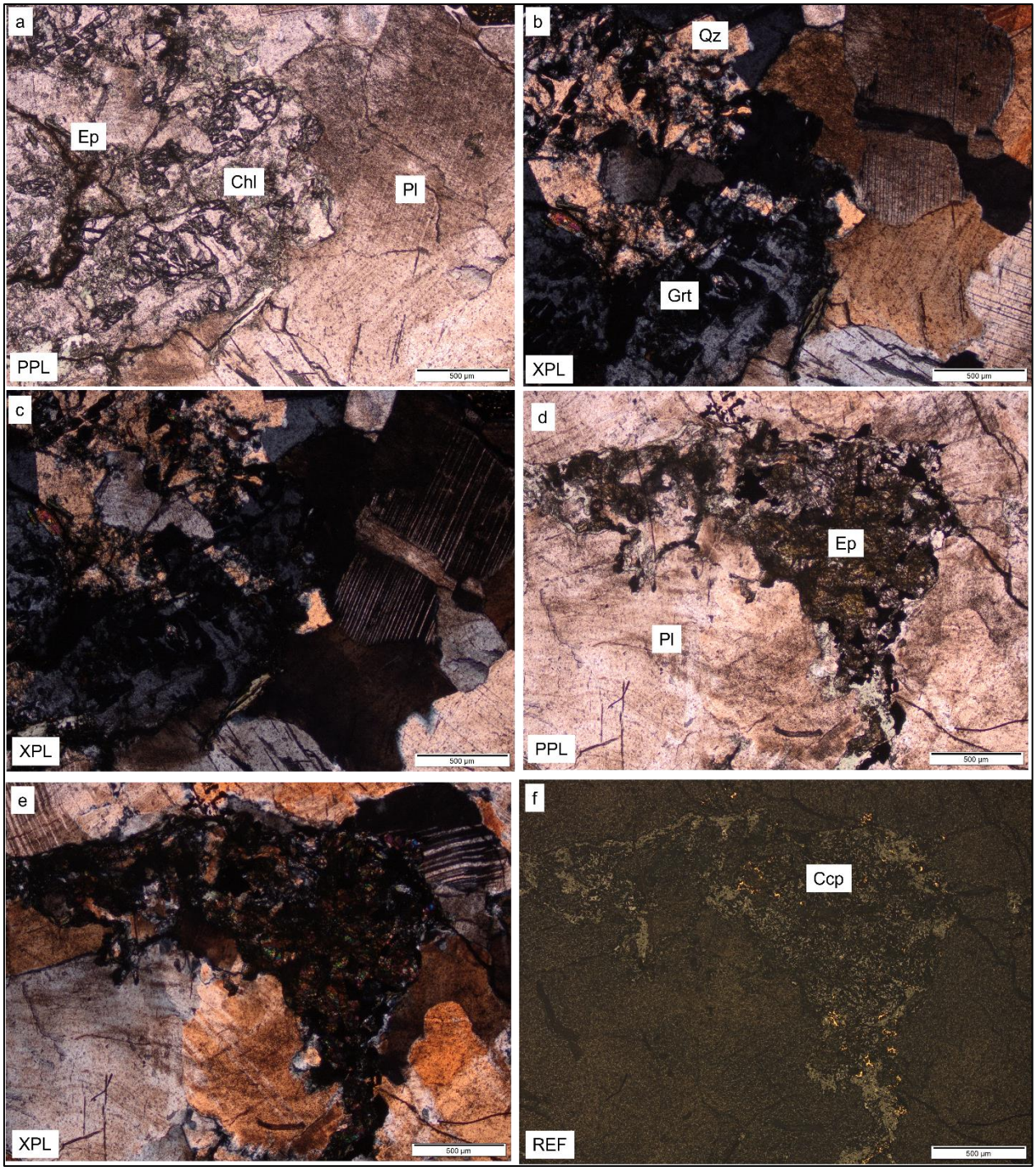
B10: Full-scan photomicrographs for Sample P613 in PPL (a), XPL (b), and REF (c). Quartz grains are intergrown with plagioclase grains. Chlorite alters biotite and garnet grains between quartz and plagioclase grains. Epidote aggregates also alter clinopyroxene and plagioclase partially. Sample size = 5 mm.



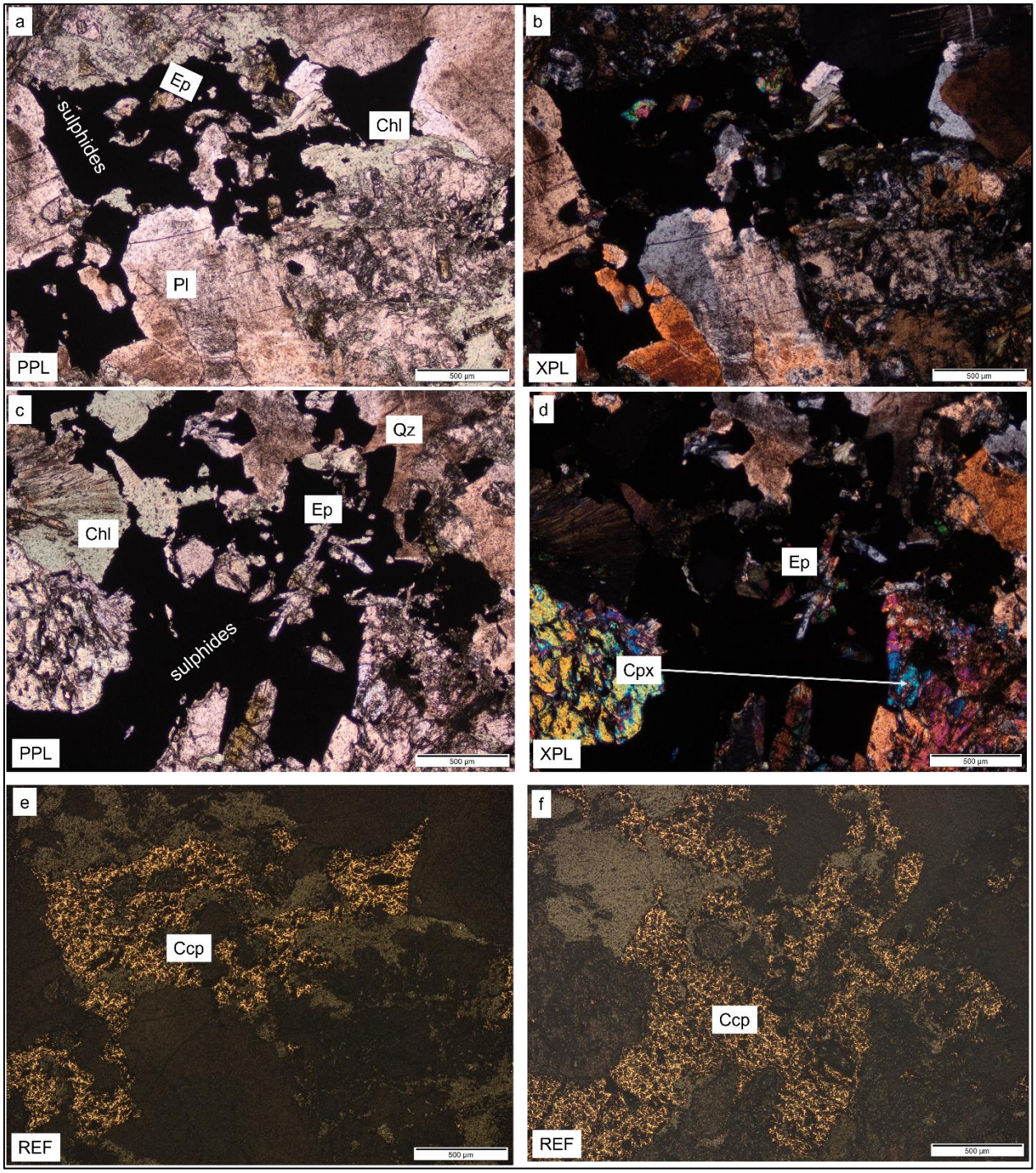
B11: (a-b) brecciated clinopyroxene (high relief and 120º cleavage) grains appear to be breaking down to epidote and occur in contact with garnet grains (isotropic in XPL) that are also breaking down to chlorite (deep blue). Biotite grains also occur in association with granular chlorite. The weakly formed chlorite and epidote enclose the opaque minerals. Slightly dismembered and brecciated quartz grains are intergrown with plagioclase grains and enclose minor disseminations of the opaque minerals; (c) oblique extinction of the sample shows undulate extinction of quartz grains; (d) subhedral chalcopyrite grains are disseminated within open spaces of all the gangue minerals.



B12: (a-b) subhedral plagioclase grains (weak albite twins) are intergrown with subhedral quartz grains and irregular fractured clinopyroxene grains. The opaque minerals occur between plagioclase, cpx, and quartz grains, as well as within the corroded spaces; (c) elongated to subhedral clinopyroxene occurs within the opaque minerals and is intergrown with subhedral quartz grains, and surround the opaque minerals; d) subhedral coarse-grained chalcopyrite represent the opaque minerals and occurs between the gangue minerals.

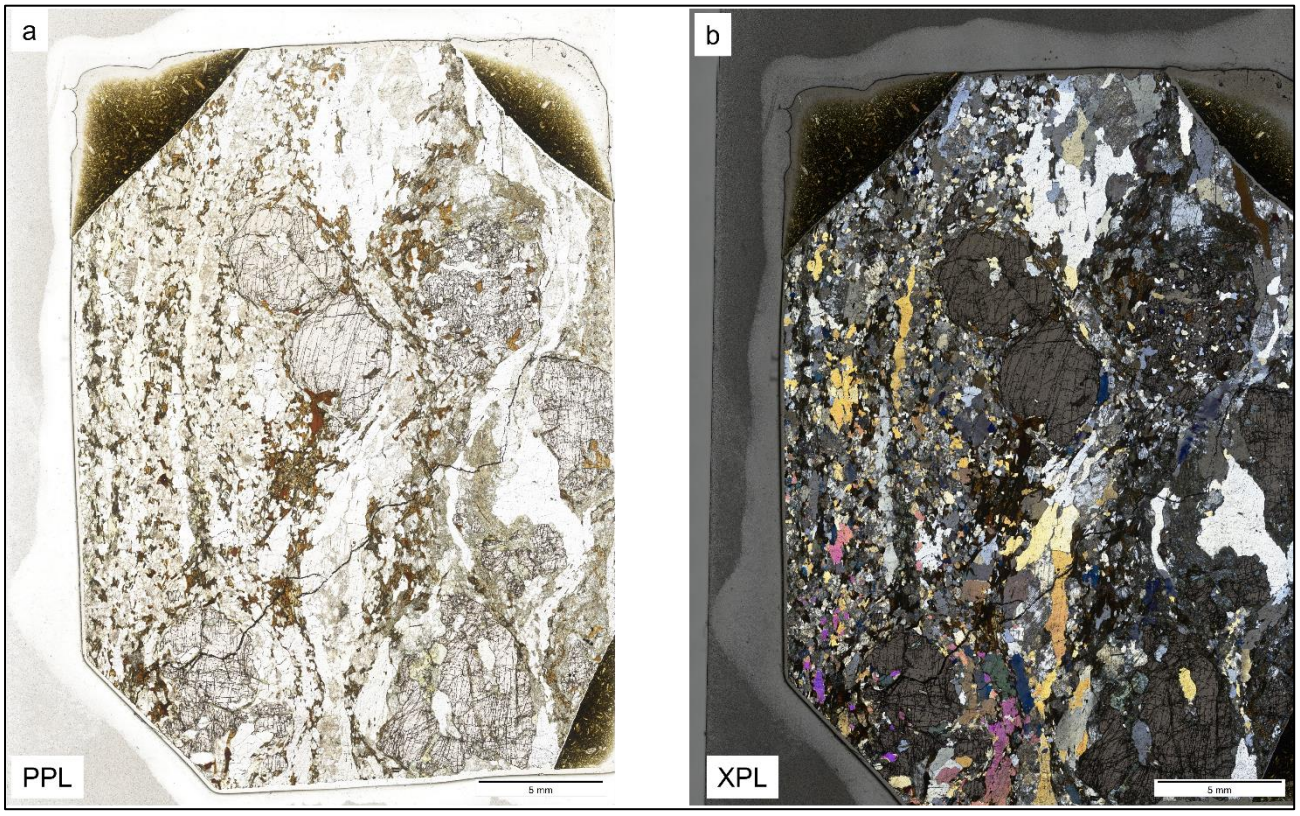


B13: (a-b) subhedral plagioclase grains with polysynthetic twins occurs in close contact with fractured garnet (high relief and isotropic) that is partially breaking down to chlorite. The chlorite in turn is being weakly replaced by epidote grains (small high interference within the garnet-chlorite). A curvy vein of epidote cuts quartz and fractured garnet grains. Subhedral micro-brecciated quartz grains are intergrown with plagioclase and the garnet; (c) oblique extinction of (a) and (b); (d-e) plagioclase grains are cut by interstitial granular epidote that appear to be filling an open space between the plagioclase grains. Opaque minerals are disseminated within the granular epidote; (e) tiny chalcopyrite grains are disseminated within the interstitial granular epidote.

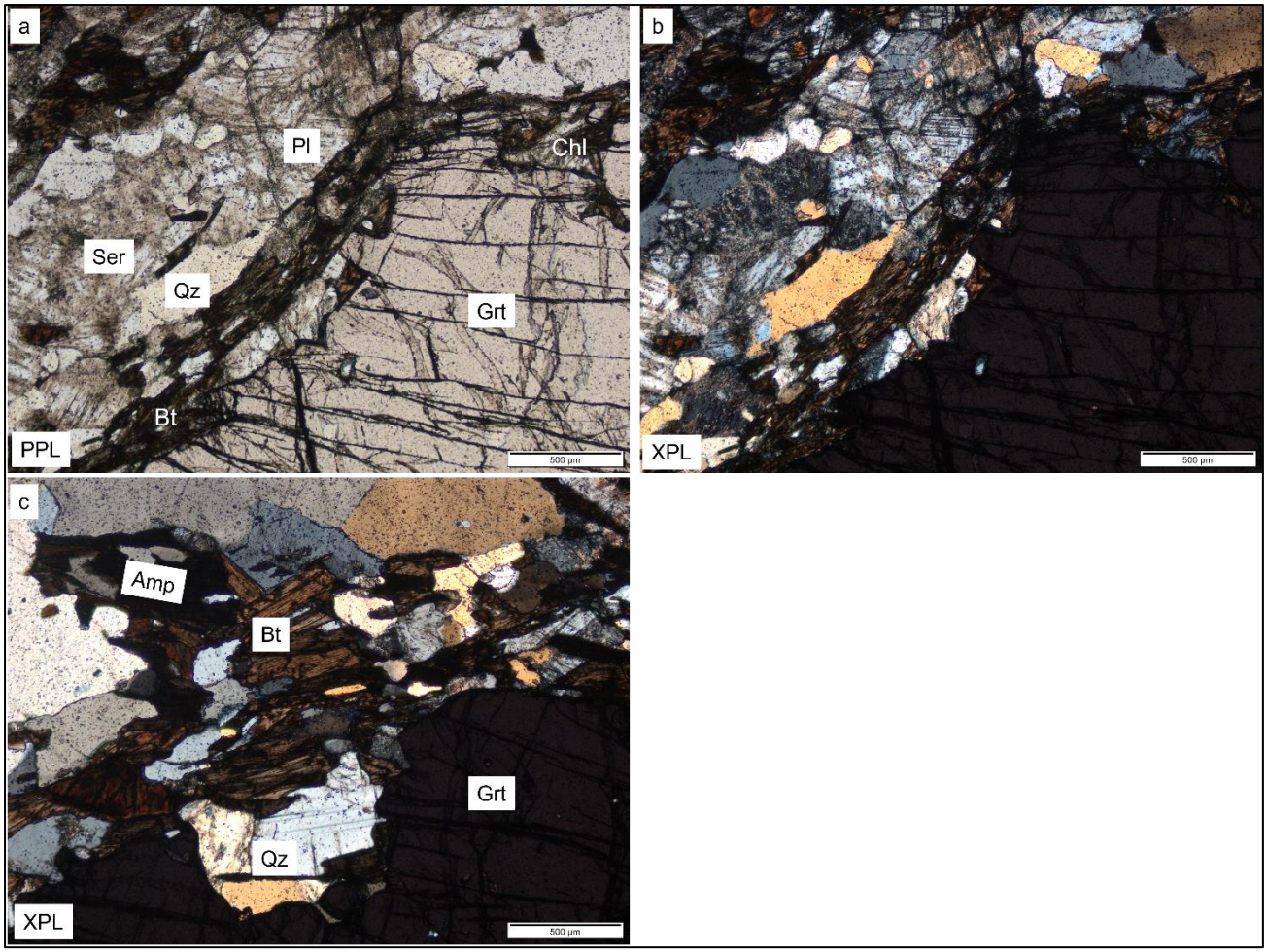


B14: (a-b) subhedral plagioclase grains (weak albite twins) are partially altering into epidote that is also altering chlorite (light green grains in PPL). Opaque minerals are enclosed by the plagioclase and minor epidote and quartz fragments are distributed within the opaque minerals; (c-d) fractured subhedral grains of clinopyroxene occur in contact with fragments of quartz, epidote, and chlorite and they enclose the opaque minerals. The elongated epidote grains and subhedral quartz fragments are isolated within the opaque minerals. The chlorite (light green in PPL and brownish-blue in XPL) appears to have completely altered biotite grains (light brown flakes in chlorite); (e-f) coarse-grained chalcopyrite occurs between the gangue minerals and within fractures of cpx and granular epidote as disseminated grains.

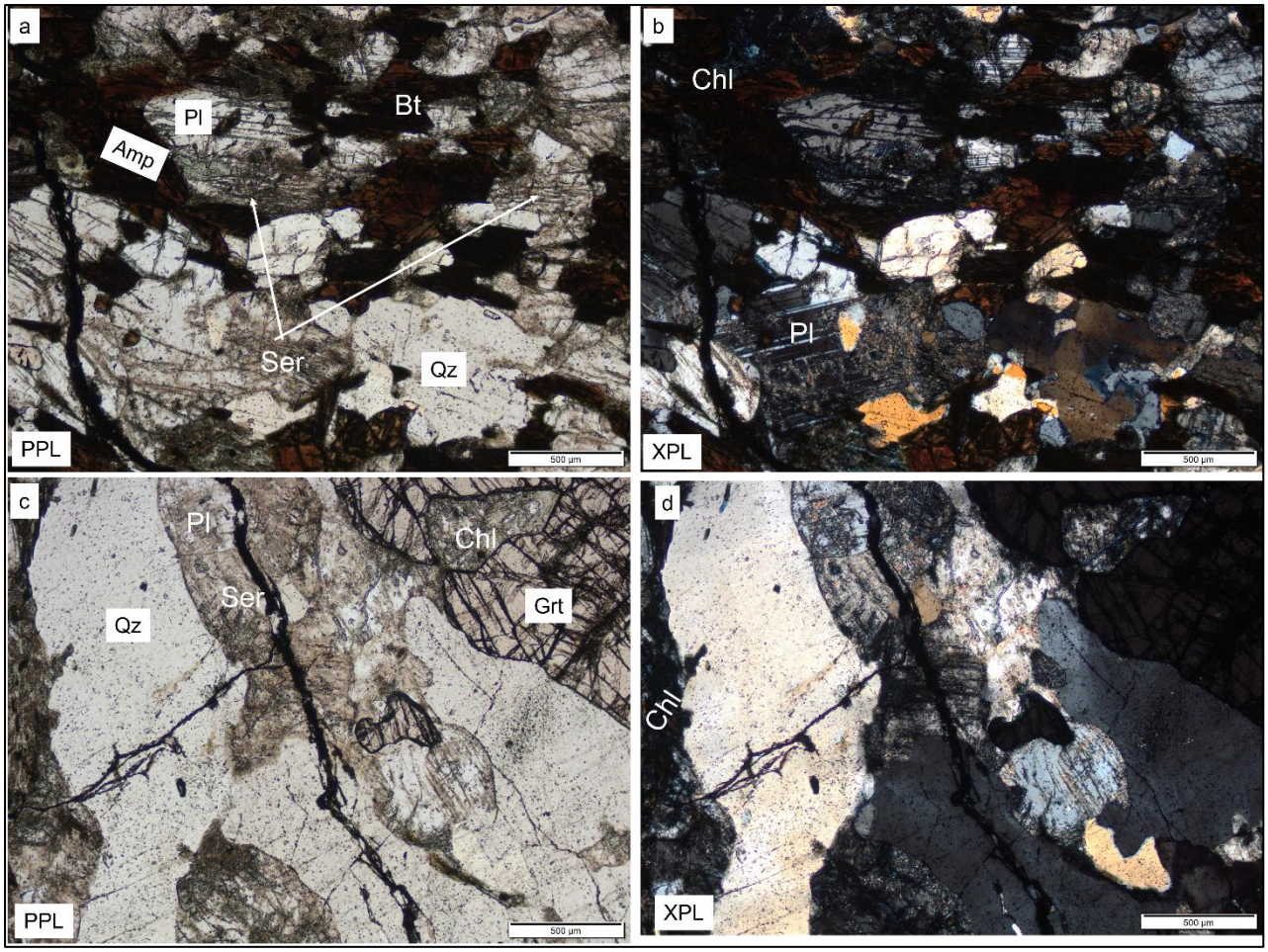
Sample P677



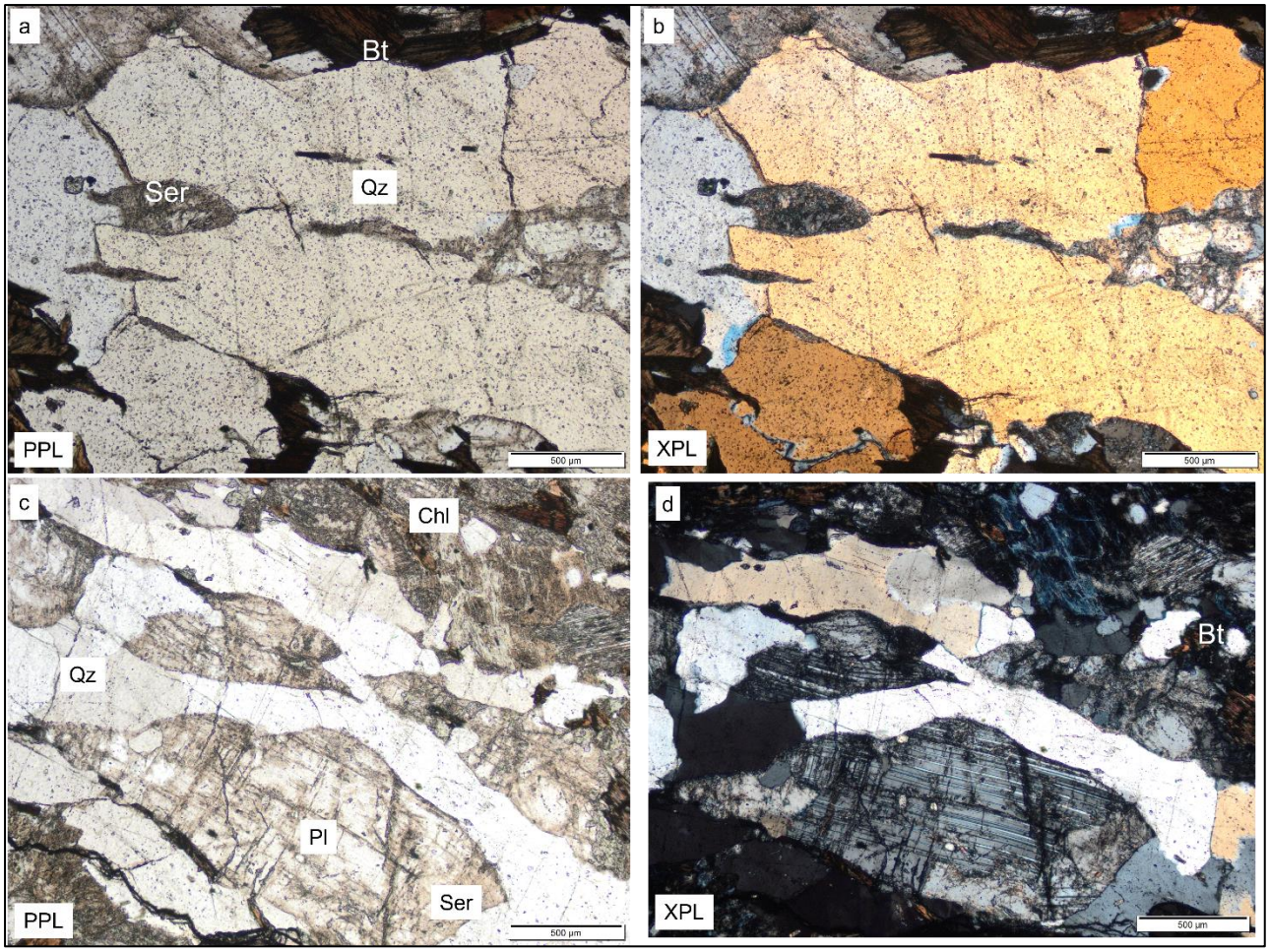
B15: Full-scan photomicrographs for Sample P677 in PPL (a) and XPL (b). This sample does not contain mineralisation. Large, rounded garnet grains are embedded within micro-brecciated quartz grains. Irregular, elongated quartz grains also occur. Elongated biotite grains and tabular grains of what could be amphibole occur within the micro-brecciated quartz grains and are preferentially aligned and surround garnet grains in places. Quartz grains also overprint garnet, biotite, and amphibole. Sample size = 5 mm.



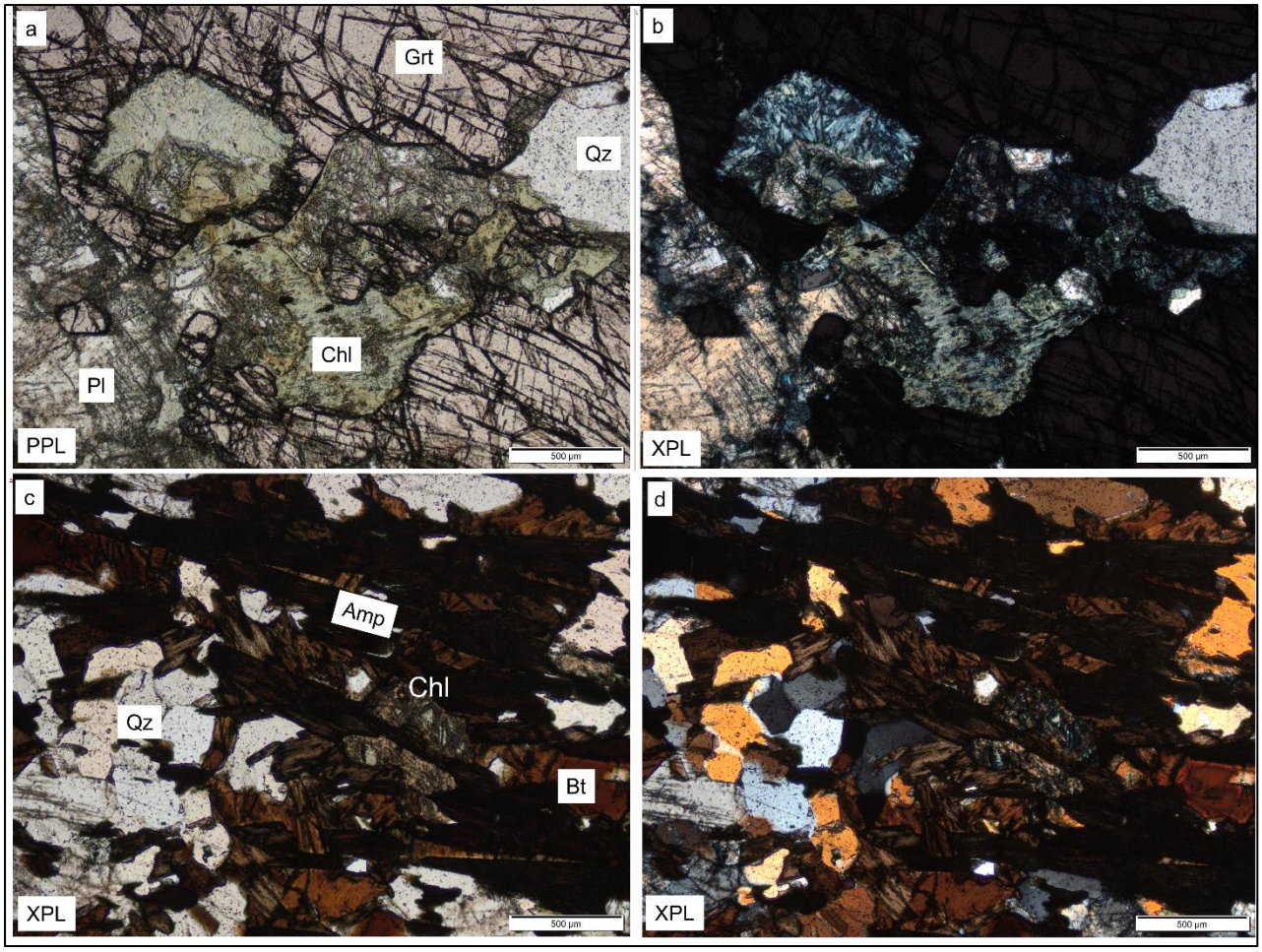
B16: (a-b) secondary quartz, biotite, fractured garnet, and fine-grained sericite are the dominant silicate minerals of this sample. The biotite flakes preferentially wrap the garnet grains and occur in contact with amphibole grains. Fine-grained sericite is altering plagioclase (recognized by multiple twinning). All the silicate minerals are overprinted by subhedral-subrounded quartz grains. The biotite and garnet grains are being partially replaced by chlorite (blue in XPL); (c) fractured garnet (isotropic) and brown biotite irregular flakes are overprinted by subhedral quartz grains.



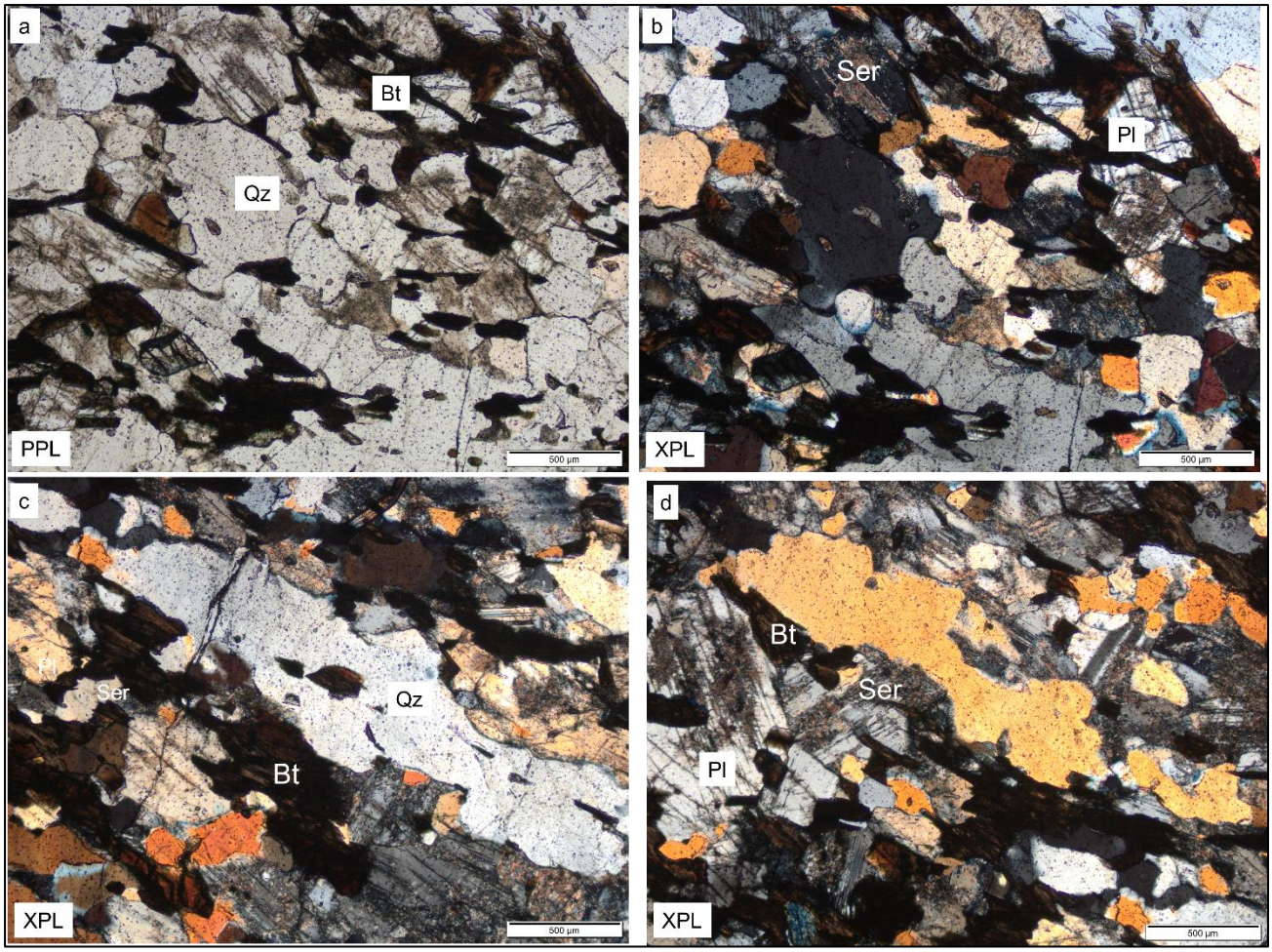
B17: (a-b) subhedral secondary Qz grains are randomly distributed and overprint primary biotite and plagioclase (albite twins) grains. The plagioclase is partially altering into fine-grained sericite. The preferentially oriented biotite and amphibole grains between plagioclase grains are partially being replaced by chlorite (anomalous blue in XPL); (c-d) elongated anhedral quartz grains occur between altered plagioclase grains and fractured garnet. The elongated quartz grains are partly fractured and the fractures contain no infilling. Chlorite is partially replacing fractured garnet grains. Some fragmented garnet and sericite occur irregularly between the elongated quartz grains and appear to have been remobilised by the hydrothermal activity.



B18: (a-b) an irregular, elongate, anhedral quartz incorporates sericitised plagioclase grains and is in contact with biotite grains and plagioclase. The elongate quartz grains appear like a single grain that became joined together to form elongated grains; c) other elongate, jelly-like (slabby) quartz grains showing undulate extinction and overprint large subhedral plagioclase (multiple twins in XPL). Micro-brecciated subrounded and angular small quartz grains overprint plagioclase, chlorite, and biotite. The plagioclase is partially replaced by fine-grains sericite; d) under crossed polarizing light, the biotite grains are seen occurring as inclusions within the anomalous blue chlorite, indicating replacement of biotite by chlorite. Magnification scale = 500 µm.

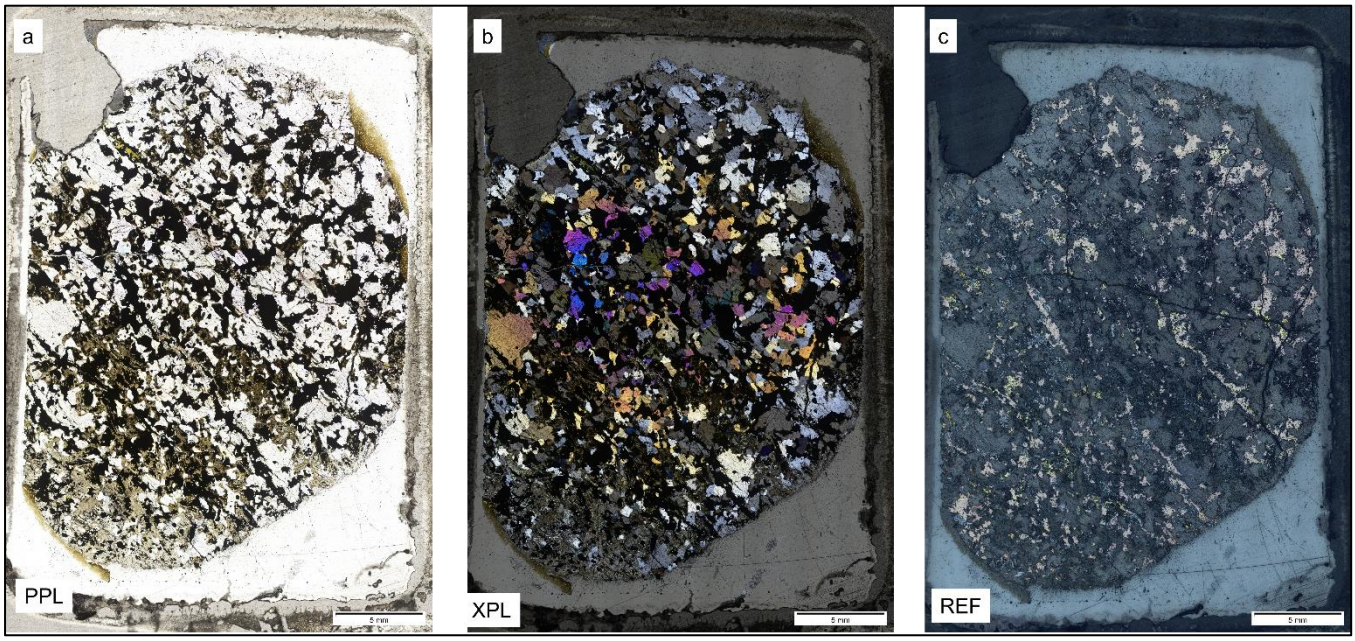


B19: (a) large garnet grains are selectively altered by irregular anhedral greenish-yellow chlorite that appears to be in contact with the secondary quartz overprinting garnet; (b) the chlorite (greenish-blue) is also encroaching into altered plagioclase along the margins. Two types of chlorite occur (i.e., blue and pale green chlorite); (c) tabular amphibole and biotite grains are preferentially oriented within the micro-brecciated quartz grains. Partial alteration of biotite/amphibole grains is possible to observe. The grains resemble brecciation texture.

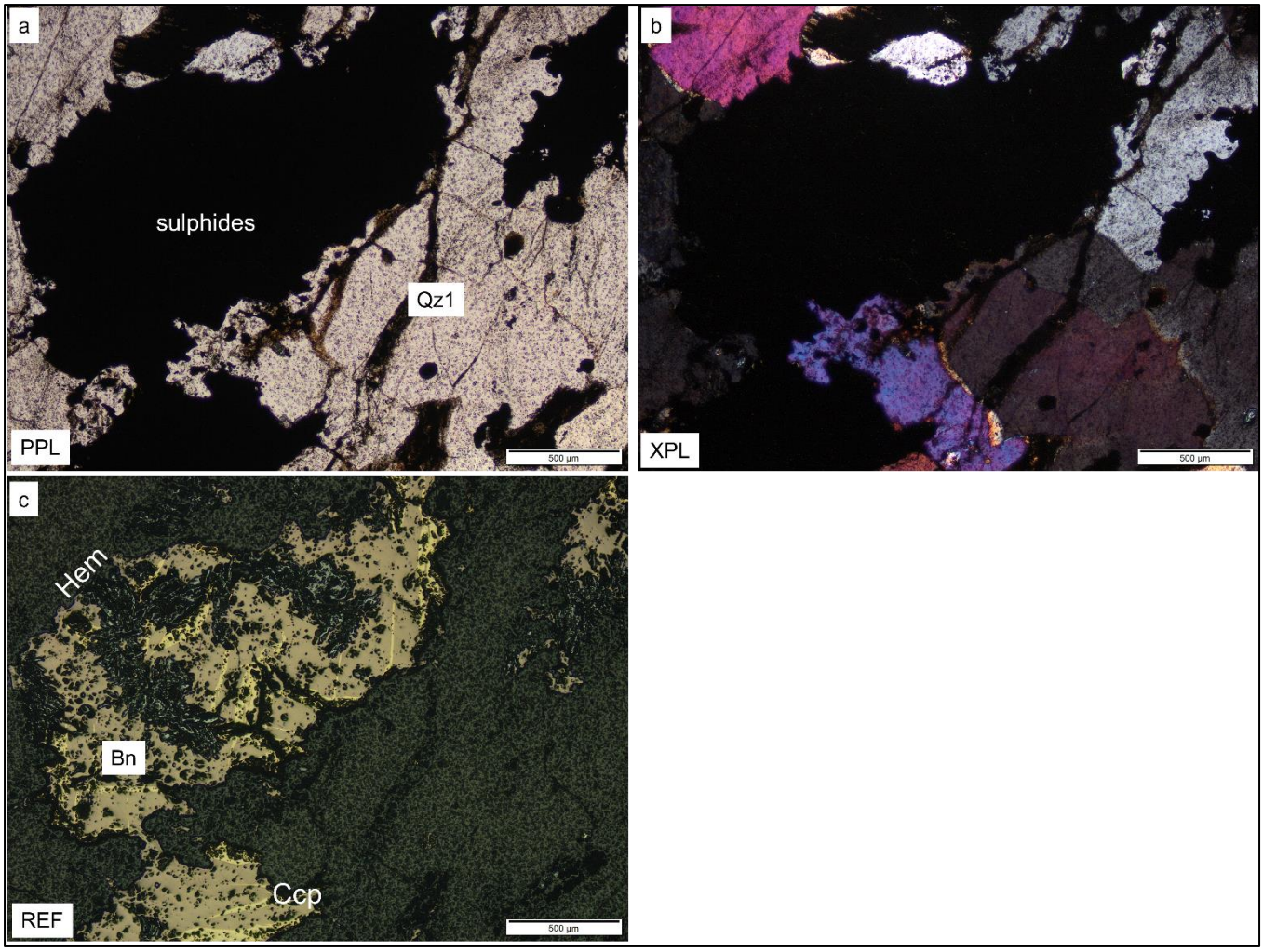


B20: (a-d) the part of the sample where garnet is absent is dominated by micro-brecciated quartz grains and randomly distributed biotite grains as inclusions within quartz grains, as well as altered plagioclase grains overprinted by quartz. Brecciation resulted in irregular and angular fragments and disorientation of minerals. Most quartz grains overprint the plagioclase that is partially altered by fine-grained sericite. Biotite alters partially into chlorite.

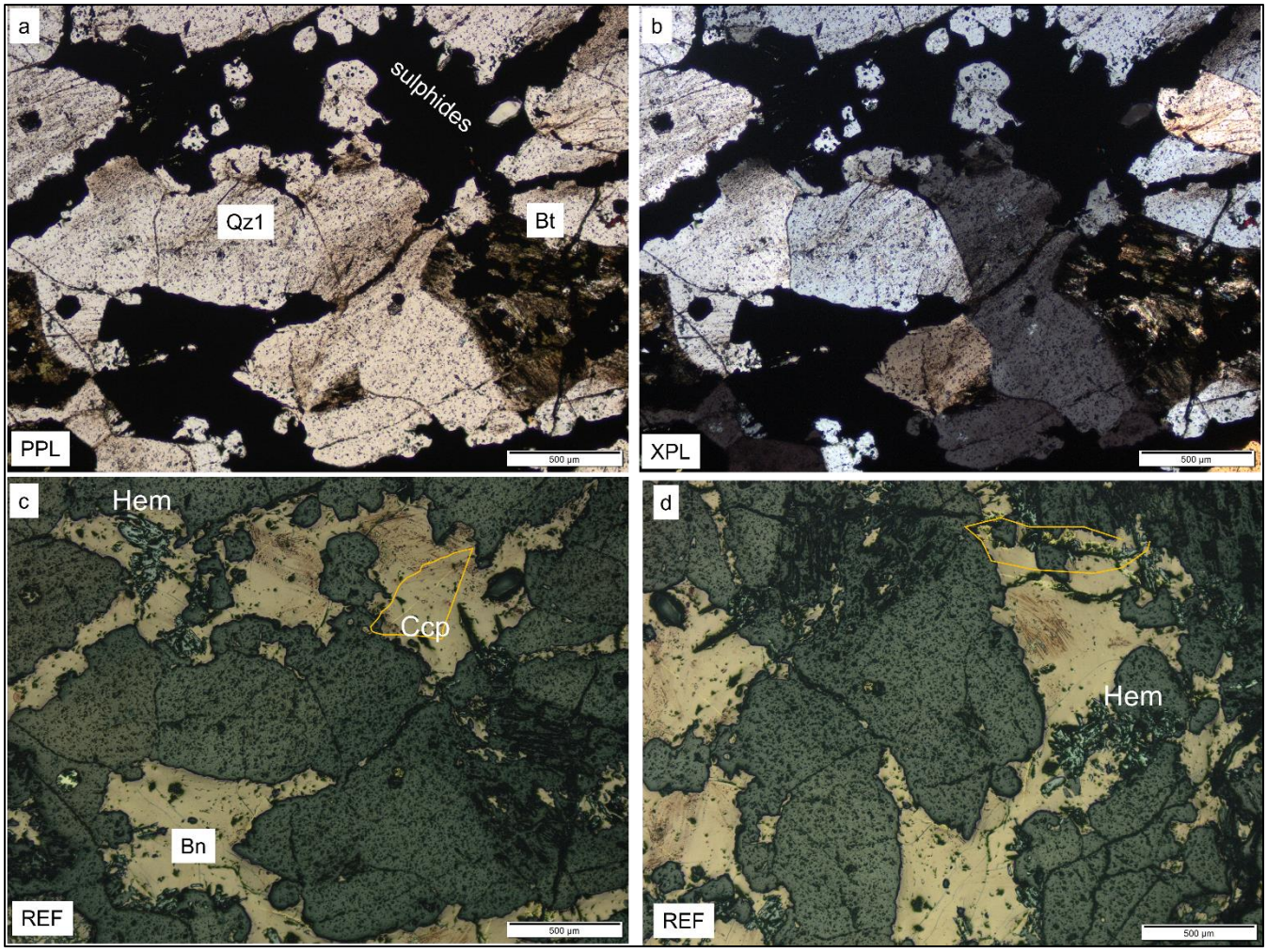
Sample P679



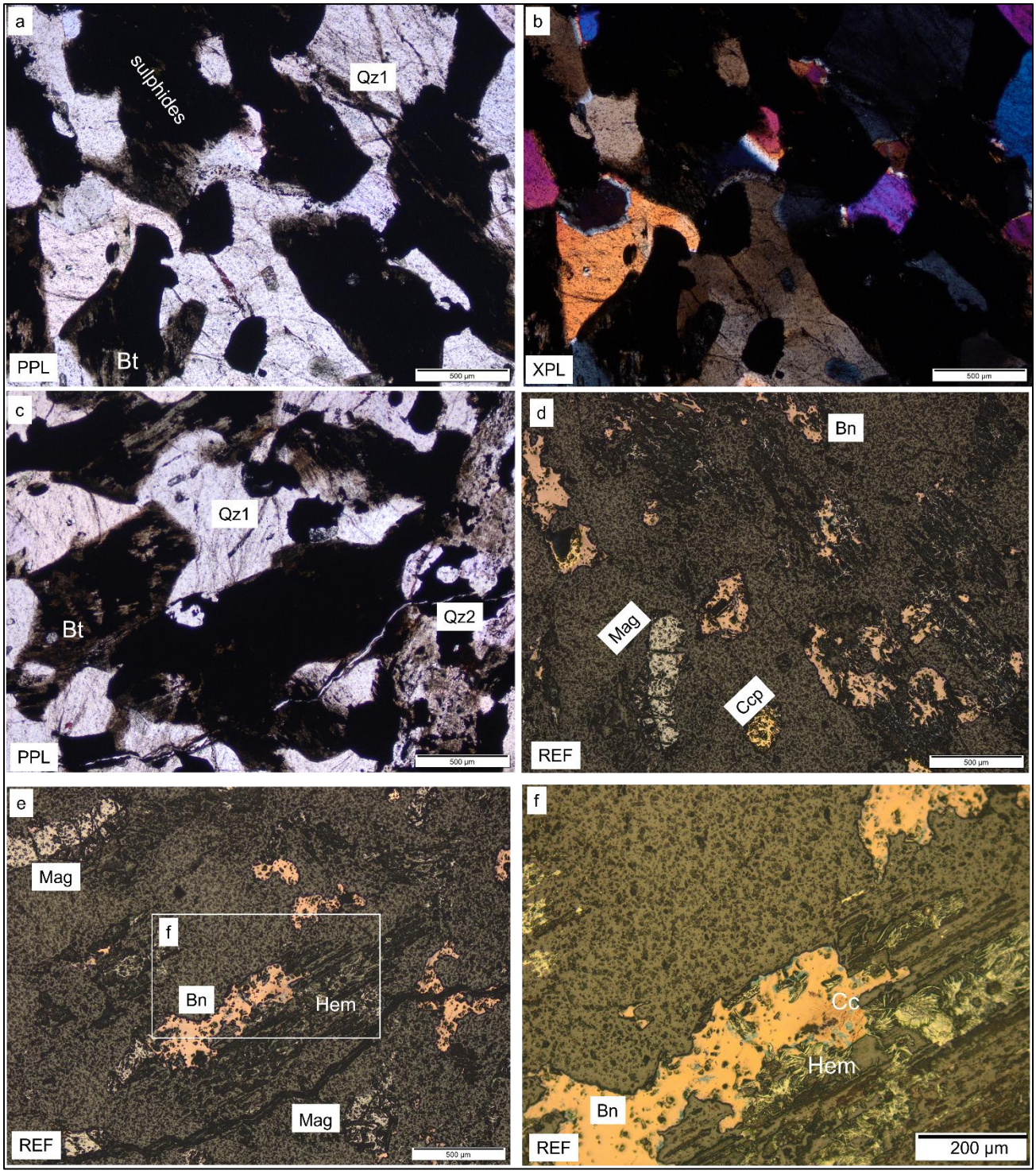
B21: Full scan photomicrographs for Sample P679 in PPL (a), XPL (b), and REF (c). The sample is dominated by brecciated quartz grains intergrown with brownish-green chlorite. Sulphides (mainly bornite) occurs between the open spaces of quartz and altered biotite as disseminations and anhedral grains. Sample size = 5 mm.



B22: (a-b) corroded and partly fractured quartz grains with distinct grain boundaries enclose the opaque minerals between them and some opaque minerals fill corrosion spaces within quartz. In crossed polarising light, the quartz grains exhibit interconnection of the grains; (c) preferential orientation of thin flame-like relics of chalcopyrite occurs within the host bornite and represents replacement of chalcopyrite by bornite. Small bladed hematite aggregates occur within the host Bn and in contact with chalcopyrite. Minor bornite grains occur as inclusions within the hematite aggregates.

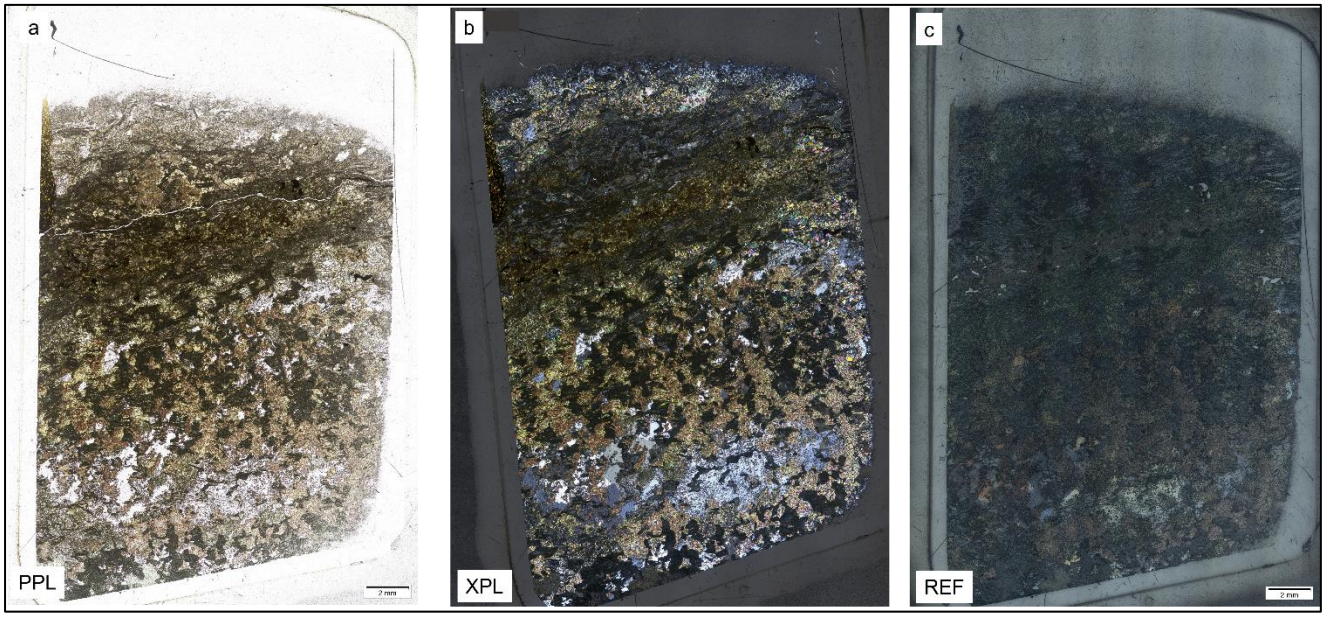


B23: (a-b) corroded quartz grains with irregular boundaries are intergrown with biotite (recognised by basal cleavage destroyed by corrosion). Quartz grains are brecciated, fractured, and dismembered whereby small fragments occur within the opaque minerals. Opaque minerals are enclosed within quartz and corrosion halos in biotite and quartz grains. Quartz grains exhibit undulose extinction; (c-d) the cleavage planes of biotite host hematite aggregates set within bornite. Hematite grains show overgrowth in places as small blades appear to be overgrowing from the fine ones. Bornite is enclosed by quartz and biotite as anhedral grains and cements the brecciated grains. Yellow chalcopyrite relics occur along the margins (orange polygons) of host bornite.

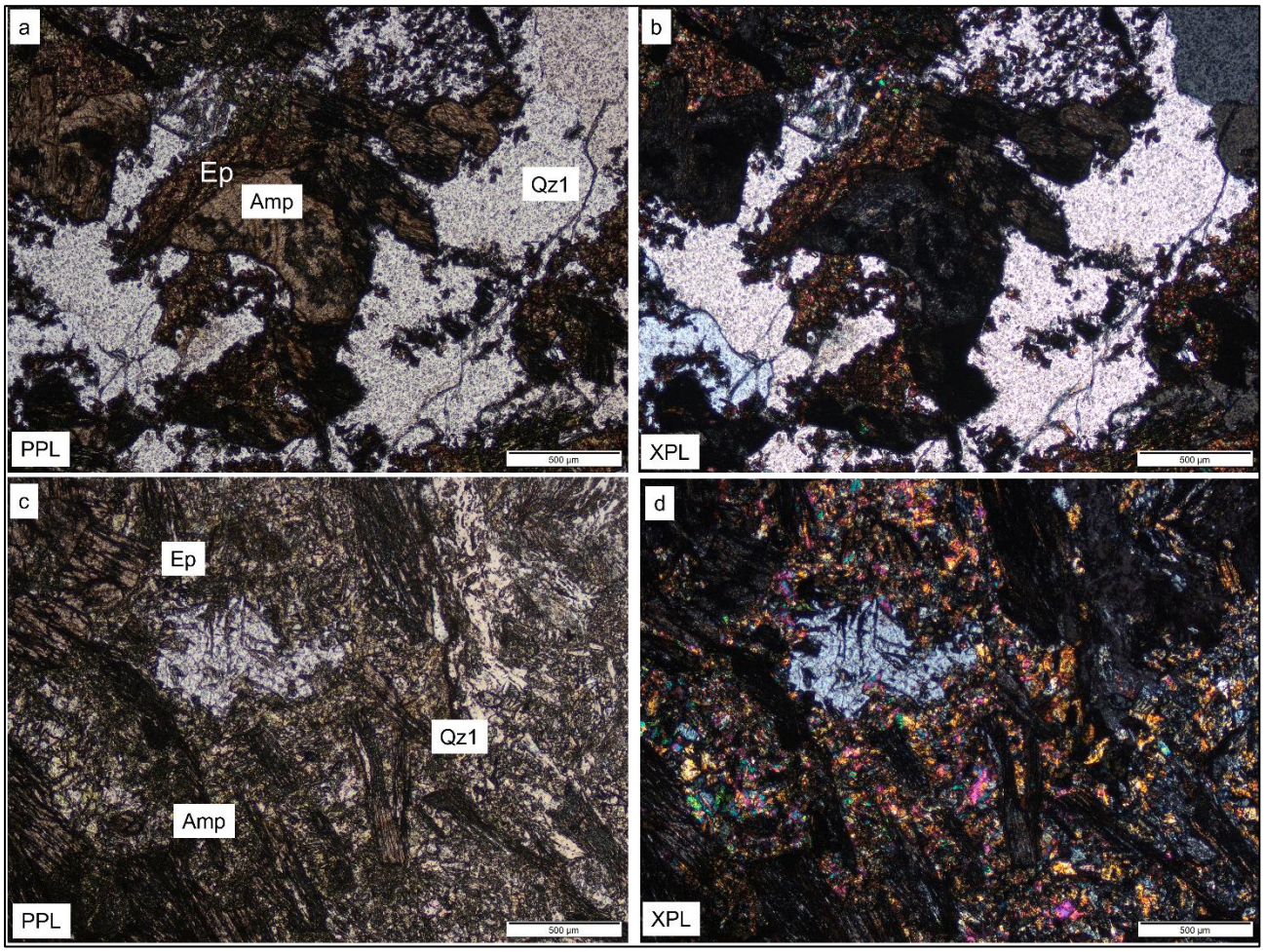


B24: (a-b) heavily corroded biotite and subhedral-angular quartz grains (light) enclose the opaque minerals; (c) inclined extinction of (a) and (b). Quartz is intergrown with corroded biotite and they are cut by a secondary thin quartz vein; (d) disseminated bornite occurs between quartz and within the corroded biotite hosting hematite. Subhedral magnetite grains are also present within the corroded biotite. The Fe-oxides could be the cause of the deep brown colour of the biotite and staining on quartz. High-magnification shows the presence of small chalcocite grains within bornite, representative of incipient replacement of bornite by chalcocite. Radial blades of hematite occur along the margins of bornite and within cleavage planes of biotite.

Sample P740

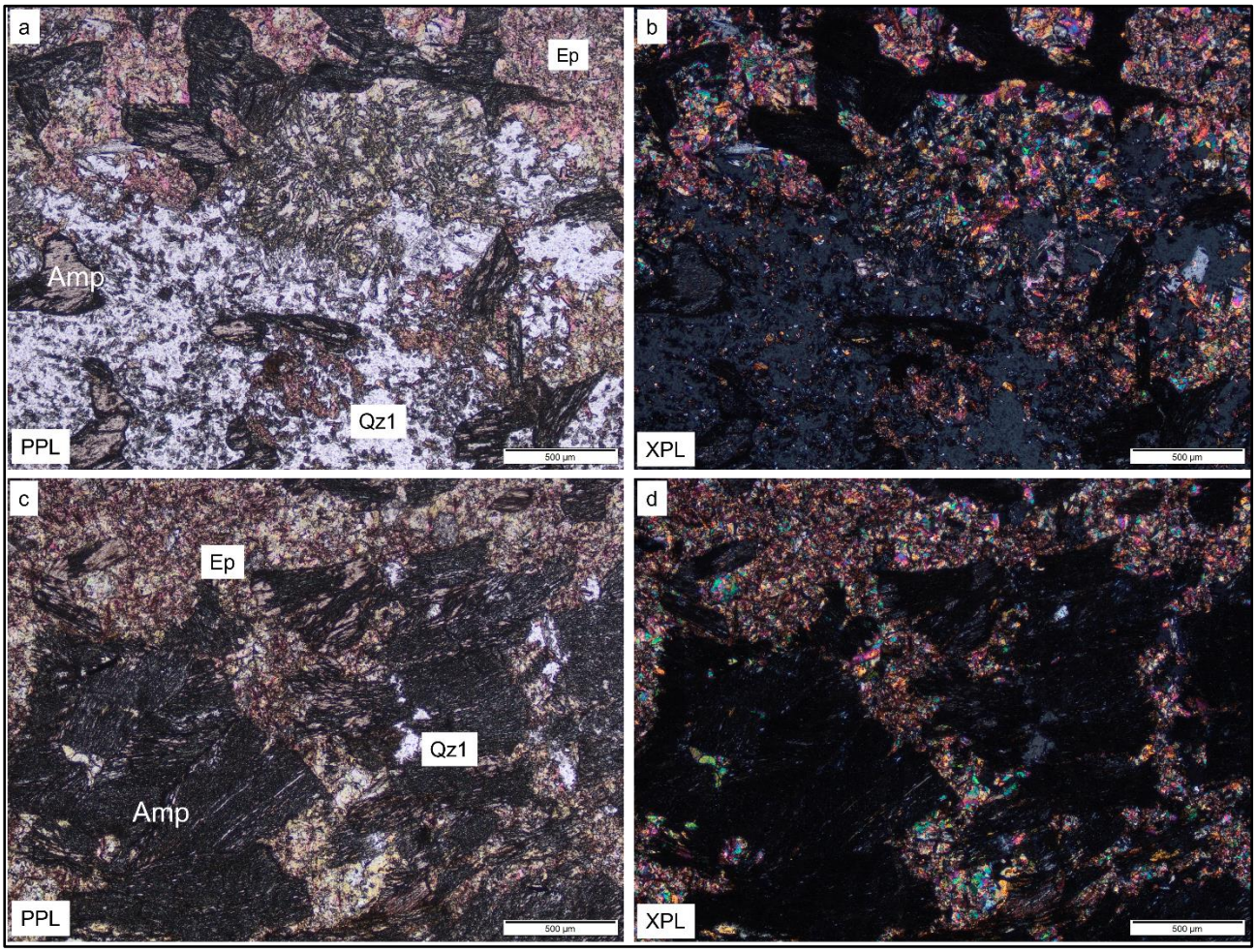


B25: Full-scan photomicrographs for Sample P740 in PPL (a), XPL (b), and REF (c). The sample represents a completely altered country rock. Epidote aggregates form the dominant silicate minerals enclosing dark brownish-black amphibole relics. Quartz grains appear to be overprinting epidote aggregates in places. Thin veins of quartz also cut across the sample. Minor grey Fe-oxides are also present. Sample size = 5 mm.



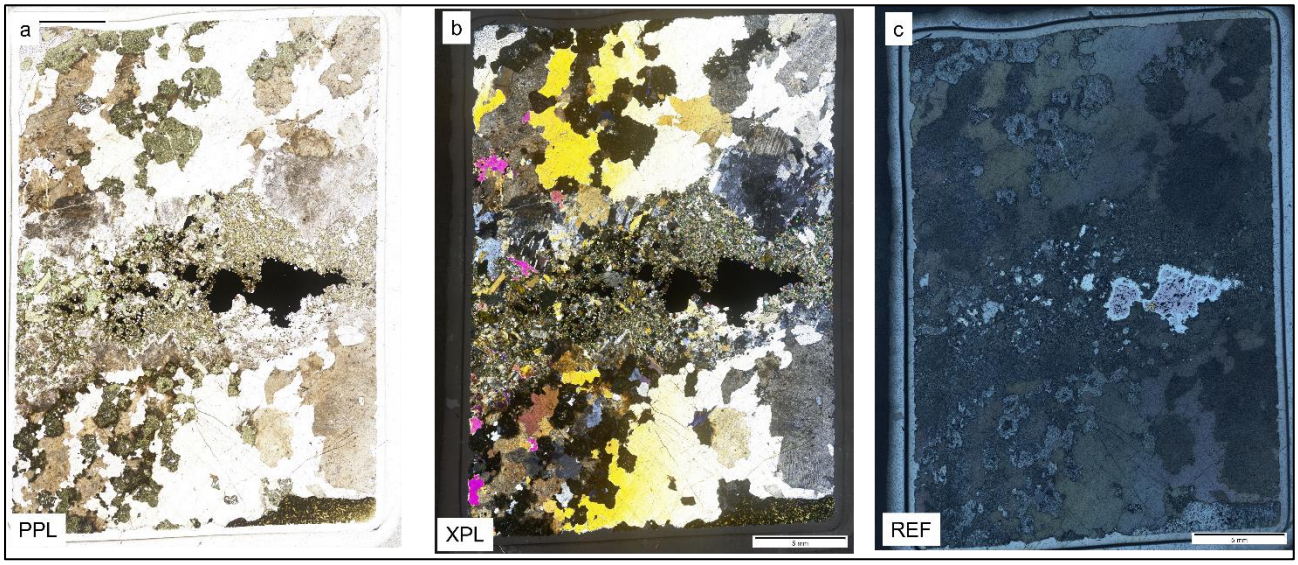
B26: (a-d) epidote aggregates enclose subhedral relict amphibole grains and are both embedded within medium-

large subhedral quartz grains. Disintegrated aggregates of epidote are seen as inclusions within quartz grains. Other quartz grains occur within the epidote and elongate amphibole grains.

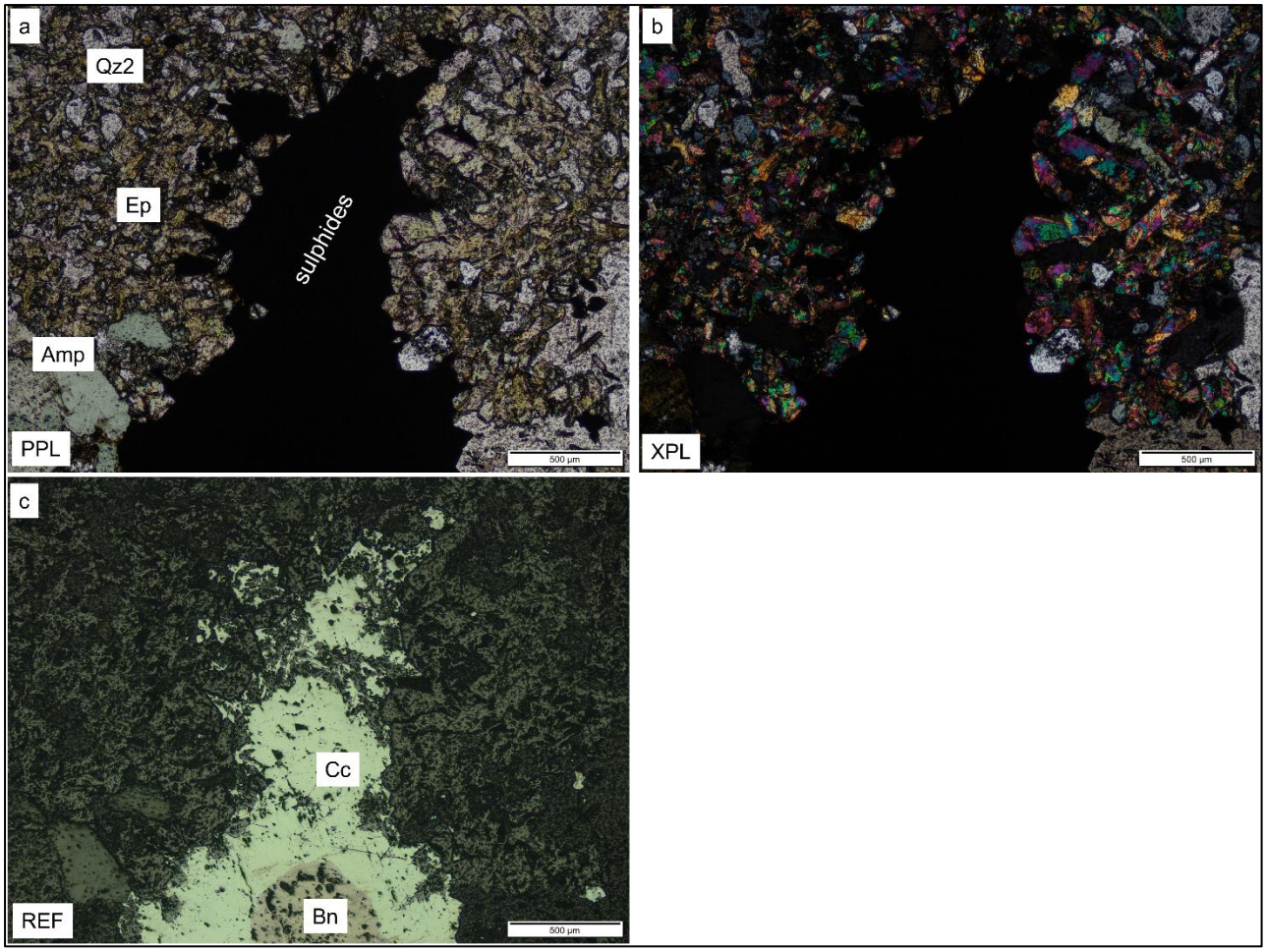


B27: (a-b) the subhedral large quartz grains appear to contain small epidote inclusions which also occur around the quartz grains as aggregates enclosing relict amphibole grains. The angular to irregular grains of amphibole also occur within quartz grains; (c-d) tabular relict amphibole grains occur within epidote aggregates which also overprint some amphibole grains. Minor angular quartz grains are also seen overprinting epidote aggregates and amphibole grains.

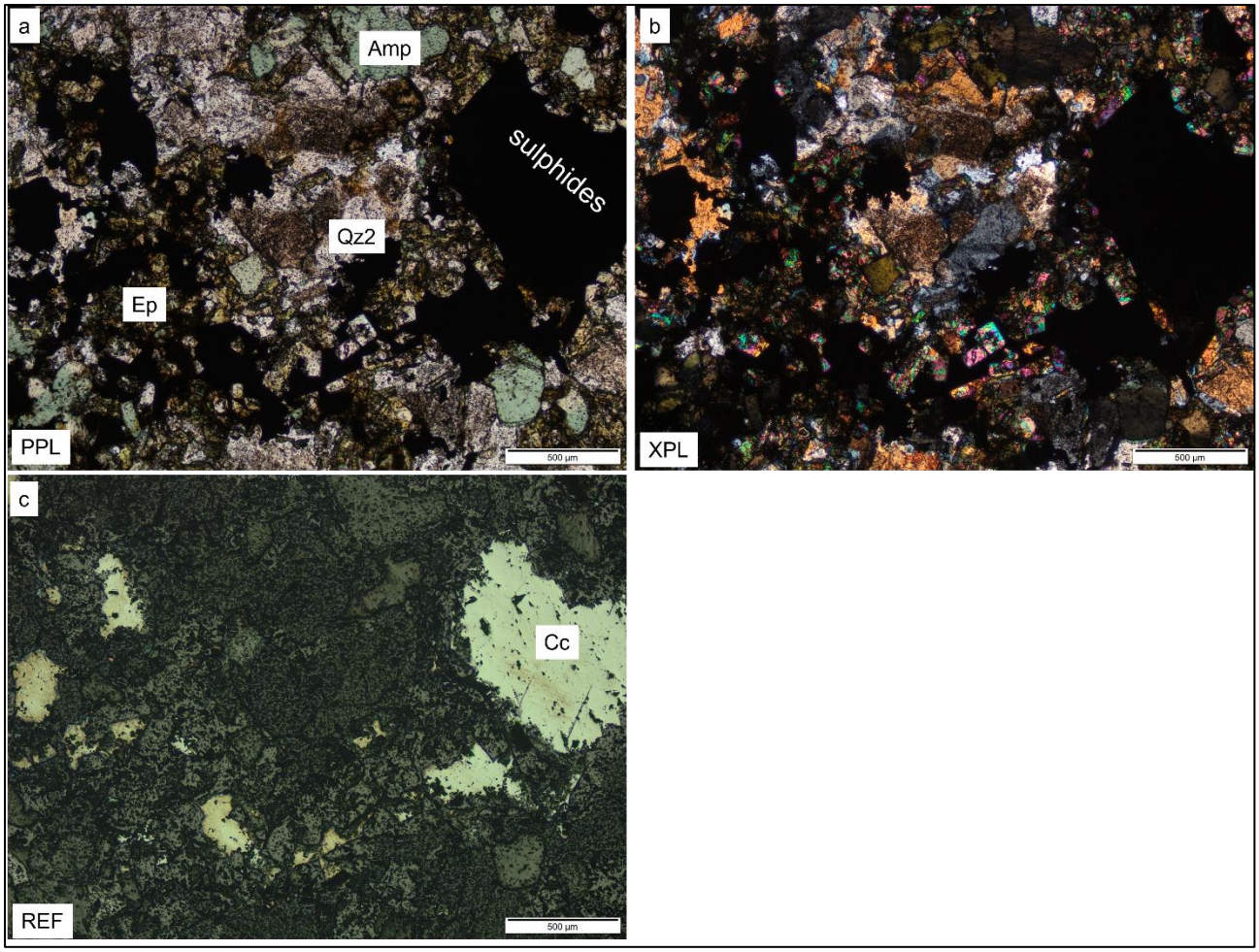
Sample P744



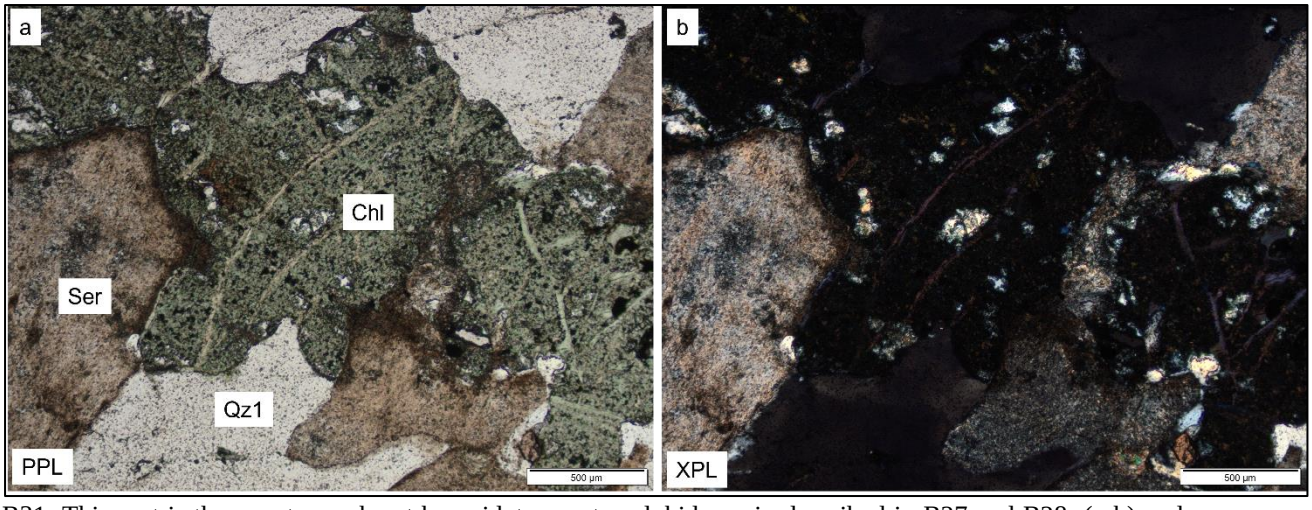
B28: Full-scan photomicrographs for Sample P744 in PPL (a), XPL (b), and REF (c). The sample is composed of a vein cutting through large, interconnected quartz grains. The vein contains micro-brecciated green epidote grains, which enclose the sulphides. Large, interconnected quartz grains are invaded by interstitial dusty brown (sericite) and dark green (chlorite). Sample size = 5 mm.



B29: (a) micro-brecciated prismatic epidote aggregates enclose relict subhedral grains of pale green amphibole and are cemented by small irregular to subrounded secondary quartz grains. The epidote aggregates are closely associated with the opaque minerals that they enclose; (b) high interference colours of epidote and light-grey, white quartz. The amphibole is brownish-black in XPL; (c) the pale blue chalcocite is replacing bornite and also occurs as disseminations within the brecciated epidote aggregates.



B30: (a-c) extension of B27 with disseminated chalcocite (small to large, 0.2-0.6 mm) within the gangue and enclosed by the gangue (mostly epidote). Epidote and amphibole occur as inclusions within the quartz grains in places.



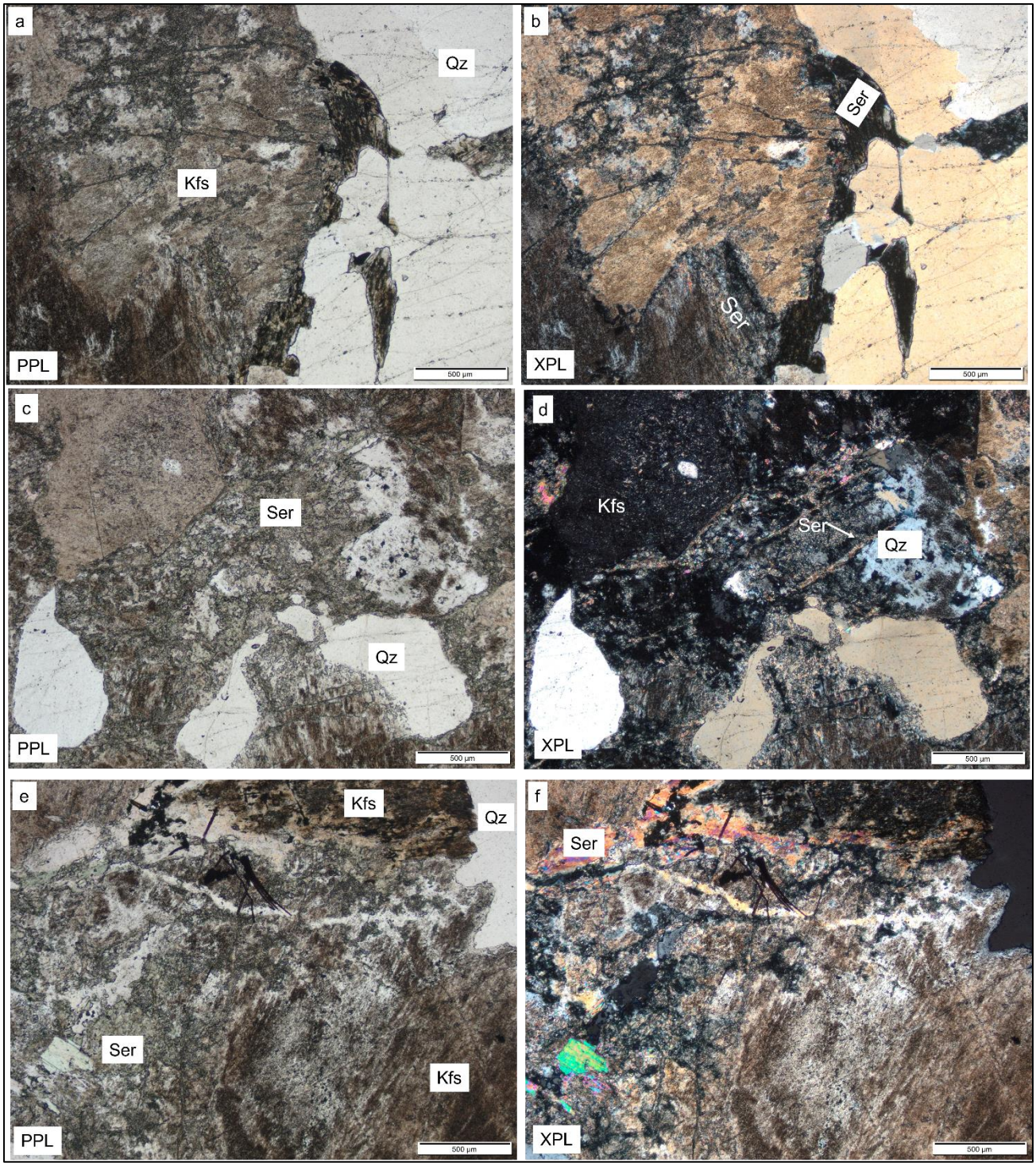
B31: This part is the country rock cut by epidote-quartz-sulphides vein described in B27 and B28; (a-b) early-formed subhedral quartz grains occur with fine-grained sericite and chlorite that are interstitial between quartz grains. The chlorite and sericite interfingers the quartz grain as irregular grains and contain small subrounded quartz grains as inclusions. Dark rims between sericite and chlorite represent reaction rims.

Sample P812

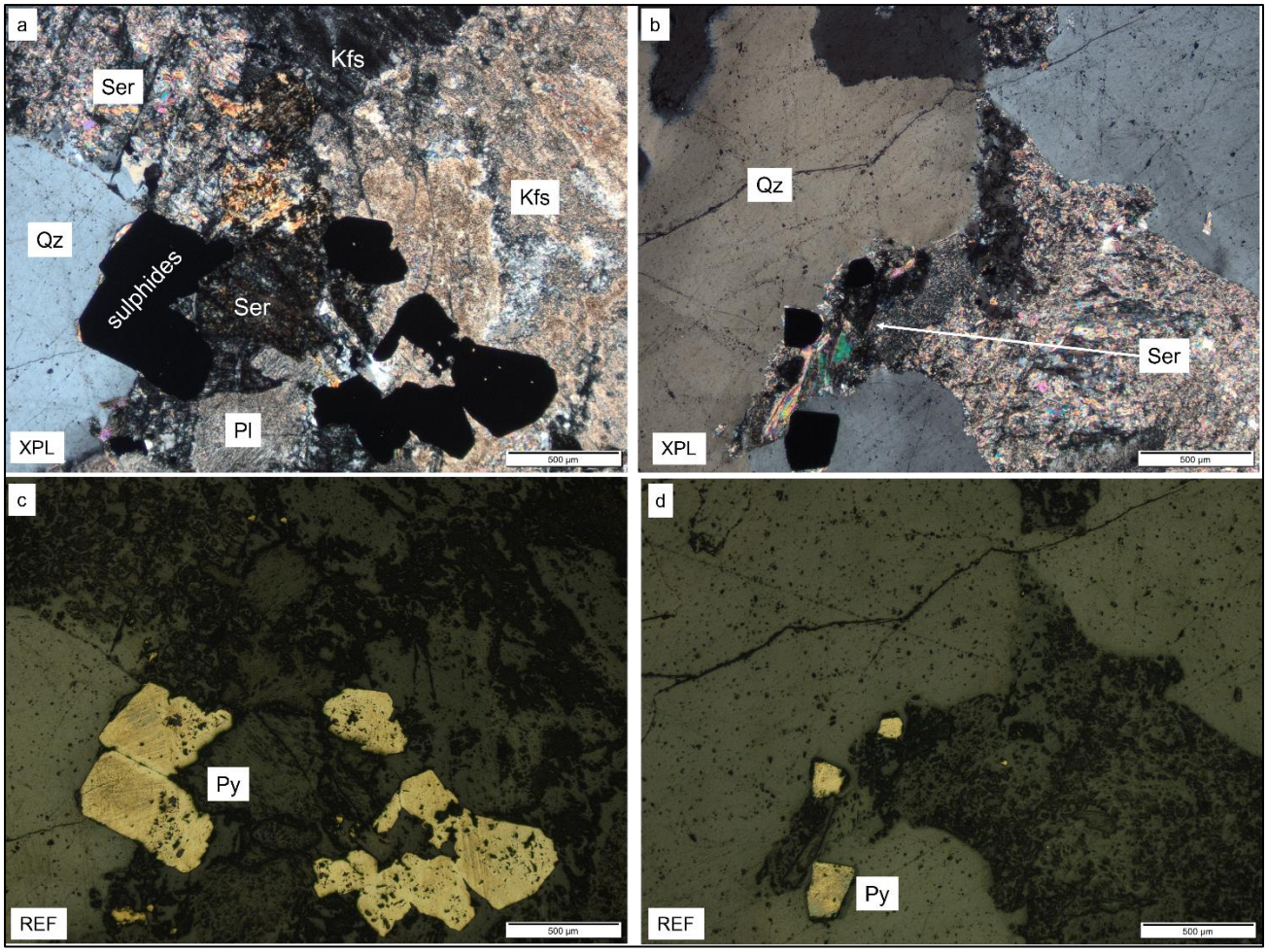
Crossed polarising light and reflected light photomicrographs could not be produced after the microscope stopped working properly as it was producing incomplete scans.



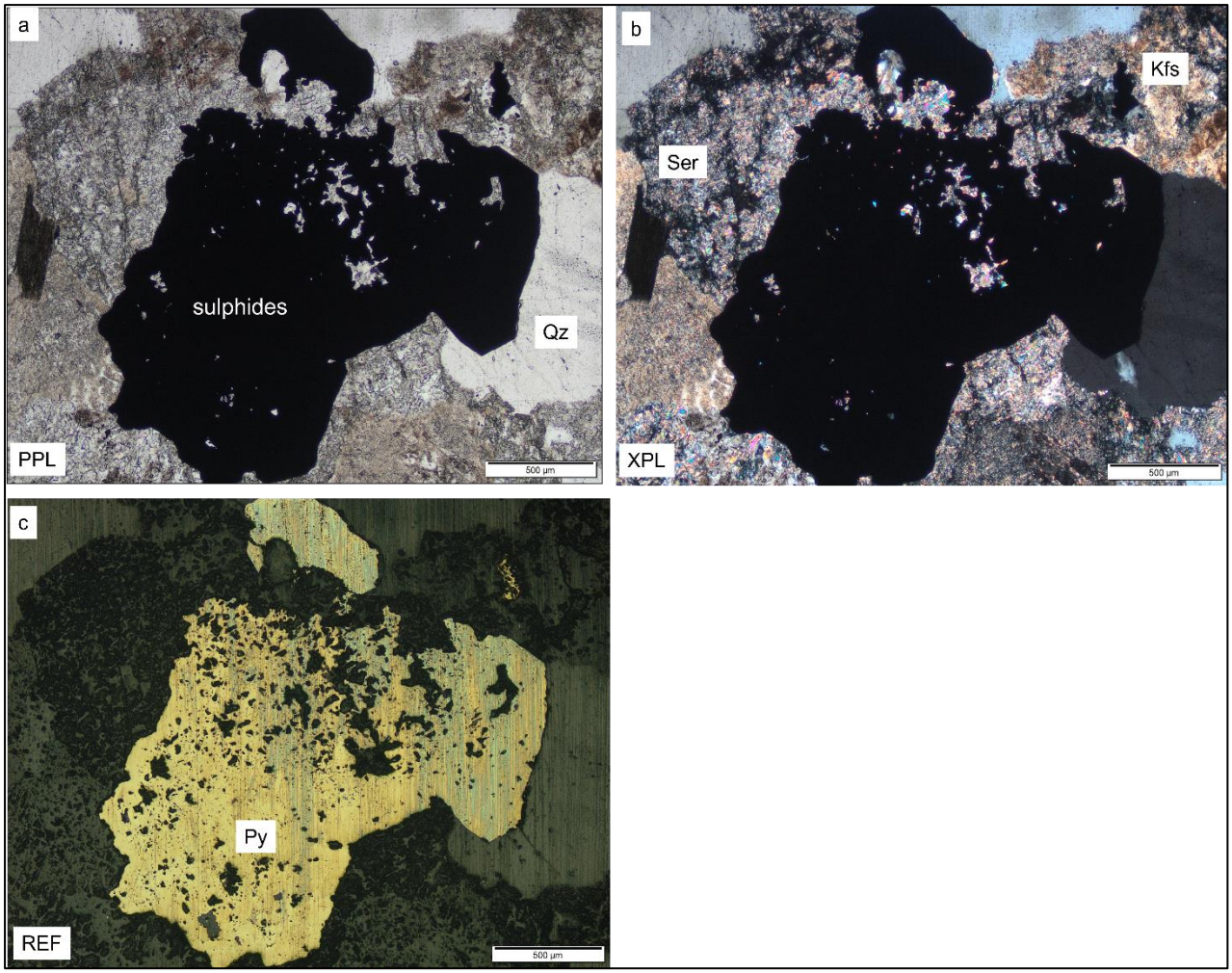
B32: Full-scan photomicrograph for Sample P812 in PPL. The sample is made up of large, interconnected quartz grains with interstitial dusty sericite and feldspars. Subhedral opaque minerals dominated by pyrite are enclosed by quartz and sericite. The large quartz grains resemble a vein.



B33: (a-b) brown Kfs is intergrown with large, subhedral, clear quartz grains and is partially altered by fine-grained sericite along grain margins. The sericite is also seen invading parts of quartz grains as irregular anhedral grains; (c-f) fine-grained sericite is replacing the Kfs and corrodes the quartz grains included within it (e.g., dark parts within sericite in (d) resemble corroded extinct quartz). Irregular subhedral Qz grains inclusions represent fragments of the vein that were dismembered during alteration or could be secondary quartz grains. Sericite also occurs as irregular veins within the K-feldspar and interfingers with quartz grain.

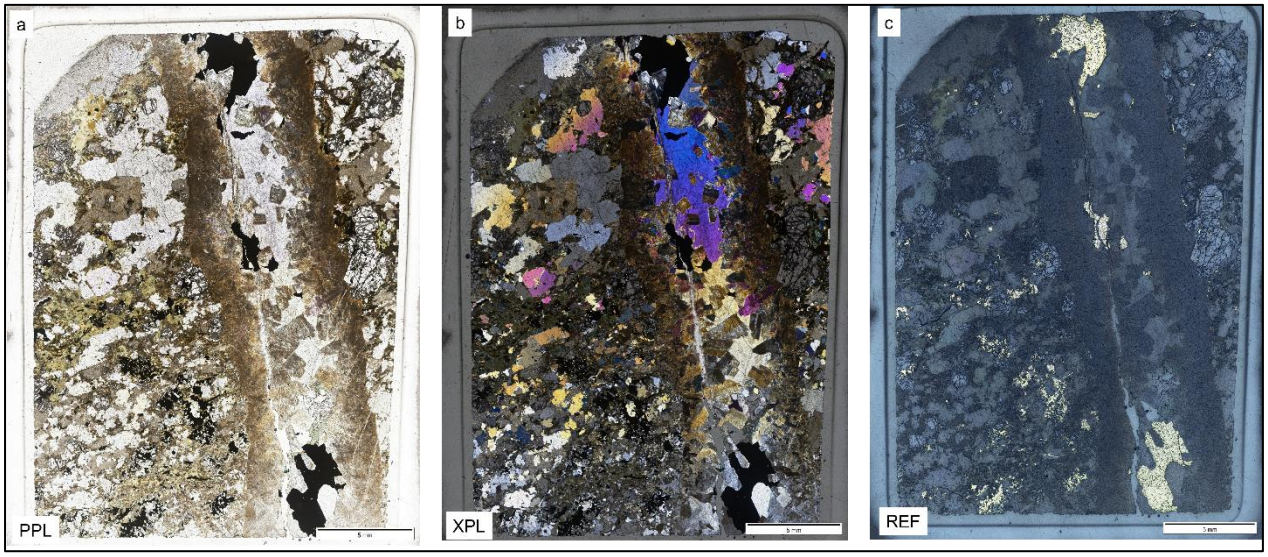


B34: (a) replacements of K-feldspar by fine-grained sericite. Some sericite occurs a partial rim between quartz and the opaque minerals; (b) sericite is interstitial between the large, interconnected quartz grains and contains inclusions of K-feldspar where it shows almost complete alteration of the K-feldspar; (c-d) small and medium (0.1-1 mm) euhedral to subhedral pyrite grains are occur within the sericite and contains corroded tiny grains of sericite. The pyrite grains also occur at the contact between quartz and sericite as well as within the quartz grains. Those within the quartz grains have smooth texture (no inclusions).

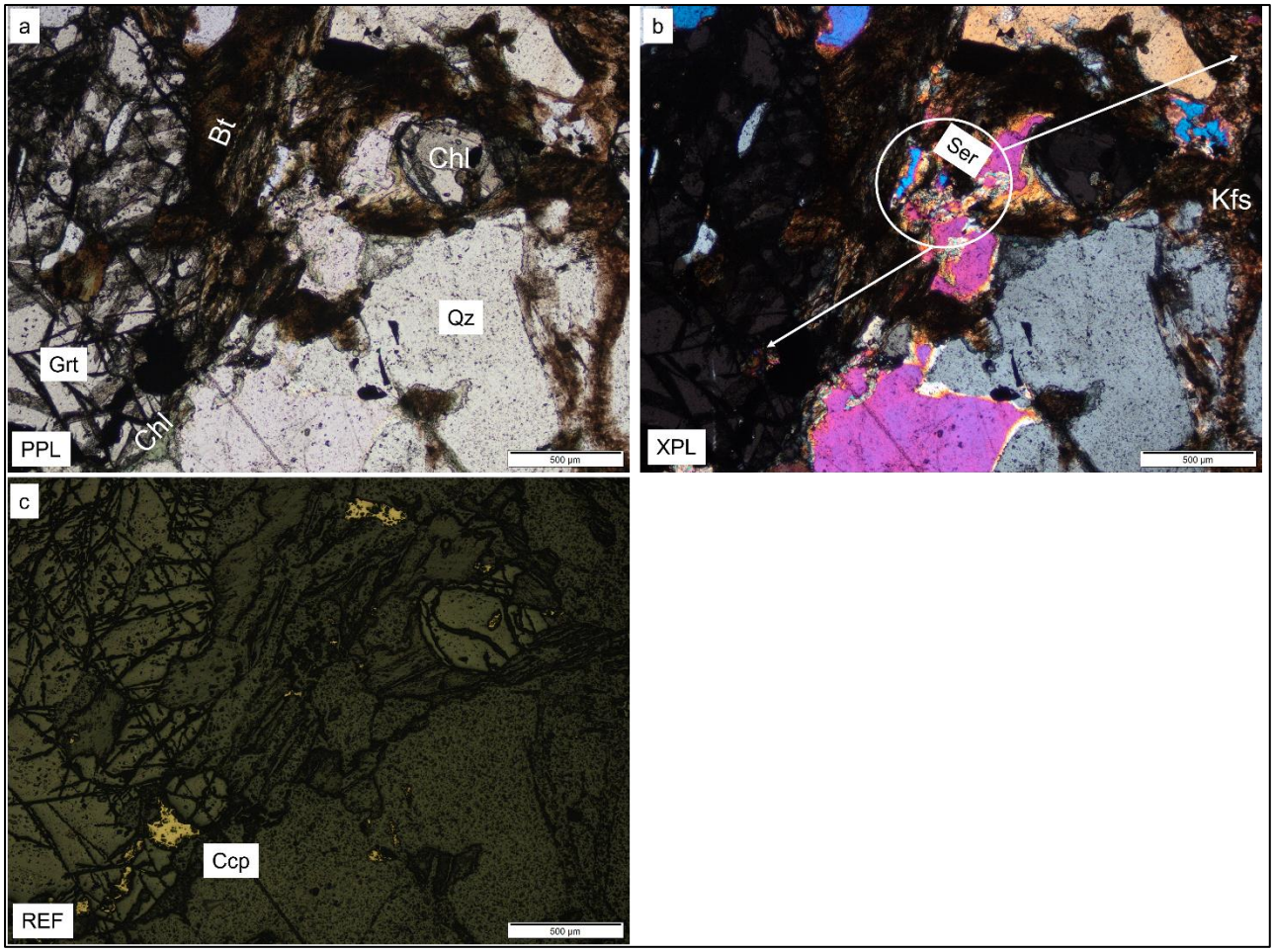


B35: (a-b) large, clear quartz grains invaded by interstitial fine-grained sericite. The opaque minerals corroded the sericite which occurs within it as irregular grains. The quartz has smooth to sharp grain boundaries with the opaque minerals but where it is associated with sericite the boundaries are irregular; (c) tarnished cluster of pyrite contains inclusions of sericite gangue (forming a porous texture on pyrite).

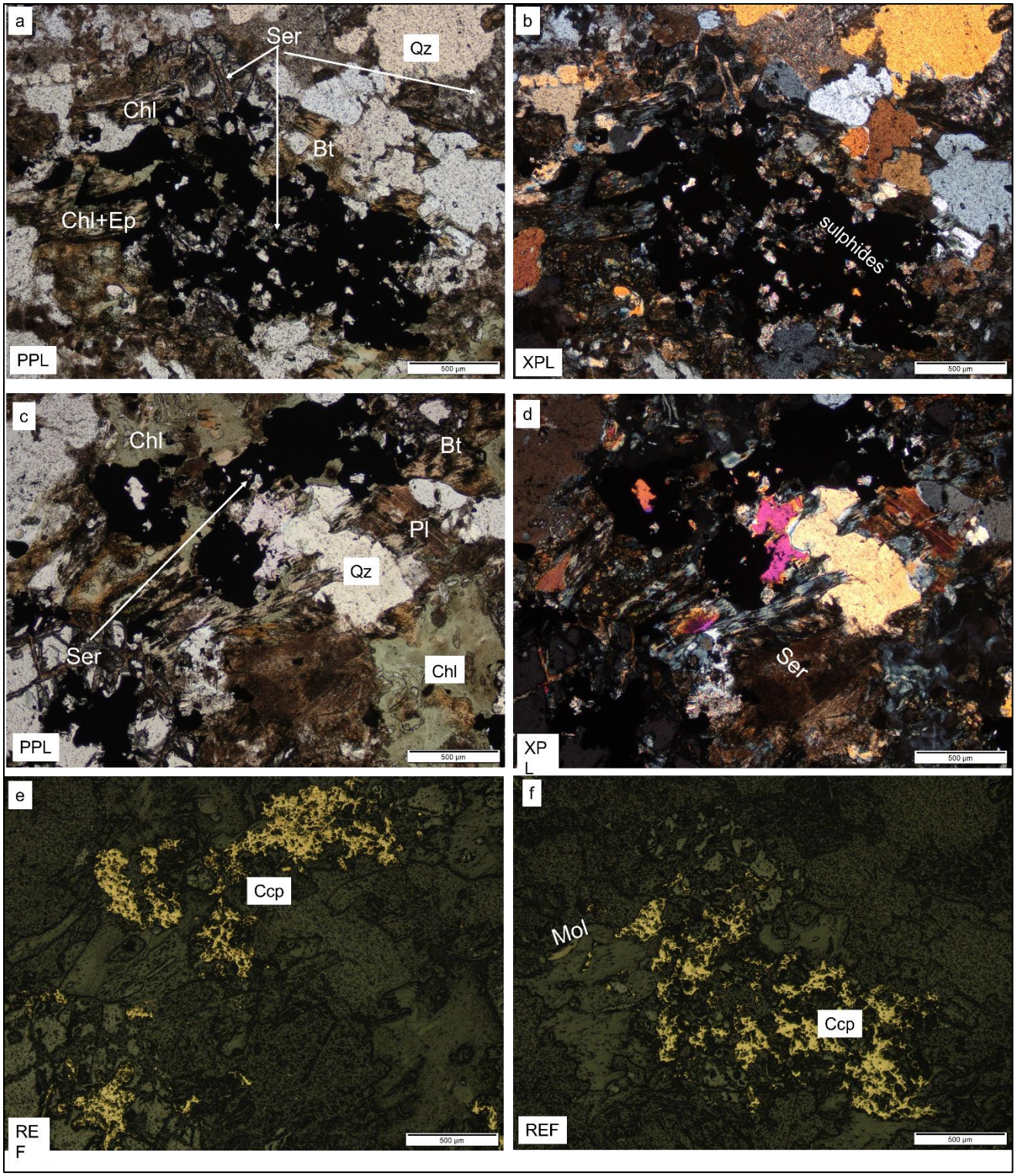
Sample P814



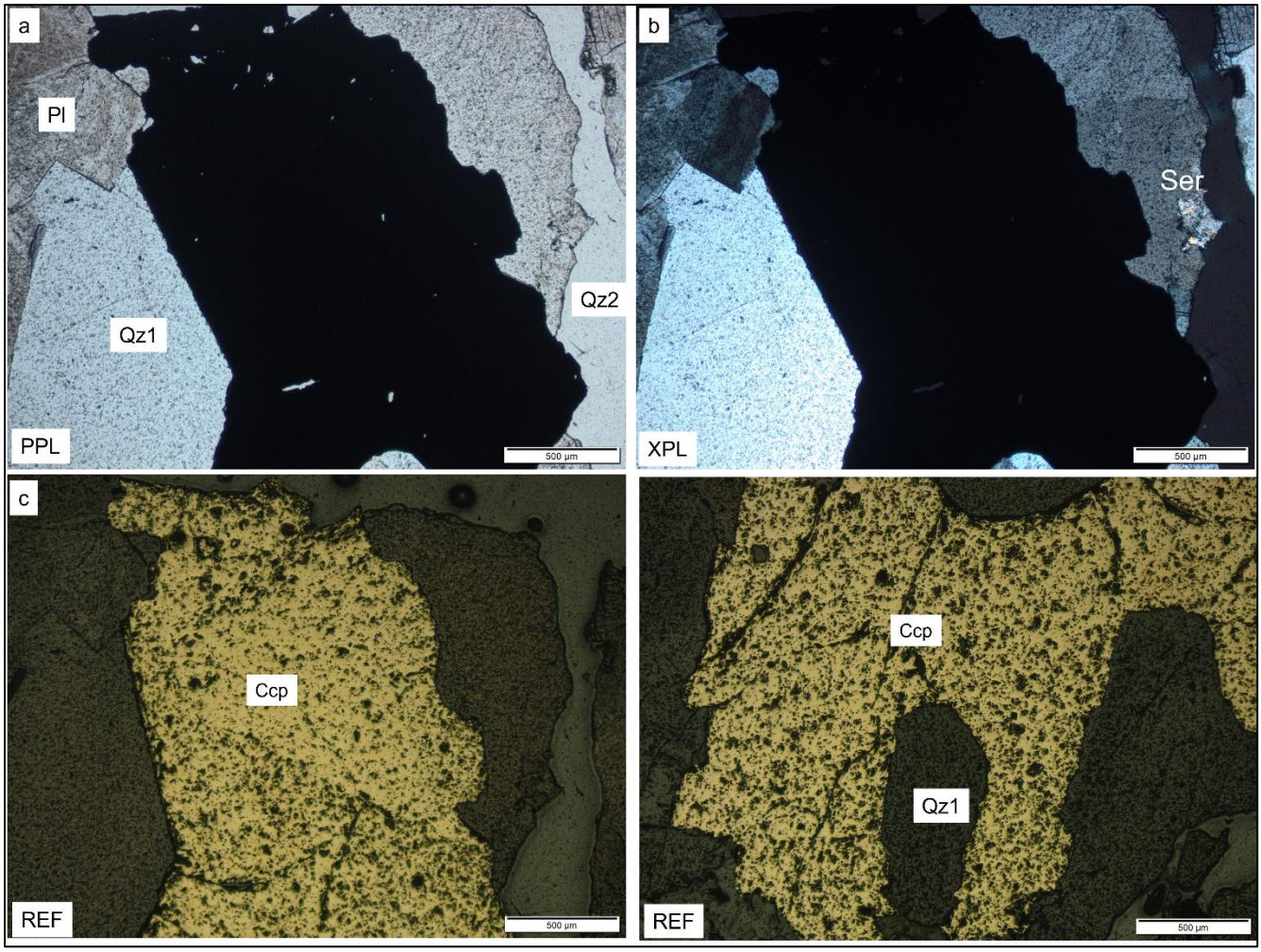
B36: Full-scan photomicrographs for Sample P814 in PPL (a), XPL (b), and REF (c). The sample consists of brecciated country rock and a vein cutting through the country rock. In the country rock, brecciated quartz and plagioclase occur with biotite that is partially altering into chlorite. Fractured garnet grains alter into chlorite as well. The thick vein is bordered by dusty feldspars and is filled by blocky quartz grains. Brecciated feldspars are also included within the vein quartz. Another thin secondary quartz vein occurs within the thick vein. Chalcopyrite dominates the sample opaque minerals and occurs within the veins and in the country rock. Sample size = 5 mm.



B37: (a-b) fractured garnet is intergrown with biotite and quartz. The garnet and biotite are partially altering into green chlorite. Quartz grains are stained or weakly fractured by K-feldspars. Fine-grained sericite is concentrated in an open space within the quartz grains (white circle), which also occurs within garnet fractures and alters K-feldspars along the margins (white arrows); (c) small chalcopyrite disseminations occur along garnet cracks and within quartz gangue.

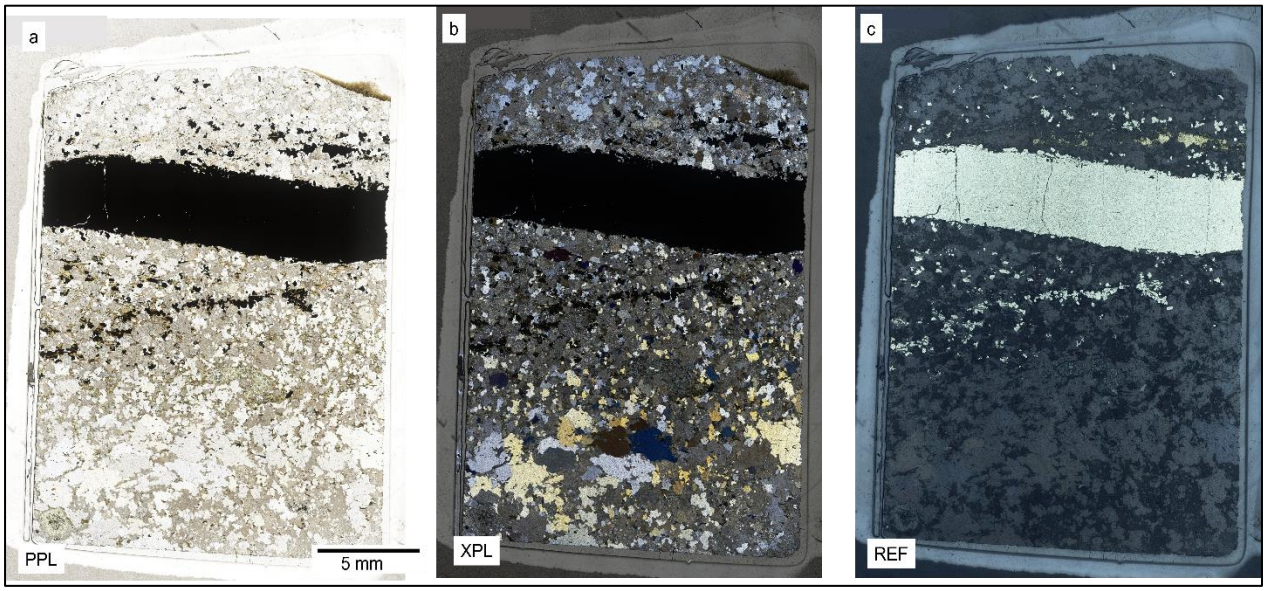


B38: (a-d) fragments of quartz grains of varying sizes are brecciated and cemented by fine-grained sericite, which is also present within the opaque minerals as distributed grains (white arrows). Brecciated chlorite (brownish-green) occurs around the quartz grains. The chlorite alters and replaces biotite. The chlorite in turn alters into epidote. Some epidote grains occur along cleavage planes of chlorite. Discrete fragmented fine grains of chlorite and quartz grains occur within the opaque minerals. Chlorite is seen replacing biotite and partially encroaching or cutting through some quartz grains. Other quartz grains appear as inclusions within biotite-chlorite (c); (e-f) coarse-grained, porous chalcopyrite is disseminated within garnet fractures and chlorite cleavage planes and between quartz grains. Thin molybdenite laths occur along the grain boundary of chlorite. This part represents mineralisation within the country rock.

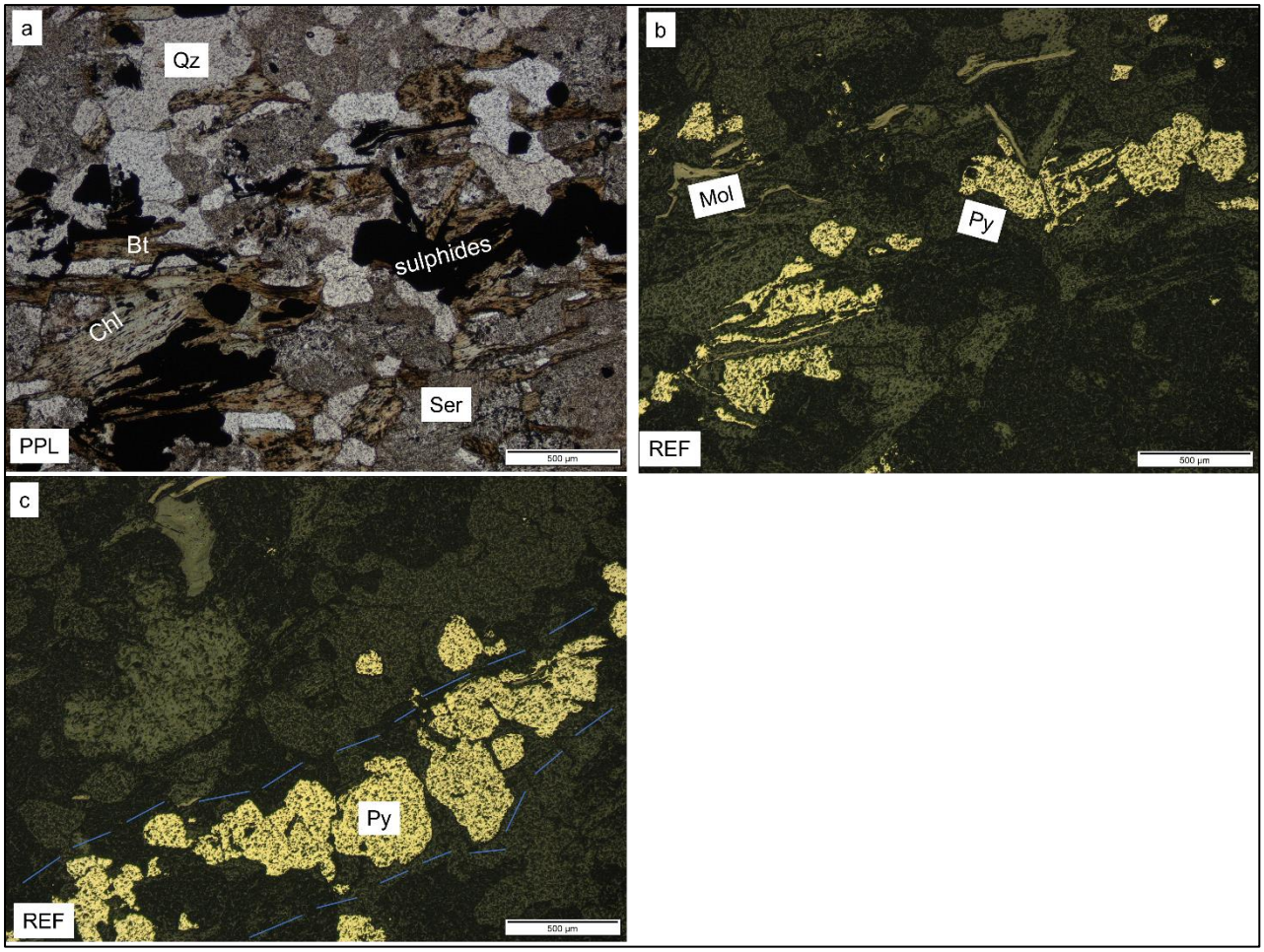


B39: (a-b) secondary quartz vein (Qz2) cut across blocky quartz within the thick vein (Qz1) that is borders by feldspars. The quartz is in contact with a subhedral plagioclase (weakly albitised in XPL). Minor fine-grained sericite occurs between plagioclase and Qz2; (c) coarse-grained chalcopyrite grains occur between the blocky quartz grains of the vein; (d) an extension of C showing isolated quartz grains within the vein and coarse-grained anhedral chalcopyrite. This part represents mineralisation within the vein.

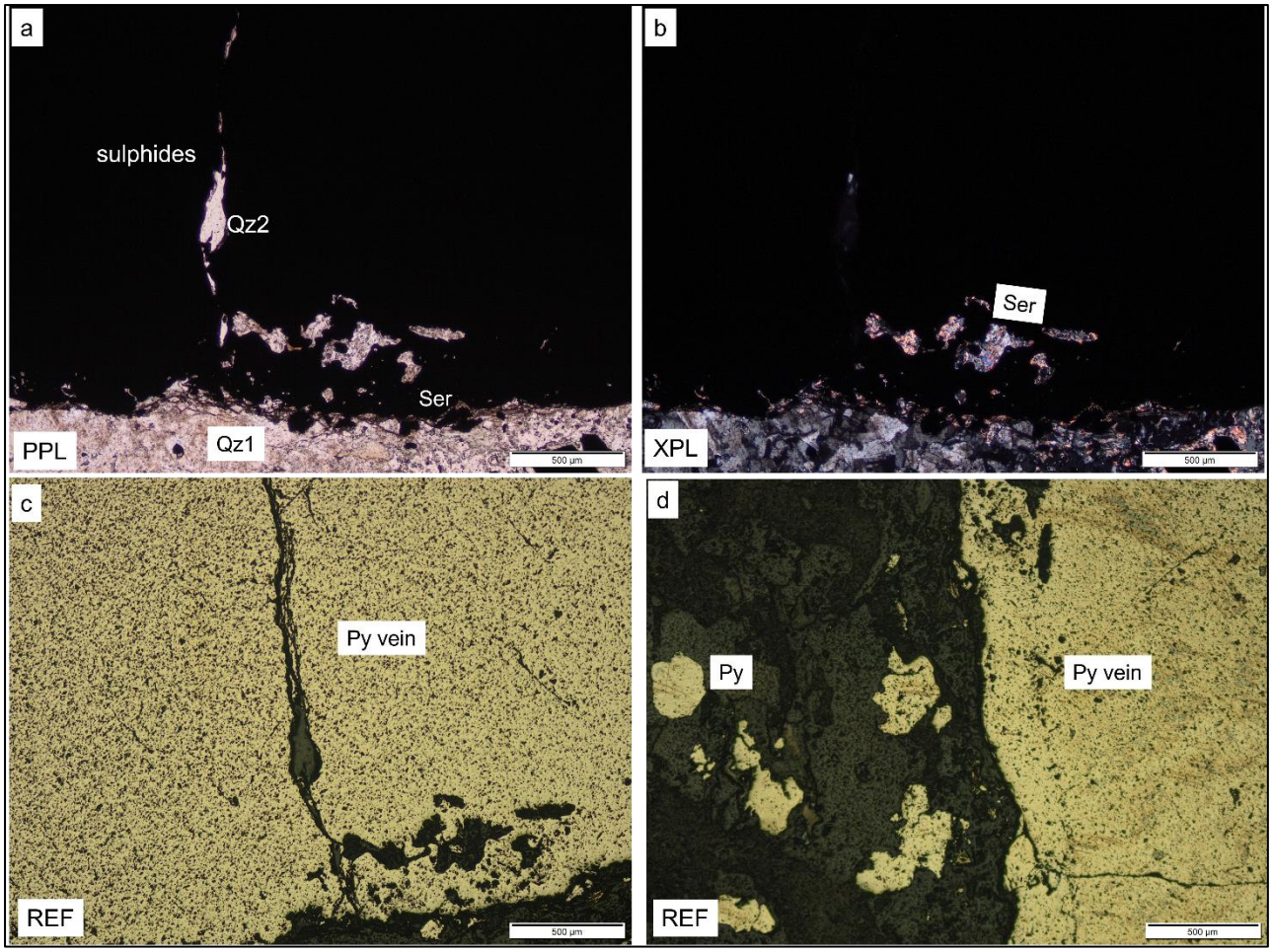
Sample P782



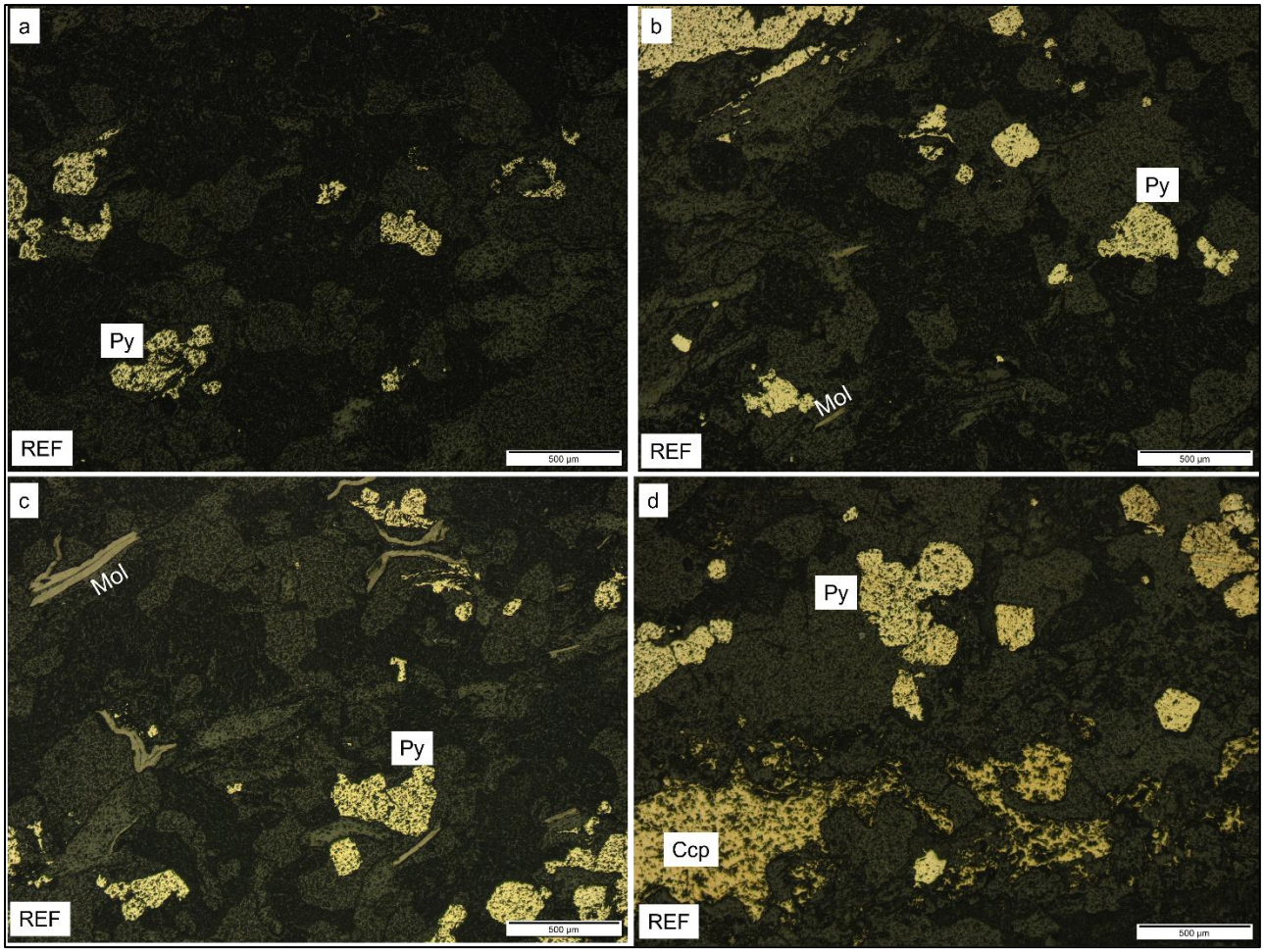
B40: Full-scan photomicrographs for Sample P782 in PPL (a), XPL (b), REF (c). The sample is dominated by dusty fine-grained sericite groundmass cementing subhedral brecciated quartz grains. Biotite and mafic minerals are embedded within the sericite groundmass and between subhedral quartz grains. The light green coloration (in PPL) on biotite and mafic mineral grains is due to chlorite alteration. The opaque minerals are enclosed within the fine-grained sericite groundmass and quartz grains as irregular veins and preferentially aligned grains. A thick vein of pyrite cut across the sample. Pyrite is the dominant sulphide mineral amongst the opaque minerals. Under reflected light, an irregular vein of chalcopyrite is seen enclosed by the silicates. Wispy, small grains of molybdenite are also present within the gangue minerals. Aligned subhedral pyrite follow what looks like a relict vein structure and are also disseminated between sericite groundmass. Sample size = 5 mm.



B41: (a) subhedral brecciated quartz grains are cemented by fine-grained sericite. The quartz grains represent inter-fragmental grains that filled open spaces within the breccia. Irregular biotite grains that are being partially replaced by chlorite occur between the quartz grains and sericite groundmass, as well as within the sericite grains. The opaque minerals occur between quartz-sericite and along cleavage planes of biotite; (b-c) subhedral-anhedral pyrite grains are disseminated between the silicates. The pyrite grains are associated with thin molybdenite laths occurring between or in contact with biotite grains. Other pyrite grains as partly clustered and aligned like a vein (blue stippled lines).

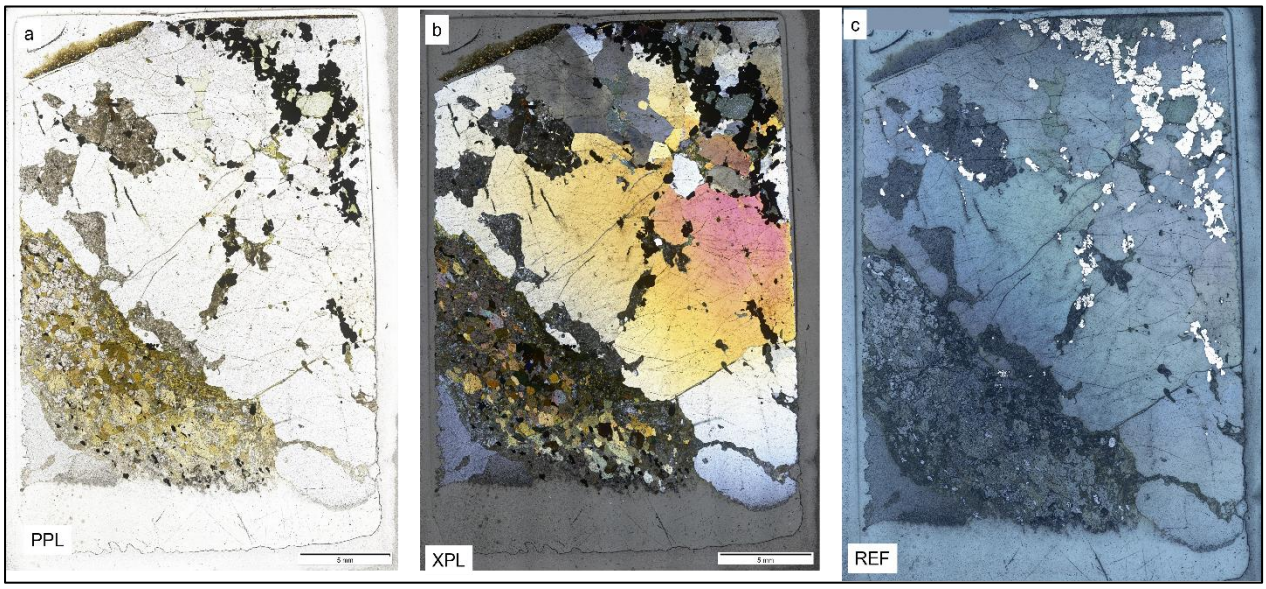


B42: (a-b) corroded fine-grained sericite grains occur within the opaque minerals. Secondary quartz cut through the opaque minerals as a discontinuous irregular vein; (c) the secondary quartz vein dissects the thick (4-5 cm) pyrite vein; (d) subhedral to subrounded pyrite grains occur within quartz grains and fine-grained sericite groundmass as disseminated grains of varying sizes and morphology. The sericite in contact with the vein appears corroded whereby some parts are broken off the fine-grained groundmass and now occur as irregular grains within the pyrite vein.



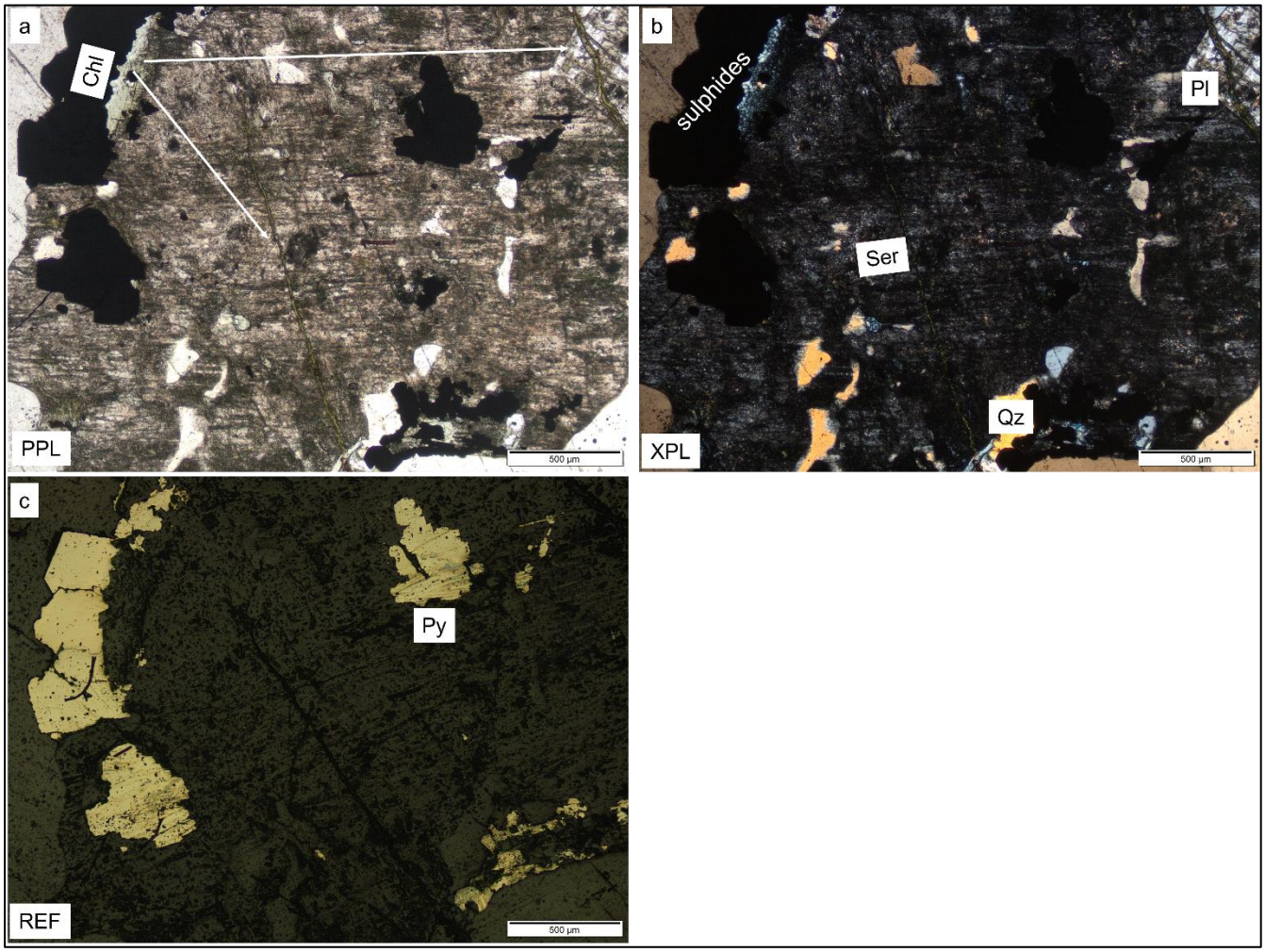
B43: (a-d) other textures of pyrite grains within the gangue minerals. Disseminated pyrite grains occur with discrete wispy and irregular molybdenite laths. There are different morphologies of pyrite grains from euhedral, subhedral, and rounded to elongated.

Sample P817

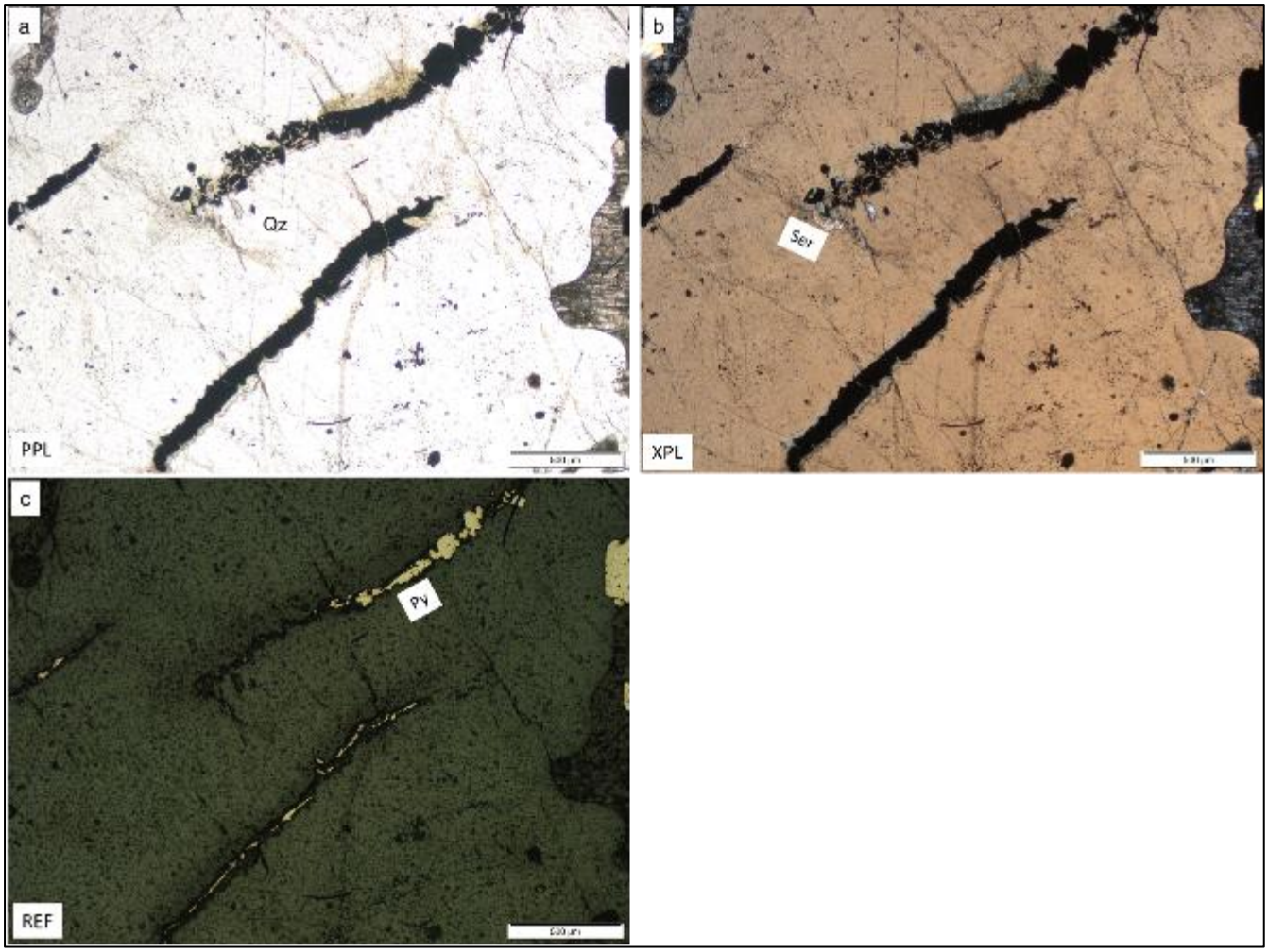


B44: Full-scan photomicrographs for Sample P817 in PPL (a), XPL (b), and REF (c). The sample consist of a thick blocky quartz vein in contact with a brecciated country rock. The country rock comprises amphiboles that are altered by light-dark green chlorite. Dusty fine-grained sericite and feldspars occur along the contact of the

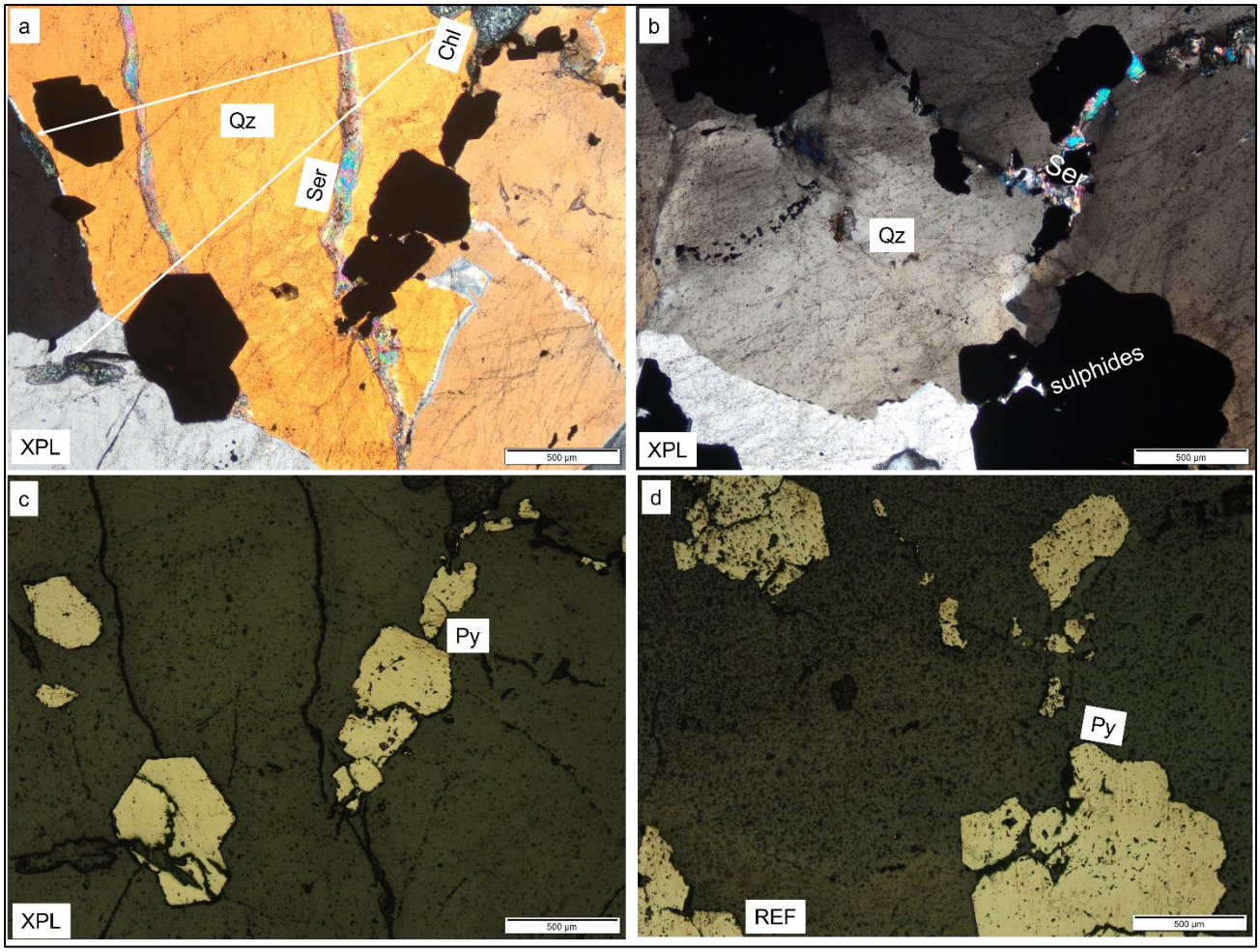
vein and country rock, as well as within the vein as anhedral mass between the large quartz grains. The quartz vein hosts subhedral to anhedral disseminations of pyrite grains. The pyrite grains also form clustered grains within the vein. In the brecciated country rock, minor grey disseminations occur as discrete grains. The grey grains in the country rock under reflected light appear to be magnetite. Sample size = 5 mm.



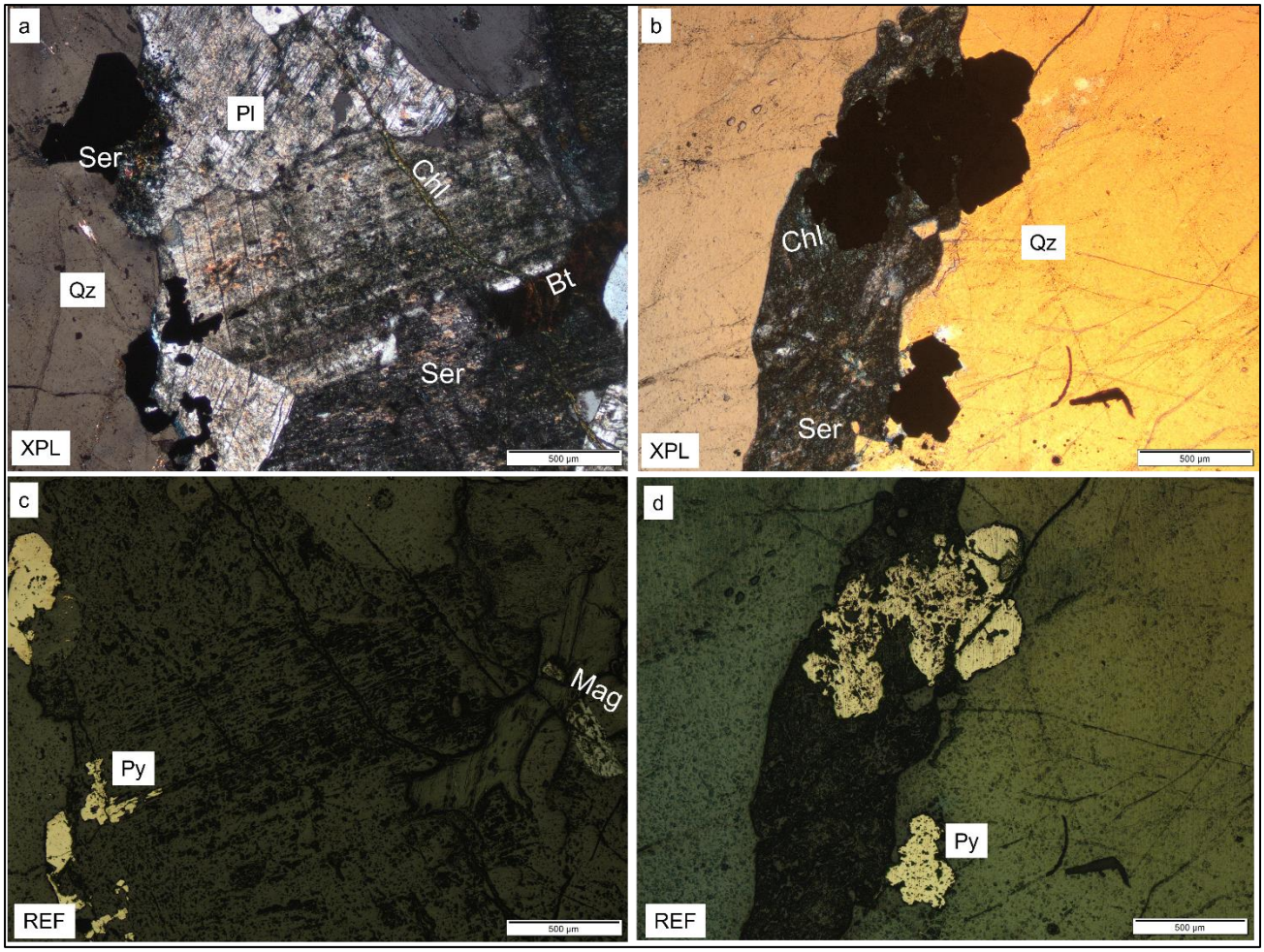
B45: (a-b) large, altered plagioclase occurs within the blocky quartz vein and contains wispy, irregular, small quartz grains. Opaque minerals preferentially occur between sericite and quartz, and some occur within the sericite as subhedral grains and thin veins (white arrows); (c) subhedral pyrite grains are intergrown together, forming a clustered grain and occur at the contact between quartz and sericite. The grains are also disseminated within the fine-grained sericite (varying shapes and sizes). Other elongated anhedral pyrite also occurs along the contact between sericite and quartz.



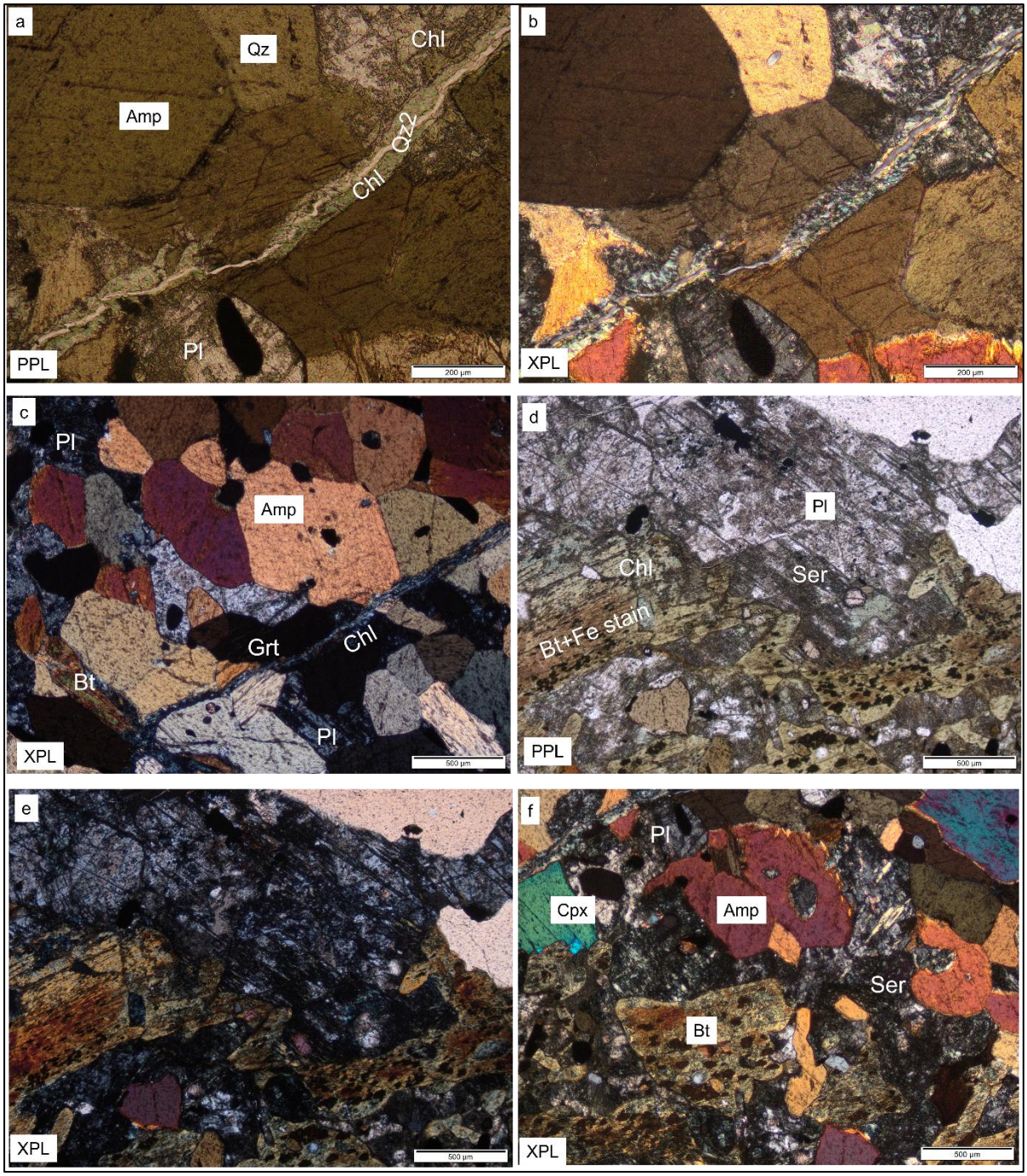
B46: (a-b) large, clear quartz grains contain isolated linear open spaces that are filled by the opaque minerals. Minor sericite is seen along the margins of the open spaces within the quartz grains. Interstitial sericite also invades the large, clear quartz grains; (c) the open spaces are filled by anhedral pyrite grains.



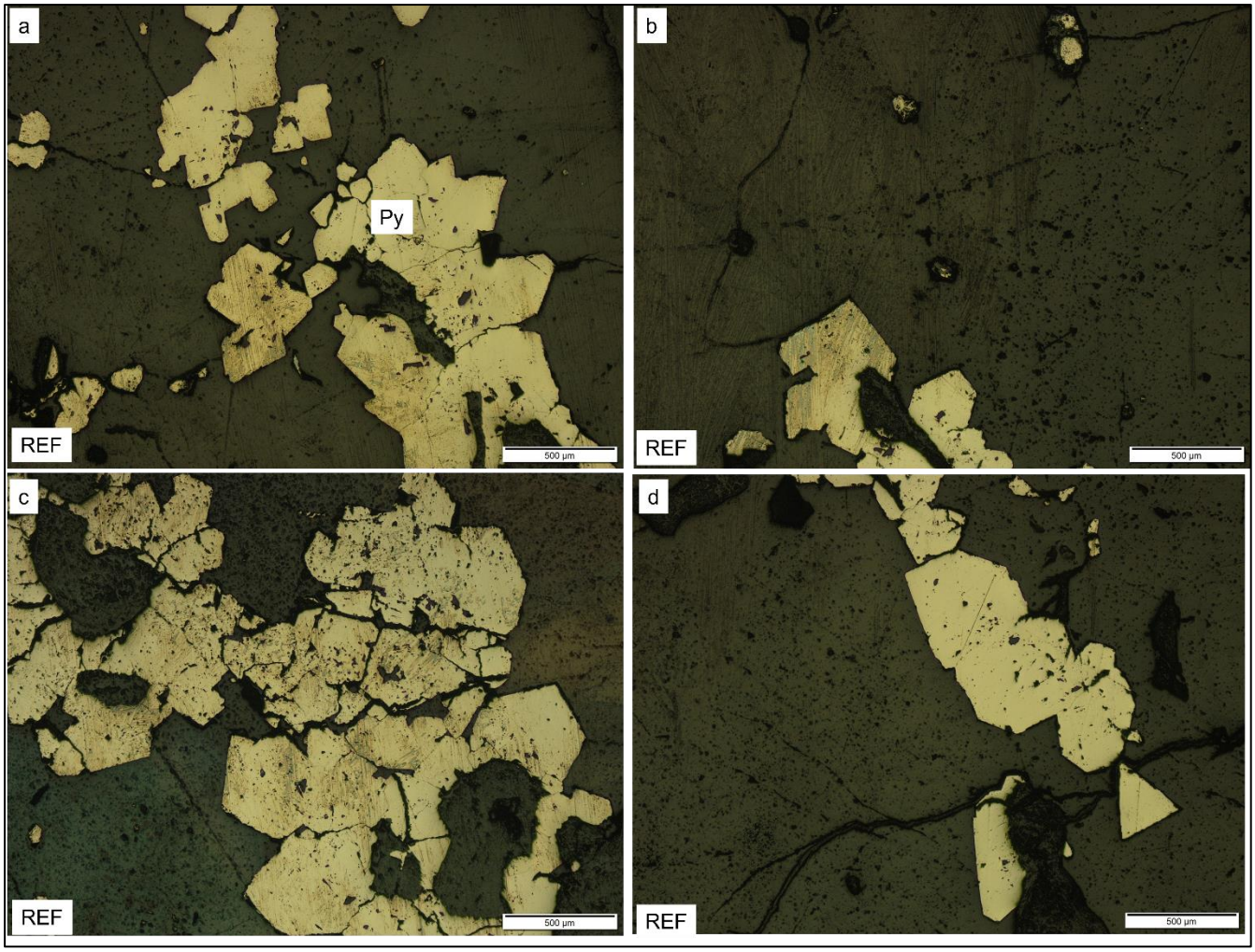
B47: (a-b) large, clear quartz grains contain what looks like weakly formed fractures filled with fine-grained sericite, which also occurs as a partial rim between quartz grains and the opaque minerals. Subhedral chlorite that also invades the quartz grains; (c-d) subhedral to euhedral pyrite grains occur between the quartz and sericite grains. Large subrounded pyrite clusters and small disseminations are present between and within open spaces of quartz grains.



B48: (a-b) invasion of the large, clear quartz grains by altered plagioclase. The plagioclase (recognised by weak multiple twins) is partially altered by fine-grained sericite and is cut by thin chlorite vein. Relict biotite is present between altered plagioclase and quartz grains. The chlorite vein appears to be forming from the biotite. The opaque minerals occur within the altered plagioclase and between the altered plagioclase and quartz grains; (c-d) disseminated subhedral pyrite grains represent the opaque minerals. A tabular magnetite grain occurs in contact with biotite and suggests that it formed by Fe release from the Fe-bearing minerals. Some pyrite grains are cut by a fracture that contains no infilling. Sericite gangue occurs within the pyrite grains, making it appear porous.



B49: (a-f) This part represents the brecciated country rock in contact with the vein quartz. Large, interconnected amphibole grains are cut by a multi-compositional vein composed of quartz in the middle and chlorite in the walls enclosing the quartz. Minor garnet grains, biotite, and plagioclase occur between the interconnected amphibole grains are also cut by a chlorite vein. Large, altered plagioclase occurs as an interstitial material hosting iron-stained tabular to elongate biotite grains that are partially altering into chlorite. Chlorite veins also occur within the plagioclase and appear to be growing from biotite grains. Brecciated clinopyroxene and angular to subhedral amphibole grains occur within the altered plagioclase together with Fe-stained biotite grains.



B50: (a-b) different morphologies and sizes of fractured and unfractured pyrite clusters. The fractures contain no infilling.